THE UNIVERSITY
of EDINBURGH

Glucocorticoids and the Diurnal Rhythm of NCC phosphorylation: Implications for Blood Pressure Control.

Jessica Ivy

Doctor of Philosophy

The University of Edinburgh

2016

Declaration

This is to certify that the work contained within has been composed by me and is entirely my own work. No part of this thesis has been submitted for any other degree or professional qualification.

Signed:

Jessica Ruth Ivy

Abstract

Reabsorbing ~7% of the sodium load, the distal convoluted tubule plays key roles in blood pressure (BP) homeostasis. Here, Na-Cl co-transport (NCC) is the major route for apical Na entry making thiazide diuretics (NCC inhibitors) a mainstay hypertension treatment. Predictive adaptations of sodium excretory rhythms are supported by an intrinsic renal clock, which regulates transporter activity according to physiological need. Peripheral clocks can be influenced by glucocorticoids, which also have a circadian rhythm. We therefore hypothesized that NCC's diurnal rhythm is regulated by glucocorticoids. C57BL6 mice were kept on a 12h light cycle with subjective day starting at 7am. Urine was collected in 12h periods and kidneys harvested at 1am (night) and 1pm (day). Slc12a3 (NCC encoding gene) mRNA and NCC protein abundance were similar between day and night but NCC phosphorylation at threonine 53 was significantly higher at night compared to day. Plasma and urinary corticosterone levels were elevated at night. Glucocorticoid inducible leucine zipper (GILZ) and serum and glucocorticoid inducible kinase (SGK1) transcripts also increased at night. Chronic corticosterone infusion flattened the plasma corticosterone rhythm within an intermediate physiological range. The diurnal rhythm of pT53 NCC was dampened in these mice but not in vehicle-treated mice. Blood pressure was monitored in the mice by radiotelemetry. After 2 weeks of baseline measurements mice received chronic corticosterone or vehicle for 3weeks, during the last 10 days of which they received ~80 mg/kg hydrochlorothiazide in their drinking water. At night systolic BP (SBP) was unaffected by any treatment whereas during the day SBP significantly increased following corticosterone but was unaffected by vehicle. Cosinor analysis of SBP in corticosterone and vehicle treated mice showed a marked reduction in rhythmicity, increased MESOR and reduced amplitude. In animals receiving corticosterone HCTZ partially rescued daytime SBP. This manoeuvre also improved SBP rhythmicity, reduced MESOR and increased amplitude. These data indicate that NCC phosphorylation has a diurnal rhythm that is in part regulated by glucocorticoids. They also show that alteration of the glucocorticoid rhythm affects the blood pressure rhythm in part through its effect on NCC phosphorylation. These findings may be clinically relevant in the pathogenesis of hypertension in conditions associated with elevated glucocorticoid levels such as metabolic syndrome and chronic stress.

Acknowledgements

First and foremost, an immense amount of thanks must go to my supervisor Matt for the unfaltering encouragement and guidance throughout this work. Your pep talks are second to none and I am so grateful for all the opportunities you've given me. I'd also like to thank Peter for all your great advice and philosophical transporter chats – the word "abrogate" will be forever spurned! A big thank you must also go to Karen for the sound advice and guidance she gave me while on my thesis advisory committee. I am also very grateful to the BHF for financial support of my PhD studentship. Thanks also to both Prof. David Ellison and Prof. Johannes Loffing for gifting us their NCC antibodies. Thanks too to Tsung Tan from iPrecio for the collaboration and opportunity to use their programmable minipumps.

I am grateful to Gillian Brooker for teaching me telemetry implant surgery and to Dawn Livingstone for adrenalectomy and tail micro-sampling training. Thank you to Emad Aldujaili for his help and advice with the urinary steroid ELISAs. I would also like to thank the BRF staff for going above and beyond to help out with my interminable requests for quiet rooms, pair housing and wild mouse hunts. Thanks too to Dr Rob for all the advice and use of his immaculate, supremely detailed protocols and to Audrey for all of her help in the lab.

Thanks must also go to my partner, Edward for the ceaseless support: you've racked up hours of listening to presentation practise and other often-trivial problems/worries and I am so grateful for you. Thanks too to all my wonderful friends and to my awesome water polo team, for all of the fun and distraction. To my parents and sisters for all their encouragement and support and in particular my Dad who has plagued me with relentless enquiries about how the thesis was coming along from PhD day 1. Thank you to my "office team": Charlotte, Amelia, Adrienne and "physics" Rob for all the hilarity, tea and encouragement. Thanks to Amelia, Charlotte, Nicole and Wilna for always being there to lend a listening ear, engage in nerdy chat and graciously accept the millions of "snap-cats" and "lab-snaps" inflicted about them!

List of publications arising from this BHF studentship

Hunter RW, Ivy JR, Flatman PW, Kenyon CJ, Craigie E, Mullins LJ, Bailey MA, Mullins JJ *Hypertrophy in the Distal Convoluted Tubule of an 11β-Hydroxysteroid Dehydrogenase Type 2 Knockout Model.* Journal of the American Society of Nephrology, 2015

Ivy JR, Dreshsler M, Catterson JH, Bodmer R, Ocorr K, Hartley PS. *KLF15 is Critical for the Development and Differentiation of Drosophila Nephrocytes.* PLoS One, 2015.

Ivy JR, Bailey MA. *Pressure Natriuresis and the renal control of arterial blood pressure.* The Journal of Physiology, 2014.

Hunter RW, Ivy JR, Bailey MA. *Glucocorticoids and renal Na+ transport: implications for hypertension and salt sensitivity.* The Journal of Physiology, 2014

Oosthuyzen W, Sime NE, Ivy JR, Turtle EJ, Street JM, Pound J, Bath LE, Webb DJ, Gregory CD, Bailey MA, Dear JW. *Quantification of human urinary exosomes by nanoparticle tracking analysis.* The Journal of Physiology, 2013

Table of Contents

List of Figures

List of Tables

1. Introduction

1.1. Non-dipping blood pressure (BP) and cardiovascular disease risk

Hypertension, defined as an average systolic blood pressure (SBP) over 140 mmHg and diastolic blood pressure (DBP) over 90 mmHg, is the leading risk factor for the global burden of disease [1]. Approximately 1/3 of adults have hypertension and this proportion is predicted to increase as the rate of new hypertensives outstrips the population expansion: by 2025 1.5 billion people will be affected [2]. It is not only hypertension per se, but the daily rhythm of BP that is an important risk factor for disease. Indeed, even if office or 24-hour BP is normal, abnormalities in circadian rhythms of blood pressure can confer an elevated risk of cardiovascular disease (CVD) [3, 4].

BP has long been known to have a circadian rhythm. In healthy individuals this is characterised by a morning surge prior to waking, a plateau during the day followed by a nocturnal decline. This nocturnal decline is ~10-20% of the day time BP in healthy individuals, but is attenuated in approximately half of hypertensive patients [5, 6]. This attenuation is known as “non-dipping”, usually defined as nocturnal BP that declines by less than 10 % compared to mean daytime levels [7]. Non-dipping is associated with a plethora of cardiovascular pathologies, including increased left ventricular hypertrophy [8], atherosclerotic plaques [9], micro albuminuria [10], cerebrovascular disease, congestive heart failure, vascular dementia [11], stroke, and myocardial infarction [12]. In a population-based study, normotensive individuals with non-dipping BP had ~double the risk for cardiovascular mortality compared to normotensive dippers [13]. Hypertensive non-dippers had a >5 times greater risk of CV-related mortality (Figure 1.1.) [13].

In other major diseases non-dipping is also a feature. It is present early in the development of diabetes preceding and predicting micro albuminuria [14] and is also associated with metabolic syndrome [15]. BP rhythmicity is lost during the earliest stages of chronic kidney disease (CKD)[16] and creatinine clearance deteriorates faster in non-dipper CKD patients compared to dippers [17]. Understanding the origins of non-dipping blood pressure and how to correct it is important to tackling the global burden of disease.

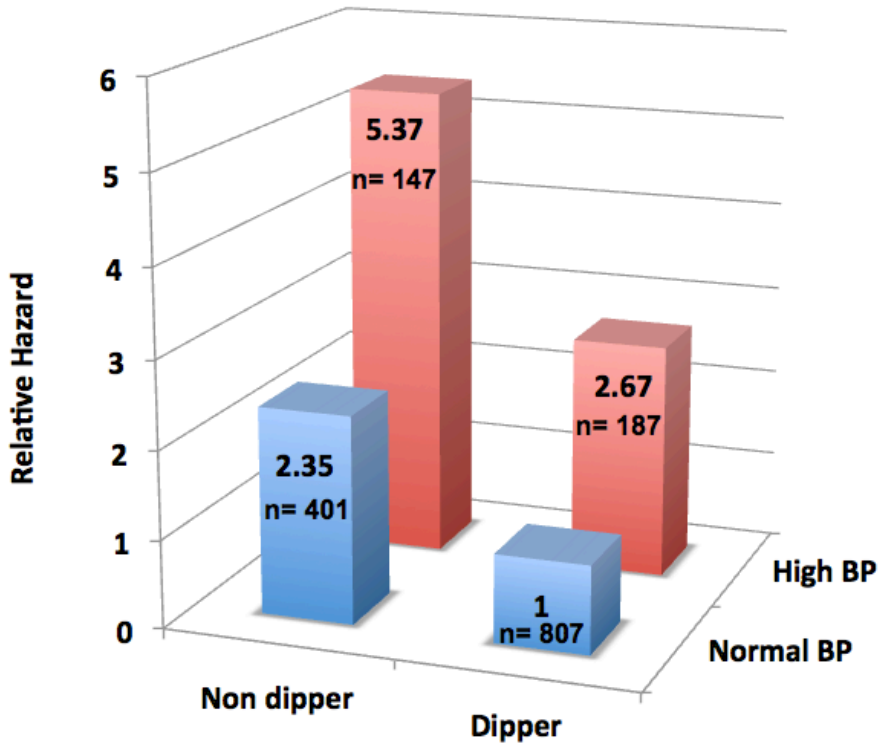

Figure 1.1: Relative Hazard or cardiovascular mortality in patients with non-dipping/dipping high/normal blood pressure.
Figure adapted from [13]

1.2. The kidney and the circadian rhythm of blood pressure

The development of non-dipping BP is multifactorial and loss of nocturnal dip has been associated with poor sleep quality [18], loss of vascular compliance [19] and increased sympathetic drive [20]. Given that the kidney, through regulation of extracellular fluid volume (ECFV), is a major regulator of long term BP [21], it is not surprising that renal impairment may also cause non-dipping. Renal function normally has a circadian rhythm with increased glomerular filtration rate (GFR), renal blood flow (RBF) and sodium excretion during the day compared to the nighttime (Reviewed in [22, 23]). Clinical studies show that the diurnal variation in BP is strongly correlated with renal sodium excretion [24]. Hypertensive and pre-hypertensive patients have a blunted diurnal pattern of sodium excretion with a larger proportion of the daily sodium output excreted at night [25, 26]. Both dietary sodium restriction and thiazide diuretics can rectify this non-dipping BP [27, 28]. Renal transplantation can rescue BP dipping in some cases [29], although pre-transplantation non-dipping can predict poor allograft survival [30].

Combined, this evidence infers a direct link between abnormal circadian BP rhythms and inappropriate renal sodium transport. Indeed, the kidney regulates BP by modulating renal sodium excretion and ECFV in response to changes in renal arterial perfusion pressure (RAP). This mechanism, called pressure natriuresis (PN), stabilises BP in the long term. For example if BP rises, the kidney senses this as a change in RAP and responds by increasing sodium excretion and thus reducing extracellular fluid volume (ECFV). Conversely if BP is low the kidney enhances renal tubular sodium reabsorption thus increasing ECFV (Reviewed in [21]). Mathematical models published by Guyton et al in 1972 predict that this PN system is one of infinite gain, such that any change in BP can be matched with an appropriate change in sodium excretion to bring BP back to a set point [31-33]. It follows that hypertension can only be sustained if the PN response is impaired.

The PN response adapts with changes in dietary sodium intake. For example if sodium intake is high, the PN curve shifts to the left and the slope steepens (Figure 1.2) so that a greater amount of sodium is excreted with a smaller change in BP to prevent an expansion of ECFV. The change in PN slope is modulated by hormonal and neuronal systems such as the renin-angiotensin-aldosterone system (RAAS) and renal sympathetic nerve activity, which trigger renal (renal sodium transporters activation/inactivation) and extra-renal (vasodilation) adaptations. Failure of these systems to respond appropriately to sodium intake can lead to an impaired PN response. In hypertension this usually means a shallower right shifted PN curve [34].

Fukuda et al hypothesised that PN impairment resulting in a diminished sodium-excretory capacity is a key step in the development of non-dipping [35]. Thus, if sodium intake is habitually high, an impaired PN means that the daytime excretory capacity is easily surpassed. Therefore sodium excretion may need to spillover into the nighttime in order to maintain 24-hour sodium balance. BP therefore remains high at nighttime because not enough sodium is excreted during the day; furthermore this BP raise enhances sodium excretion.

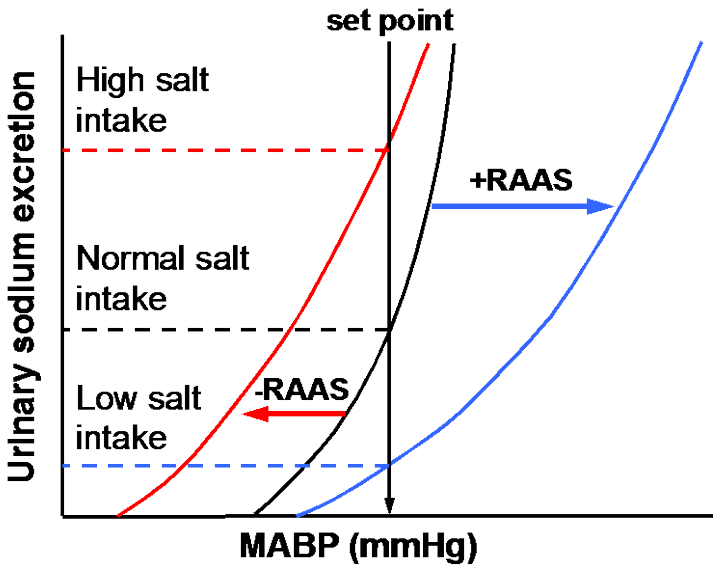

Figure 1.2: Pressure natriuresis curve
Shifting of the pressure natriuresis curve occurs as an adaptation to dietary sodium intake. Low sodium intake causes a shift of the PN curve to the right through an activation of the renin angiotensin aldosterone system (RAAS) and increased renal sympathetic nerve activity (rSNA). Conversely high sodium shifts the PN curve left through an inhibition of the RAAS and rSNA. These shifts cause a change in sodium excretion to maintain mean arterial pressure (MABP) at a set point. Figure adapted from [34, 36].

1.3. Circadian control of renal sodium transport

Vogel and Zadek first described rhythms in urinary excretion in the 1800s (Reviewed in: [22]). These are synchronised with activity and feeding but are unlikely to be merely cause and effect. Electrolyte excretory rhythms have been shown to persist over extended periods under experimental conditions where external factors are kept constant [37, 38], suggesting that these rhythms are under the control of an intrinsic renal clock.

The 24-hour rotation of the Earth confers a predictable daily cycle of fluctuations in temperature and light to the environment. Endogenous biological oscillators or clocks, which are pervasive within the biosphere, are an evolutionary adaptation to these cycles (Reviewed in: [39]). They allow the organism to schedule behavioural and biological functions at the appropriate time within the daily cycle and coordinate internal physiology.

Endogenous molecular clock machinery has been identified in nearly every peripheral tissue in the body. Nucleated cells operate via a simple transcription and translation feedback (TTF) loop involving 4 core clock genes: bmal1, clock, cry and per. The transcription factors *brain and muscle arntl-like 1* (*bmal1*) and *circadian locomotor output cycles kaput* (*clock*) are positive activators of the TTF loop. These are produced and form heterodimers, which

bind to E-box response elements within promoter regions of target genes. These target genes include *period* (per, homologs 1,2,3) and cryptochrome (cry, homologs 1,2). Per and cry proteins are transcribed, translated and accumulate in the cytoplasm where they form heterodimers and homodimers of various combinations before translocating to the nucleus. Upon reaching a critical nuclear concentration, they inhibit bmal1 and cry1, thus repressing their own transcription. When per and cry concentrations decrease below a level required for efficient bmal1 and clock repression, a new transcription cycle can begin.

In order for these transcription and translation oscillatory loops to function, the RNA and protein products of the core clock genes must undergo controlled and rapid degradation. Post-translational modifications modulate this degradation. In particular, phosphorylation of per protein by casein kinase 1ε destabilises per and increases its turnover [40]. Other accessory components of the molecular clock include rev-erbα, DBP and RORA, which modulate the activity of the loop (Figure 1.2,[41]). Importantly in addition to regulating each other to sustain oscillation the clock components also transactivate genes that mediate downstream physiological functions.

Components of the core molecular clock are expressed in the kidney with robust rhythmicity. Furthermore a significant number of renal genes exhibit a circadian profile of expression. Zuber and colleagues demonstrated in microarray analysis of DCT/CNT and CCD micro-dissected kidney segments, that 356 and 504 genes respectively, exhibited a circadian expression pattern (defined by amplitude >1.8 and ~24-hour period)[42]. Using RNA sequencing Hogenesh and colleagues looked at circadian rhythms in several whole organs, including the kidney, with greater resolution (2-hourly compared to 4-hourly)[43]. Of the 12 organs studied, the kidney, with circadian gene expression in 13 % of genes, was second only to the liver with 16% [43].

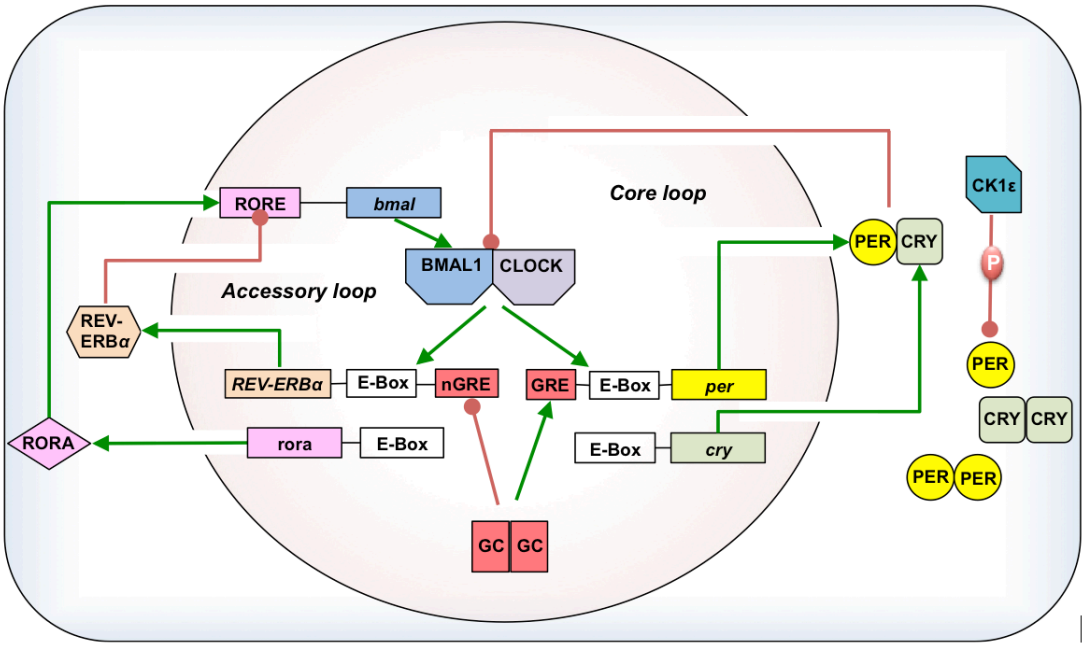

Figure 1.3: Transcription translation feedback loop model of the endogenous clock
The molecular clock mechanism consists of a "Core Clock Loop" in which bmal1 and clock heterodimers bind E-box regions within promoters of *per* and *cry* genes activating their transcription. Per and cry constitute the negative arm of the loop. These accumulate in the nucleus where they form combinations of homodimers and heterodimers. These dimers translocate to the nucleus where they inhibit bmal1 and clock activity thus inhibiting their own transcription. Phosphorylation of per by casein kinase 1 (CK1E) accelerates the degradation of per adding another level of control to the clock. Post-translational modifications modify the accumulation of per in the cytoplasm leading to the ~24-hour rhythm. The "Accessory Loop" is also triggered by clock and bmal1 heterodimers. These bind E-box regions in the promoters of *rev-erbα* and *rora* genes. RORA activates *bmal1* transcription through a RORE element in the *bmal1* promoter. REV-ERBα competes with RORA for the RORE binding site of *bmal1* and inhibits its transcription. Glucocorticoids (GC) can modulate transcription of both *per*1 and *rev-erbα* by binding glucocorticoid response elements in their promoter regions. The GRE in the per1 promoter causes transactivation and increased production of per1 whereas the rev-erbα gene promoter contains a negative GRE (nGRE), which facilitates repression of rev-erbα. Figure adapted from [44, 45].

A micro-array approach identified several gene families with rhythmic expression, including the solute carrier (SLC) family of genes and those encoding enzymes involved in the metabolism of xenobiotics [42]. Genes involved in sodium and water homeostasis have also been identified as being circadian including the vasopressin receptors (V2R, V1aR) and the aquaporins: AQP2 and AQP4 [42]. A candidate gene approach has uncovered several more important renal transporters with circadian rhythms. The sodium hydrogen exchanger (NHE3) in the proximal tubule exhibits circadian oscillations of both its mRNA and protein [46]. These oscillations are directly regulated by bmal1/clock through their interaction with an E-box region in the NHE3 promoter region[46]. Similarly ENaCα, which is the rate-limiting transcript for epithelial sodium transport in the distal nephron, displays a circadian rhythm of expression. This rhythm is per-dependent and can be modulated by aldosterone through aldosterone's induction of per, which requires both MR and GR [47].

The importance of circadian clocks in renal physiology and BP homeostasis is exemplified by gene-targeting approaches in mice (summarised in Table 1.1). Many of these models have sodium transport defects and all exhibit changes in BP level or rhythm. Interestingly some clock mutants were able to maintain their diurnal rhythm of BP (KS bmal1-/-, clock-/- and per1-/-) while others are not (cry1/2-/- and global bmal1-/-). Most of these clock mutants have deformations in their corticosteroid rhythms. Therefore although the intrinsic renal clock is likely important and can function autonomously [48], *in vivo* the kidney clock is modulated by a hierarchical timing system.

Table 1.1: Effects of targeted disruption of clock genes on blood pressure (BP) and sodium balance
"Rhythmic" in the context of Aldo/GC defect means that difference in daytime versus nighttime corticosteroids is intact. SS (salt sensitive) BP, KS (kidney specific, in this case Cre Bmal1$^{lox/lox}$/Ren1d/Cre mice)

Clock gene	BP effect	BP dipping?	E_{Na} defect	Aldo/GC defect	Transporters defects?	References
bmal	↓	non-dipping	**unknown**	Aldo unknown GC rhythmic	**unknown**	[49] [50]
bmal (KS*)	↓	dipping	✓	Aldo ↓ (*rhythmic*?) GC unknown	αENaC, NCC, ROMK, AQP2, AQP3, AQP4	[51]
clock	↓	dipping	✓	Aldo ↓ arrhythmic GC rhythmic	AQP2, AQP4, V2R, V1aR	[42] [52] [50]
cry1/cry2	↑ (SS BP)	non-dipping	✓	Aldo ↑ (arrhythmic) GC ↑ (arrhythmic)	NHE3	[53] [54] [46]
per1	↓	dipping	✓	Aldo ↓ (arrhythmic) GC ↑ (rhythmic)	ENaCα, NCC	[55] [56] [57] [47] [58]

1.4. Entraining renal clocks to the external world

Molecular clocks can only approximate 24 hours and require periodic entrainment by external cues or Zeitgeibers. Zeitgeiber translates as “time giver” and describes exogenous stimuli, which act to synchronise molecular clocks. The photoperiod is the most dominant environmental Zeitgeiber and this information is conveyed within an opaque organism by the activation of the central or master clock within the superchiasmatic nucleus (SCN) of the hypothalamus in the brain (Figure 1.3). The SCN receives light information via non-image forming photoreceptors called photosensitive retinal ganglion cells (pRGC). These ganglion cells express their own photopigment, melanopsin and sense light independently of rods and cones [59]. They signal directly to the SCN through the retinohypothalamic tract and activate several signalling pathways within the SCN (Reviewed in [45]). These signals culminate in chromatin remodelling and the induction of clock genes, adjusting the “metronome” of the SCN.

The SCN then relays this rhythm via neuronal and hormonal signals to the billions of individual clocks within every cell of the body, thus daily establishing “phase coherence” of the organism. Initially this arrangement was thought of as a master and slave situation whereby the peripheral slave clocks are fully dependent or, answer only to, the master clock. However it is now apparent that the peripheral clocks are cell-autonomous and self-sustained. An analogy for this that I particularly like is that of an orchestra and a conductor [60]. Each orchestra performer is capable of playing his/her own tune and each section has a slightly different melody/harmony but the conductor sets the tempo and unifies the performers. Importantly adjacent peripheral cells do not appear to couple their molecular clocks via paracrine signalling therefore the SCN is required for phase coherence of cells within the same tissue [61]. Extending the orchestra analogy, it is as if the performers within the same section cannot hear each other thus are dependent on the conductor’s signalling to keep in time. Whole-organ RNA sequencing experiments by Hogenesch and colleagues show that while the clock genes oscillated in phase in all 12 organs studied (including kidney), the vast majority of other circadian gene expression is organ-specific with very little overlap of circadian genes between organs [43]. Therefore although the peripheral clock is “in time” throughout the body, its effects are organ dependent.

Most data on circadian clock origin, mechanism and function have been obtained in nocturnal rodents but humans are diurnal. The genes and networks of the circadian oscillators are highly conserved between mice and humans [62]. Therefore the mouse

represents a tractable model for disease relating to human circadian disorder. The major difference between nocturnal and diurnal animals appears to be in how the SCN signals are interpreted by the brain. Nocturnal and diurnal animals' SCN clocks are entrained to light in the same manner with increased SCN neuronal firing during light conditions. However, downstream peripheral clocks in nocturnal and diurnal animals are in anti-phase to each other. Therefore nocturnality or diurnality arises from signals downstream of the SCN but upstream of any circadian entrainment relay centres such as the pituitary, which are in phase with the periphery. These pathways are not well defined but comparisons between diurnal and nocturnal rats indicate that the interaction between the SCN and ventral subparaventricular zone (SPVz) may modulate the effect of SCN signals at its targets[63]. Others indicate a developmental difference in how and when the SCN connects to the hypothalamus may confer diurnality [64].

1.5. Glucocorticoids (GCs): peripheral clock synchronisers

How the SCN transmits signals to the rest of the body is the subject of on-going research. A major candidate for peripheral clock entrainment is glucocorticoids (GCs). These steroid hormones have a robust and striking circadian rhythm, their receptors are ubiquitous and they regulate the mRNA expression of ~20 % of the genome [65]. Furthermore glucocorticoid receptors (GR) are not expressed in the SCN [66] so GCs are unlikely to modulate central clock function through their cognate receptor.

GC release is usually governed by the hypothalamic pituitary adrenal (HPA) axis particularly during stress (Figure 1.4). Corticotrophin releasing factor (CRH) from the hypothalamus triggers adrenocorticotropic hormone (ACTH) release from the pituitary, which ultimately increases production and secretion of GCs from the adrenal zona fasciculata. The circadian rhythm of GCs is under the control of the SCN [67]. The SCN projects to the hypothalamus both directly and via several other brain regions (including the subPVZ potentially important for nocturnality/diurnality). Translation of these signals mainly through the paraventricular nucleus of the hypothalamus stimulates CRH-releasing neurones and arginine vasopressin (AVP) releasing neurones triggering rhythmic ACTH excretion, which stimulates corticosterone production and secretion from the adrenal gland (Figure 1.4).

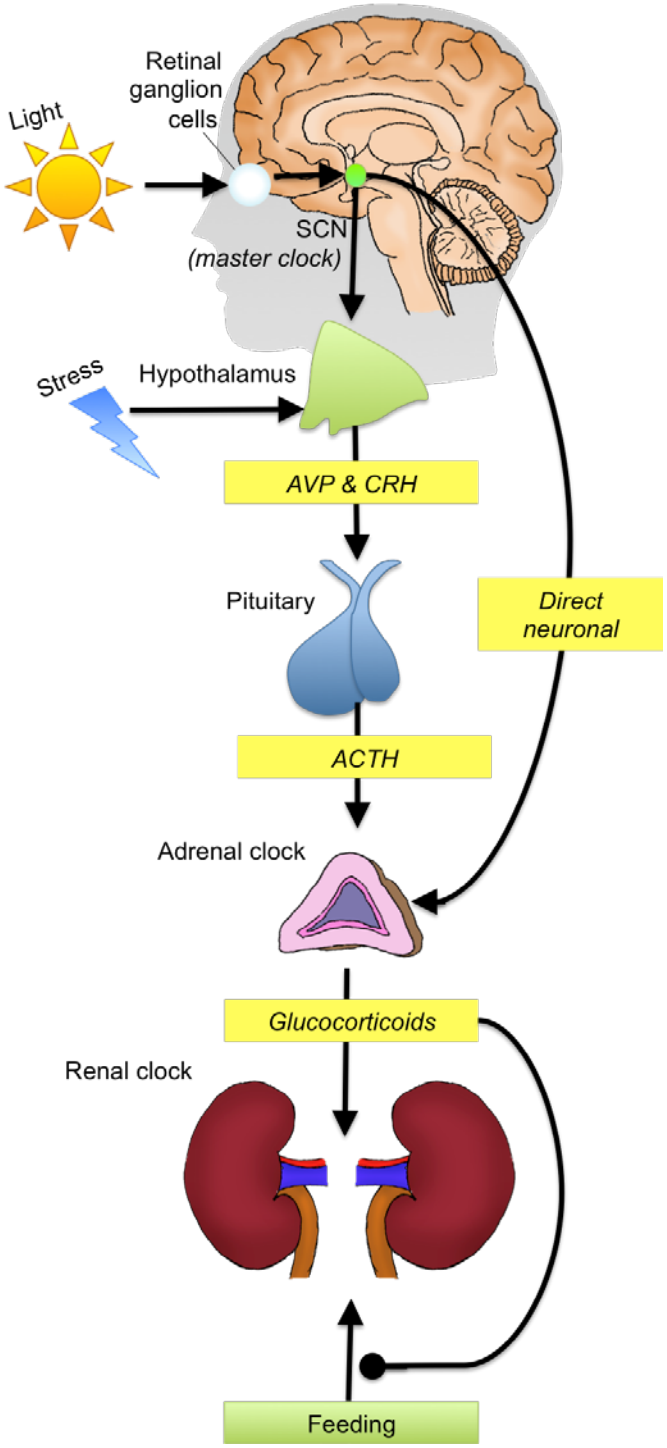

Figure 1.4: Hierarchical arrangement of the circadian timing system and integration with the HPA axis

Light detected by retinal ganglion cells entrain the SCN clock. The master clock integrates with the hypothalamus, which can also receive stress signals from high brain regions. This results in the release of arginine vasopressin (AVP) and corticotrophin releasing hormone into the median eminence triggering the release of adrenocorticotropic hormone (ACTH), which stimulates glucocorticoid (GC) release from the adrenal. GCs go on to entrain peripheral clocks such as those in the kidney. The GC rhythm can also be directly stimulated by the SCN through neuronal connections. For clarity the hypothalamus and pituitary are shown outwith the brain. Adapted from [45, 68].

There is also evidence for direct neuronal connections between the SCN and the adrenal gland, since rhythmic corticosterone release persists in hypophysectomised rats [69] but not in hypophysectomised adrenal denervated rats [70].

GCs have been shown to strongly entrain molecular clocks in many peripheral tissues. Following SCN ablation in rats, a single bolus dose of the synthetic GC, dexamethasone induced the synchronisation of 60% of the circadian transcriptome of the liver [71]. In corneas of adrenalectomised (ADX) rats dexamethasone treatment improved rhythmicity [72]. In human peripheral mononuclear cells, exogenous GCs increased PER1 expression and after several days of treatment caused an 11-13 hour phase shift of PER2-3 and BMAL1 expression [73]. Administration of exogenous GCs causes a strong phase resetting of the circadian oscillators in fibroblasts [74]. And a single injection of GC causes a phase shift of peripheral clocks in the kidney and liver in *in vivo* rat experiments [75]. In primary mouse mesenchimal stem cells GCs stimulated the transcriptional oscillation of 10 of the known clock genes (per1-3, cry 1-2 rev-erbα, dbp, npas2, bmal1) [76].

GCs act by binding to GR in the cytoplasm, which then dimerise and translocate to the nucleus. GR act like transcription factors to transrepress or transactivate genes by binding to glucocorticoid response elements (GREs) and can therefore target clock genes directly or indirectly. GREs have been found in both the core and accessory loops of the circadian clock including per 1 [77], per2 [76, 78] and Rev-verbα [79]. Interestingly clock genes also seem to play a role in the transcriptional activity of the GCs. BMAL and CLOCK dimers can modulate the effects of GCs through enzymatically targeting the GR and attenuating its binding to GREs[80]. Cry1 also appears to associate with and modulate the activity of GRs [54].

It is important to note that GCs are not the only peripheral clock entrainers and many clock protein rhythms are maintained in ADX rats [75]. However GCs do seem to be a dominant stimulus for changing the phase of peripheral clocks. There is evidence that GCs act to oppose the uncoupling of SCN and periphery during phase advancement. This is exemplified in ADX animals or GR ablation in peripheral tissues [81]. In these animals, peripheral clocks entrain more rapidly to feeding cues than adrenal intact animals despite being out of sync with the SCN. Rhythmic GC synchronises peripheral clocks, providing resistance to sporadic environmental changes and thus ensuring any shifts in phase are co-ordinated.

1.6. GCs in the regulation of renal sodium transport

Renal sodium excretion is controlled by complex neuro-hormonal interactions. The RAAS is a major regulatory pathway for BP control, being activated by volume depletion to produce angiotensin II and ultimately aldosterone. Aldosterone promotes sodium retention by activating transporter pathways in the aldosterone-sensitive distal nephron (ASDN) through the mineralocorticoid receptor (MR, Figure 1.5). Aldosterone has a circadian rhythm much akin to GCs and is key in the circadian rhythm of the epithelial sodium channel within the connecting tubule (CNT) and collecting ducts (CD) [47]. Furthermore all clock mutant animals described thus far exhibit aldosterone rhythm abnormalities (Table 1.1).

GCs may have a role in circadian control of renal transport by regulating clock genes, which then regulate sodium transport. GCs are not normally considered a major regulator of sodium transport in the ASDN even though GRs are expressed in cells of the distal convoluted tubule (DCT), CNT and CD [82, 83] (Figure 1.5). Moreover GCs bind MR with a similar affinity as aldosterone [84]. However, in the epithelial cells of the distal nephron the enzyme 11β-hydroxysteroid dehydrogenase 2 (11βHSD2), converts active glucocorticoids (corticosterone/cortisol) into their inactive metabolites (11-dehydro-corticosterone/cortisone) (Figure 1.6). These metabolites have little affinity for MR/GR and therefore 11βHSD2 allows aldosterone to access the receptors (Reviewed in: [85]). The presence of both 11βHSD2 and aldosterone defines the ASDN.

It is likely that the paradigm of an “aldosterone sensitive distal nephron” does not extend to the DCT. In C57BL6 mice, double-immunofluorescence staining indicated that 11βHSD2 and DCT markers were not co-expressed [86]. 11βHSD2 mRNA was not detected in microdissected DCTs [86]. Another approach using HSD2iCre-ROSA26 reporter mice showed 11βHSD2 was present in the connecting tubule (CNT) and collecting duct (CD) but not in the DCT [87]. In other older studies in mice 11βHSD2 immuno-staining was present but very low and only confined to the most distal ends of the DCT[88]. Similarly in rats expression of 11βHSD2 was low restricted to the most distal portions of the DCT [89]. Therefore 11βHSD2-expression is low if present at all in the DCT. Consequently, in the DCT GCs may have a major direct effect on sodium transporter activation and circadian rhythm in the DCT. Furthermore in an environment of habitually high sodium intake, sodium restriction and thus raised aldosterone is likely a rare occurrence. Therefore, one could argue that GCs are more relevant to sodium transport in the DCT in modern society.

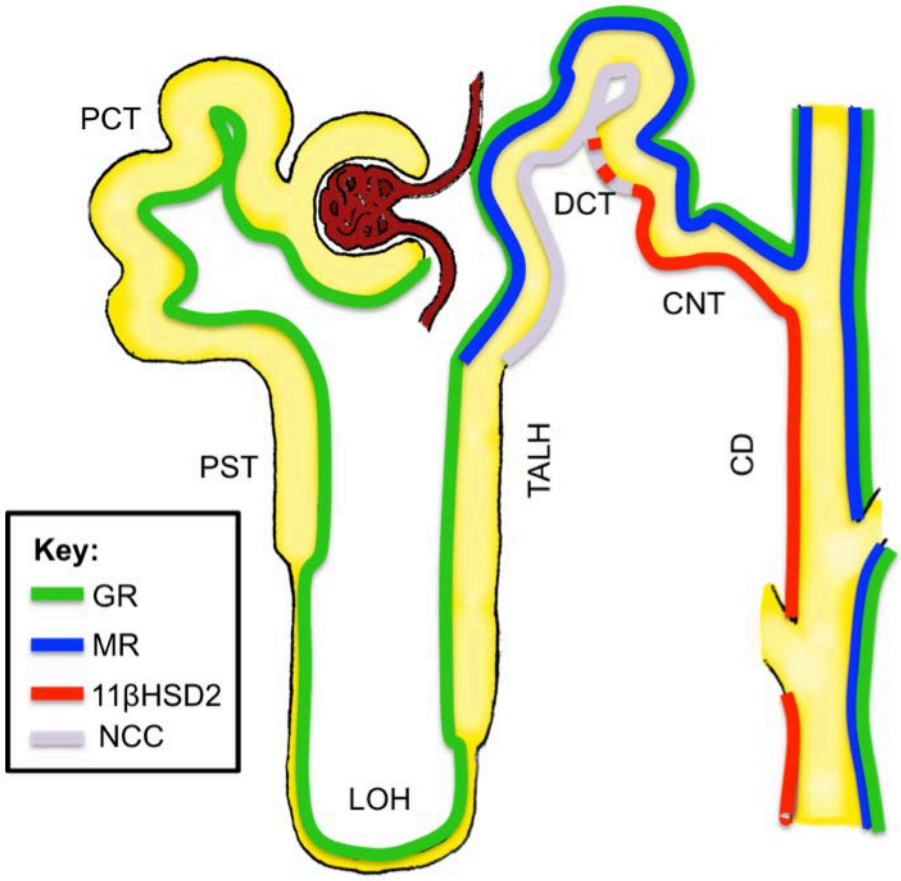

Figure 1.5: Nephron with localisation of MR, GR, 11βHSD2 and NCC
Glucocorticoid receptor (GR) is expressed throughout the tubule and glomerulus, whereas mineralocorticoid receptor (MR) expression tapers off towards the thick ascending limb of Henle's loop (TALH). 11βHSD2 expression is low/absent in the DCT where the thiazide sensitive sodium chloride co-transporter (NCC) is expressed. PCT, proximal convoluted tubule, PST, proximal straight tubule, LOH, loop of Henle, CNT, connecting tubule, CD, collecting duct.

In common with many regions of the nephron the sodium gradient in the DCT is established and maintained energetically by the basolateral K+/Na+ATPase, which extrudes sodium into the renal interstitium from where it is taken back into the circulatory system. This provides an electrochemical driving force that allows passive influx of luminal Na+ through the sodium transporters. In the DCT, passive influx of sodium across the apical membrane occurs through the thiazide-sensitive sodium transporter (NCC, Figure 1.6). There are two studies that demonstrate GC-mediated activation of the NCC. In adrenalectomised rats, both aldosterone and dexamethasone can increase the number of [3H]-metolazone binding sites[90]. [3H]-metolazone is a thiazide-like diuretic and its binding was used to roughly quantify the number of NCC channels in the apical membrane. They also found that the effect of dexamethasone and aldosterone on NCC quantity was additive, indicating two mutually exclusive GR and MR-mediated pathways of NCC upregulation [90]. Another

group found that dexamethasone caused an increase in thiazide-sensitive sodium reabsorption in micro-perfused DCTs of ADX rats [91].

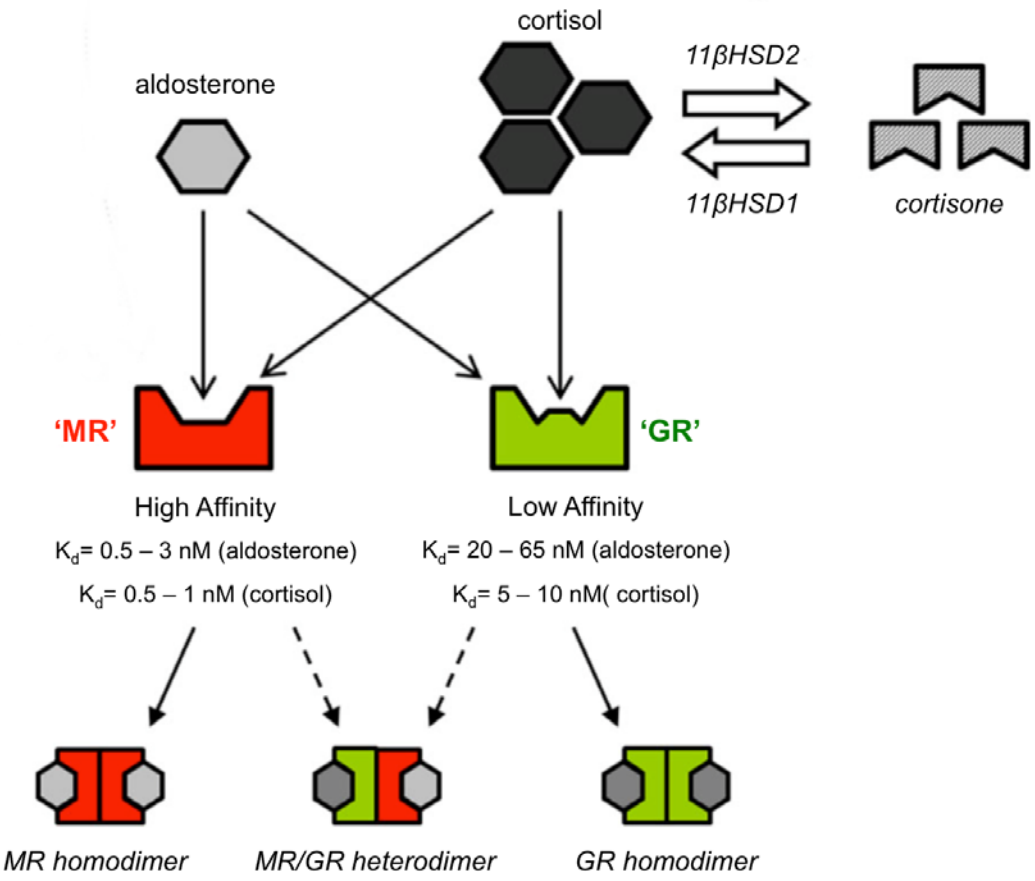

Figure 1.6: Glucocorticoid signal transduction machinery
Glucocorticoids (cortisol in humans or corticosterone in rodents) can bind both the classical low affinity glucocorticoid receptors (GR) and high affinity mineralocorticoid receptors (MR). *In vivo,* glucocorticoids are usually prevented from binding MRs in aldosterone-sensitive tissues, by 11βHSD2, which converts cortisol to inactive cortisone (or corticosterone to 11-dehydro-corticosterone in mice). GR and MR form homodimers and translocate to the nucleus where they can trans-activate or trans-repress genes. GR and MR may also form heterodimers but the physiological significance of this is unknown. Adapted from [92].

1.7. The thiazide sensitive co-transporter

NCC, encoded by the gene *slc12a3*, is part of the solute carrier (SLC) protein family and transports sodium via an electro-neutral route. It consists of 12 trans-membrane domains with intracellular amino and carboxyterminal regions (Figure 1.7). Although only responsible for the reabsorption of around ~7% of the total sodium load it is physiologically important for sodium and BP homeostasis. This is shown by the effectiveness of its inhibitors, the thiazide diuretics, for BP control. Thiazide-diuretics revolutionised BP treatment in the 1950s and are still a frontline-treatment for high BP today [21]. NCC's physiological importance is further exemplified by rare-inherited diseases such as Gitelman's syndrome in which hypotension and renal salt wasting arise from an inactivating mutation of the SLC12A3 gene [93, 94] and conversely Gordon's disease, which causes constitutive NCC activation, low-renin hypertension and hyperkalaemia [95] [96].

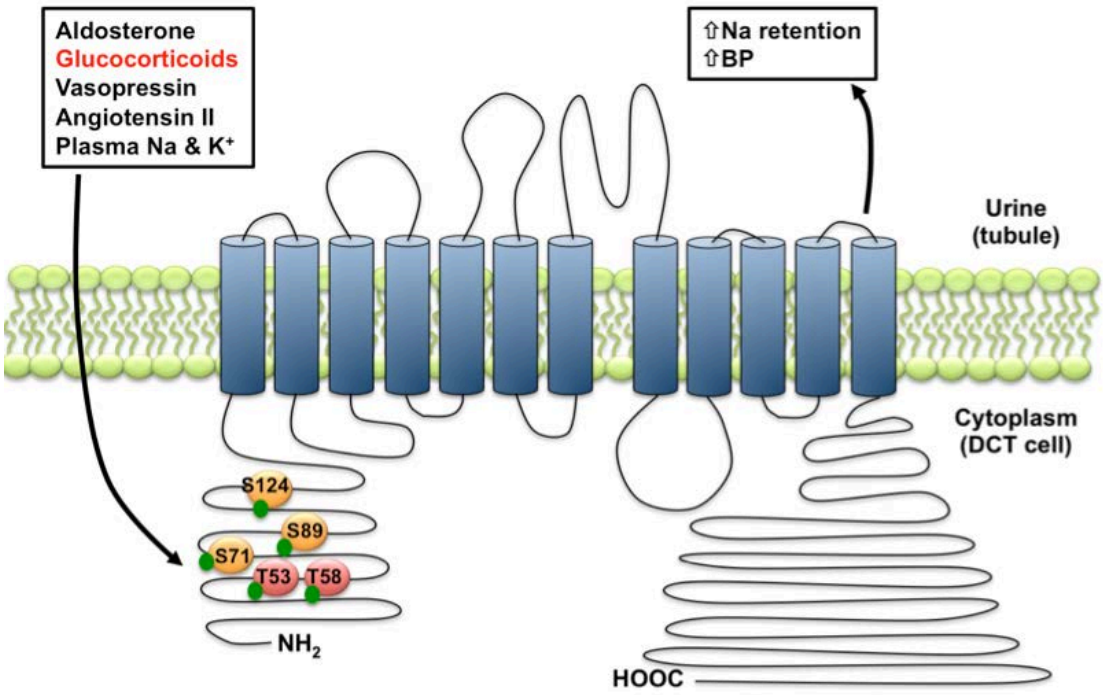

Figure 1.6: 12-transmembrane domain structure of the thiazide-sensitive sodium chloride-cotransporter (NCC).
Activation of NCC within the apical membrane of distal convoluted tubule cells requires its phosphorylation at key threonine and serine residues in the intracellular amino terminus as illustrated. The hormonal regulators that can ultimately cause an increase or decrease in NCC phosphorylation are listed. Enhanced NCC phosphorylation causes an increase in sodium retention and blood pressure.

1.8. Activation and regulation of NCC

NCC regulation occurs through alterations of both the amount of protein inserted into the apical membrane and through the activation of this apical membrane protein. Activation of NCC relies upon its phosphorylation. Phosphorylated NCC is found exclusively in the apical plasma membrane of the DCT [97] suggesting phosphorylation is involved in the activation of NCC rather than forward trafficking of NCC to the membrane. The major phosphorylation sites of NCC in mice include threonine 53 (T53), threonine 58 (T58) and serine 71 (S71). In a *Xenopus laevis* oocyte expression system, mutation of any of these three residues reduces the activity of NCC [98, 99]. In cell models of the DCT, the phosphorylation of NCC correlates with activity rather than an increase in surface expression and it has been speculated that phosphorylation may facilitate dimerization of NCC, which promotes activity of the transporter but this is yet to be confirmed *in vivo* [100]. NCC phosphorylation delays its ubiquitinylation, endocytosis and degradation [101]. In NCC mutant T58 phospho-incompetent homozygous knock-in mice, a decreased NCC total and membrane abundance was found, indicating that phosphorylation at T58 may be important for its stability in the membrane [102].

Much of the work on NCC intra-cellular regulation has been elucidated using *Xenopus laevis* oocytes and cell lines with aldosterone as the hormonal stimulator. Therefore in this section a provisional model is described with aldosterone as hormonal stimulator of the NCC regulatory pathways but note that GCs could activate the same pathways through MR. Furthermore other NCC regulators such as rSNA [103, 104], vasopressin [97], AngII [105] also contribute to NCC regulation through manipulation of these intracellular regulators. Finally although DCTs express GR, its role in NCC regulation is unclear. The model described here is a simplified summary of the major intra-cellular machinery that may be involved in NCC activation (Figure 1.8).

Many of the known regulatory pathways centre around the *with no lysine kinase* proteins 1 and 4 (WNK1 and WNK4 respectively). These two kinases emerged in the pursuit of the genetic basis for Gordon's Syndrome [106]. This syndrome of hypertension with hyperkalaemia is hyper-responsive to thiazide diuretics, but does not involve any mutations of NCC. Instead, linkage studies found mutations in WNK1 and WNK4 [107], which triggered a surge of research into the regulatory effects of these kinases. The majority of studies, including those in animals and native DCT cell models, indicate that WNK4 acts as

an inhibitor of NCC activity. Indeed overexpression of wild type WNK4 in mice causes hypotension and a decrease in thiazide sensitive sodium transport [108], indicating an inhibitory role for WNK4. WNK4 is thought to inhibit NCC activity through the inhibition of the STE20/SPS-1-related-proline/alanine-rich kinase and oxidative stress response kinase 1 (SPAK/OSR1) complex [109]. SPAK/OSR1 phosphorylates NCC at three residues present in its amino terminal (murine Threonine 53, threonine 58 and serine 71) promoting activation as described earlier.

WNK4 also decreases the transport of NCC from the trans-Golgi network to the apical plasma membrane [110] and promotes the association of NCC with the mouse adaptor protein 3 (AP-3), which recruits NCC to lysosomes for degradation [111]. Another pathway through which WNK4 is thought to inhibit NCC activity is through the ERK1/2 pathway, which is promoted by WNK4-dependent phosphorylation [112]. That WNK4 is solely inhibitory is not clear-cut as conflictingly, several studies have alluded to a stimulatory role for WNK4 under some conditions. In cells WNK4 promotes SPAK/OSR1 phosphorylation and WNK4 null mice lack the ability to phosphorylate NCC and SPAK/OSR1 appropriately upon low salt or angiotensin II stimulation [113]. WNK4 is not constitutively active and although its expression is inhibited by aldosterone [112], the protein/s or pathways that activate WNK4 remain unidentified. It is likely that WNK4 can have both inhibitory and stimulatory roles on NCC regulation in the same cell depending on the stimuli present and its state of activation [114].

WNK1 on the other hand is constitutively active upon expression [115]. It exists in two forms in the kidney: a long form (L-WNK1) that is ubiquitously expressed throughout the epithelia of the body and a truncated form that has its own separate promoter and is specific to the kidney hence its name kidney-specific WNK1 (KS-WNK1)[109]. L-WNK1 does not directly alter NCC activity but promotes its phosphorylation by phosphorylating SPAK/OSR1 and by direct inhibition of WNK4[116]. KS-WNK1 is a negative regulator of L-WNK1, therefore KS-WNK1 relieves WNK4 inhibition [117, 118]. Although no mutations have been found in WNK3 that link it to Gordon's disease, it is nevertheless an important NCC regulatory kinase. WNK3 directly stimulates NCC, increasing its phosphorylation as well as apical abundance [109]. Furthermore, WNK3 and WNK4 are reciprocally inhibitory, therefore adjustments in the concentration of these kinases is thought to allow a range of NCC activity [109].

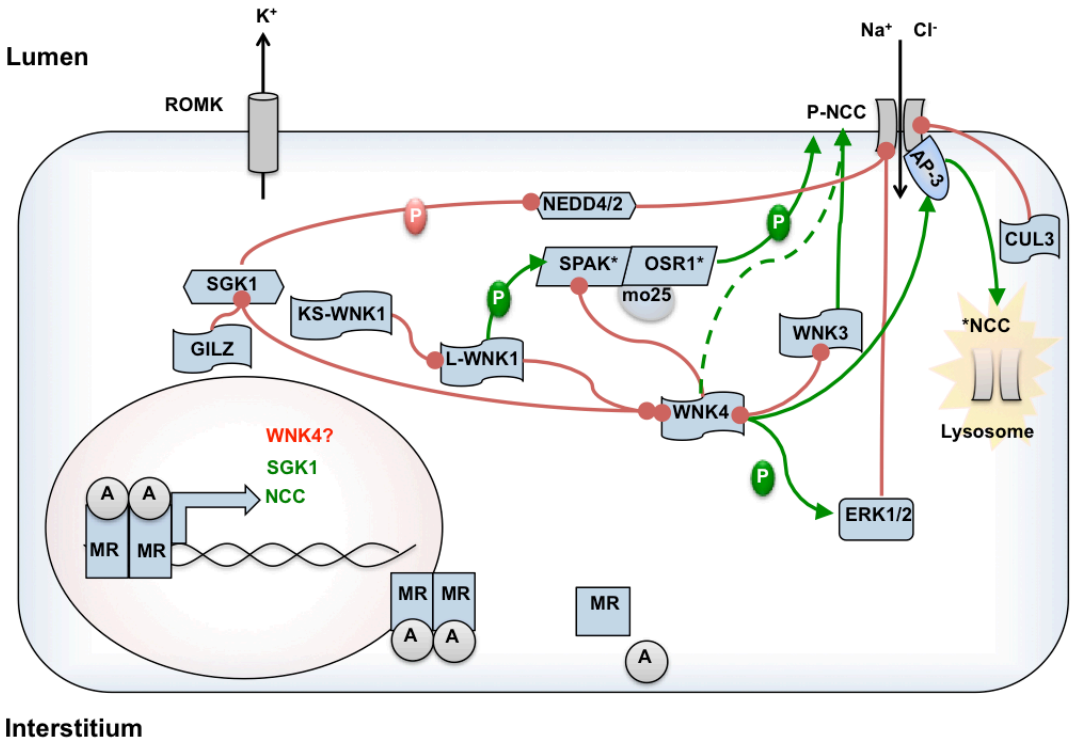

Figure 1.7: Provisional model for the intra-cellular regulation of the sodium chloride co-transporter (NCC).
Aldosterone is thought to upregulate the sodium chloride co-transporter in the distal nephron although it is not clear how this is achieved. MR activation, dimerization and translocation to the nucleus, promotes the transcription of NCC and inhibits WNK4 expression following prolonged aldosterone exposure. WNK4 is generally accepted to be an inhibitory regulatory kinase of NCC and how WNK4 is activated is still unknown. SGK1 and L-WNK1 inhibit WNK4 and thus promote NCC activity through relief of WNK4-mediated inhibition of the STE20/SPS-1-related-proline/alanine-rich kinase and oxidative stress response kinase 1 (SPAK/OSR1) complex. Mouse protein 25 (mo25) is a positive regulator of SPAK/OSR1. SGK1 is also postulated to inhibit Nedd4/2, which can also ubiquitinylate NCC. Kidney specific WNK1 (KS-WNK1) is a negative regulator of L-WNK1 and thus promotes WNK4 driven inhibition of NCC. Further WNK4-mediated inhibitory pathways include inhibition of the NCC-stimulatory kinase WNK3 and stimulation of inhibitory protein ERK1/2 and the adaptor protein 3 (AP3). AP-3 facilitates lysosomal transport and thus WNK4 redirects NCC to the lysosome. (Red connectors represent inhibition through phosphorylation (P) or otherwise, while green arrows indicate stimulation by phosphorylation (P) or otherwise. Interrupted green arrows represent unknown or controversial events.)

Although interactions between WNKs and NCC have been the subject of much investigation, less attention has been paid to the connection of these pathways to stimulatory hormones or neuronal activity. There is evidence that GR can interact with a nGRE in the WNK4 promoter and is essential in the development of salt-sensitive BP induced by β adrenergic stimulation [103]. Chronically, aldosterone increases NCC transcription and inhibits WNK4 transcription through MR activation [112]. Acutely, however, the aldosterone-induced increase in NCC abundance [119] is a post-transcriptional phenomenon as no changes in NCC mRNA are seen [116]. Increased NCC abundance could be achieved

through prolonging its half-life through adjustments of the WNK1 and WNK4 pathways (Figure 1.8). However, the only transcript within this NCC pathway that aldosterone has been shown to increase in DCT cells acutely thus far is SGK1 [120, 121]. SGK1 could link aldosterone stimulation, WNK4 kinase pathways and NCC upregulation. *In vitro*, SGK1 inhibits WNK4 through phosphorylation and this relieves the inhibition upon NCC thus promoting its activity [122]. Furthermore *sgk1-/-* mice fail to phosphorylate and upregulate the expression of NCC under low salt conditions despite dramatically increased plasma aldosterone levels [123]. Negative regulators of WNK4 and WNK1 have recently been discovered and include kelch-like family member 3 (KLHL3) and cullin3. These proteins form the KLHL3-Cullin E3 ligase. This complex ubiquitinylates WNK1 and WNK4 and promotes their degradation [95, 124, 125]. Very recently, aldosterone has been shown to mediate the interaction between NEDD4/2 and WNK1 through SGK1 [126]. NEDD4/2 targets WNK1 for degradation. Aldosterone-induced SGK1 upregulation therefore causes an inactivation of NEDD4/2, limiting its interaction with WNK1 and thus allowing more WNK1 to accumulate [126].

Finally, we know from experiments on NKCC1, that the role of phosphorylation in regulating the rate of ion transport can be overridden by changes to the cytoskeleton (protein-protein interactions)[127]. It is therefore possible that this could be an important, if not overlooked, aspect of NCC regulation too.

1.9. Does the clock regulate NCC?

There are clearly many aspects to the regulation of NCC that are not understood including the role of the molecular clock in to the NCC signalling cascade. The clock must integrate with this pathway at some level, since *per1* and *bmal-KS* null mice demonstrate altered NCC expression [51, 56] (Table 1.1). Clock genes could directly affect NCC activation by acting as transcription factors to genes within the NCC regulation pathways. Work by Gumz and colleagues has shown that E-BOX binding sites, which per1 and cry1 interact with, exist on WNK4 and WNK1 [56]. It is unclear how or if these affect *in vivo* NCC activation.

The second major question is how are clocks activated in the DCT? Does GC-entrainment of the renal clock have a role in this signalling cascade and how? As explored, GCs can alter the level of per1, per2 and rev-erbα directly through GREs and thus influence the renal clock. But GCs could also interact with the NCC pathway independently of the clock, for example through induction of SGK1, which as the name suggests is a GC-induced kinase.

1.10. Summary, hypothesis and aims

Rhythmic renal sodium transport likely contributes to a circadian rhythm of BP. GCs are a major entrainer of peripheral circadian clocks. Limited 11βHSD2 expression in the DCT of the kidney means that this nephron segment's circadian rhythms are likely influenced by GCs over mineralocorticoids. Here, NCC is the major apical sodium transporter and has key roles in BP homeostasis.

In my thesis I hypothesise that:

Glucocorticoids impose a diurnal rhythm on NCC, which contributes to the diurnal rhythm of blood pressure.

The overarching aim of this work was to investigate the presence of a circadian rhythm for NCC activity and it's relationship with GCs and BP. The diurnal rhythm of sodium excretion, corticosteroid secretion, BP and NCC phosphorylation is initially defined in Chapter 3. The effect of GC manipulations on NCC phosphorylation and sodium excretion is investigated in Chapter 4. Temporal variation of components of the NCC regulatory pathways and clock machinery and the effect of GCs on these was investigated in Chapters 3 & 4. An attempt to define temporal changes in NCC function (by looking at temporal thiazide-sensitive sodium transport) was made in Chapter 5. The indirect effects of temporal variations in NCC activity were investigated by monitoring thiazide-induced changes in rhythmic BP in mice undergoing chronic GC treatment (Chapter 5). Finally the receptor (MR/GR) through which GCs stimulate NCC phosphorylation was investigated in Chapter 6.

Circadian comes from the latin circa-diem meaning "about a day". In chronobiology the term is used stringently to only include ~24-hour processes that have autonomous rhythmicity i.e. can occur in the absence of exogenous stimuli or Zeitgeibers. In this thesis "diurnal" is used in place of circadian to denote processes that occur daily but are yet to be defined as truly circadian as they have not been tested under free running conditions (i.e. constant dark or light.)

2. Methods

2.1. Animals

2.1.1. Husbandry

All experiments were performed in line with United Kingdom Home Office regulations and in accordance with the Animals (Scientific procedures) Act 1986. Breeding and husbandry was carried out in the Biological Research Facility, University of Edinburgh. Mice were housed in groups ($n \leq 5$, unless otherwise stated) and given *ad libitum* access to water and standard chow, (rat and mouse maintenance diet 1: Special Diet Services) containing 0.25% Na, 0.38 % Cl and 0.67 % K, unless otherwise stated. All mice used were adults aged between 2-4 months. Mice were housed at 50% humidity and 22-26^{o}C with 12:12 light:dark cycles starting at 7am local time, unless otherwise stated.

2.1.2. Source of Animals and Breeding

Male C57BL6J/Ola mice used for breeding and experiments were bought in from Harlan and allowed at least a week between transportation and the start of any experiment, to minimise stress.

2.2. Qualitative Immunofluorescence Staining

2.2.1. Perfusion fixation of the kidney

Deep anaesthesia was achieved using 50 mg/kg Pentobarbital Sodique, (Tocris) and the kidneys and aorta accessed via a laparotomy. The intestines and other internal organs were gently brushed to the side using a cotton bud, in order to clearly visualise the left kidney and the descending aorta. The left renal artery/vein bundle was occluded using a micro-haemoclamp and the kidney was removed and snap-frozen and stored at -80^{o}C. The aorta was gently isolated from the overlying connective tissue using a cotton bud and blunt forceps. A micro-haemoclamp was applied anteriorly just below the renal vascular branches and another was applied about 2 cm postural to this. An abdominal incision was made and the aorta was catheterised using p50 tubing primed with filter-sterilised 140 units/ml heparin saline (porcine heparin sodium salt, Sigma-Aldrich) attached to a heparin saline filled syringe. Care was taken to ensure no air bubbles were present within the tubing or aorta. The anterior micro-haemoclamp was moved to hold the catheter in place and correct positioning within the aorta was confirmed by the pulsatile backflow of blood into the tubing. The vena cava was then punctured just below the postural micro-haemoclamp.

The aorta catheter tubing was connected to a peristaltic perfusion pump (Gilson Minipuls® 3) with PVC perfusion tubing (2.79 mm internal diameter, Scientific Laboratory Supplies). The peristaltic perfusion tubing was primed with heparinised PBS (140 units/ml heparin (porcine heparin salt, Sigma) in PBS) for 1 minute followed by 4 % PFA (Paraformaldehyde, Sigma-Adrich) for 20 seconds at a rate of 15 ml/min. The mouse was perfused for 4 minutes before the right kidney was excised and its poles removed. The kidney next immersed in 4% PFA at ten times their volume (5-7 ml) for 24 hours at 4ºC. They were then transferred to 70% ethanol for up to 1 week before embedding in paraffin wax (pole end down). Sections (5 μm) were dried onto glass slides at 37ºC over night.

2.2.2. Immunofluorescence with tyramide signal amplification

Double-immunostaining, (using two different fluorophores to detect two different targets on the same sample), was performed by the Immunodetection and Imaging Facility at The University of Edinburgh. Slides were processed in batches using a Leica BOND-MAX™ robot, following de-waxing and hydration. An antigen retrieval step was included and involved heating in the presence of Novocastra Bond Epitope Solution 1, pH 6 (ER1, Leica). Slides were then heated to 125ºC for 10 seconds, cooled to 90ºC over 40 minutes and loaded onto the BOND-MAX™ robot, which carried out the following steps: peroxidase block (3% H_2O_2 in wash buffer, 10 minutes), serum block (serum from the species that the secondary antibody was raised in, diluted 1:5 in TBS; 10 minutes), primary antibody (Table 2.1, 2 hours), HRP-conjugated secondary antibody (Table 2.1, 30 minutes) and tyramide-labelled fluorophore (either Cy5 or Cy3, 10 minutes). Three 4-minute washes (0.1% Tween in TBS) were carried out between each of the above steps. After the first immunofluorescence detection step, antigen retrieval was performed, by heating samples in ER1 solution for 10 minutes on the robot and the second detection step was performed, exactly as the first above. Finally the slides were counter-stained with DAPI and a glass coverslip was mounted on an aqueous medium (PermaFluor™, Thermo Scientific).

2.2.3. Image acquisition and analysis

Images were acquired using a Zeiss LSM 510 Meta Confocal Laser Scanning Microscope. DAPI, Cy3 and Cy5 were excited using a blue diode 405 nm laser and HeNe 546 and 633 lasers respectively. Tiled images (~7x7) were captured through a 20X objective lens.

Table 2.1: Primary and secondary antibodies used in immunofluorescence

Target	Dilution (primary)	Source/host/ catalog#	Dilution (secondary)	Source /host
NCC	1:2500	Millipore/rabbit/AB3553	1:500 (anti-rabbit)	Santa Cruz/ goat
11β-HSD2	1:2000	Millipore/sheep/AB1296	1:500 (anti-sheep)	Nordic Immunology/rabbit
MR	1:500	Abcam/rabbit/ AB64457	1:500 (anti-rabbit)	Santa Cruz/ goat
GR	1:1000	Santa Cruz/rabbit /SC1004	1:500 (anti-rabbit)	Santa Cruz/ goat

2.3. Western analysis of renal protein and phosphoproteins

Western analyses of phosphoproteins involved in the regulation of NCC were performed on whole kidney to gain insight into some of the molecular pathways controlling sodium transport.

2.3.1. Tissue harvest procedure

Mice were acclimatised to various treatments; 12 hour light cycles (with light on at 7 am local time/ZT0 and lights off at 7 pm local time/ZT12) and housed either singly or in groups of 2 for at least a week (described in methods sections of results chapters: Chapter 3, 4, 5) prior to cull. Mice were then culled by cervical dislocation within 1 minute of removal from the holding room. A laparotomy was performed and using a pair of curved 7 cm curved forceps the left kidney was prised from the renal artery, decapsulated and snap frozen on dry ice and stored at -80^{o}C for western analysis. The right kidney was excised and frozen in the same way, but halved after decapsulation for qPCR analysis. A terminal plasma sample was taken via cardiocentesis (see plasma sampling post mortem section).

In initial culls, mice were housed in groups of three and culled by an increasing concentation of carbon dioxide followed by a cervical dislocation to confirm death. However using this approach, we noted that the mouse culled third in every batch of three displayed a lower level of phosphorylation compared to the other mice (Figure 2.1), regardless of the time point of cull (the phenomenon occurred both at night and during the day time culls). The reason for this is not known but one possibility relates to an increase in plasma potassium levels following death by CO_2 [128]. Plasma potassium in mice culled by CO_2 was almost twice as high (7 mmol/l) as mice culled by ketamine/xylene overdose [128]. It is also shown

that an oral gavage to increase plasma potassium to 10 mM induces a rapid and sustained decrease in the phosphorylation of NCC at pT53 [129]. We do not know if this accounts for the phenomenon observed in the third mouse of each batch but we rejected this approach. For all experimental data in results chapters, mice were housed either single or in pairs and culled by rapid cervical dislocation. No kidney weights were taken at the time of cull, but all mice were of similar body weights and no differences were found in renal protein abundance (assessed post-homogenisation by BCA assay).

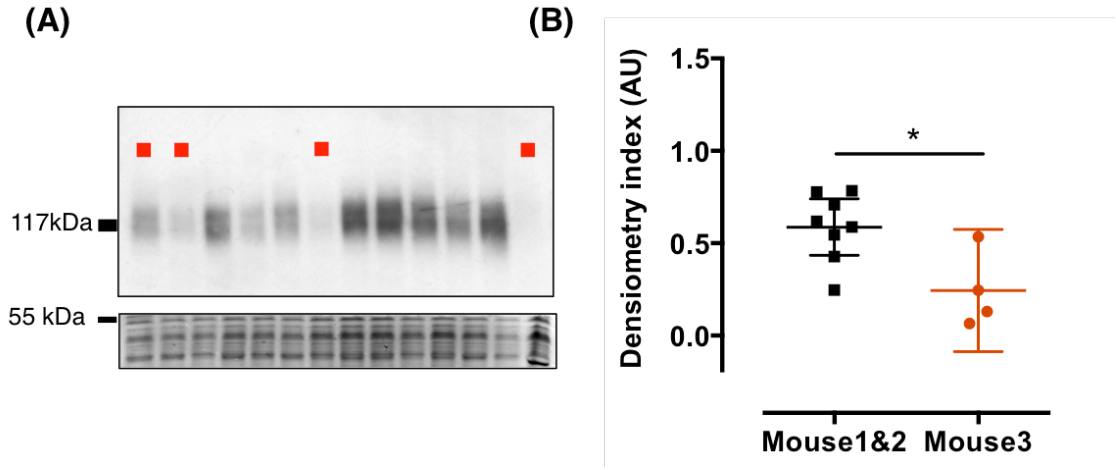

Figure 2.1: Reduced phosphorylation in the third mouse, in mice culled by CO_2 in batches of threes
(A) Western blot of pT53 NCC and coomassie gel, red squares demarcate the "third mouse" sample in each of the 4 groups culled. All mice herein were culled during the active phase, i.e. at night (B) densitometry analysis, with pT53 NCC normalised to the coomassie. Data are mean ±95% CI, *p<0.05.

2.3.2. Kidney homogenization and sample preparation

In order to minimise any dephosphorylation or protein degradation a buffer containing phosphatase and kinase inhibitors and protease inhibitors was prepared. All solutions were bought from Sigma-Adrich unless otherwise stated. Protein and protease inhibitor buffer (PIB): 250 mmol/l sucrose, 10 mmol/l thriethanolamine, 2 mmol/l EDTA, 50 mmol/l NaF, 25 mmol/l Na β-glycerophosphate, 5 mmol/l Na pyrophosphate, 1 mmol/l Na orthovanadate, dH_2O pH to 7.6. A 200 mmol/l stock solution of Na orthovanadate was in the biologically active monomeric state. This was achieved by dissolving 2.94 g Na orthovanadate in 60 ml dH_2O and adjusting the pH to 10. This caused a colour change to yellow (indicating a change to decavanadate). The solution was then boiled until transparent (indicating a change to monomeric vanadate) and pH readjusted to 10. PIB was filter sterilised 0.45 µm filter and frozen at -20ºC in 20 ml aliquots. The buffer was defrosted on ice and protease inhibitors added prior to use (10 µl per 1 ml protease inhibitors (Protease inhibitor cocktail set III,

Calbiochem, Merck-Millipore). Frozen, decapsulated whole kidneys were kept on ice-water slurry and immersed in 2 mL of ice-cold PIB. The kidneys were homogenised in a mixer mill (Mixer Mill MM301, Retsch®) for 60 seconds at top speed three times, cooling on ice between mixes. The homogenate was incubated (on ice-water slurry, 15mins) and centrifuged (4ºC, 4000 g, 15 minutes). The supernatant was collected and the pellet re-suspended in 1 ml ice-cold PIB, homogenised and centrifuged as previous and the supernatants were pooled. Aliquots of protein were made at this point to take forward for protein quantification and for western analysis. All aliquots were made up on ice-water slurry in a cold room (4ºC) to minimise any dephosphorylation or protein degradation. Aliquots were stored at -80ºC, thawed once for use and then discarded.

2.3.3. Protein preparation and Gel Electrophoresis

The protein content of the kidney homogenates was quantified by BCA assay (Pierce™, Thermo Scientific™) according to the manufacturer's instructions. A protein load of 10-20 µg was loaded for electrophoresis as this was in the linear range of detection for NCC and phospho-NCC (Figure 2.2). While on ice, protein samples were adjusted to the desired concentration with protein isolation buffer (PIB), LDS sample buffer (NuPAGE®, 4X) and DTT (final concentration of 100 mM) and the sample preparation heated (70 ºC, 15 minutes) to reduce the proteins. Half and double protein loads from one or two designated lane(s) were prepared to run as linearity controls The samples were centrifuged briefly and vortexed before loading. Fifteen well, 3-8 % Tris-Acetate precast protein gels (NuPAGE®, Novex ®, Life Technologies) were rinsed and loaded into an electrophoresis cell (SE300 MiniVE, Hoefer®). Electrophoresis running buffer (Tris-Acetate SDS running buffer, NuPAGE®) was poured into the gel chambers, 250 µl antioxidant (NuPAGE®) was added to each chamber and the tank was ½ filled. To remove excess gel storage buffer each well was flushed with 100 µl running buffer twice. Protein samples (10 µl) and protein ladder (HiMark™, Life Technologies) were resolved on the gels at constant voltage (100 V) for 60 minutes.

2.3.4. Protein Transfer

Transfer buffer contained 25 ml 20X NuPAGE ® Transfer Buffer, 100 ml absolute methanol, topped up to 500 ml dH2O with 500 µl NuPAGE® antioxidant added fresh with every use. Following use it was stored at 4ºC and could be re-used u to 3 times. Gels were removed from their plastic casing and equilibrated in cold (~4ºC) transfer buffer for 15 minutes. PDVF membrane (AMERSHAM Hybond®-P, GE Healthsciences) was cut to size

and immersed for 10 seconds in absolute methanol and then allowed to equilibrate for 10 minutes in transfer buffer. Extra-thick filter paper (BioRad®) was soaked in transfer buffer. Avoiding bubbles, the membrane followed by the gel was assembled between two pieces of filter paper in a BioRad Trans-blot SD semi-dry electrophoretic transfer cell (BioRad®). The gel was transferred for 30 minutes at constant voltage (10 V).

2.3.5. Immunoblotting

The membrane was removed from the transfer apparatus and rolled into a 30 ml Falcon tube and incubated (RT°, 1 hour) with 20 ml blocking buffer (5% w/v non-fat dry milk powder in wash buffer: 0.2%v/v Tween in phosphate buffered saline (PBS: 20 tablets for 2 l, Dulbecco A, Oxoid™). Primary antibody (see Table 5 for dilution) was added to 5 ml blocking buffer and incubated with the membrane (4°C, overnight). The membrane was washed with wash buffer (3 x 10 minutes). The HRP-conjugated secondary antibodies were diluted in 5 ml blocking buffer as appropriate (see Table 2.2) and incubated with the membrane (RT°, 1 hour). The membrane was washed as previous and incubated with ECL reagent (Pierce™, Thermo Scientific™) (RT°, 5 minutes). Excess ECL reagent was removed and the membranes were covered in clear plastic film, exposed to X-ray film, developed (Compact 4x, Xograph) and scanned. The membrane was then rinsed in wash buffer and stored in PBS for up to a month.

2.3.6. Coomassie blue staining for normalization

Coomassie blue staining was adapted for use as a loading control to normalise the immuno-blot results for the amount of protein loaded on the gel. A dose curve indicated that densitometry of the Coomassie blue staining was linear in range of 10-40 μg protein (Figure 2.2). Regular housekeeping genes such as β actin and GAPDH were previously found to supersaturate at these protein loading concentration [130]. The bottom of the gel, just above the 55 kDa mark, was trimmed and incubated in Coomassie blue solution (Coomassie Blue R (0.025 g), methanol (40 ml), acetic acid (7 ml) and dH_2O (53 mL)) on a rotary shaker (RT°, 3-4 hours). The solution was replaced with de-staining solution 1 (in mL: methanol 200, acetic acid 35 and dH_2O 265) and incubated (RT°, 30 minutes). De-staining solution 1 was replaced with de-staining solution 2 (in ml: methanol 25, acetic acid 35 and dH_2O 440) and incubated overnight. De-staining solution 2 was changed once the next day and gels scanned (Epson Perfection 1640SU, Epson) for quantification by densitometry analysis.

Table 2.2: Concentration and source of primary and secondary antibodies used for Western analysis

Primary Antibody	Dilution (primary)	Source of primary	Dilution (secondary)	Source /host
Anti-NCC	1:2500	Chemicon, Millipore	1:5000 (anti-rabbit)	Santa Cruz /goat
Anti-phospho NCC T53	1:500	MRC Protein Phosphorylation and Ubiquitinylation Unit (PPU), University of Dundee	1:10 000 (anti-sheep)	Sigma Aldrich /donkey
Anti-phospho NCC T58	1:500	MRC PPU, University of Dundee	1:10 000 (anti-goat)	Sigma Aldrich/ donkey
Anti-phospho NCC S71	1:100	MRC PPU, University of Dundee	1:10 000 (anti-goat)	Sigma Aldrich /donkey
Anti-NCC	1:1000	Gift from Prof D. Ellison, University of Oregon	1:5000 (anti-rabbit)	Santa Cruz /goat
Anti-NCC	1:1000	Stressmarq, Bioline	1:5000 (anti-rabbit)	Santa Cruz /goat
Anti-NKCC2	1:1000	MRC PPU, University of Dundee	1:5000 (anti-rabbit)	Santa Cruz /goat

2.3.7. Stripping and re-probing the membrane

Following analysis of phosphorylated NCC the membrane was stripped and re-probed for total NCC or NKCC2. This protocol could not be used the other way around since the phospho-antibodies failed to detect a signal once the membrane had been stripped. Stripping and re-probing made little difference to the quantity or the linearity of NCC/NKCC2 detected. The membrane was incubated in stripping buffer (glycine (3.75 g), SDS (0.25 g), Tween20 (2.5 ml), pH to 2.2 and topped up to 250 ml) for 10 minutes on a rotary shaker at room temperature. This step was repeated before washing the membrane for 10 minutes three times. The membrane was then immediately transferred to blocking buffer and subjected to all the steps undertaken as per "Immunoblotting" section.

2.3.8. Densitometry and quantification

The band intensity was quantified by densitometry analysis using Image J (a detailed method is available: http://lukemiller.org/index.php/2010/11/analyzing-gels-and-western-blots-with-image-j/). For occasions where two or more western blots were required to run the samples,

a reference load was prepared from a pool of homogenate and run on each gel in order to normalise the data to account for inter-run differences. Gel lanes were normalised for differences in protein loading as quantified by densitometry of the Coomassie stained gel segments and further adjusted so that the control group (for consistency this is defined throughout this work as "day time" and/or vehicle group) = 1.

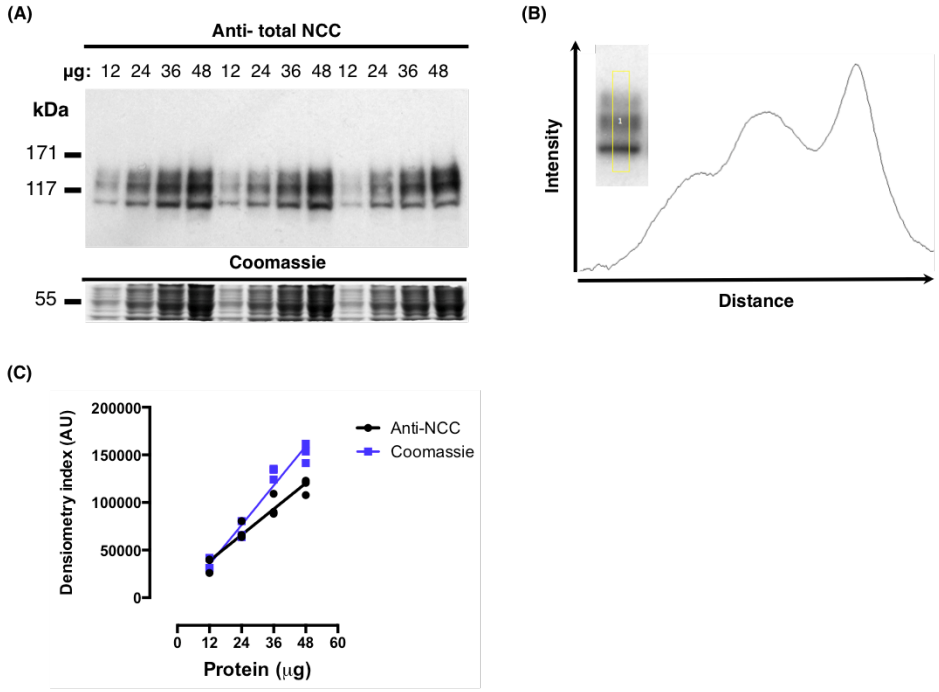

Figure 2.2: Defining the linear range of detection for total NCC and coomassie.
(A) Protein loads from 12-48 µg were loaded and immunoblotted for anti-NCC. The bottom of the gel was coomassie stained. (B) Example of how densitometry was performed. A region of interest was selected within ImageJ and the relative intensity of each pixel was given across the distance selected. To quantify this intensity over distance an area under the curve was taken. (C) Results of densitometry analysis of (A) indicate both anti-NCC and coomassie are within the linear range between 12-48 µg of protein, with R-square values of 0.93 and 0.95 respectively and both p values <0.0001.

2.3.9. Selection of antibodies for analysis of NCC phosphorylation

2.3.9.1. Comparison of Total NCC antibodies

The total NCC antibody identified three products of sizes: ~ 111, 128, 143 kDa. The predicted molecular weight of NCC is 110 kDa [131], with higher bands thought to be as a result of N-glycosylation, which is essential for surface expression and activity of NCC [132]. The literature gives a range of sizes of NCC in whole kidney homogenates depending on the gel system and conditions used. For example, Fenton et al find a diffuse protein band(s) at ~100-150 kDa using the StressMarq antibody [97], Loffing and colleagues reports a triplet band very similar to ours at ~130 kDa [129] and Ellison's group report a double

band at ~111 kDa and a very faint thin band at <111 kDa using a Bis-Tris gel system [133]. This lower band is likely to be the core non-glycosylated protein with the heavier two bands (which are often seen in the literature as a single large band) being the glycosylated protein [132]. Experiments in which whole kidney homogenate is incubated with a de-glycosylating agent, such as N-glycosidase, result in the complete disappearance of the two heavy bands, leaving behind only the ~110 kDa band i.e. "core non-glycosylated NCC [132].

In order to assess whether the reported differences in protein sizes and banding patterns were a result of a discrepancy in the antibodies' target epitopes, three different antibodies to NCC were tested under the same conditions. Professor Ellison's antibody was a generous gift. Stressmarq (Bioline) and Chemicon (AB3553, Millipore) antibodies were purchased. Whole kidney homogenate was prepared and samples of 10, 20, 40 μg total protein loaded on a single gel three times along with a ladder (Himark^{TM}, Life Technologies). The western analysis was run as described in Methods (2.3.4 - 2.3.8) but after transfer the membrane was cut into 3 sections and incubated overnight with the Ellison, StressMarq or Chemicon and anti-NCC antibody. All membranes were probed with a goat anti-rabbit HRP-conjugated secondary antibody (Santa Cruz) and visualised using chemiluminescence. All three total antibodies showed the same thick middle two bands at the same molecular weight ~120-150 kDa when resolved on the same gels (Figure 2.3). The thin, lower molecular weight band was present with both stressmarq and chemicon but was not detected using the Ellison antibody under the conditions used here. The origin of the thin, higher molecular weight band present with StressMarq is not clear. The chemicon antibody resolved the best with our gel system and was comparable with the other available antibodies.

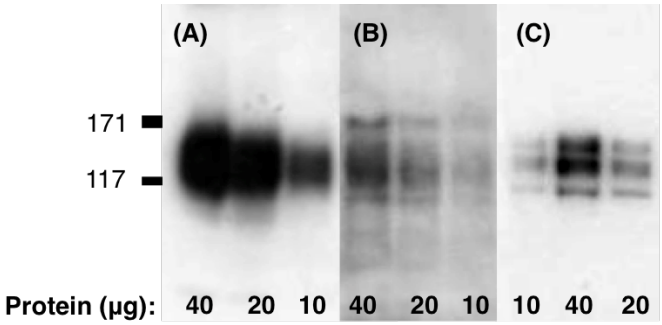

Figure 2.3: Comparison of total NCC antibodies.
(A) Prof David Ellison's NCC antibody. (B) Stressmarq NCC antibody (C) Chemicon NCC antibody.

2.3.9.2. Specificity of phospho antibodies for NCC over NKCC2

The NCC phospho-motifs are conserved in other related transporters, particularly NKCC2. Threonine 53 and 58 on NCC shares homology with Threonine 96 and 101 on NKCC2 (Figure 2.4). The pS71 antibody is unlikely to cross react with NKCC, as there is not a homologous serine site. Other groups have raised similar concerns, particularly with the specificity of the pT58 NCC phospho-antibody [105] [134]. Immunofluorescent staining showed total NCC antibody was restricted to the apical and sub-apical membrane of the cortex. However, pT58 immunofluorescent staining was much more abundant, with detection in the medulla as well as the cortex [105] [134]. There is no basolateral staining with anti-pT58, indicating that it is unlikely to cross react with NKCC1, which is located on the basolateral membrane [135]. In this short series of validation experiments we utilise immunoprecipitation (IP) to separately "pull down" NCC and NKCC2 and probe the IP products using pT58, pT53 and pS71 antibodies.

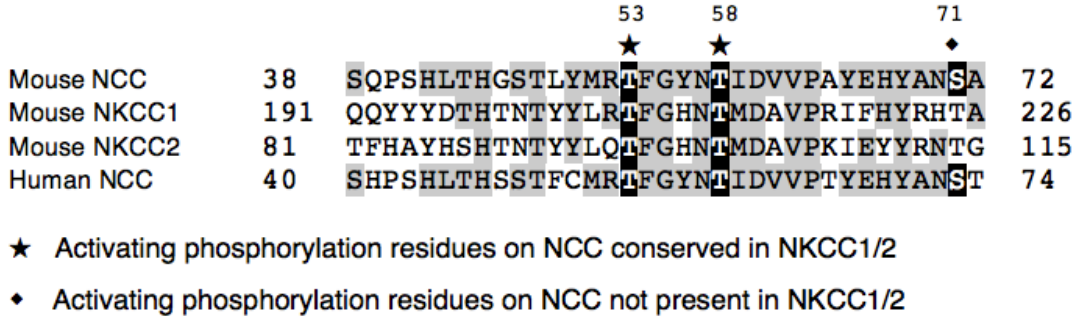

Figure 2.4: Sequence alignment of the N-terminal region of SLC12 electro-neutral NaCl co-transporters, exhibiting several homologous phosphorylation sites
Grey highlights regions on mouse NKCC1/NKCC2 and human NCC that are homologous with mouse NCC. Black highlights phosphorylation sites that are important for transporter activation. Adapted from [136].

Superparamagnetic beads (Dynabeads™ Protein G, Life Technologies) were resuspended in a homogenous solution by gentle shaking and rolling on a roller at room temperature. 50 µL was added to a 1.5 ml eppendorf tube and placed on a magnet (Dynal magnetic particle concentrator, Invitrogen). Within 1 minute the beads stuck to the side of the tube and the clear supernatant was aspirated and discarded. Primary antibody was diluted in Antibody washing and binding buffer (ABB, Dynabeads™ Protein G Immunoprecipitation Kit, Life Technologies) 10 µl anti-NKCC2 (Dario, Alessi, Dundee) in 190 µl ABB or 20 µl anti-NCC (Chemicon, Millipore) in 180 µl ABB and added to the beads. The antibody-bead solution was removed from the magnet and incubated for 10 minutes at room temperature on rotation to allow the antibody to conjugate to the beads.

The mixture was placed back on the magnet and supernatant removed. 400 μl kidney homogenate (approximately 2500 mg protein) was added to the beads, taken off the magnet and incubated for 1 hour at 4°C. The homogenate-bead-antibody mixture was placed back on the magnet and supernatant removed. The beads-antibody-antigen was washed 3X in PIB by removing the mixture from the magnet resuspending the mixture by pipetting carefully up and down and removing the supernatant once placed back on the magnet. The antigen was eluted with 20 μl elution buffer (Dynabead® Protein G Immunoprecipitation Kit, Life Technologies), 3 μl DTT (Sigma-Adrich) and LDS (NuPAGE®, Life Technologies) and heated at 70°C for 15 minutes. The mixture was placed back on the magnet for a final time and the suspension was separated on 3-8% Tris acetate gels and immunoblotted as previously described. A standard kidney homogenate (no IP) was prepared contemporaneously and separated by electrophoresis alongside the IP sample. Following transfer to a membrane, the membrane was cut in 4 with each piece containing a ladder, IP product and 12 mg total protein from whole kidney homogenate. Each piece of membrane was probed with anti-pT53, pT58, pS71 or NKCC2 antibodies. There was some cross reactivity with NKCC2 for the pT58 antibody (Figure 2.5) and therefore this antibody was not used to detect NCC specific phosphorylation. All experiments in this work are carried out using the pT53 and pS71 antibodies, which do very specifically bind NCC (Figure 2.5).

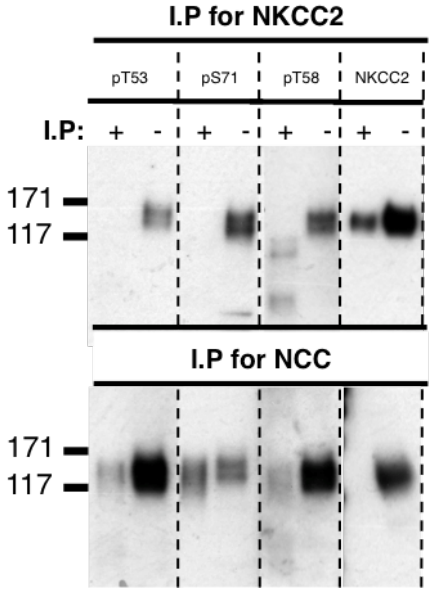

Figure 2.5: Cross-reactivity of anti-NCC antibodies
Immunoprecipitation was used to "pull down" NCC or NKCC2 from 2500 μg of total kidney homogenate. These immunoprecipitation products (+) were then separated on 3-8% Tris Acetate gel, transferred to Hybond P membrane and immunoblotted for the NCC phospho-antibodies and NKCC2. 12 μg of total kidney homogenate (-) was run alongside the IP products and probed directly as a positive control.

2.4. Estimating the abundance of mRNA transcripts by Q-PCR

Real time quantitative RT-PCR was performed on whole kidney to gain an insight into some of the molecular pathways controlling sodium transport. Tissue was harvested as per "Tissue Harvest Procedure" see 2.3.2.

2.4.1. Sample preparation

2.4.1.1. Extraction of RNA

mRNA was prepared from half kidneys using RNeasy spin columns (QIAGEN) according to the manufacturer's instructions. Briefly, half kidneys were removed from -80°C onto ice/water slurry. A steel bead and 600 µl RLT buffer (QIAGEN) was added to the 2 ml eppendorf tube containing the kidney, which was then homogenised for 2 minutes at top speed (Mixer Mill MM301, Retsch®). The samples were centrifuged at 8 000 g (Heraeus Biofuge pica, DJB Labcare) for 3 minutes to pellet the debris. 150 µl of supernatant was removed to a fresh 2 ml eppendorf and 300 µl 70% ethanol and 150 µl RLT buffer was added and the sample mixed briefly by inversion and loaded on to a spin column (QIAGEN). The spin steps were carried out exactly as instructed in the product manual and RNA finally eluted in 50 µl RNAse free water (QIAGEN). A DNAse step was carried out using DNA-free™ Kit (Ambion® Life technologies). Briefly 5 µl 10X DNAse1 buffer and 1 µl nDNasel was added to the 50 µl RNA sample gently mixed and incubated at 37°C for 30 minutes. 5 µl inactivation reagent was added and vortexed thoroughly before centrifugation at 16 000 g for 2 minutes. The supernatant was carefully transferred to a clean tube. RNA was stored at -80°C until use.

2.4.1.2. Quantification and quality control of RNA

2 µl of the RNA sample was taken forward to quantify the RNA concentration using a Nanodrop 1000 spectrophotometer. This gives a sample concentration in ng/mL based on the absorbance at 260 nm. RNA concentrations were 200-700 ng/µl. RNA purity was also assessed using the A260/280 and A260/230 ratios given by the Nanodrop analyser. A A260/280 ratio of <1.7 is indicative of contamination by phenols, which can affect downstream applications. All samples taken forward for reverse transcription had A260/280 ratios 1.7-2.1. The A260/230 ratios were usually in the range of 1.8-2.2. Several samples were lower than this indicating the presence of co-purified contaminants. An agreement about the acceptable lower limit of this ratio is not available but the RNA spin column manufacturers have expressed that this ratio is very likely a result of contamination by

guanidine thiocyanate salt. Experiments using high concentrations of this salt (up to 100 mM) in real time PCR, did not compromise the reliability of the assay [137] and therefore the very small volume taken forward to reverse transcription (as a result of a high yield of RNA), was unlikely to affect the qPCR results. To check the RNA was intact, 500 ng of each sample mixed with 6X DNA Gel loading dye (Life technologies) and resolved at 80 V for 1 hour on a 0.8 % agarose, 0.5 % TBE gel and stained with 0.05 % ethidium bromide. This enabled the detection of two clear sharp bands of 28S ribosomal RNA and 18S ribosomal RNA. The top 28S band was approximately twice the intensity as the lower 18S band and no smearing was detected, indicating intact RNA (Figure 2.6).

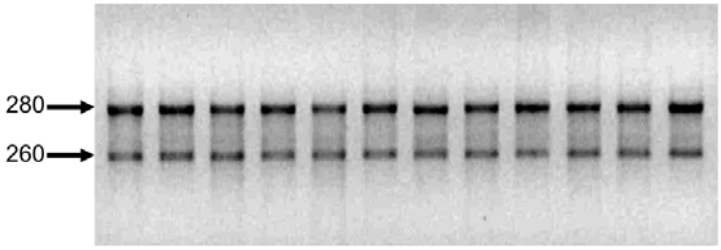

Figure 2.6: Representative example of agarose gel electrophoresis of RNA samples. 500 ng of each RNA sample was resolved on a 0.8 % agarose in 0.5 % TBE buffer and visualised with 0.05 % ethidium bromide. The clear, sharp bands of 28S (top) and 18S (bottom) rRNA indicate that the RNA preparations were not degraded. Furthermore, the intensity of the 28S band was approximately double that of the 18S band in each sample.

2.4.1.3. Reverse transcription

Reverse transcription was carried out on 500 ng RNA using a AB High capacity RT kit (Life Technologies) using a total reaction volume of 20 µl. Constituents per sample include (in µl): 10X RT buffer (2), 25 X dNTP mix (0.8), 10 X RT random primers (2), Reverse transcriptase (1) and 500 ng RNA & nuclease free water mix (14.2). Prepared RT samples were briefly centrifuged and run under the following RT PCR conditions: 2 5ºC (10 minutes), 37 ºC (120 minutes), 85 ºC (5 minutes), 4 ºC (continuous). Included in each RT PCR round were a no template control and a no reverse transcriptase control. Resultant cDNA samples were stored at -20 ºC prior to dilution for qRT-PCR.

2.4.2. qRT-PCR Assay

2.4.2.1. 2.3.3.1. Assay design

Assays were designed using the Roche Universal Probe library "assay design centre" application (URL:
http://lifescience.roche.com/shop/CategoryDisplay?identifier=Universal+Probe+Library).
All assays were designed so that the amplicon spanned an intron excluding the first or last intron (to avoid targeting any SNPs, as these areas have a higher frequency of SNPs [138]).

Primers were also run through the Integrated DNA technologies oligo analyser tool (https://www.idtdna.com/calc/analyzer) to flag up those with any hairpins, self-dimers and heterodimers. All primers were purchased from Eurofins Scientific. The assay was rejected if the standard curve error exceeded 0.05 (i.e. the mean squared error of the data points making up the standard curve) or the efficiency was outwith the range 1.7-2.1 and a second or third assay attempted (Table 2.3). PCR products were ran with loading dye (DNA Gel Loading Dye, 6X, Life Technologies) on a 4 % TBE agarose gel with 0.05 % ethidium bromide to ensure the amplicons conformed to the expected lengths (Figure 2.7).

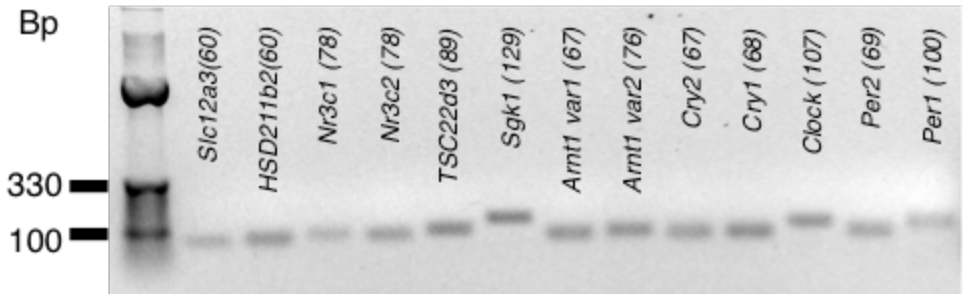

Figure 2.7: Representative example of qRT-PCR products resolved on a 4 % TBE agarose gel with 0.05% ethidium bromide
Expected lengths of qRT-PCR products are in brackets. The cDNA ladder used was a 10 bp Trackit ladder (Life Technologies).

Table 2.3 (overleaf): Table of qRT-PCR assays.

Efficiency and error values here are those from exploratory qRT-PCR performed in Chapter 3. All other assay's efficiency and error values were not wildly different from those presented here and were not outwith the acceptable range.

gene	protein	accession number	forward primer	reverse primer	probe	amplicon (nt)	error	efficiency
Rn18s	18S rRNA	NR_003278.1	ctcaacacgggaaacctcac	cgctccaccaactaagaacg	77	110	0.013	1.750
Tbp	TBP	NM_013684	gggagaatcatggaccagaa	gatgggaattccaggagtca	97	90	0.020	2.067
HPRT	HPRT	NM_013556.2	cctcctcagaccgcttttt	aacctggttcatcatcgctaa	95	91	0.022	1.946
per1	PER1	NM_001159367.1	gcttcgtggacttgacacct	tgctttagatcggcagtggt	71	100	0.037	1.750
per2	PER2	NM_011066	gcttcgtggacttgacacct	tgctttagatcggcagtggt	5	69	0.016	1.784
clock-201	CLOCK	NM_007715.5	ccagtcagttggtccatcatt	tggctcctaactgagctgaaa	76	107	0.015	1.996
cry1	CRY1	NM_007771.3	ggcagagcagtaactgatacga	tgactttcccaccaacttca	52	68	0.011	2.100
cry2	CRY2	NM_009963.4	ggagcatcagcaacacagg	ccgcttggtcagttcttcac	11	67	0.018	1.998
arnt1 var1	BMAL1	NM_001243048	gaatacattgtctcaaccaacactg	ttagctgcgggaaggttg	97	76	0.037	2.082
arnt1 var2	BMAL1	ENSMUST00000106637.1	agtacgcctccccctgat	tgtctggagtccctccattt	79	67	0.007	2.010
Sgk1	SGK1	NM_001161845	gattgccagcaacacctatg	ttgatttgttgagagggacttg	91	129	0.019	1.940
TSC22d3 v2	GILZ	NM_010286.3	tccgttaaactggataacagtgc	tggttcttcacgaggtccat	49	89	0.015	1.700
MR	Nr3c2	NM_001083906	caaaagagccgtggaagg	tttctccgaatcttatcaataatgc	11	78	0.015	1.786
GR	Mr3c1	NM_008173	tgacgtgtggaagctgtaaagt	catttcttccagcacaaaggt	56	78	0.035	1.720
Hsd11b2	11βHSD2	NM_008289.2	cactcgaggggacgtattgt	gcaggggtatggcatgtct	26	60	0.024	1.817
Slc12a3	*NCC*	*NM_019415*	*cctccatcaccaactcacct*	*ccgcccacttgctgtagta*	12	60	0.017	1.945
Oxsr1	OSR-1	NM_133985	tgccttcaaaaggatccaga	tggaaaaatttgtgcctcaac	84	65	0.024	1.846
Stk39	L-SPAK	ENSMUST00000102715	gtacgagctccaggaggttatc	tcttgcctgggtttgcat	27	75	0.014	1.700
Stk39	KS-SPAK	JN368425	ttaccgtcattcctaactttactgc	gaatgcgcttactccaaaatct	18	146	0.039	1.913
Wnk1	WNK1-L	AY309076	cttttgccaagagtgtgataggt	caacggattcatcatatttctcc	92	78	0.024	1.775
Wnk1	WNK1-KS	AY311934 / AY309076	tgctgctgttctcaaaagga	acttcaggaattgctactttgtca	20	77	0.009	1.970
Wnk4	WNK4	NM_175638	tccgatttgatctggatgg	gggcaggatgaactcattgta	26	74	0.026	1.729
Nedd4	NEDD4	NM_010890	acgtgctgttcactgctgat	tcacaactcgtgtgtcatcg	1	60	0.023	1.754
Cab39	MO25-alpha	NM_133781	tgagaaggagcctcagacaga	aaaatttgagccacgtcttttt	17	132	0.016	1.814
Cul3	cullin3	NM_016716.4	agaagggaagaatcctgttgact	gccggtcattattgaaggatt	69	95	0.015	1.978

2.4.2.2. qRT-PCR and Analysis

An 8-point standard curve was prepared by pooling all cDNA samples. The top standard consisted of a pool of all assay samples diluted 1:8 with nuclease-free water, serial dilutions (1:2) were made for standards 2-7 and the final with the last standard left as a blank (just water). The final standard curve consisted of 1:8, 1:16, 1:32, 1:64, 1:128, 1:256, 1:512 and blank. Samples were diluted 1:32, so as to fit in the middle of the standard curve. The standard curve and samples were aliquotted and stored at -20ºC such that only 2 freeze-thaw cycles were required to complete all qRT-PCR analyses. qRT-PCR assays were performed using the probes and primers outlined in Table 2.3.

Each assay was setup in a 10 µl total reaction volume comprising 2 µL cDNA, 0.1 µl of each primer (from a 20 µM stock, Eurofins Scientific), 0.1 µL probe (Universal Probe Library, Roche) and 5 µl MasterMix (PerfeCTa, FastMix® II, Quanta Biosciences) and 2.8 µl nuclease-free water (QIAGEN). Each standard and sample qRT-PCR reaction was assembled on a 384 well plate in triplicate using repeat multichannel pipettors to minimise inter-replicate variability. No template and reverse transcriptase (RT) negative controls were run alongside each assay. Reactions were run on a Roche Lightcycler 480 using the following cycling conditions: 95ºC for 5 minutes, 95ºC for 10 seconds, 60ºC for 30 seconds, repeated for 60 cycles, then 40ºC for 30 seconds. Quantitation was achieved using the automated LightCycler 480 software, which identifies the threshold cycle (Cp) value for each well by finding the maximum value from a plot of second derivative of fluorescence versus time (Figure 2.8). Each triplicate value was analysed and replicates excluded if the Cp standard deviation was >0.5. Results were accepted if the standard curve was adequate, as assessed by efficiency within the range 1.7-2.1 and error <0.5 (i.e. the mean squared error of the data points making up the standard curve).

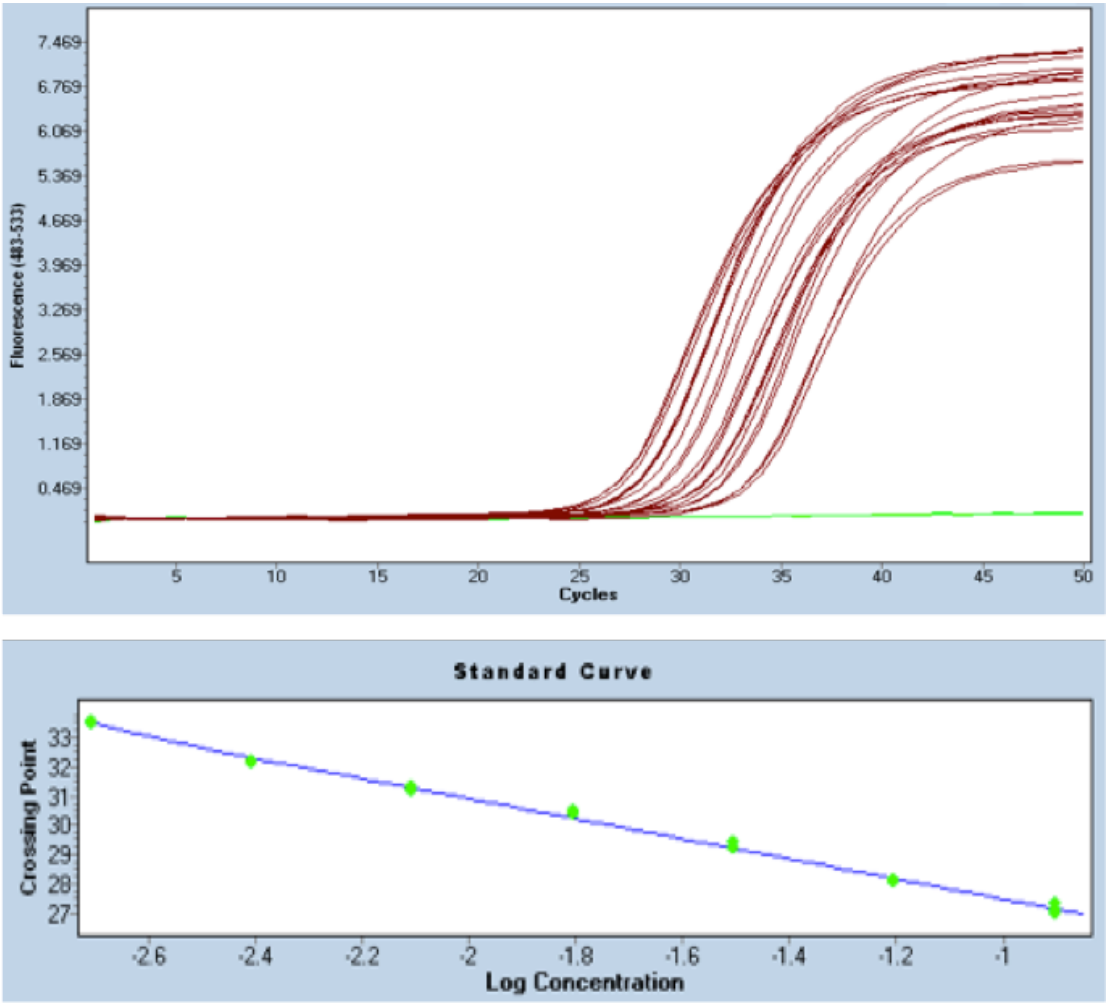

Figure 2.8: Example standard curve for a qPCR assay (TBP)
(A) Plots of florescence intensity versus cycle number for 7 point serial dilutions of pooled cDNA template and no template negative control (green) performed in triplicate. (B) Standard curve constructed from Cp values obtained from A (there are three data points for each concentration).

2.4.2.3. Selection of endogenous control genes

Endogenous control genes were used to normalise the experimental gene values. Following a literature search, a panel of three endogenous control genes was selected to include tat box binding protein (TBP), hypoxanthine-guanine phospho-ribosyltransferase (HPRT) and 18S ribosomal RNA [139] [118] [140]. The expression of these control genes did not differ across any of the experimental groups (Figure 2.9) and CT values were approximately 25-33, 22-28, 7-15 for TBP, HPRT and 18S respectively. Test gene CT values ranged from 22-37. The level of endogenous control genes was normalised such that day/vehicle/sham was equal to 1 (so as not to give greater weight any one of the control genes, this may be particularly important for 18S which has much higher expression than HPRT and TBP) and the mean of all three control-genes was taken. The experimental gene expression was calculated as the

mean level normalised to the mean of the control genes and adjusted so day/vehicle/sham was equal to 1 and log10 transformed to normalise the spread of data.

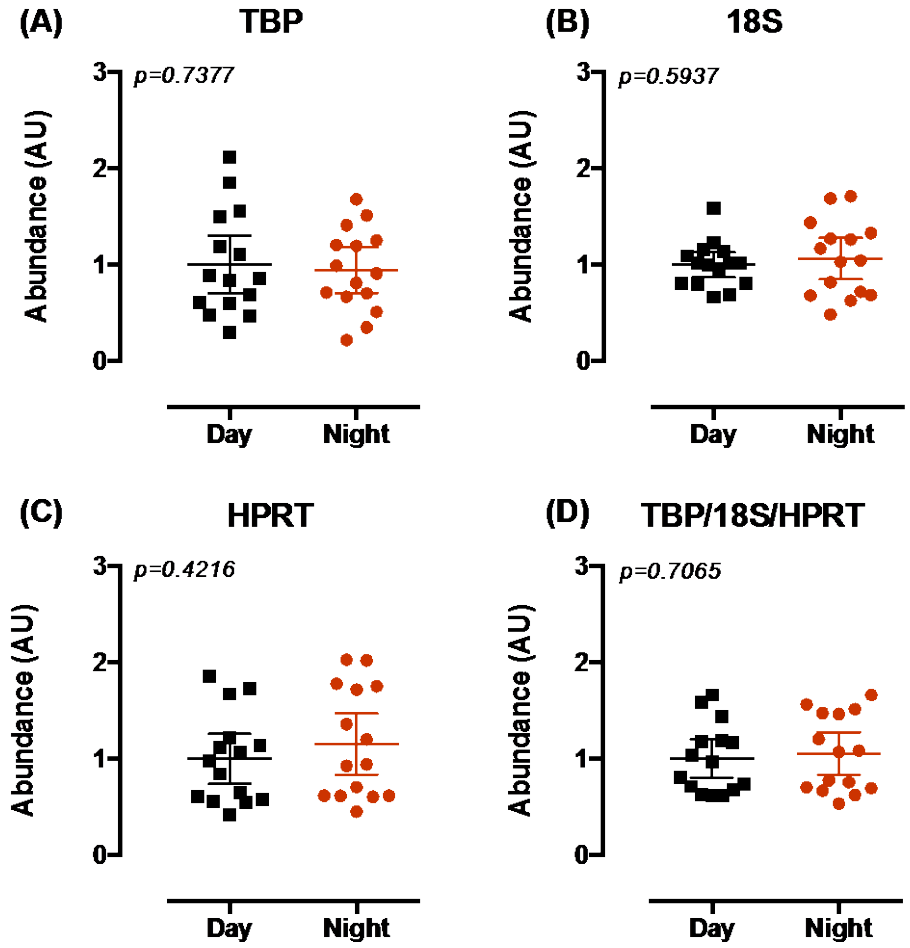

Figure 2.9: Exogenous control genes in C57BL6 mouse kidneys
(A)-(C) Abundance of TBP, 18S and HPRT during the day versus at night adjusted such that day= 1 (D) Mean value obtained for all 3 assays. Each "experimental" gene was expressed relative to this mean abundance of these 3 genes as shown in (D). Data here are from experiments described in chapter 3 and are presented as mean ±95 % CI. P values are from unpaired Student's t tests. No differences were found in any of the endogenous control genes between any of the experimental groups (n=15).

2.5. Metabolic Cage Experiments

2.5.1. Experimental design

This section outlines general methods that apply for all metabolic cage experiments carried out. Metabolic cage protocols for individual experiments are outlined within the brief methods section for chapters 3-5. Mice were single housed in metabolic cages with 12 hour light dark cycling (starting at 7 am). There was a ~10 % loss of body weight in all mice,

which stabilised out after 4-5 days but did not return to pre-experimental body weight. Food intake, water intake, urine output and body weight were measured at least daily.

2.5.2. Gelled diet

To minimise the contamination of urine with food, a gelled diet was used all metabolic cage experiments unless otherwise stated. The mice adapted well to the diet and considerably less was scattered out of the food hoppers compared to standard powdered diets previously used in our lab group. The gelled diet also increased urine flow permitting collection of a urine sample during the day. One sachet of gelatin (Dr Oetker, UK) was dissolved in deionised water (750 ml, heated to ~70ºC). The gelatin-water was thoroughly mixed with powdered RM1 diet (250 g, Special Diet Services) in a zip-lock bag. A hole was made in the bottom of the bag and diet "piped" out into strips and stored at 4ºC for up to 1 week or at -20ºC for up to 1 month. The resulting sodium content was 0.21% dry weight. Approximately 40 g gelled diet was given in double food hoppers daily to allow ad libitum feeding.

2.5.3. Urine Analysis

2.5.3.1. Urinary Electrolyte Analysis by Flame Photometry

A flame photometer (BWB-1, BWB technologies) was used to analyse sodium potassium and calcium levels in urinary samples collected from metabolic cages. Urine was diluted 1:50 with "blank" diluent (BWB technologies). Results in ppm were then converted to molar values and multiplied by urinary flow rate to get μmol/hour(s).

2.5.3.2. Urinary Steroid Analysis by ELISA

Urine was extracted and assayed according to the method developed by Dr Emad Al Dujaili [141, 142]. Briefly, 1800 μl diethyl ether (CROMOSOLV®, Sigma Aldrich) was added to 200 μl urine and very thoroughly vortexed for 15 minutes using a multi vortex. To test the recovery of extraction a sample of known aldosterone/corticosterone concentrations was extracted along with the test samples. Samples were placed in an -80ºC freezer for 15 minutes and top ethyl layer poured off into a clean glass tube (12x75 mm). Samples were desiccated at 50ºC under nitrogen. Samples were reconstituted in 0.5 ml assay buffer (20 ml Blocking buffer (0.5g BSA (Sigma Aldrich) in 100 ml PBS) in 80 ml PBS), thoroughly vortexed and incubated at room temperature for an hour (reconstituted samples could also be vortexed and incubated overnight at 4ºC). Two 96 well ELISA assay plates (medium-bind, Griener Bio-One), 1 for each aldosterone or corticosterone assay, were coated with 200 μl diluted steroid-3-carboxymethyloxime-BSA conjugateor (50 μl conjugate diluted in 20 ml

PBS) and incubated overnight at 4ºC. Plates were washed 3 times with wash buffer 0.05% Tween 20 (Sigma Aldrich) in PBS) and incubated with 190 µl blocking buffer (0.5 g BSA in 100 mL PBS) for 1 hour at 37ºC. The following 5 standards were prepared in assay buffer: aldosterone: 0.01 nM, 0.1 nM, 1 nM, 10 nM, 100 nM and corticosterone: 0.2, 1, 4, 20, 100 ng/ml (0.6, 2.9, 11.5, 57.7, 288.6 nM) and 50 µl of each standard and sample was loaded onto the plate. Antibodies were produced in house and described in [141], [142]. 100 µl diluted antibody (corticosterone antibody: 60 µl antibody +12 mLs assay buffer or aldosterone antibody: 40 µl + 12 ml assay buffer) was added to each well and the plates incubated in the dark at room temperature for 2 hours.

Plates were washed four times and 100 µl HRP-goat anti-rabbit IgG enzyme conjugate (Upstate, 10 µl in 11 ml for corticosterone) or HRP – Donkey-anti-sheep IgG enzyme conjugate (produced in-house, 10 µl in 11 ml for aldosterone) added to each well and incubated in the dark at room temperature for 1 hour. 100 µl substrate (11 ml 0.2 M sodium acetate/citrate buffer pH to 4.2 with sodium citrate, 0.300 ml 10 mg/ml tetramethylbenzadine in DMSO and 0.060 ml hydrogen peroxide) was added to each well and incubated for 15 minutes. 50 µl stop solution (2 M sulphuric acid in water) was added to each well and plate read at 450 nm (MRX plate reader, Dynex). Results were extrapolated from a standard curve using a third order polynomial (Figure 2.6) and multiplied by 5 to get ng/ml. The aldosterone samples were just within the limit of detection but a detectable reduction in urinary aldosterone excretion following high salt diet was observed (Figure 2.10).

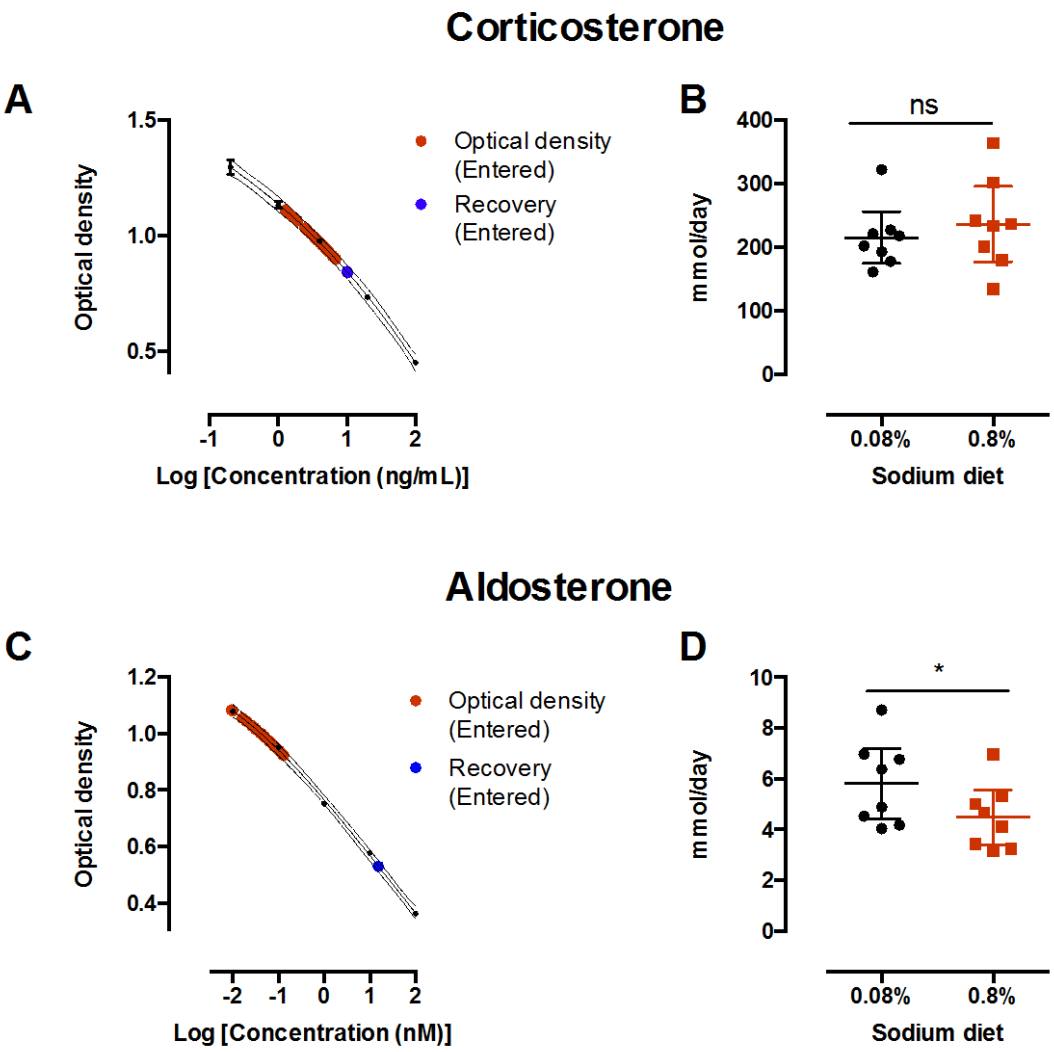

Figure 2.10: Representative examples of cubic polynormial curves obtained from corticosterone (A) and aldosterone (C) assays, along with validation experiment results, showing the assay is capable of detecting a difference in aldosterone levels following a high salt diet (D), while corticosterone level remains unchanged (B).
Data is mean ±95 % CI (A-D). Red circles (A&D) are the sample values and blue circles (A&D) are spiked samples to test recovery of extraction process. *p<0.05 by paired Student's t tests, n=8.

2.6. BP measurements by Radiotelemetry

Radiotelemetry allows the remote, real-time analysis of BP, HR and activity in conscious, unrestrained mice and is the gold standard approach for cardiovascular physiology in rodents.

2.6.1. Device calibration and setup

Miniature radio telemeter devices PA-C10 (Data Science International) were electronically coupled with their receiver pads and assigned to a mouse. The offset of each device was tested and recorded (this was in the range of -2 to +2 mmHg). All details of the mouse, devices and offset could be recorded using the DSI software accompanying the devices.

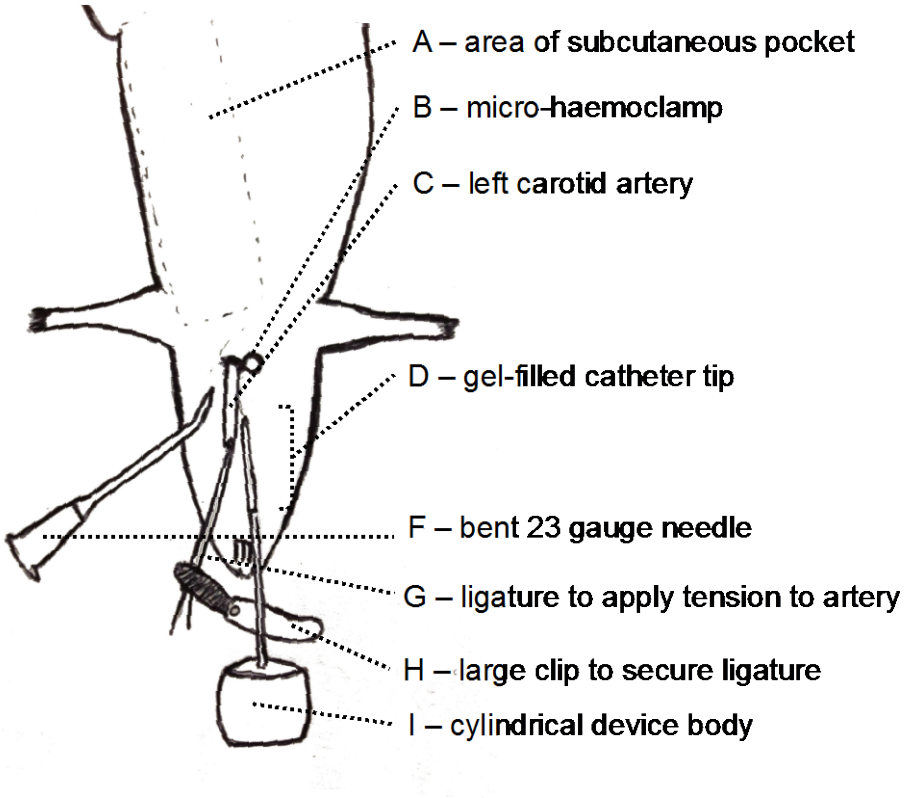

Figure 2.11: Diagram of components and set up of telemetry surgery
(The incision and loose ligature are not shown for clarity)

2.6.2. Telemetry implant surgery

All surgical work was carried out using aseptic technique [143]. To minimise stress caused by single housing, mice were single housed for a week prior to surgery in order to build a nest and acclimatise to single housing and conditions in the telemetry suite. Anaesthesia was achieved using isofluorane in oxygen, with initial induction at 3 % reduced to 1-2 % to maintain unconsciousness. The isofluorane delivery tubing was tapered using a 5mL syringe with the plunger removed, which fit snugly around the mouse's face. Buprenorphine (Vetergesic®) at a dose of 0.1 mg/kg was given subcutaneously along with a 1 mL bolus injection of 0.9 % sterile saline. Ocular lubricant (Lacri-lube®) was applied to the animal's eyes to prevent them drying out during the procedure. The mouse was then positioned in dorsal recumbency and the ventral neck area was shaved and bathed in iodine scrub (Vetersept®). A ventral cervical skin incision was made and a subcutaneous pocket was made down the left flank of the animal (Figure 2.11 A). Blunt dissection was utilised to isolate the carotid artery (Figure 2.11, C) and separate it from the vagus nerve gently, ensuring the nerve was not disturbed. A tight double-knotted ligature was applied to the anterior end of the carotid artery (Figure 2.11, G) and loose ends secured with a large haemoclip (Figure 2.11, H) to produce light tension on the artery. A loose ligature was applied to the carotid artery and postural end was occluded with a micro-haemoclamp (Figure 2.11 B, Microserrefine, FST). A bent 23 gauge blue (Figure 2.11 F, BD Microlance, FST) needle was used to make an incision in the artery and to gently hold it open. The device catheter (Figure 2.11 D, Data Sciences International) was fed gently into the carotid artery using vessel cannulation forceps and secured by tightening the loose ligature around it. The antithrombotic, gel-filled tip was extremely delicate and care was taken to avoid crushing it. A radio was used to gauge the level of interference caused by gripping the catheter and upon opening of the postural occlusion a pulsing sound was heard over the radio if the catheter was still patent.

The micro-haemoclamp was gently removed from the postural end of the artery and the catheter fed in until resistance was felt (approximately 1-2 mm before the joint between the gel-filled segment and rest of the fluid filled portion of the catheter). Both anterior and initial securing ligatures were double knotted and tissue adhesive (3M^{TM} VetBond^{TM}) was applied to the knots. The device body was then fed into the pre-made subcutaneous pocket, this could be aided by wetting the pocket with <1 ml saline, and the wound was closed with 3-5 silk sutures (size 5.0, non absorbable, Vicryl). Tissue adhesive was used to seal the wound and oxygen was fed through the nose cone for 3-5 minutes until consciousness was regained. The mouse was allowed to recover in a hot box (34^{o}C) until full mobility was regained (<30

minutes) after which it was returned to its cage and allowed *ad libitum* access to vetergesic-laced jelly (0.02 mg/ml buprenorphine in 45 ml water, 2 cubes jelly (Hartley's, UK)) and mash (RM1 pellets soaked for >1 hour to overnight in drinking water). Body weight, wound healing and general activity were monitored for 5 days and accounting for device weight, body weight usually matched pre-operative levels within this time.

2.6.3. `Collection and analysis of telemetry data

The transmitter device was set to record once every half hour over a period of 1 minute. How the telemetry data are presented is outlined in each specific results chapter. Common to both chapters is the use of a cosinor analysis, the details of which are outlined here. Cosinor analysis is suited for analysis of rhythmic variables calculating midline estimating statistic of rhythm (MESOR), rather than the arithmetic mean as the central tendency. This rhythm adjusted mean (also known as the time-structured mean or chronome adjusted mean) is a more accurate estimation of central tendency than the arithmetic mean particularly in instances where the data is not equidistant – for example if there are missing data points. The cosinor analysis also calculates period, amplitude and acrophase (Figure 2.12). The period is the time taken for a full cycle, or the time from one peak to the next. The amplitude is the distance between the MESOR and the peak or half of the full extent of the oscillation. Acrophase is the time at which the peak occurs. The movement of the acrophase can give an estimate of any shifts in "phase" that is any movements in time of the wave. Finally "robustness" or prominence, which is the strength and endurance of a rhythm, is a measure of signal-to-noise ratio. Levels below 20 % are likely biological noise [144]. Mathematically robustness/prominence is calculated as the percentage of the variance accounted for by the cosinor model. Statistical significance of the goodness of fit did not exceed $p<0.000001$ for each analysis and was corrected for multiple tests (with 5 periods used for each analysis). The data was first smoothed using a moving average over 5 hours; this improved the "robustness" of the cosinor fit. The smoothed data for each individual mouse for each of the 5-day bins was fitted to a cosinor curve using software designed by Refinetti et al (available at: www.circadian.org), which fits the data by the least squares method [144]). Acrophase data was plotted on a polar diagram using Grapher 2.1 software (Apple Inc).

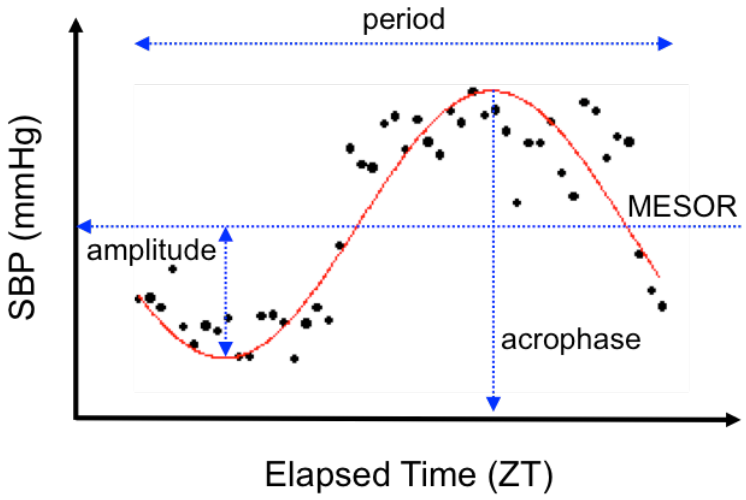

Figure 2.12: Cosinor fit of an example baseline data set in order to visualise how period, amplitude, MESOR and acrophase are acquired from a cosinor curve fit.

2.7. Manipulation of Plasma Corticosteroids

2.7.1. Bilateral Adrenalectomy Surgery

Mice were anaesthetised under isofluorane (as previous) without a nose-cone adaptation. Buprenorphine (Vetergesic® 0.1 mg/kg) and 0.3 ml of 0.9 % sterile saline was administered subcutaneously. Mice were positioned in lateral recumbency and an area just caudal to the rib cage and just ventral to the spine on both sides was shaved with hair clippers. Just prior to incision the area was scrubbed with iodine solution (Vetersept®) and a small 10-15 mm transverse skin incision made just beneath the ribs. A smaller incision was made in the abdominal wall just caudal to the last rib and adrenal gland located near the anterior pole of each kidney using 7 cm curved serrated forceps (Fine Science Tools, 11065-07). On the left side the spleen was gently moved laterally and on the right side the liver was gently held cranially to expose the adrenal gland. Once exposed a second pair of curved forceps was positioned underneath the adrenal gland and peri-adrenal fat and both were gently exteriorised while using the other forceps to tease the connective tissue, fat and blood vessels apart from the adrenal gland beneath the curved forceps. No haemostasis was necessary here as any bleeding from the adrenal blood vessels was minimal. Extra care was taken not to grasp the adrenal gland itself as this can cause it to tear and leave functioning residue within the peritoneum. The abdominal muscle was closed using a single silk suture (size 5.0, non absorbable, Vicryl) and skin closed using three Michel suture clips (7.5 x 1.75 mm, Fine Science Tools). The other adrenal gland was removed in the same way and the mice allowed to recover in a hot box (34^{o}C) until full mobility was regained (this took <30 minutes) after which they were singly housed to prevent fighting, which may lead to greater chance of

sudden death in ADX animals. Mice had access to vetergesic-laced jelly and mash (as previous) as well as ad lib access to 0.9 % saline and tap water to maintain electrolyte homeostasis. Body weight, wound healing and general activity were monitored for 3 days post-operatively and body weight usually matched pre-operative levels within this time.

2.7.2. Corticosterone Pellet experiments

2.7.2.1. Pellet preparation

Corticosterone silastic slow-release pellets were prepared for implantation in mice in order to inhibit their existing rhythm of plasma corticosterone. Corticosterone (1 g, Sigma, UK) and Silastic® (1.8 g, Silastic® F RTV rubber base, Dow Corning) were mixed together into a uniform paste in a weigh boat and curing agent (0.01 g, Silastic® F RTV curing agent, Dow Corning) added in a drop-wise fashion on a fine balance and mixed into the paste. The mixture was then aspirated into a 1 ml syringe. To remove bubbles from the mixture, the syringe was trimmed and inserted into a 15 ml falcon tube and centrifuged at 800 g for 10 minutes to remove the bubbles. The mixture was incubated in the syringe and falcon tube at 37^{o}C overnight to set. The pellet was cut out of the syringe and it's length: weight ratio calculated in order to work out the length of a 25 mg slice. The vehicle pellet was produced in the same way excluding the corticosterone and cut to the same length. This is a rough estimate of the release rate estimated by quantifying the level of corticosterone present by its UV absorption. The release rate of the pellet is estimated to be 3.67 mg/kg/day and is steady over 4 weeks. This was calculated by soaking a 25 mg pellet in a sealed glass flask of 27 ml of PBS at 37^{o}C for up to 6 weeks (Figure 2.13) and analysing 200 μl sample from it weekly. The 200 μl sample was loaded into a microcuvette (10 mm Lightpath precision cell, Hellma) and measured at 240 nm on a UV machine (UV-1201 spectrophotometer, Shimadzu) and returned to the glass flask. Microcuvettes were rinsed with methanol between sample applications and air-dried. These data were plotted with reference to a 100 μm corticosterone standard. The change in corticosterone concentration was worked out to be approximately 10 μM/day, which converts to a release rate of 0.1 mg/day thus giving a dose of around 3.7 mg/kg/day (assuming a 30 g mouse, all experimental C57Bl6/J mice were within range 27-32 g). The range of release rate values was between 3 mg/kg/day and 4.33 mg/kg/day (for 5 pellets). The release rate appeared to taper off towards the end, this may be as a result of reaching the limit of detection with this setup. It was unlikely that all the corticosterone had leached from the pellet, as only 2.8 mg out of 25 mg was detected. Furthermore plasma samples taken at day 21 show flat lining of corticosterone levels, which is consistent with release rate still being constant.

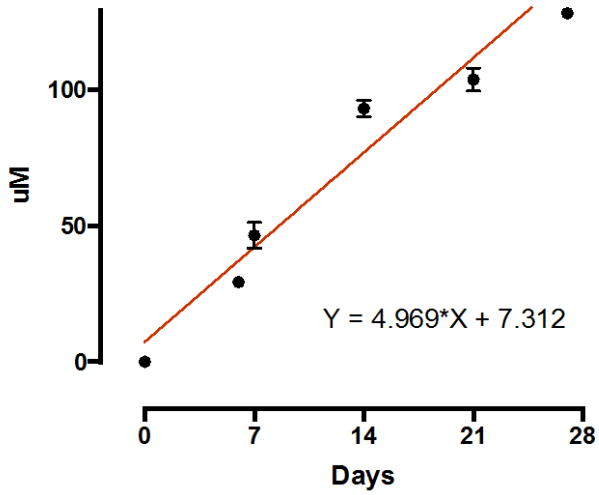

Figure 2.13: Release rate of corticosterone pellets over 4 weeks *in vitro*
Data presented is mean ±95% CI and n= 5.

2.7.2.2. Pellet implantation surgery

Mice were anaesthetised under isofluorane using a 5 ml syringe nose-cone adaptation, given buprenorphine (Vetergesic ®) and positioned in ventral recumbency. Hair was removed from the dorsal cervical area and scrubbed with iodine (Vetersept®). A small ~5 mm transverse dorsal cervical incision was made and a subcutaneous pocket made down the midline into which the Silastic® pellet was implanted. The wound was closed with a Michel suture clip (7.5 x 1.75 mm, Fine Science Tools). Mice regained consciousness in a hotbox (as previous) within 5 minutes and were returned to their home cages.

2.7.3. Plasma corticosterone measurements

2.7.3.1. Tail venesection

Tail vessel micro sampling was performed just after the lights came on, ~ 7 am and just before lights out at ~ 6.45 pm, unless otherwise stated. Mice were removed from their home cages and placed on top of an empty cage. While securing the mouse by the tail <1 mm was snipped off the using sharp sterile scissors. The mouse was minimally restrained by the tail and allowed to explore the cage surface while the tail was gently massaged from base to tip until ~20 µl of blood was collected into a 300ul EDTA coated tube (Microvette CB 300 EDTA, Sarstedt). Blood was collected within 1 minute of the mouse's removal from its cage and placed on wet ice. The second sample was taken by gently nicking the scab from the tail wound and collected as before. Blood samples were centrifuged at 10 000 rpm for 5 minutes and plasma removed using gel-loading pipette tips and stored at -80ºC.

2.7.3.2. Plasma sampling post mortem

A larger sample of blood could be taken post mortem by cardiocentesis. This was performed by roughly excising the ribcage to expose the heart and while holding the apex of the heart with 7 cm forceps a bent 23 gauge needle (attached to a 1 ml syringe rinsed with heparin saline (20units/L porcine heparin saline, Sigma Aldrich) was inserted into the right ventricle and blood very gently aspirated to prevent the ventricle heart collapsing.

2.7.3.3. Plasma Corticosterone Assay

Plasma corticosterone was measured using a commercially available corticosterone EIA kit (Enzo Life Sciences). All reagents were provided in the kit. Plasma corticosterone was extracted from plasma samples by incubating 10 µl of sample 10 µl of steroid displacement reagent (SDR: diluted 1:100 with assay buffer 15 (AB15)) for 5 minutes at room temperature (RT^{o}) in sterile glass tubes. AB15 (280 µl) was then added along with 3 ml ethyl acetate (Sigma Aldrich) and the glass tube was vortexed thoroughly, incubated (RT^{o}, 2 minutes) and vortexed again. The clear organic upper layer was aspirated to a new glass tube. The samples were desiccated under nitrogen at 60^{o}C. Standards and samples were prepared in duplicate and assayed according to the manufacturer's instructions. Absorbance measurements (405 nm and corrected with 580 nm) were plotted against the known standard values using GraphPad software and the r2 value for the sigmoidal curve produced was >0.98 and the concentrations of the unknown samples were interpolated onto the line.

2.8. Estimation of NCC activity in anaesthetised animals by renal clearance

Renal clearance experiments enabled the measurement of mean arterial BP and the estimation of renal haemodynamic parameters

2.8.1. Surgical protocol

General anaesthesia was induced by intra-peritoneal injection of 100 mg/kg thiopentalbarbitol (Inactin®, Sigma). Small bolus doses of anaesthetic (50 mg/kg) were applied judiciously during surgery to maintain unconsciousness (as assessed by blink or toe pinch reflexes) but minimise cardiovascular suppression. Unconscious mice were kept in dorsal recumbency on a heated pad to conserve body heat during the surgery. Ligatures were made with size 5 suture silk (Fine Science Tools) and lidocaine-HCl (1 % w/w in 0.9 % saline, Sigma Aldrich) was used to provide local anaesthetic and maintain tissue moisture during surgery.

2.8.1.1. Tracheostomy

In order to maintain a clear airway throughout the surgery a tracheostomy was performed. A ventral cervical skin incision was made and the muscles immediately beneath were dissected to expose the trachea. An incision was made between the tracheal cartilage rings and a tracheostomy tube, contrived from a 1 cm piece of P90 tubing (Smith's medical) was inserted and secured.

2.8.1.2. Jugular Vein cannula

In order to administer infusate, anaesthetic and drugs during renal clearance experiments, the jugular vein was cannulated. The left jugular vein was exposed and perivascular fat gently removed with fine forceps. The anterior end of the exposed vein was ligated and light tension was applied to elevate the vein. A small incision was made just postural to the ligature and a piece of P10 (Smiths medical) tubing containing 0.9 % saline connected to a 1 mL syringe, was inserted and secured with a second ligature.

2.8.1.3. Carotid Artery Cannula

For continuous blood pressure monitoring and blood collection, the carotid artery was cannulated. The carotid artery was exposed between the tracheal muscle and salivary gland and gently isolated from the adjacent vagus nerve. The carotid was tightly ligated at the anterior end and tension applied to elevate the artery. The posterior end was ligated to prevent blood loss. A small incision between the ligatures was made and P10 tubing containing 20units/L porcine heparin saline (Sigma Aldrich) attached to a 1 mL syringe was inserted and secured with a third ligature. The anterior ligature was carefully untied to restore blood flow and the cannula was advanced further into the carotid and firmly secured.

2.8.1.4. Bladder Catheter

The bladder was catheterised for urine collections. The catheter tube was fashioned from a ~1 cm length of P50 (Smiths medical) into which a ~10 cm length of P10 tubing was inserted to minimise the dead space. A lower abdominal incision was made, the bladder located and gently lifted out through an incision in the peritoneum. A hole was made in the bladder using a 23 gauge blue needle (BD Microlance) and the catheter was inserted and secured with surgical suture.

2.8.2. Renal Clearance protocol

The particular renal clearance protocols used in each experiment are presented in the in-chapter methods. Presented here is a general outline of procedures common to all protocols. Once surgery was completed a bolus of 0.1 ml/10gbw I.V. infusate (in mM: NaCl 100, KCl 5, $NaHCO_3$- 15, sodium para amino-hippurate (PAH, Sigma Aldrich) 25, and 0.25 % FITC-inulin (Sigma Aldrich), pH to 7.4 by bubbling with CO2) was administered to hasten equilibration and replace fluid losses during surgery. The venous cannula was connected to an infusion pump (AL2000, World Precision Instruments) for administration of infusate at a constant rate of 0.2 ml/10gbw/hour. The carotid cannula was connected to a ML224 Bridge Amp (AD Instruments) for continuous monitoring of arterial blood pressure through PowerLab data acquisition software. An equilibration period of 1 hour was allowed before any experimental collections. During all protocols 20 µl blood samples were taken prior and post urine collection and a final large terminal blood sample was taken via the carotid artery. These were collected into Lithium-heparinised capillary tubes or 500 µl Li-heparinised tubes (Microvette CB 300 LH, Sarstedt). Urine samples were collected into pre-weighed 500 µl eppendorf tubes containing mineral oil to prevent sample evaporation. Bolus injections of thiazides or vehicle were administered via the jugular vein cannula and the animal was euthanized via cervical dislocation following the final blood collection.

2.8.3. Sample Analysis

2.8.3.1. FITC-Inulin Assay

FITC-inulin is freely filtered at the glomerulus but is neither secreted nor reabsorbed along the nephron, therefore its clearance gives a very accurate measurement of the glomerular filtration rate (GFR). The FITC fluorescence was measured in samples of urine and plasma. Briefly, urine and plasma samples were diluted 1:10000 and 1:100 respectively in HEPES buffer (as the fluorescence reaction is pH dependent). A five point 2 fold dilution series was performed for FITC standard curve with 1 mg/ml as top standard. These were diluted 1:100 in HEPES buffer. 190 µl of samples and standards were loaded in duplicate into Microfluor black 96 well plates (Thermoscientific). The plate was then read on a microplate reader (infinite M1000, TECAN) with samples excited at 485 nm and read at 538 nm. GFR could then be calculated:

GFR (clearance of inulin) = (Urinary[inulin] x Urinary flow rate)/ Plasma [inulin]

2.8.3.2. PAH Assay

In order to calculate renal blood flow (RBF), plasma and urinary para amino-hippurate (PAH) was measured. Effective renal plasma flow was calculated on the assumption of complete extraction of PAH from plasma into the urine [145, 146]. In brief, standards were prepared in serial dilution using water with 0.2 $mg.ml^{-1}$ as the top standard. Plasma and urine samples were diluted in 3.2 % trichloroacetic acid (TCA, Sigma Aldrich). Plasma was vortexed and incubated for 5 minutes at room temperature, this step was repeated before centrifugation at 10 000 g for 3minutes to pellet and remove the plasma protein. Mix A (40 µl 0.2 N HCl and 20 µl 0.1 % $NaNO_2$) was added to the all the samples/standards, vortexed and incubated (RT^o, 5 minutes). Mix B (20 µL 0.5% $NH_2S0_3NH_4$ and 20 µl 0.1% N-(1-naphthyl)-ethylenediamine dihydrochloride) was added to the samples/standards, followed by a thorough vortex and incubation (RT^o, 40mins). 200 µl was transferred into a clear 96 well plate in duplicate. The absorbance was measured at 535 nm on a Victor plate reader (Perkin). Renal plasma flow (RPF) could then be calculated:

RPF (clearance of PAH) = (Urinary [PAH] x Urinary flow rate)/ plasma [PAH]

RPF was converted to RBF by adjusting for the cellular fraction using the haematocrit values.

2.8.3.3. Electrolyte Analysis

An electrolyte analyser (Roche, UK) was used to measure plasma and urinary sodium, according to the manufacturer's guidelines. Urine was first diluted 1:5 with dH_2O and in turn this was diluted again with 2:3 parts 120 mM NaCl. Plasma samples were run undiluted. In order to account for any inter-animal changes in renal haemodynamics the fractional sodium excretion was calculated to assess tubular sodium reabsorption:

FENa = (Urinary sodium x Urinary flow rate)/ (Plasma sodium x GFR) x100)

2.9. Quantifying HCTZ by liquid chromatography-tandem mass spectroscopy (LCMS)

The method for quantification of urinary and plasma HCTZ was developed by Dr Robert Hunter and Dr Natalie Homer [147]. The Clinical Research Facility carried out all analyses. 20 µl plasma or urine was spiked with 20ng trichlorothiazide (TCTZ), which acted as an internal standard to correct for variations in HCTZ extraction efficiency. Samples were extracted with 200 µl ethyl acetate through agitation for 30 minutes and room temperature. The organic phase was desiccated to dryness at 40^oC under nitrogen and reconstituted in 100

μl 5% acetonitrile and 95 % 0.5mM ammonium acetate. LCMS was performed using an Aria-Quantum CTC Turboflow autosampler and HPLC system (Thermo Fisher) used with a TSQ Quantum Discovery triple-quadropole mass spectrometer. A T3 Atlantis (100 x 2.1mm, 3.5 μm, Waters, Manchester) HPLC column was used for quantitation with a flow rate of 0.3 ml/min at 40^{o}C with a mobile phase of 5mM ammonium acetate and 0.1 % formic acid in methanol. The mass spectrometer was operated in negative ion electrospray ionisation mode with 3-kv spray voltage, 60/5 sheath and auxiliary nitrogen gas and 1.5- mTorr argon collision gas. Results for each sample were compared to a pre-determined standard curve ranging from 10 – 5000 ng.

2.10. Data analysis and statistics

All data are presented and analysed using GraphPad Prism software version 6.0. Data are presented as mean ±95% confidence interval (CI). The number of biological replicates (n) for each experimental group is given in the figure legends along with the test used for statistical analysis. As two-way ANOVAs are used frequently in this work, these will be described in greater detail here. Two-way ANOVAs were used when analysing differences between groups that have been split by two independent variables, most commonly used in this thesis a treatment, such as adrenalectomy and a time point, such as day or night. The output for these tests, given in boxes within the figures, gives the p values for each of these independent variables as well as the "interaction" and "matching" (where appropriate). The interaction effect tests the null hypothesis that any differences within the first independent variable (eg. time of day) are the same for each group within the second independent variable (eg. adrenalectomy or adrenal intact). Repeated measures two-way ANOVA is used if the data are matched, for example if it is the same mouse that is treated with HCTZ it's BP will be "matched" for before and after treatment. Where "matching" has been effective for controlling experimental variability this is marked as significant. Sidak tests were employed for post hoc analysis. This test gives high power (thus preventing false negatives), while still being stringent in adjusting the family-wise error rate in order to counteract the problem of false positives following multiple comparisons.

3. Diurnal rhythm of NCC phosphorylation

3.1. Introduction

In the kidney 13% of genes exhibit a circadian profile of expression [43]. This does not include NCC (*slc12a3*) expression [42, 43]. However, as explored in chapter 1, NCC activity is regulated predominantly through posttranslational modifications, such as phosphorylation and ubiquitinylation. Therefore the primary purpose of this chapter is to investigate temporal variation in NCC phosphorylation.

3.1.1. Aims

1. Confirm the presence of a circadian rhythm of behaviour, BP, urinary excretion in normal C57BL6 mice under controlled 12-hour light and dark conditions.
2. Determine whether there is any difference in NCC phosphorylation during the active phase (night) compared to the inactive phase (day) in C57BL6 mice.
3. Explore potential mechanisms that may contribute to any such difference in activity.

3.1.2. Strategy for addressing the chapter aims:

1. The rhythms of urinary excretion, feeding and drinking behaviour were determined in conscious C57BL6 mice using metabolic cages. Radiotelemetry in conscious unrestrained C57BL6 mice was employed to define the rhythms of BP, activity and heart rate.
2. NCC phosphorylation status was measured by probing whole kidney homogenate with phospho-antibodies. Tissue was collected when day:night BP differences were maximal i.e. between peak and nadir.
3. Potential mechanisms for the rhythmic regulation of NCC were investigated by exploring the diurnal rhythms present in candidate genes and hormonal systems that could regulate NCC phosphorylation. This was further probed by defining the localisation of MR, GR and 11βHSD2 by immunohistochemistry.

3.2. Methods

Detailed methods of each of the procedures in this chapter are outlined in the main methods section, however for clarity, an outline of the experiments carried out and cohorts of mice used are presented here.

3.2.1. Metabolic cage experiment

Male C57BL6 mice (n=10) were housed in metabolic cages with a 12-hour light/dark cycle and allowed to acclimatize for 5days (See Methods 2.5). Food and water intake was measured and urine collected for 12-hour periods over 3 consecutive days (ZT0-12 “Day” and ZT12-0 “Night”).

3.2.2. Telemetry

Male C57BL6 mice (n=4) were implanted with radiotelemetry devices (PA C10, DSI). The mice were housed in a room with a 12-hour light/dark cycle with *ad libitum* access to standard RM1 diet and tap water. After 5 days postoperative recovery, recordings were taken every 30 minutes for 1 minute. The baseline data presented here is the mean at each half hour time point, averaged over 5 consecutive days and smoothed using a rolling average over 5 consecutive data points. Each 5-day data set for each mouse was fitted to a cosinor curve (See Methods 2.6).

3.2.3. Timed Culls

In order to assess NCC phosphorylation at night versus day, timed culls were performed. Two time points were selected. The rationale for selecting these time points was to remove the kidney during steady-state blood pressure at both peak and nadir, reasoning that the transporter activity may be at its highest and lowest at these time points. Kidneys underwent western analysis and RT qPCR (see Methods 2.3 & 2.4 respectively).

3.2.4. Plasma corticosterone sampling

The circadian rhythm of corticosterone was compiled using plasma samples collected from 5 separate groups of male mice; each group was housed under the conditions previously described (Methods 2.1). Terminal plasma samples were taken at cull at ZT 6 and ZT 18 in 3 separate cohorts (n=22). Plasma was also taken by tail venesection in 2 groups of conscious mice, one group (n=4) was sampled from at ZT0 and ZT12 and another group (n=10) was sampled from at ZT6 and ZT18 so as to be comparable with the terminal samples. Plasma was analysed by EIA (see Methods 2.7.3).

3.2.5. Perfusion Fixation

Male C57BL6 mice (n=3) were perfusion fixed between 8am-4pm and kidneys excised for analysis (see Methods 2.2).

3.3. Results

3.3.1. Diurnal rhythm of food and water intake

Consistent with literature reports [148], food and water intake exhibit a strong diurnal rhythm, with more consumed during the 12 hour night period (ZT12- ZT0) than during the 12 hour day period (ZT0- ZT12) (Figure 3.1).

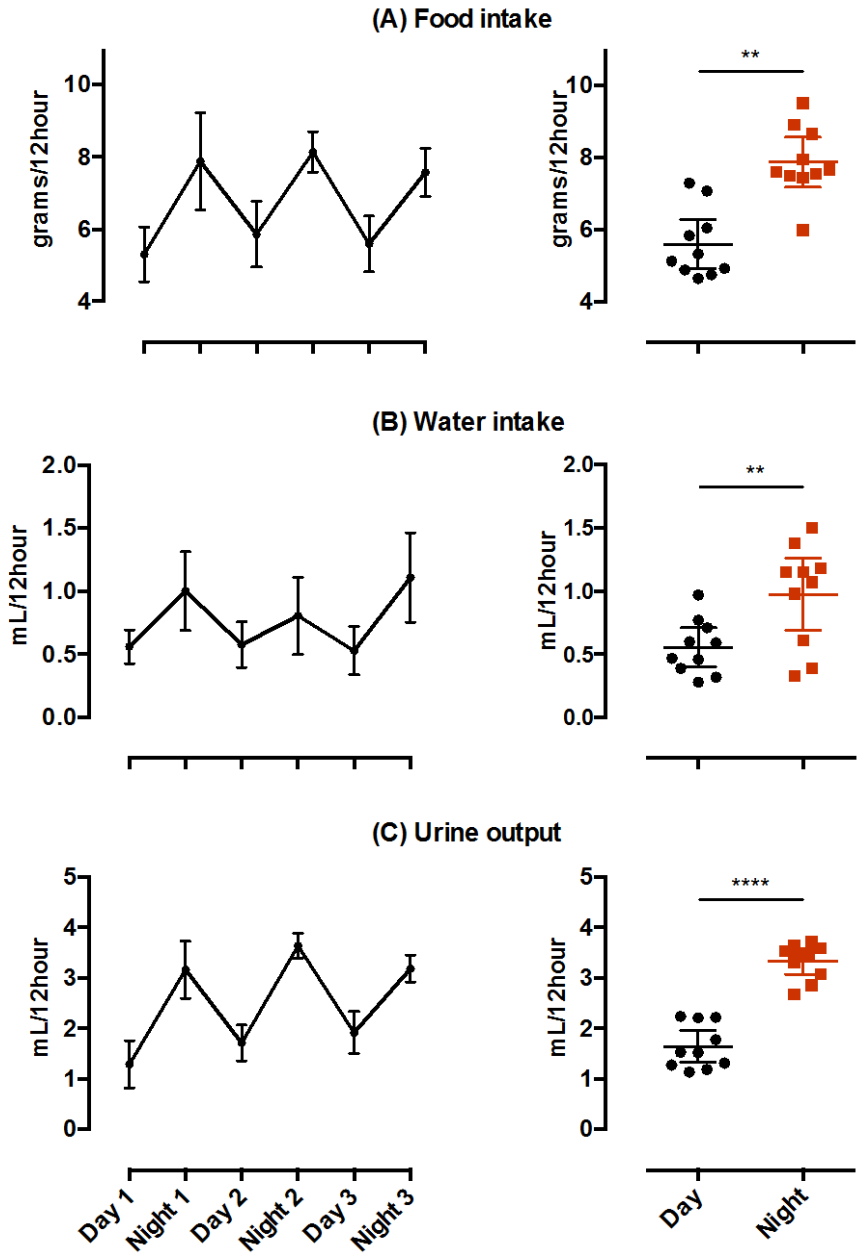

Figure 3.1: Food (A) and water intake (B) and urine output (C) in C57Bl6 mice over 12-hour day and 12-hour night.
Water intake is that drank, with water in the gelled diet included in the food intake. Data are mean±95% CI. Data were analysed by paired Student's t-tests,****p<0.0001 **p<0.01 (n=10).

3.3.2. Diurnal rhythm of electrolyte excretion

As shown in Figure 3.2, sodium and potassium excretion was markedly increased at nighttime (ZT12-ZT0) compared to the daytime (ZT0- ZT12).

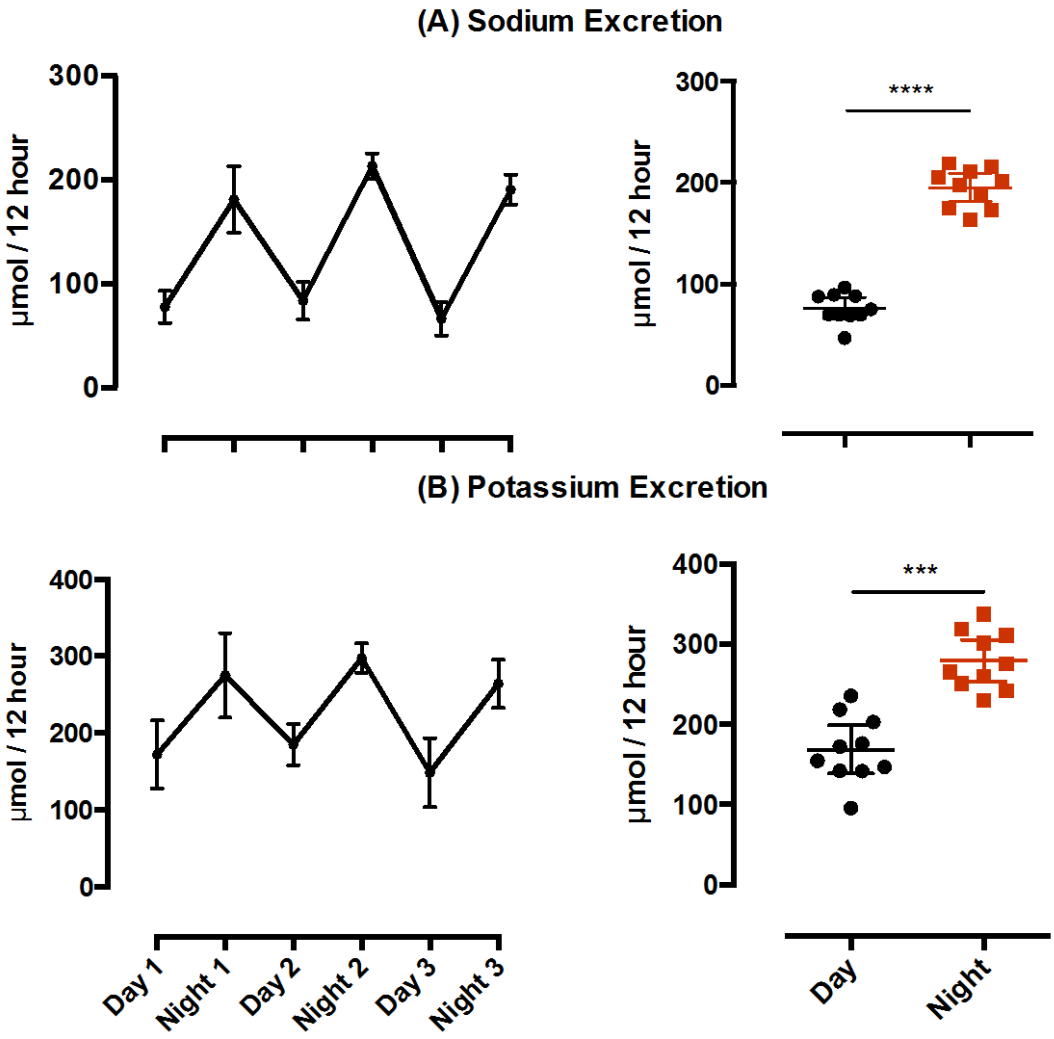

Figure 3.2: Urinary sodium (A) and potassium (B) in C57Bl6 mice.
Urine was collected 12 hourly between ZT0 and ZT12 and electrolyte concentrations measured by flame photometry. Data are mean±95% CI. Data were analysed by paired Student's t tests where ****p<0.0001, ***p<0.001 (n=10).

3.3.3. Diurnal rhythm of BP, heart rate (HR) and activity in C57BL6 mice

As shown in Figure 3.3 systolic blood pressure (SBP) and diastolic blood pressure (DBP), HR and activity were all increased at night (ZT12-0) compared to the day (ZT0-12). The mean period for SBP was 23.9 ±0.22 (95% CI) and the acrophase was roughly ~ ZT 18h10 ±0h47 (Table 3.1). Robustness is a measure of rhythmicity, or how well the data fit a cosinor waveform. Values of >20% are above noise-level and exhibit significant rhythmicity. SBP, DBP and activity exhibited significant rhythmicity, with robustness values exceeding 20%. However, HR was below threshold (at 12.5%) with high noise levels.

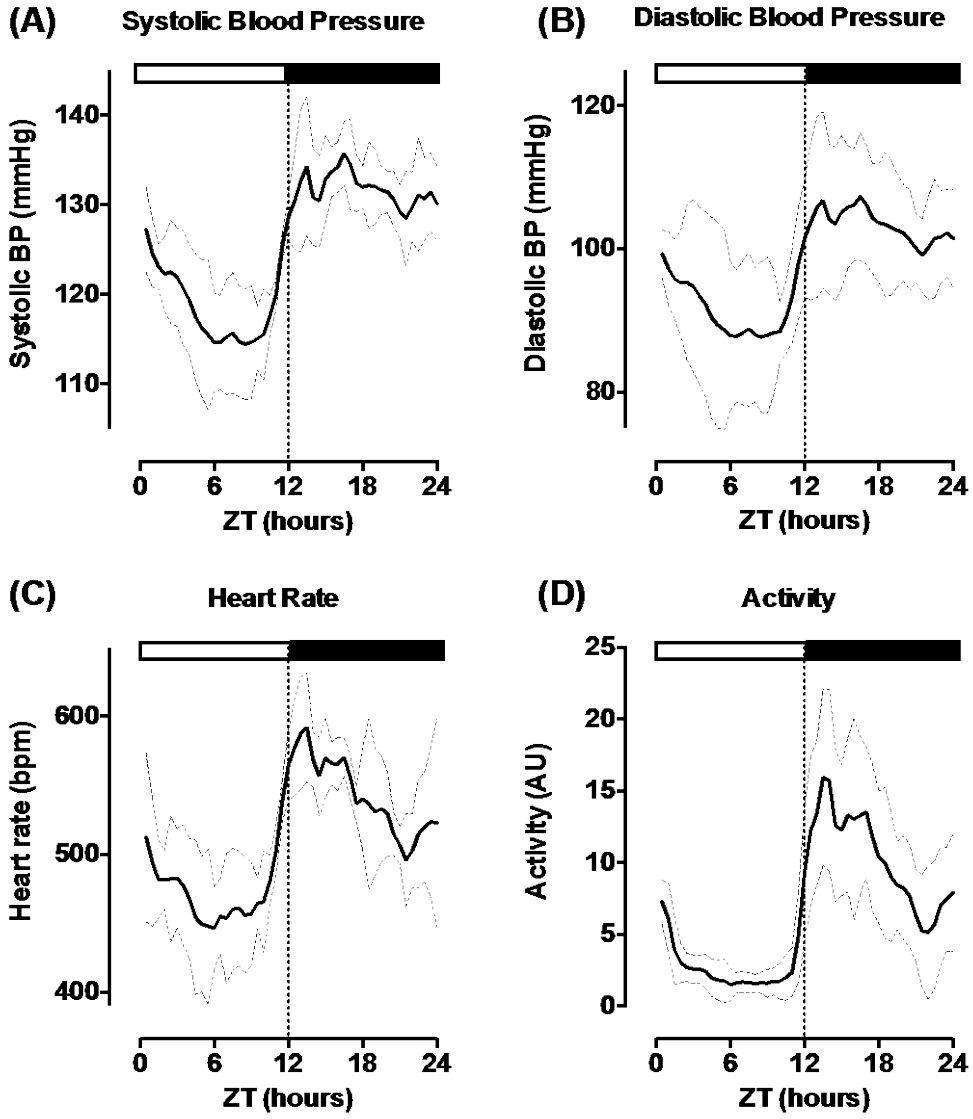

Figure 3.3: 24 hour systolic blood pressure (A), diastolic blood pressure (B), heart rate (C) and activity (D) Data are mean±95% CI (n=4) Black line and white line indicates the subjective night and day respectively.

Table 3.1: Parameters obtained from cosinor analysis of C57BL6 mice telemetry data
SBP (systolic blood pressure), DBP (diastolic blood pressure), HR (heart rate). Data are mean± 95% CI. (n=4)

	SBP	DBP	HR	Activity
Period (hours)	23h09 ± 0h22	23h09 ±0h18	23h48 ± 0h12	23.48 ±0h12
Acrophase (ZT)	18h10 ± 0h47	18h09 ± 0h49	16h36 ± 0h14	17h06 ±0h05
Amplitude (mmHg/ / bpm/ counts)	10.0 ± 1.8	9.8 ± 1.5	57.0 ± 22	6.24 ± 1.2
MESOR (mmHg/ bpm/ counts)	125.2 ± 1.6	95 ± 4.9	506.9 ± 6.6	7.17± 1.9
Robustness (%)	26.3 ± 4.3	23.9 ± 3.3	12.5±5.0	28.5 ± 1.9

3.3.4. Diurnal rhythm of NCC phosphorylation

The peak of SBP as estimated by cosinor analysis was at approximately ~ ZT18h10 and with a period of ~ 24 h the nadir can be calculated as approximately 12 hours prior at ~ZT 6. Therefore these two time points, at which blood pressure was most different, were selected for kidney collection and quantification of NCC phosphorylation by western analysis. As shown in figure 3, pT53, pS71 and total NCC were measured in whole kidneys taken at night (ZT 18) or day (ZT 6). Phosphorylation of NCC at T53 showed a marked diurnal rhythm: the levels at night being significantly greater than during the day ($p<0.0001$, Fig 3.4). No such rhythm was evident for phosphorylation at S71 ($p=0.13$, Figure 3.4B) or total NCC ($p=0.52$, Figure: 3.4C). This experiment was also performed in a cohort of female C57BL6 mice. As shown in Figure 3.4D, pT53 was higher at night than during the day ($p=0.009$). No changes were observed for pS71 or total NCC (data not shown). The effect on pT53 was more variable than in the males, possibly due to heterogeneity of the oestrous cycles. Studies in the rest of this thesis were performed only on male mice.

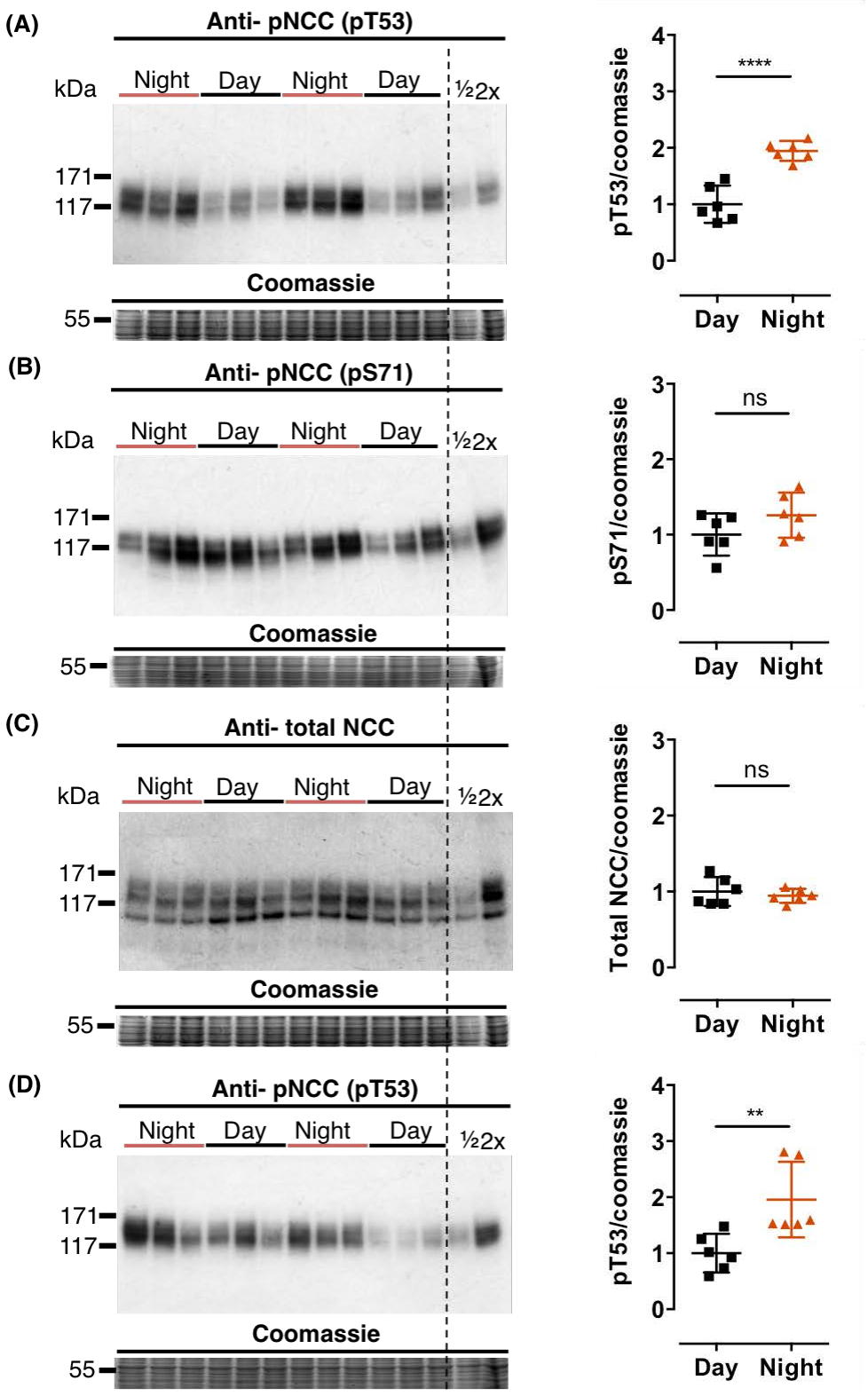

Figure 3.4: Western blots for (A) pT53 NCC, (B) pS71 NCC, (C) total NCC in male C57BL6 mice and (D) pT53 NCC in female C57B6L6 mice and their corresponding densitometry analyses.

Data are mean ±95% CI. Unpaired Student's t tests were carried out on the densitometry analyses ****p<0.0001 **p0.001 ns p>0.05 (n=6)

3.3.5. *Diurnal rhythm of renal mRNA transcripts*

Of 21 transcripts assessed, 5 were upregulated at night compared to day, including the clock genes: per2, cry1 and bmal1 (Figure 3.5). Both glucocorticoid-induced genes, SGK1 and GILZ were upregulated at night. None of the genes within the NCC regulation cascade were different at night, which is perhaps unsurprising as the proteins encoded by these genes are regulated on an acute scale by post-translational modifications such as phosphorylation.

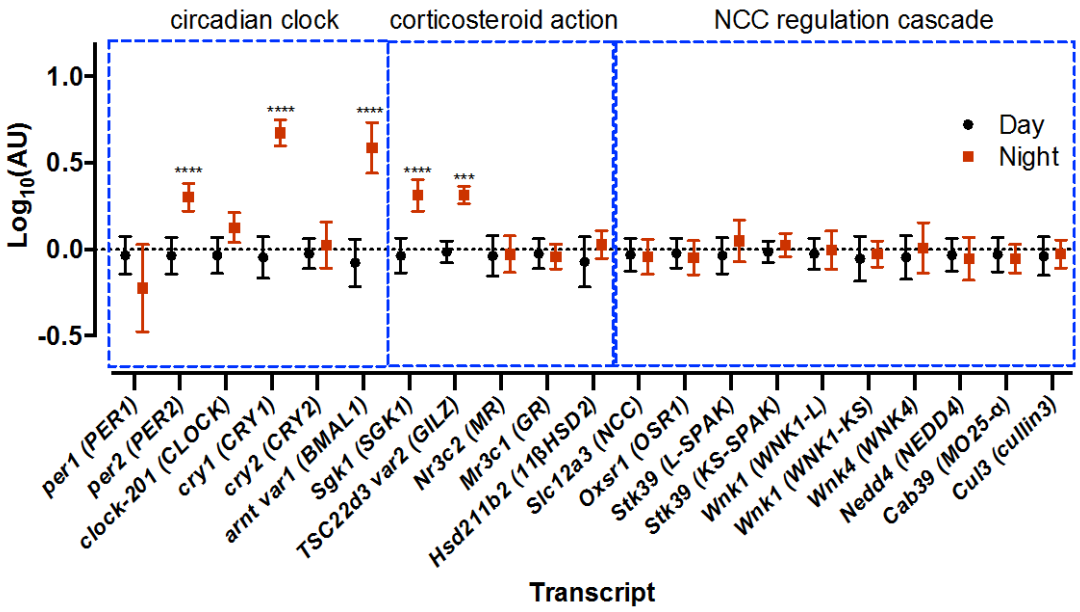

Figure 3.5: Renal gene expression in C57BL6 mice culled at night or during the day. Gene expression of each gene was normalised to the average expression of 18S, TBP and HPRT. Data are mean±95% CI. ****p<0.0001, ***p<0.001 with Sidak post hoc tests (n=15).

The gene expression data sets were further analysed using correlation to identify transcripts whose expression associated with NCC pT53. This analysis was performed "within group" for day and night to avoid "between group" correlation, which is almost certainly present in many of the samples [149]. During the day, no positive correlations were identified (Table 3.2); Stk39 (SPAK KS) displayed a moderate negative correlation with the level of NCC phosphorylation at T53. During the night several genes were positively correlated at a moderate level: *per1*, *per2*, *clock*, *Nr3c2* (but not *Nr3c1*), *Oxsr1* and *Slc12a3*. Stronger positive correlations were found between pT53 NCC and *stk39* (SPAK-L) and *SGK1*.

Table 3.2: Correlation between phosphorylation at T53 and expression of genes involved in the circadian clock, corticosterone action and NCC regulation cascade.

		DAY		NIGHT	
	Gene	**Pearson's r value**	**P value**	**Pearson's r value**	**P value**
Circadian clock	*per1*	+0.34	0.22	**+0.58**	**0.022**
	per2	+0.12	0.67	**+0.53**	**0.043**
	clock-201	-0.042	0.88	**+0.57**	**0.026**
	cry1	-0.081	0.77	-0.13	0.63
	cry2	0.089	0.75	+0.48	0.072
	arntl1 (BMAL1)	-0.17	0.55	+0.41	0.13
Corticosteroid action	*sgk1* (SGK1)	+0.12	0.67	**+0.65**	**0.0082**
	TSC22d3 (GILZ)	+0.24	0.40	+0.51	0.052
	Nr3c2 (MR)	+0.27	0.31	**+0.57**	**0.023**
	Nr3c1 (GR)	-0.32	0.24	+0.46	0.086
	Hsd11b2	-0.14	0.61	+0.25	0.37
NCC regulation cascade	*Slc12a3* (NCC)	+0.015	0.96	**+0.55**	**0.034**
	Oxsr1 (OSR1)	-0.0046	0.99	**+0.59**	**0.021**
	Stk39 (SPAK-L)	+0.31	0.27	**+0.62**	**0.014**
	Stk39 (SPAK-KS)	**-0.53**	**0.041**	+0.30	0.28
	Wnk1 (WNK1-L)	-0.19	0.49	+0.33	0.23
	Wnk1 (WNK1-KS)	-0.23	0.42	+0.25	0.38
	Wnk4	+0.45	0.092	+0.44	0.11
	Nedd4	+0.15	0.60	+0.35	0.20
	Cab39 (MO25-α)	-0.12	0.67	+0.37	0.17
	Cul3 (cullin3)	-0.11	0.69	+0.35	0.20

3.3.6. Circadian rhythm of corticosteroids

Corticosteroids have a 24-hour rhythm. The following experiments aimed to define this rhythm, in the context of our ZT6 and ZT18 culls.

3.3.6.1. Rhythm of plasma corticosterone

Figure 3.6A, illustrates the general rhythm of plasma corticosterone in C57BL6 mice. It is a composite data set composed from a mixture of terminal or conscious plasma samples taken from several different groups of C57BL6 mice. Plasma corticosterone reached a peak of ~300 nmol/l at ~ZT12 and a nadir of ~50 nmol/l at approximately ZT0 (Figure 3.6A). Blue

arrows indicate the times of culls. Assessing only the plasma samples taken at these times (ZT 6 and ZT 18) in either conscious (Figure 3.6B) or terminal (Figure 3.6C) experiments, a trend towards elevated plasma corticosterone at ZT 18 is seen. This was statistically significant in the terminal samples (p=0.013) but failed to reach threshold (p=0.062) in conscious mice.

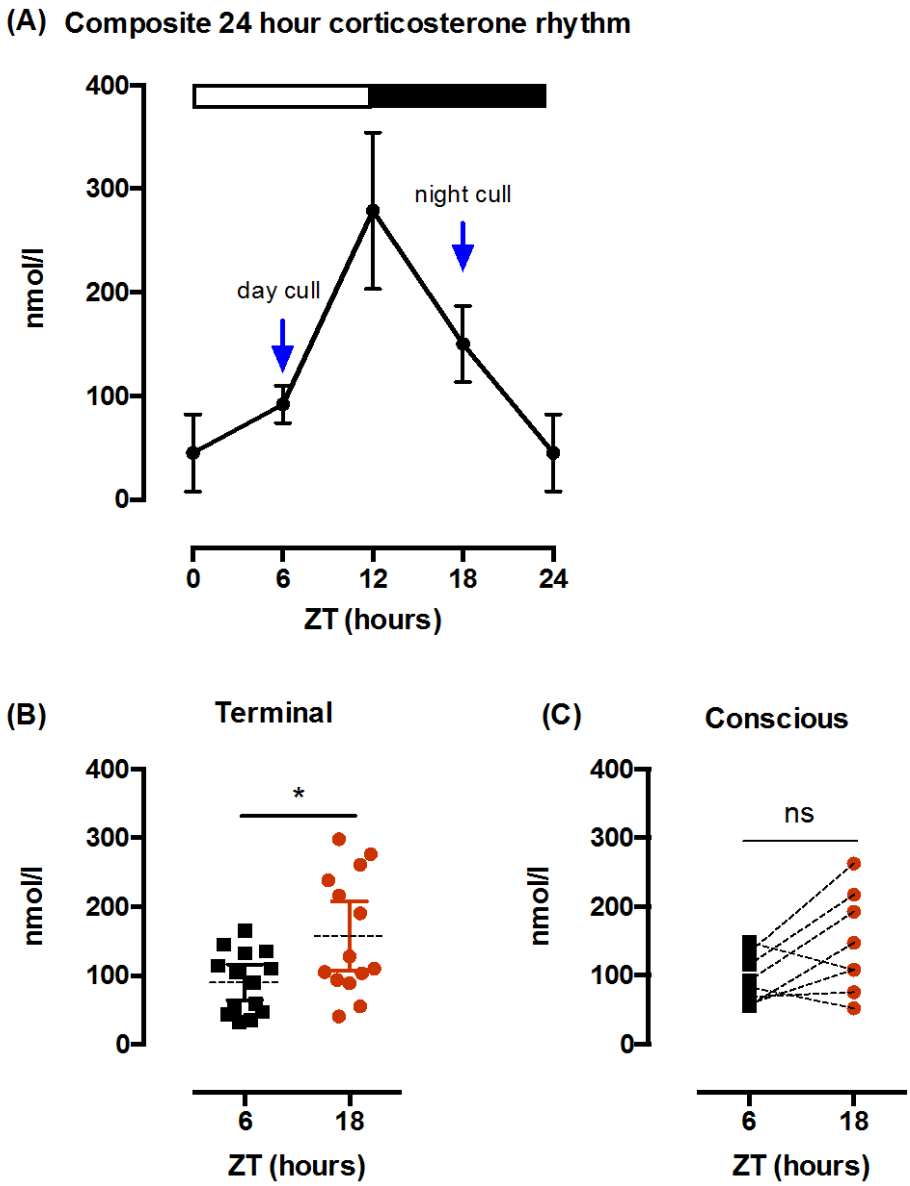

Figure 3.6: Plasma corticosterone levels in C57BL6 mice.
(A) Composite graph of plasma samples taken from several groups of mice, (B) corticosterone measured in terminal plasma samples, (C) corticosterone measured in tail micro-samples in conscious animals. Data are mean ±95% CI. Unpaired t-tests were carried out on terminal samples (B, n=22), paired Student's t tests were carried out on conscious tail micro-sampling groups (C, n=8). No statistical analyses carried out on composite graph as this is for illustrative purposes only.

3.3.6.2. *Diurnal rhythm of urinary corticosterone and aldosterone*

Plasma aldosterone was not measured, as the assay requires a volume of plasma that exceeds the volume we were able to obtain following the removal of both kidneys during the timed culls. As a surrogate for plasma aldosterone, urinary aldosterone excretion was measured in 12-hour urine samples collected over the day (ZT 0 – ZT12) and night (ZT 12 – ZT 0) as a surrogate for plasma aldosterone [142]. As shown in figure 3.7 the urinary excretion of both aldosterone (Figure 3.7A $p<0.01$) and corticosterone (Figure 3.7B, $p<0.0001$) was significantly higher at night than the day.

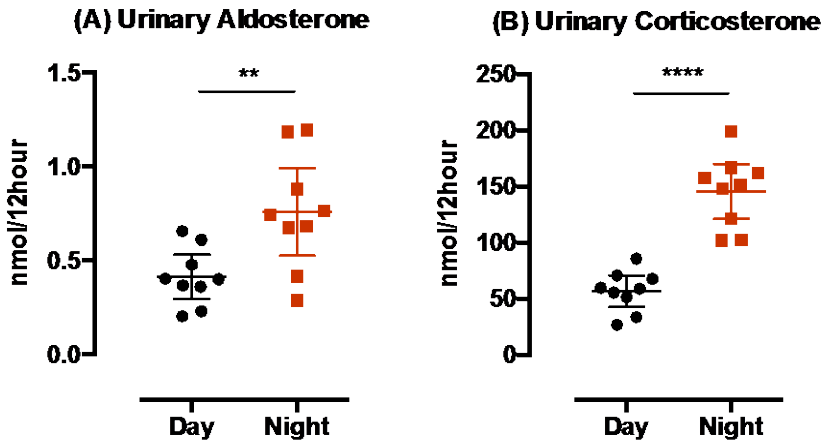

Figure 3.7: Urinary aldosterone (A) and corticosterone (B) in 12-hour day and 12-hour night samples from C57BL6 mice.
Urinary aldosterone and corticosterone was measured in pooled 12-hour urine from day and 12-hour urine overnight, collected between ZT0 and ZT12 and ZT12 and ZT0 respectively. Data are mean ±95% CI. Statistical comparisons were made using paired Student's t tests, ****p<0.0001 **p<0.001 (n=10)

3.3.7. *Localisation of NCC, GR and 11βHSD2 in the kidney*

Given the differences in the urinary excretion of corticosterone and aldosterone (corticosterone excretion is ~100X greater than aldosterone), it would be expected that aldosterone should only exert specific effects on NCC phosphorylation if MR in DCT cells is protected by 11βHSD2. The DCT can be split into 2 segments, with 11βHSD2 defining "DCT2", in which both NCC and ENaC are present [150] and absence of both 11βHSD2 and ENaC characterising DCT1. As we have recently described [86], 11βHSD2 and NCC seldom co-localise in the mouse. In each of the DCTs examined here co-localisation was only found on 1-2 occasions (Figure 3.8, illustrated by blue arrows). MR staining was sparse in the kidney but colocalised with NCC in all of the DCTs examined (Figure 3.9 A). GR was

abundantly expressed throughout the kidney and co-localised with NCC in all sections examined (Fig 3.9 B).

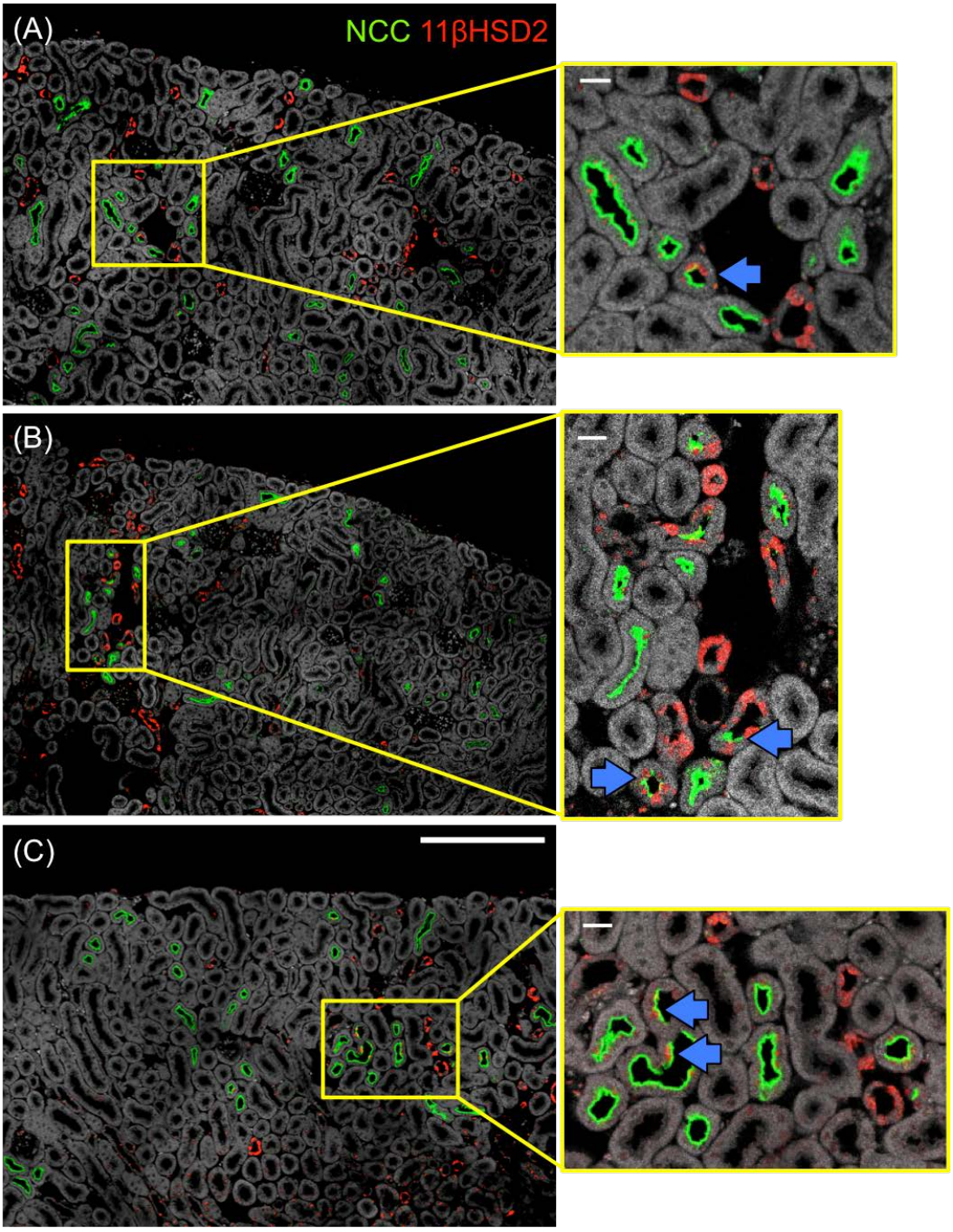

Figure 3.8: Immunofluorescent staining for NCC (green) and 11HSD2 (red) in 3 (A-C) male C57BL6 mice

High-powered views of yellow-boxed regions are given on the right where blue arrows indicate regions in which 11βHSD2 and NCC staining are within the same cell/tubule. Bar, 100 μm (left-hand panels); 10 μm (right hand panels).

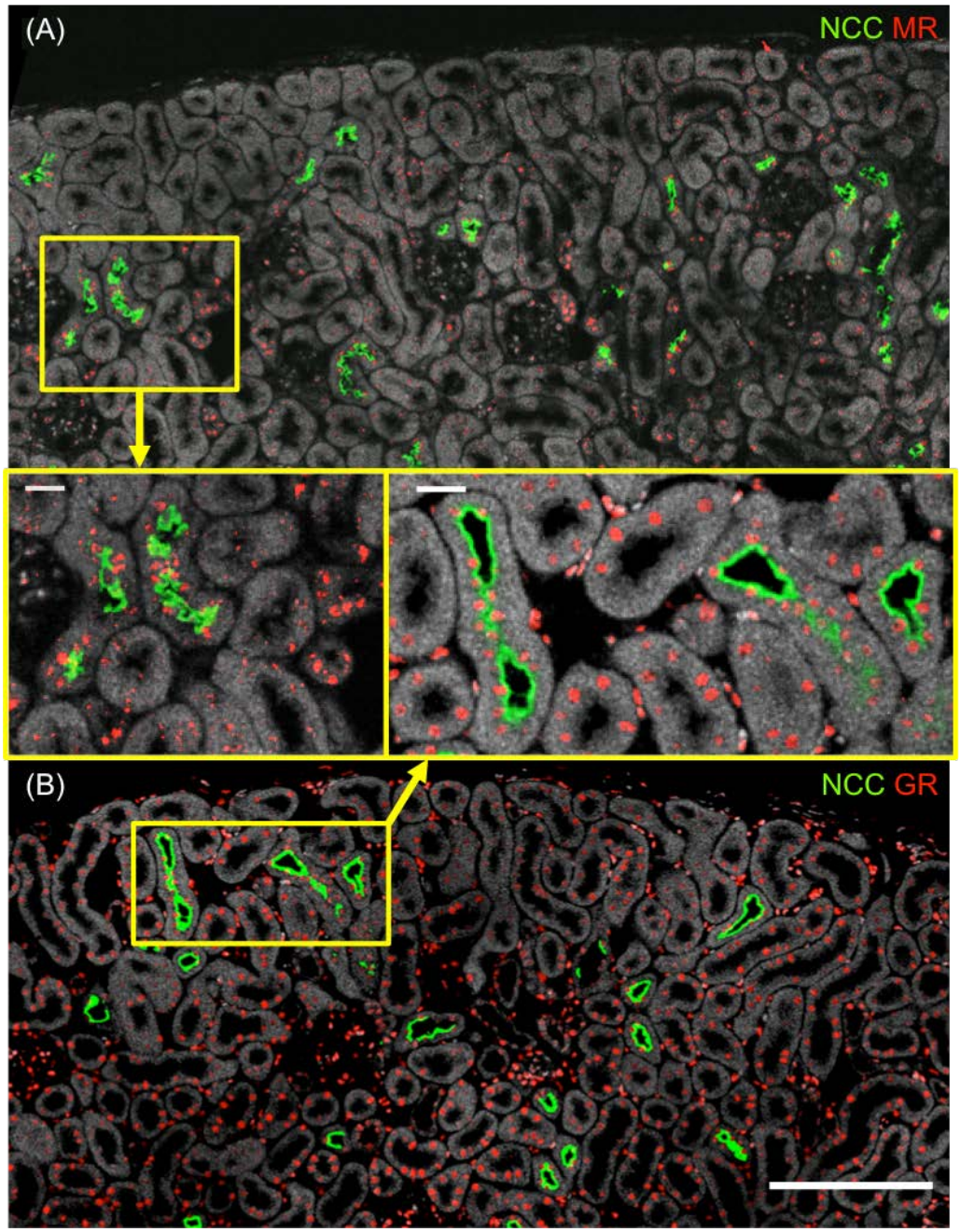

Figure 3.9: Representative images of immunofluorescent staining of (A) NCC (green) and MR (red) and (B) NCC (green) and GR (red) in male C57BL6 mice.
High-powered views of yellow-boxed regions are displayed. Bar, 100 μm in large top/bottom panels; 10 μm in high-powered middle panels.

3.4. Discussion

In this chapter the diurnal variation in food intake, renal sodium excretion and BP was assessed in male C57BL6 mice, finding that each of these variables was higher in the subjective night when the mice were active. NCC did not have a diurnal rhythm at either the mRNA or protein levels but phosphorylation of the transporter at a site critical for its activity was higher at night than day. Since it was found that MR in the DCT is not protected from GC activation by 11βHSD2, it is likely that corticosterone rather than aldosterone plays a dominant regulatory role for this transporter.

3.4.1. Rhythms of BP, feeding and urinary excretion

These experiments aimed to confirm the day/night differences in BP, activity, heart rate, feeding, drinking and urinary excretion in C57BL6 mice under our experimental conditions (as outlined in Methods 2.1.1). Our findings confirm that the animals were asleep during the day as the activity as measured by radiotelemetry was minimal and feeding, drinking and urinating was all reduced during the 12-hour day collection (ZT0-ZT12). At nighttime all the parameters investigated increased including BP, HR, activity, feeding, drinking and urinary excretion. This is in keeping with the literature for C57BL6 mice [148, 151, 152] and confirms that the conditions in these experiments facilitate normal behaviour, with minimal disturbance of circadian behavioural rhythms by husbandry staff or the experimenter.

We have shown in this work that the excretion of sodium and potassium have a strong diurnal rhythm of excretion, with twice as much excreted at night compared to the day. Such rhythms of electrolyte excretion have been defined in animal models and humans for decades [148, 153, 154]. This rhythm is the product of both hormonal factors and rhythmic feeding and drinking as it still persists to some extent even if a constant sodium load is applied [153]. Furthermore several groups suggest that perturbations to this rhythm of excretion affect an individual's ability to reduce BP while at rest, i.e. if not enough sodium is excreted during the active phase, then BP is maintained at a high level in order to excrete it in the inactive phase [26]. Indeed high nocturnal (in humans) BP is correlated strongly with nocturnal sodium excretion [25, 155, 156].

3.4.2. NCC has a diurnal rhythm of phosphorylation

The acrophase of SBP in these animals was ~ ZT 18 and nadir was ~ ZT 6. These two time points, at which BP was most different, were chosen as a starting point for timed culls to measure NCC phosphorylation. The major finding of this chapter was that NCC

phosphorylation has a diurnal rhythm with increased phosphorylation at T53 at night compared to day. Transcript levels of *slc12a3* were unchanged as was total NCC protein at these time points. NCC requires phosphorylation at several key residues in its amino terminus for its activity. These include but are not limited to T53, T58 and S71. Phosphorylation at T53 is associated particularly strongly with transporter activity, as measured by thiazide-sensitive sodium current in cells [99, 157], and in thiazide renal clearance experiments in mice [86] and rats [158]. Therefore phosphorylation at T53 and often T58 is commonly used as a surrogate for transporter activity. However, caution must be taken as transporter activity (as measured by thiazide-sensitive sodium transport) *in vivo*, does not always correlate with phosphorylation [86, 159], this is further discussed in Chapter 5. Our initial immunoprecipitation experiments indicated that in whole kidney homogenate, the antibody that recognises phosphorylation of T58 in NCC also recognises phosphorylation of residues in NKCC1 and NKCC2 (with all these proteins running at similar apparent molecular masses on SDS gels).

Interestingly, while large changes were seen in pT53, no changes in phosphorylation were seen at the S71 site. A similar finding was made with mice treated with chronic furosemide treated, which displayed increases in T58, T53 phosphorylation and thiazide-sensitive sodium transport but no differences in pS71 [86]. It is possible that phosphorylation at this residue is not critical for transporter activity; the evidence for its involvement is less convincing than for the other phospho-sites [99]. However, SPAK, which phosphorylates NCC does not appear to discriminate between T53, T58 and S71 *in vitro*. Therefore it is more likely that the S71 phospho-antibody is not as sensitive as the pT53 antibody.

The circadian clock allows predictive adaptations that prepare the body for daily activity such as feeding. NCC reabsorbs around 5-10 % of the total sodium load and has key roles in maintaining sodium homeostasis. Sodium intake is at its highest during the active phase, during which sodium requirement is greatest for the maintenance of sodium gradients for the myriad of metabolic functions this facilitates such as nutrient absorption, muscle contraction, action potential firing etc. Therefore it makes sense to have an activated transporter during the active phase to match body sodium levels with demand and compensate for insensible losses through defecation and sweating, which is also increased during activity. However, we haven't tested whether NCC phosphorylation is a predictive adaptation or if it occurs as a result of increased activity or feeding. It is not clear what effect acute sodium or electrolyte intake, which mice would experience daily during their active phase, would have on NCC

phosphorylation. Work by Sorensen et al offers some insights[129]. This group initially showed that a gavage of sucrose and 2% potassium caused rapid and sustained NCC dephosphorylation (lasting up to 6 hours) but this was not seen with a high sodium gavage [129]. The maintenance diet used throughout our experiments in this chapter is 0.67% w/w potassium and so we are unlikely to get this dramatic dephosphorylation with nighttime food intake. The group also then fasted the mice and presented mouse diet containing either 2% potassium or 0.5% potassium, the latter of which is much akin to our diet. The 2% K diet caused rapid NCC dephosphorylation but the 0.5% diet did not markedly alter NCC phosphorylation. Therefore it is likely that the NCC phosphorylation rhythm is not merely a feeding induced phenomenon and that hormonal and other factors are at work to balance extracellular sodium.

Two papers, published after this work was started, have also examined temporal differences in NCC expression. Uchida's group employed a similar approach to ours but addressed the question with increased temporal resolution, culling groups of mice every 4 hours over a 24-hour period. That study reported much lower variability in NCC expression and phosphorylation than found in our laboratory and also defined a diurnal rhythm of NCC phosphorylation, rather than total NCC [160]. However, the peak (ZT12) and nadir (ZT0) were phase shifted by about 6 hours compared to our study; no difference in NCC phosphorylation was reported at points corresponding to our culls. We cannot fully account for this difference, as the day/night feeding conditions were the comparable to ours. However the study does not define exactly which phospho-antibody was being used. Cross-referencing their methods, it seems that only the pS71 is being employed. This raises the intriguing possibility that pS71 has a different cycle of phosphorylation compared to pT53 but this remains to be substantiated. Interestingly, based on their findings, the group suggest that NCC is switched off on waking up to ensure enough excretion occurs during the active phase to counteract intake and switches on at the beginning of the inactive period to ensure enough sodium is absorbed at night, when intake is reduced.

The second paper examined NCC rhythm in healthy humans, measuring NCC expression in urinary exosomes over 5 time points from 7am to 11.30pm [161]. Exosomes are a specific sub-type of micro-vesicle, 20-100nm in diameter, which are released from most cells in the body [162]. In the kidney, exosomes are a major route of apical membrane protein excretion into the urine. The assumption is that these exosomes therefore may give a snapshot of the protein abundance of the apical membrane. NCC activity peaks during active phase (day in

humans; night in mice) coinciding with greatest need in terms of requirement for reabsorption. There are major caveats to this study: the authors do not correct for urinary volume or creatinine and rely on the assumption that temporal differences in total urinary exosomal release will be minimal within the same subject. The subjects were allowed to eat and drink freely and there is no indication of when eating or drinking took place. Hydration, nutrition status and the resulting urinary flow rate and concentration are likely to affect the concentration of urinary exosomes, therefore this assumption that total exosomal release is constant throughout the day is likely an oversimplification. This is perhaps also hinted at in the observation that all the urinary exosomal proteins studied in the paper (aquaporin 2, prostatin, NCC) follow a similar temporal pattern of concentration, which could simply reflect the pattern of total exosomal release throughout the day.

3.4.3. Transcriptional changes: links to NCC phosphorylation rhythm?

A panel of 21 genes was chosen for qPCR analysis. The rationale behind the selection of these genes was threefold. In the first instance it was to confirm the mice had a "normal" circadian rhythm – as indicated by the differential expression of key clock genes (bmal1, per1, per2, cry1, clock). Next was to identify any genes within the known NCC regulation pathway that may be differentially regulated at our time points. The current paradigm for how these transcripts contribute to the regulation of NCC is outlined in Figure 3.10. Finally, NCC is known to be regulated by corticosteroids, therefore genes involved in corticosteroid action such as the receptors (MR, GR), inactivating enzyme (11βHSD2) and induced genes (SGK1, GILZ) were tested to investigate any changes in these that could be linked to NCC activity.

Various transcripts including *SGK1*, *GILZ*, *per2*, *bmal1* and *cry1*, were upregulated during the active phase at ZT18 compared to the inactive day phase at ZT6 in C57BL6 mice. This is consistent with microarray experiments performed by two independent groups [42, 43]. Hogenesh and colleagues allowed mice to "free run" in dark/dark settings and culled 3 mice every 2 hours and whole kidney was taken forward to microarray analysis [43]. The resulting microarray and RNAseq data is available on their database: http://bioinf.itmat.upenn.edu/circa/query. All the genes with a significant difference in gene expression in our q-RT-PCR experiments exhibit strong circadian rhythms as assessed by the JTK_CYCLE algorithm, which is defined and described in detail [163]. Genes that have circadian expression but were missed by our timed culls include *PER1*, *cul3*, *wnk1* and *mo25α*. This appears to be as a result of either their zenith being near the day:night transition

(*WNK1*, *PER1*), or as a result of low amplitudes (*CUL3*, *mo25*). In Zuber's work culls were made every 4 hours of mice exposed to dark/light conditions. The DCT/CNT and CCD were micro-dissected from the collected kidneys. In conflict with our results and those of Hogenesh, Zuber did not find any diurnal variation in SGK1 expression in either DCT/CNT or CCD sections, which is perhaps owing to the temporal resolution not being high enough or amplitude not large enough for detection in their experimental setup.

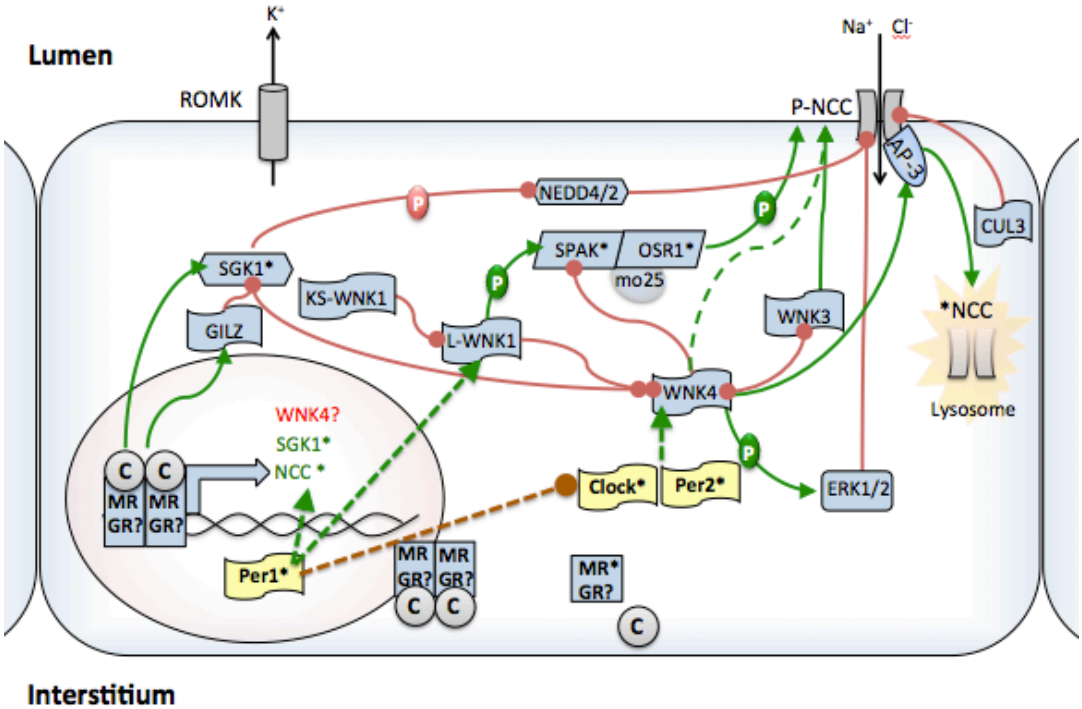

Figure 3.10: Diagram illustrating the current paradigm for the regulation of the sodium chloride co-transporter (NCC) including implicated clock genes.
Corticosteroid (C) induced MR or GR activation, dimerization and translocation to the nucleus, promotes the transcription of NCC and inhibits WNK4 expression following prolonged corticosteroid exposure. WNK4 is generally accepted to be an inhibitory regulatory kinase of NCC and how WNK4 is activated is still unknown. SGK1 and L-WNK1 inhibit WNK4 and thus promote NCC activity through relief of WNK4-mediated inhibition of the STE20/SPS-1-related-proline/alanine-rich kinase and oxidative stress response kinase 1 (SPAK/OSR1) complex. Mouse protein 25 (mo25) is a positive regulator of SPAK/OSR1. SGK1 is also postulated to inhibit Nedd4/2, which can also ubiquitinylate NCC. GILZ on the other hand acts in opposition to SGK1. Kidney specific WNK1 (KS-WNK1) is a negative regulator of L-WNK1 and thus promotes WNK4 driven inhibition of NCC. Further WNK4-mediated inhibitory pathways include inhibition of the NCC-stimulatory kinase WNK3 and stimulation of inhibitory protein ERK1/2 and the adaptor protein 3 (AP3). AP-3 facilitates lysosomal transport and thus WNK4 redirects NCC to the lysosome. Cullin 3 (CUL3) acts to promote NCC ubiquitinylation. Per1 has recently been shown to promote NCC and WNK1 transcription and prevent the binding of clock and per2 to the WNK4 promoter. (Red connectors represent inhibition through phosphorylation (P) or otherwise, while green arrows indicate stimulation by phosphorylation (P) or otherwise. Interrupted green arrows represent unknown or controversial events, *indicates transcripts that were positively correlated with NCC phosphorylation at nighttime).

It is intriguing that many genes within the NCC regulation cascade that promote NCC activation, such as *SPAKL*, *OSR1*, *WNK1*, *WNK4*, *N3cr2* (MR) are positively correlated with NCC phosphorylation at night, when phosphorylation is high but not during the day, when the system may be in a dormant or "off" state. Transcripts that positively correlated with NCC phosphorylation are highlighted in Figure 3.10 (with an asterix). pNCC is also correlated strongly with clock genes: *PER1, PER2* and *clock-201*. Richard's et al recently explored how the circadian clock may integrate with the downstream NCC regulatory pathways [56]. This group showed that *PER1* regulated NCC transcription *in vivo* and pharmacological inhibition of PER1 nuclear entry (by inhibiting its phosphorylation with the drug casein kinase 1delta/epsilon) reduced NCC and *WNK1* mRNA but increased *WNK4* mRNA [56]. They went on to demonstrate that PER1 block increases levels of Cry1/Cry2 and Per2 mRNA. This PER1 blockade also increased occupancy of CLOCK and PER2 on the WNK4 promoter and decreased occupancy in the *WNK1* promoter and Slc12a3 (NCC) promoter in mDCT15 cells. *WNK1* is constitutively active upon expression and promotes NCC phosphorylation through the activation of *SPAK*/*OSR1*, which in turn phosphorylates NCC. It is therefore feasible that an increase in WNK1 mRNA could promote NCC phosphorylation over a relatively short period. This is particularly interesting in light of our work, as we've shown that although *PER1* is not differentially expressed at our time points, it is strongly correlated with pNCC at night.

3.4.4. Regulation of NCC phosphorylation rhythm by corticosteroids

Both plasma corticosterone and aldosterone have similar circadian rhythms and both can bind the MR and GR, which are expressed in the DCT. In Uchida's temporal NCC phosphorylation experiments, blockade of the MR using eplerenone, attenuated the rhythm of NCC phosphorylation [160]. GCs are well known to entrain local clocks in peripheral tissues [75] [164] [44, 74] and circulate at levels 100-1000 times greater than that of aldosterone [165]. The enzyme 11βHSD2 acts like a specific pre-receptor blocker of GC access, presumably to both receptors and it confers aldosterone sensitivity to the distal nephron. However the data in this chapter suggest that 11βHSD2 and NCC co-expression is limited. This confirms recent micro-dissection experiments performed in this lab [130] and other studies in reporter mice [87]. This suggests that NCC is GC sensitive, but the receptor through which GCs act is unknown. In light of Uchida's work, one would speculate GCs would act through MR rather than GR. GR and MR are nuclear receptors, acting like transcription factors in order to promote transcription or inhibition of multiple downstream

processes. These genomic actions take in the region of 1-6 hours [166-168] and therefore we could expect this length of delay between the corticosterone zenith and downstream events. This fits with our work where marked NCC phosphorylation is preceded by a corticosterone peak 6 hours prior.

It is important to note that, several other hormonal systems can induce phosphorylation of NCC including angiotensin II [169], AVP [97] and renal sympathetic nerve activity [104]. Although these hormonal systems also have circadian rhythms of release [170-173] and may contribute to the rhythmic control of NCC, their role was not investigated during my PhD studies.

3.4.5. Summary of Chapter Findings:

1. NCC phosphorylation at T53 has a diurnal rhythm
2. Genes associated with the circadian clock and glucocorticoid action are also upregulated at our time points
3. Plasma corticosterone levels are marginally raised at ZT18 compared with and ZT6 but peak at approximately 6hours prior to ZT18, giving enough time for genomic actions to occur and trigger downstream events that culminate in increased NCC phosphorylation.
4. We've established that C57BL6 mice have a marked urinary excretory rhythm of sodium and potassium.

4. Effect of chronic GC manipulation on the diurnal rhythm of NCC phosphorylation

4.1. Introduction

In the previous chapter it was shown that NCC phosphorylation at T53 has a diurnal rhythm, with increased phosphorylation at night compared to the day in C57BL6 mice. There were correlations between NCC phosphorylation and corticosteroid-activated transcripts: SGK1 and GILZ. Furthermore, urinary corticosterone was elevated at night with levels 200 times higher than urinary aldosterone. Although aldosterone can stimulate NCC phosphorylation [98, 99, 157], IHC experiments in the previous chapter indicate that the enzyme 11βHSD2 seldom colocalises with NCC [87, 130]. Therefore the primary purpose of this chapter is to investigate the hypothesis that GCs regulate the diurnal rhythm of NCC phosphorylation.

Two different approaches were taken to investigate this hypothesis. The first was examine the effect of adrenalectomy (ADX) on the diurnal rhythm of NCC phosphorylation. ADX reduces circulating aldosterone, GCs and catecholamines. Therefore we complemented this strategy with a more refined approach in adrenal intact animals, in which the diurnal rhythm of plasma corticosterone specifically was attenuated and plasma levels clamped within a mid-physiological range. The rationale behind this approach was that the rhythmicity of other adrenal hormone levels might still persist.

4.1.1. Specific chapter aims

1. Investigate whether ADX affects the diurnal rhythm of NCC phosphorylation and the abundance of key transcripts within the NCC regulation cascade, corticosteroid pathway and circadian clock
2. Investigate whether clamping plasma corticosterone levels in adrenal intact mice affects the diurnal rhythm of NCC phosphorylation, abundance of key transcripts within the NCC regulation cascade, corticosteroid pathway and circadian clock and food and water intake, urine output and sodium and potassium excretion.

4.2. Methods

Detailed methods of each of the procedures in this chapter are outlined in the main methods section. For clarity, an outline of the experiments carried out and cohorts of mice used are presented here.

4.2.1. Timed culls in adrenalectomised mice

ADX was performed under isofluorane anaesthetic (Methods 2.7.1) after which these mice and adrenal intact controls were individually housed and allowed to recover and acclimatise for 9 days prior to timed culls. Following ADX mice were given *ad libitim* access to 0.9% saline as well as water. 9 days is sufficient for recovery and restoration of circadian rhythms of BP post anaesthetic yet should be before extra-nodular adrenal tissue regrowth [174]. As in the previous chapter these mice were then culled at 1am (ZT18) and 1pm (ZT6). Mice were culled on two separate days (batch 1 and batch 2), with 3 ADX and 3 intact animals culled each time to make up 6 in each group. Details of the cull and techniques used to analyse the tissue are presented in (Methods 2.3 and 2.4). A separate cohort of 4 ADX and 4 adrenal intact mice underwent tail venesection for blood micro sampling at 7.15am (ZT 0.15) and 6.45pm (ZT 11.45). ADX animals were not subject to the additional stress of metabolic cage experiments, due to welfare concerns. ADX animals are more prone to sudden death from adrenal insufficiency as they are unable to mount a full stress response. Saline intake was assessed by weighing water bottles daily on days 6-7 post-ADX.

4.2.2. Metabolic cage and tail micro-sampling in mice implanted with corticosterone or vehicle pellets

Corticosterone or vehicle pellets were subcutaneously implanted into C57BL6 mice under isofluorane anaesthetic (Methods 2.7.2). The mice were then individually housed in standard cages and allowed to recover for 5 days. Tail venesection was performed to sample blood at 7.15am (ZT 0.15) and 6.45pm (ZT 11.45) on day 6. The animals were then housed in metabolic cages with a 12hour light/dark cycle and allowed to acclimatize for 5days. Food and water intake was measured and urine collected for 12-hour periods over 2 consecutive days (ZT0-12 “Day” and ZT12-0 “Night”). Details of the techniques used to analyse the urine samples are presented in (Methods 2.5).

4.2.3. Timed culls of mice implanted with corticosterone or vehicle pellets

Corticosterone or vehicle pellets were subcutaneously implanted into C57BL6 mice. Mice were pair housed and allowed to recover for 5 days. On day 5, the mice were culled at 1am

(ZT 18) and 1pm (ZT 6). Mice were culled on 3 separate days (batch 1-3), with 3 corticosterone and 3 vehicle-treated mice culled at a time to make up 9 in each group. Details of the cull and techniques used to analyse the tissue are presented in Methods 2.3 & 2.4.

4.3. Results

4.3.1. Effect of Adrenalectomy (ADX) on plasma corticosterone

Figure 3.1A illustrates the reduction of corticosterone achieved by ADX in C57BL6 mice 9 days following ADX surgery. It is a composite data set composed from a mixture of terminal or conscious plasma samples taken from several groups of adrenal intact or ADX C57BL6 mice. Blue arrows indicate the times of culls. Assessing the plasma samples taken at these times (ZT 6 and ZT 18) in terminal experiments, plasma corticosterone was elevated at ZT 18 in the intact group compared to the ADX animals but corticosterone levels were comparable at ZT 6 (Figure 3.1B).

In a separate cohort of conscious mice, blood samples were taken via tail venesection at ZT 0 and ZT 12 (Figure 4.1C). In intact mice, plasma corticosterone increased 4 fold at ZT 12 compared to ZT 0 ($p<0.0001$, Figure 4.1C), whereas no such increase was seen in ADX mice ($p>0.05$, Figure 4.1C). Increased saline appetite is well described in ADX rats [175] but no such appetite has been found in mice [176]. Here we found that ADX animals drank ~ 2 fold greater proportion of saline than the intact animals ($p=0.0004$, Fig 4.1D). In terms of absolute volumes, ADX animals drank more saline than the intact group (3.16 ±0.92 ml/48 hour compared to 1.86 ±0.28 ml/ 48 hour, mean ±95%CI, $p=0.016$, by t test with Welch's correction, n= 11 ADX, n= 12 intact) but also drank less water than the intact animals (7.720±1.115 ml/48 hour compared to 9.80 ±0.66 ml/48 hour, mean ±95% CI, $p=0.0015$, by Student's t test, n= 11 ADX, n= 12 intact). The total fluid intake was not different (5.896 ±0.556 ml/48 hour compared to 5.59 ±0.47 ml/48 hour, mean±95% CI, $p=0.37$, by Student's t test, n=11 ADX, n=12 intact).

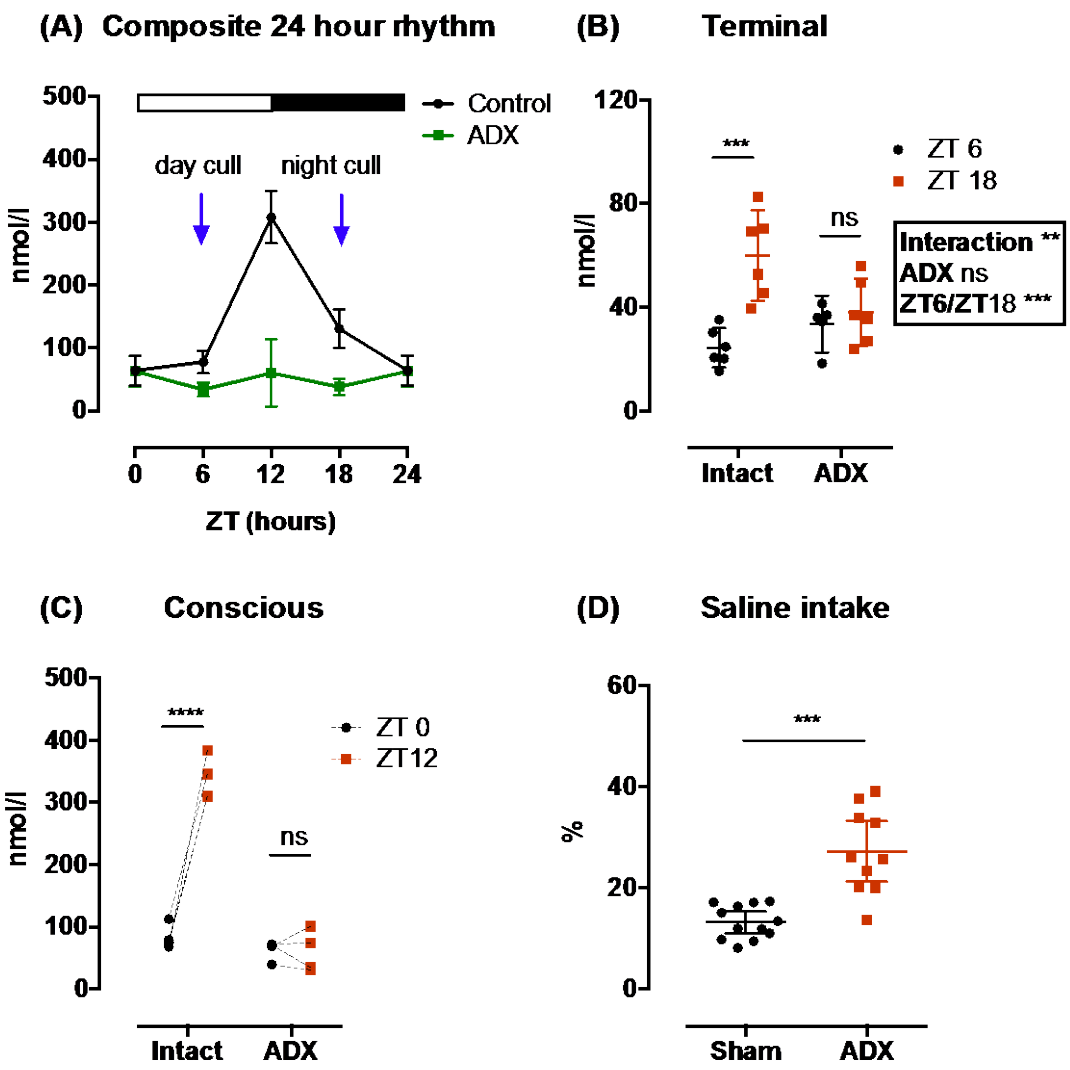

Figure 4.1: Composite graph of 24-hour plasma corticosterone in adrenal intact and adrenalectomised (ADX) mice (A), plasma corticosterone measured in terminal (B) and conscious (C) experiments and saline preference (D) in intact and ADX mice.
Composite graph includes all samples taken in control mice (n=8-29). The terminal and conscious samples were taken from 2 different cohorts of ADX or adrenal intact mice (n=6 & n=4 respectively). Saline and water intake was measured over 2 days (day 6-7 post ADX). Saline intake here is expressed as a % of total fluid intake. Two-way ANOVA was carried out on data from terminal experiments, and matched two-way ANOVA carried out on the conscious experiments, with post hoc Sidak tests used for both. Saline intake data were analysed by t test with Welch's correction for unequal variance. ****p<0.0001, ***p<0.001 ns, p>0.05. No statistical analyses were carried out on composite graph as this is for illustrative purposes only.

4.3.2. Effect of ADX on the diurnal rhythm of NCC phosphorylation

As shown in Figure 4.2A & 4.3A, NCC phosphorylation at T53 was significantly higher at night compared to day in the adrenal intact group. This difference was absent in the adrenalectomised group and phosphorylation levels were not significantly increased at night. There were no day/night changes in pS71 levels in either the intact or ADX group, however levels of the phosphoprotein were significantly reduced by at nighttime compared to controls (Figure 4.2 & 4.3B). Total NCC protein was reduced at both night and day in the adrenalectomised group compared to the intact group (Figure 4.2 & 4.3C).

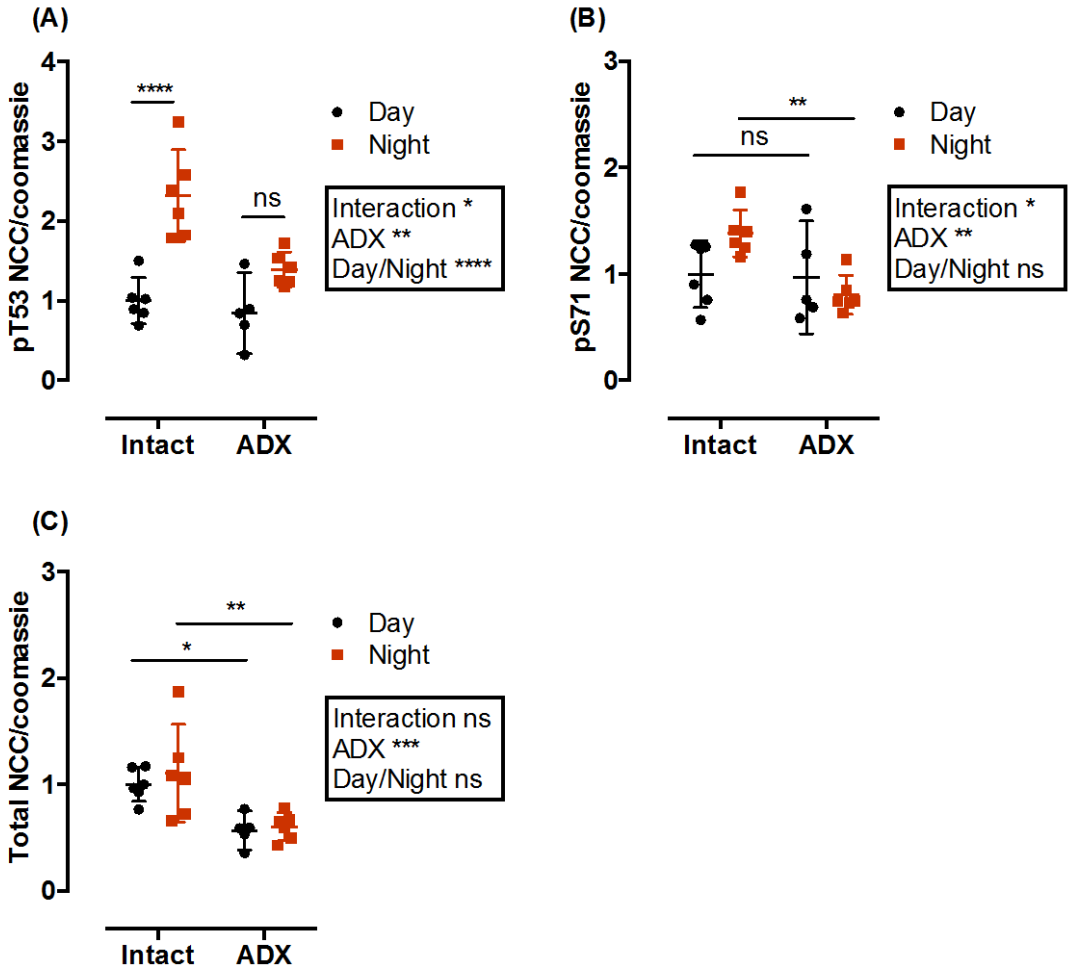

Figure 4.2: Densitometry analysis of western blots for pT53 NCC (A), pS71 NCC (B) and total NCC (C) in intact and adrenalectomised (ADX) mice culled at night (ZT 18) or during the day (ZT 6).
Data presented as mean±95% CI. Two way ANOVA was performed with post hoc Sidak tests where ****p<0.0001, ***p<0.001 **p<0.01 *p<0.05 and ns p>0.05.

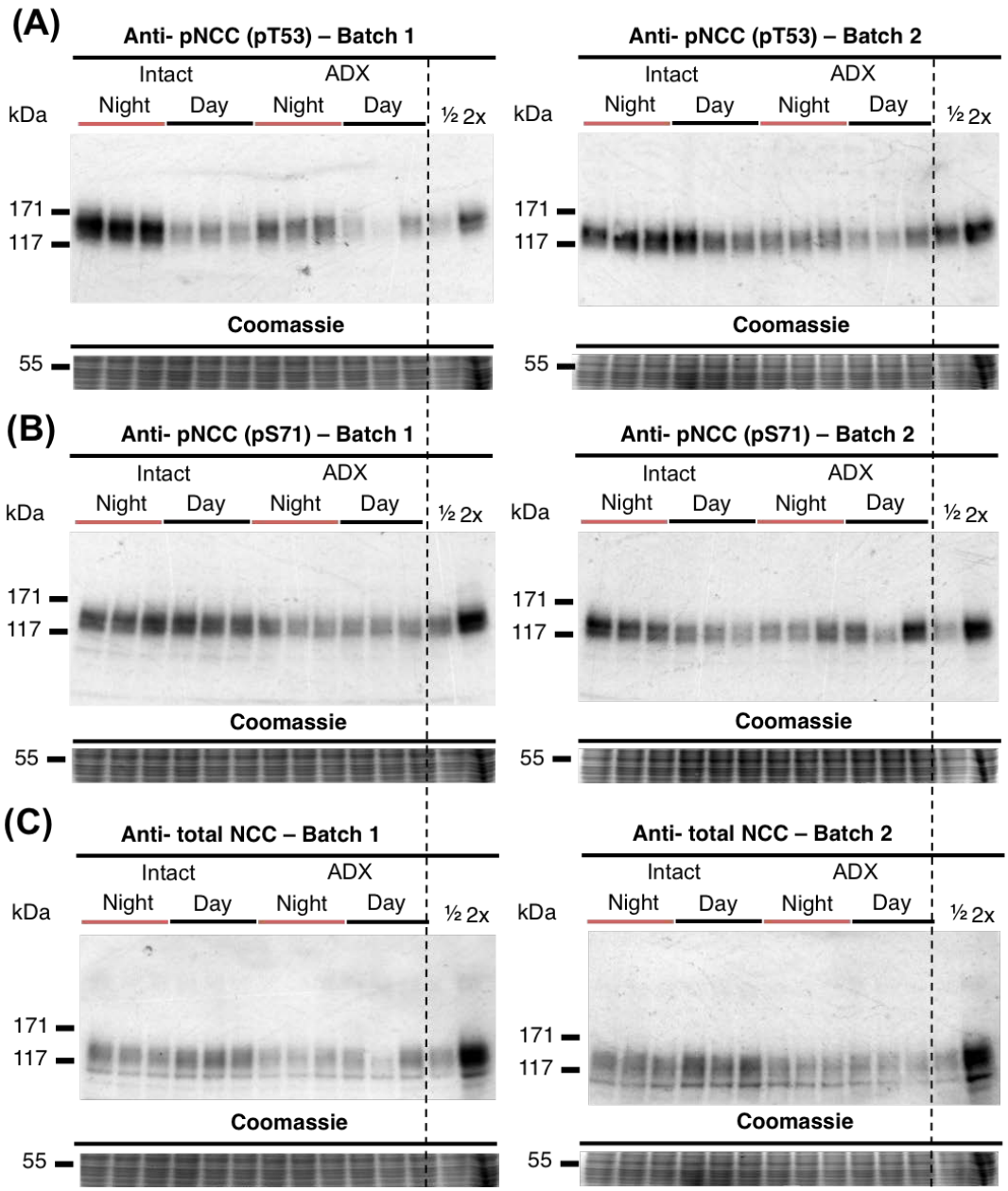

Figure 4.3: Western blots for (A) pT53 NCC, (B) pS71 NCC and (C) total NCC in intact and adrenalectomised (ADX) mice culled at night (ZT 18) or during the day (ZT 6). Western blots were performed in 2 batches. A sample from the first batch was ran again in the third batch and used as a reference lane to normalise across the batches. ½ and 2x are linearity control lanes.

4.3.3. Effect of ADX on the diurnal variation of renal mRNA

Nine genes were selected from the larger panel of 21 candidate genes presented in chapter 3, for testing in this intact and ADX experimental cohort. These genes were selected on the basis that they were either: i) shown to be differentially expressed between day and night in Chapter 3; or ii) are key transcripts within the NCC regulation pathway (*slc12a3* and WNK4). ADX had little effect on the diurnal rhythms of the selected genes. GILZ had a blunted diurnal rhythm in the ADX group, but all other rhythms of clock genes were similar between the intact and ADX group (Figure 4.4). SGK1 was not differentially expressed between day and night in either ADX or intact animals.

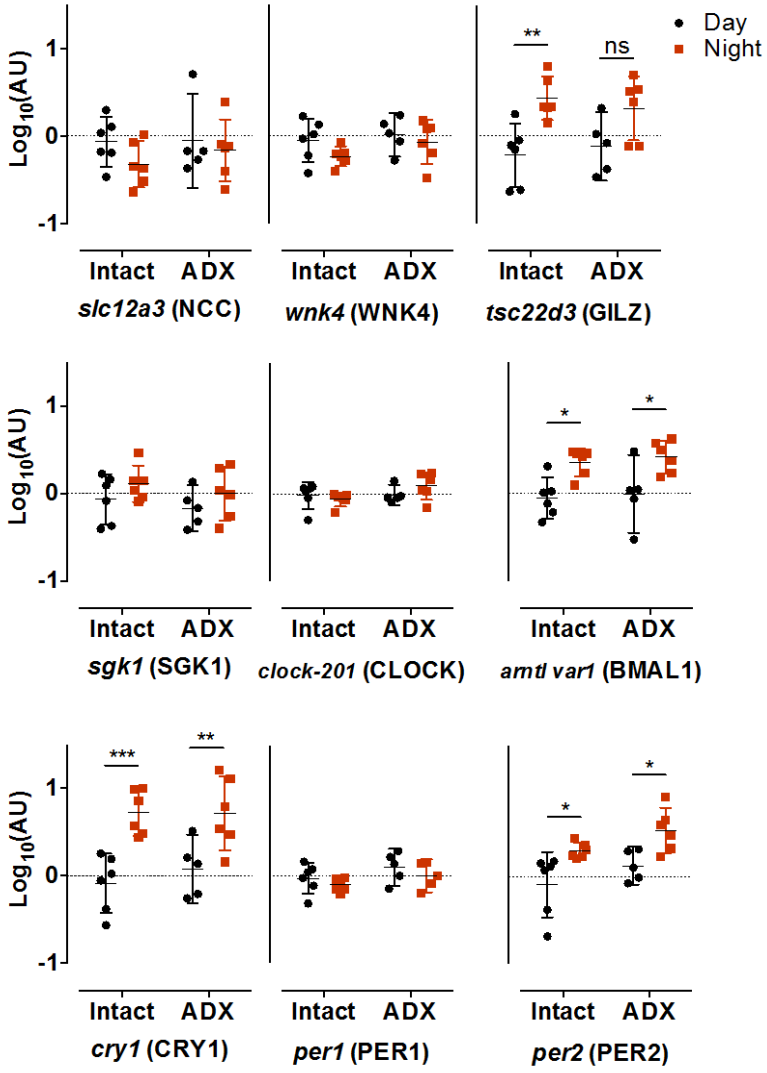

Figure 4.4: Gene expression in kidneys of adrenalectomised (ADX) and adrenal intact C57BL6 mice culled at night (ZT 18) or during the day (ZT 6).
Protein the gene transcribes is in brackets. Gene expression of each gene was normalised to the average expression of 18S, TBP and HPRT. Data are mean±95% CI. Data was analysed with two way ANOVA followed by post hoc Sidak tests, where ***p<0.001, **p<0.01 *p<0.05, ns p>0.05 (n=5-6)

4.3.4. Effect of chronic corticosterone treatment on plasma corticosterone levels

Adrenalectomy reduces to various degrees the level of endogenous glucocorticoids, mineralocorticoids and catecholamines [177-180]. In order to assess whether corticosterone in particular affects the rhythm of NCC phosphorylation in C57BL6 mice, the levels of plasma corticosterone were clamped at a constant physiologically intermediate between the normal peak and nadir. Figure 4.5 C illustrates the midpoint level of plasma corticosterone achieved using silastic slow release pellets. It is a composite data set composed from a mixture of terminal or conscious plasma samples taken from several different groups of C57BL6 mice with or without subcutaneous slow release pellet implants.

Blue arrows indicate the times of culls. Assessing only the plasma samples taken at these times (ZT 6 and ZT 18), corticosterone pellets significantly increased the plasma corticosterone levels at ZT 6 (Figure 4.5 A). In a separate cohort of mice, blood samples were taken at the known trough (ZT0) and peak (ZT 12) time points for plasma corticosterone levels. In vehicle treated mice a significant difference was seen in plasma corticosterone in blood sampled by tail venesection at ZT 0 compared to that from ZT 12 (Figure 4.5C) but this was not seen in the corticosterone treated animals, which exhibited slightly higher day time plasma corticosterone and slightly lower night time corticosterone (Figure 4.5B).

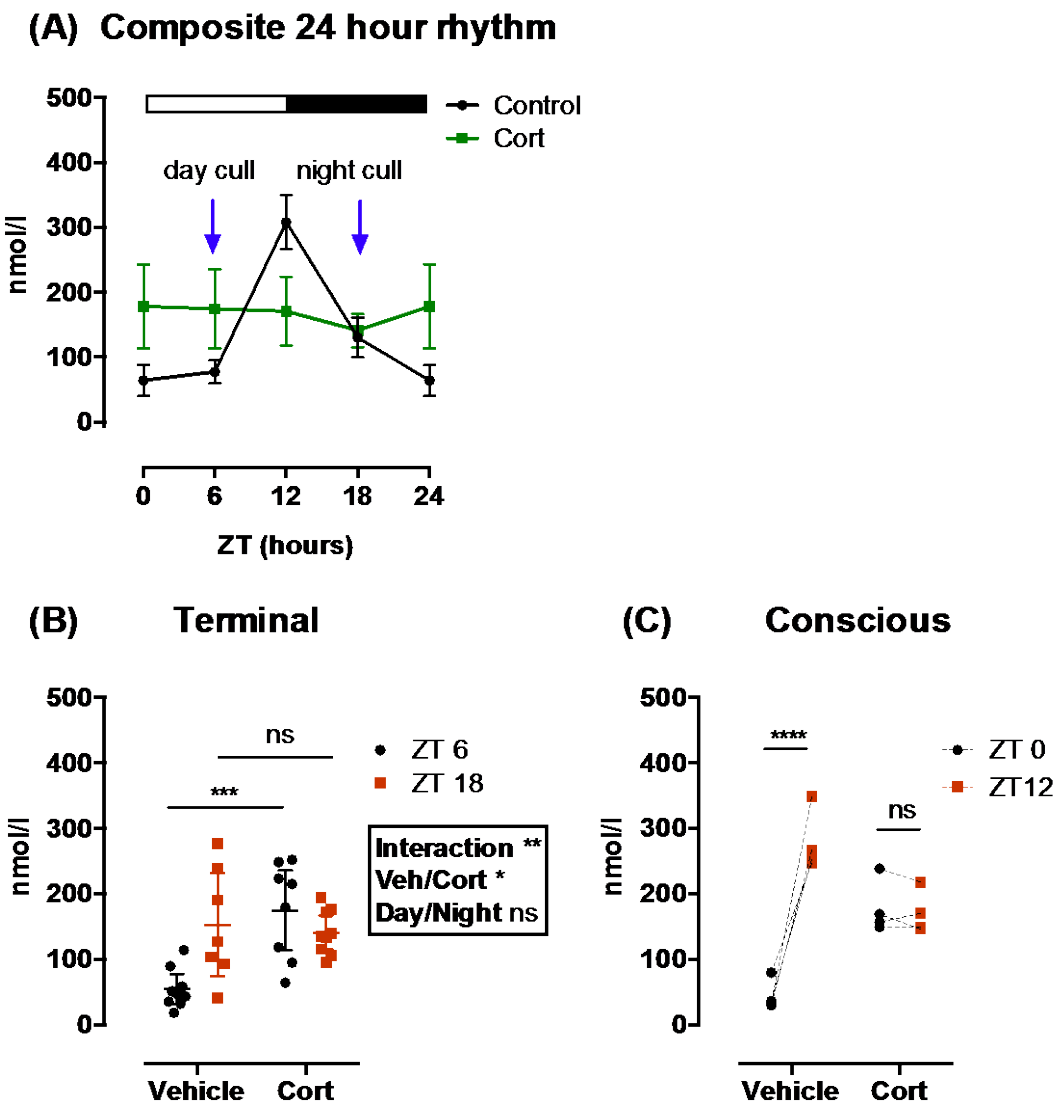

Figure 4.5: Composite graph of 24-hour plasma corticosteorne in control mice and mice receiving chronic corticosterone (A), plasma corticosterone measured in terminal (B) and concious (C) experiments.
Composite graph includes all samples taken in control mice (n=8-29). The terminal and conscious samples were taken from 2 different cohorts of corticosterone or vehicle treated mice (n=9 & n=4 respectively). Two-way ANOVA was carried out on data from terminal experiments, and matched two-way ANOVA carried out on the conscious experiments, with post hoc Sidak test results for both indicated by ***p<0.0001, ***p<0.001 ns, p>0.05. No statistical analyses were carried out on composite graph as this is for illustrative purposes only.

4.3.5. *Effect of chronic corticosterone administration on urinary corticosterone and aldosterone*

In the absence of sufficient plasma for the measurement of aldosterone, urinary aldosterone as measured urine samples taken over 12-hour night (ZT 0 - ZT 12) and 12-hour day (ZT 0 – ZT 12) was used as a surrogate. Urinary aldosterone exhibited a diurnal rhythm of excretion with significantly more excreted during the night than the day in both corticosterone and vehicle treated groups (Figure 4.6 A). In contrast, the diurnal rhythm of urinary corticosterone was absent in corticosterone treated animals ($p>0.05$, Figure 4.6 B) but present in vehicle treated animals ($p<0.01$ for day/night differences in urinary corticosterone, Figure 4.6 B).

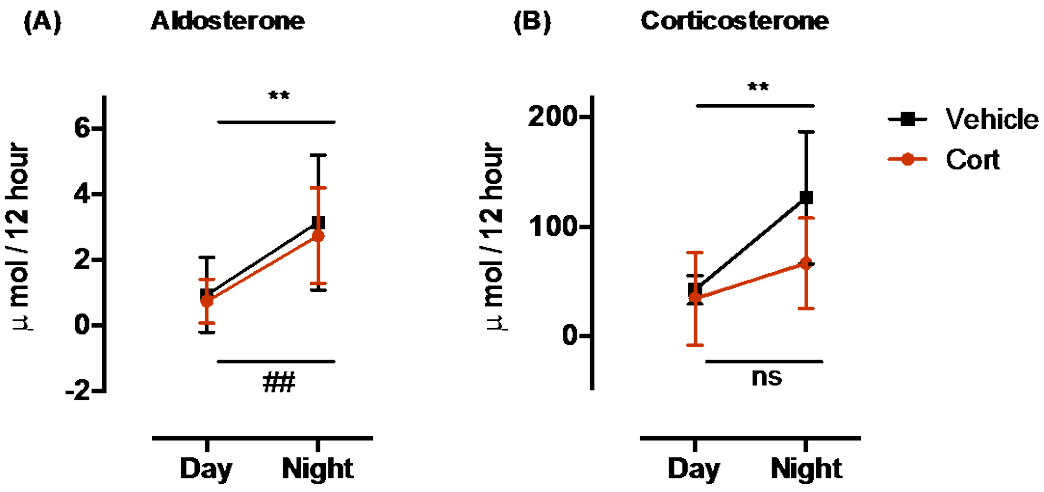

Figure 4.6: Urinary aldosterone (A) and corticosterone (B) in C57BL6 mice receiving chronic vehicle or corticosterone treatment.
Urinary aldosterone and corticosterone was measured in pooled 12-hour urine samples from day and 12-hour urine overnight, collected between ZT0 and ZT12. Data presented as mean±95% CI. Data analysed by matched two way ANOVA with post hoc Sidak's tests where **p<0.01 (vehicle) ##p<0.01 (corticosterone) ns p>0.05 (n=4).

4.3.6. *Effect of chronic corticosterone administration on the diurnal rhythm of NCC phosphorylation*

There was batch variability as seen in Figure 4.7 and 4.8 but overall NCC phosphorylation at pT53 was significantly increased at night compared to day in the vehicle treated group and this difference was not present in the corticosterone-treated group. Furthermore, NCC phosphorylation at pT53 was significantly raised during the day in corticosterone-treated animals ($p<0.001$, Figure 4.7A). Total NCC protein was unchanged by any of the treatments or at any of the time points (Figure 4.7C). pS71 NCC exhibited a significant difference

between night and day in the vehicle treated group ($p<0.01$, Figure 4.7 B) which was not present in the corticosterone treated animals ($p>0.05$, Figure 4.7 B).

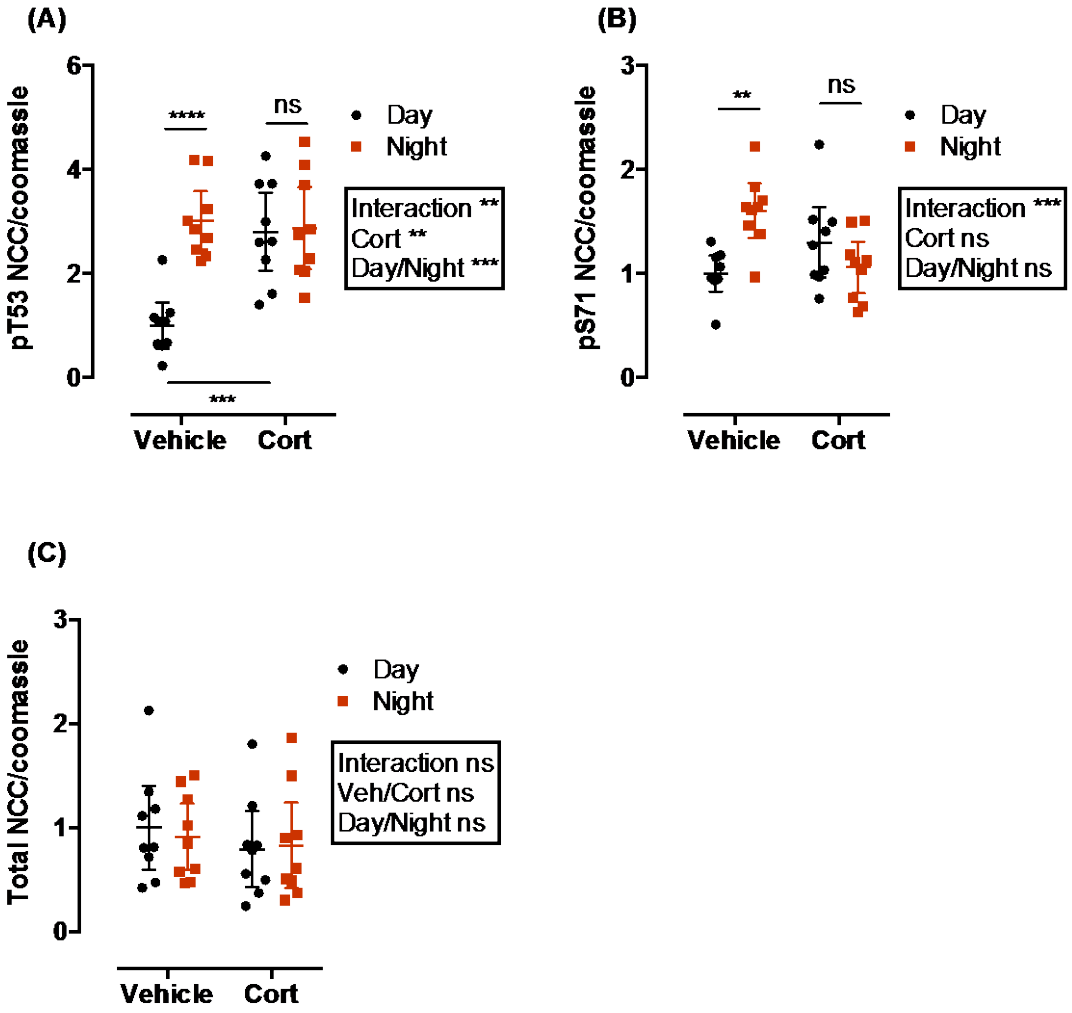

Figure 4.7: Densitometry analysis of western blots for pT53 NCC (A), pS71 NCC (B) and total NCC (C) in vehicle and corticosterone treated mice culled at night (ZT 18) or during the day (ZT 6).
Data presented as mean±95% CI. Two way ANOVA was performed with post hoc Sidak tests where ****$p<0.0001$, ***$p<0.001$ **$p<0.01$ and ns $p>0.05$.

Figure 4.8 (overleaf): Western blots for pT53 NCC (A) pS71 NCC (B) and total NCC (C) in vehicle and corticosterone treated mice culled at night (ZT 18) or during the day (ZT 6).
Westerns were performed in 3 batches (1-3). "R" is reference load, which was a pooled sample used to normalise across the three batches of western blots.

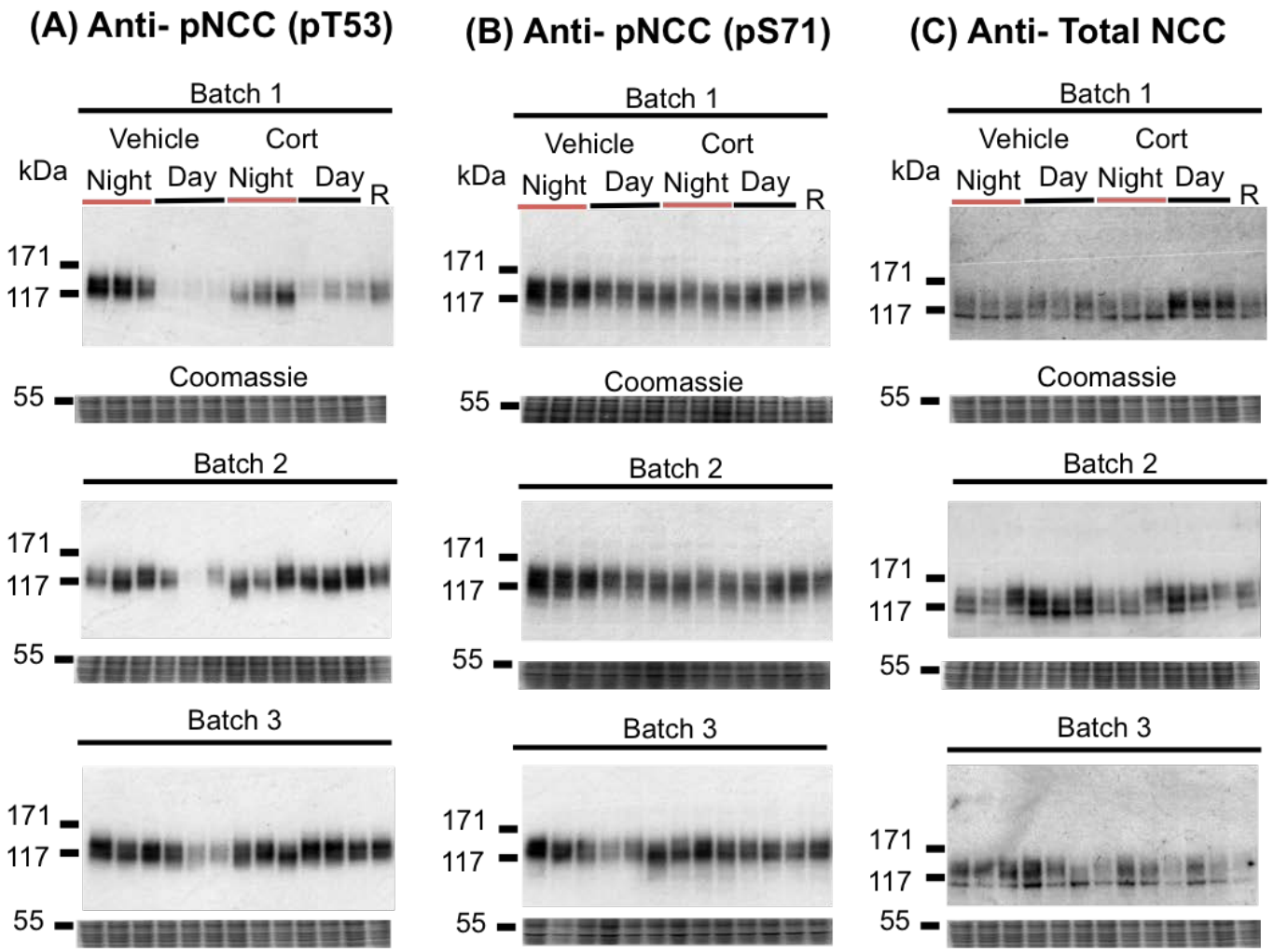
(A) Anti- pNCC (pT53)
(B) Anti- pNCC (pS71)
(C) Anti- Total NCC
Batch 1
Vehicle
Cort
kDa
Night
Day
Night
Day
R
171
117
Coomassie
55
Batch 2
Batch 3

4.3.6. Effect of chronic corticosterone administration on the diurnal regulation of renal mRNA transcripts

Nine genes were selected from the larger panel of candidate genes presented in chapter 3, for testing in this experimental cohort. As with the initial experiments, we found no differences in *slc12a3* (NCC), WNK4 or clock-201 mRNA between night and day in any of the treatment groups (Figure 4.9). Both *GILZ* and *SGK1* were significantly increased during the day in the corticosterone group compared to the vehicle group. Clamped plasma corticosterone levels affected several clock genes, such as bmal1 and cry1, which were moderately increased during the day in the corticosterone-treated group compared to the vehicle group (Figure 4.9). Per2 mRNA was unaffected by corticosterone treatment and the diurnal rhythm was maintained. However, Per1 mRNA levels were increased at both day and night in the corticosterone treated group compared to vehicle, with no day-night differences.

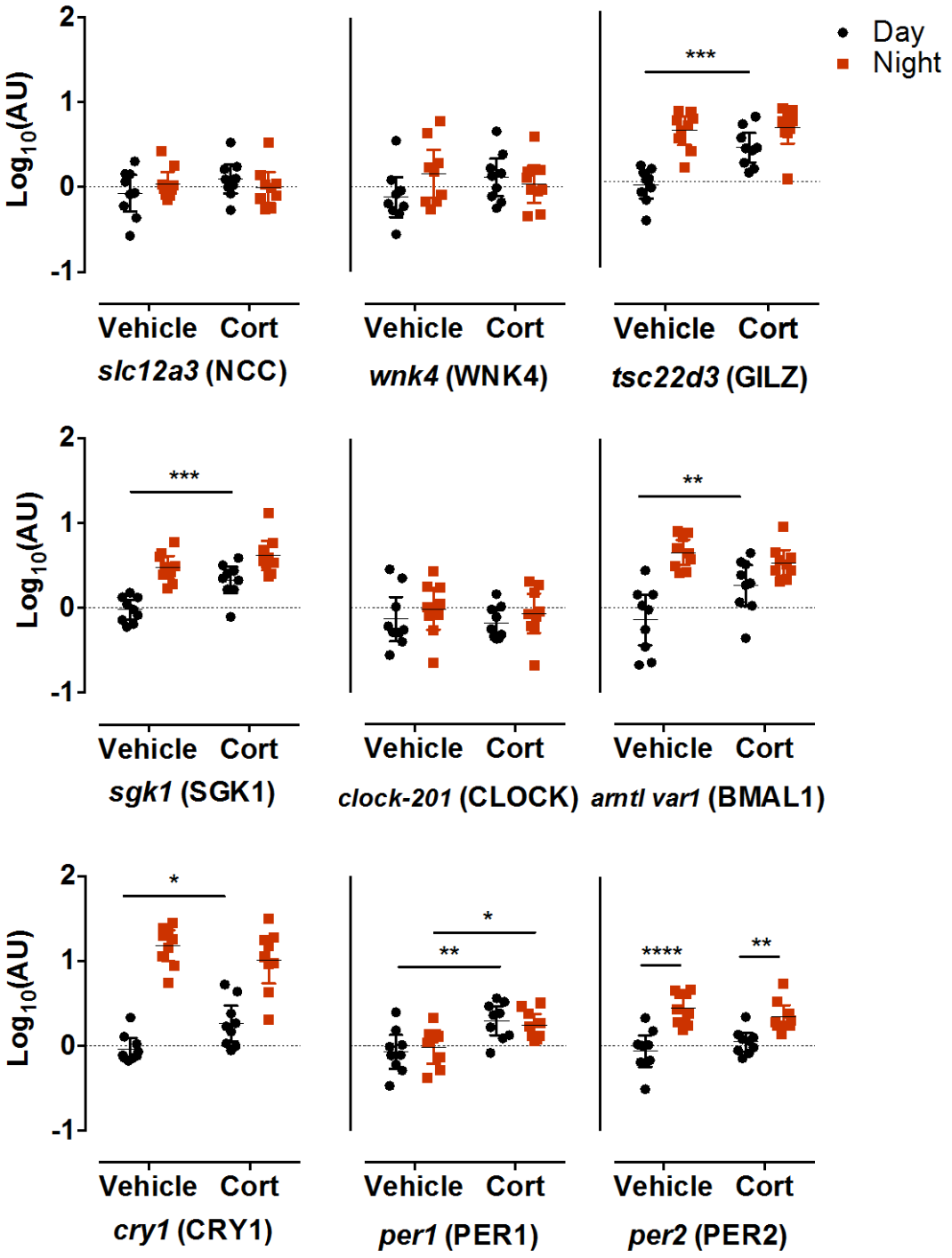

Figure 4.9: Gene expression in kidneys of corticosterone (Cort) or vehicle treated C57BL6 mice culled at night (ZT 18) or during the day (ZT 6).
Protein the gene transcribes is in brackets. Gene expression of each test gene was normalised to the average expression of 18S, TBP and HPRT. Data are mean ± 95% CI. Data were analysed with two way ANOVA followed by post hoc Sidak tests, where ***p<0.001, **p<0.01 *p<0.05, ns p>0.05 (n=9)

4.3.7. Effect of chronic corticosterone administration on the diurnal rhythm of feeding and drinking

Both treatment groups exhibited modest diurnal differences in food and water intake and urine output, with no significant differences between treatment groups but a significant day/night effect (Figure 10 A, B, C respectively).

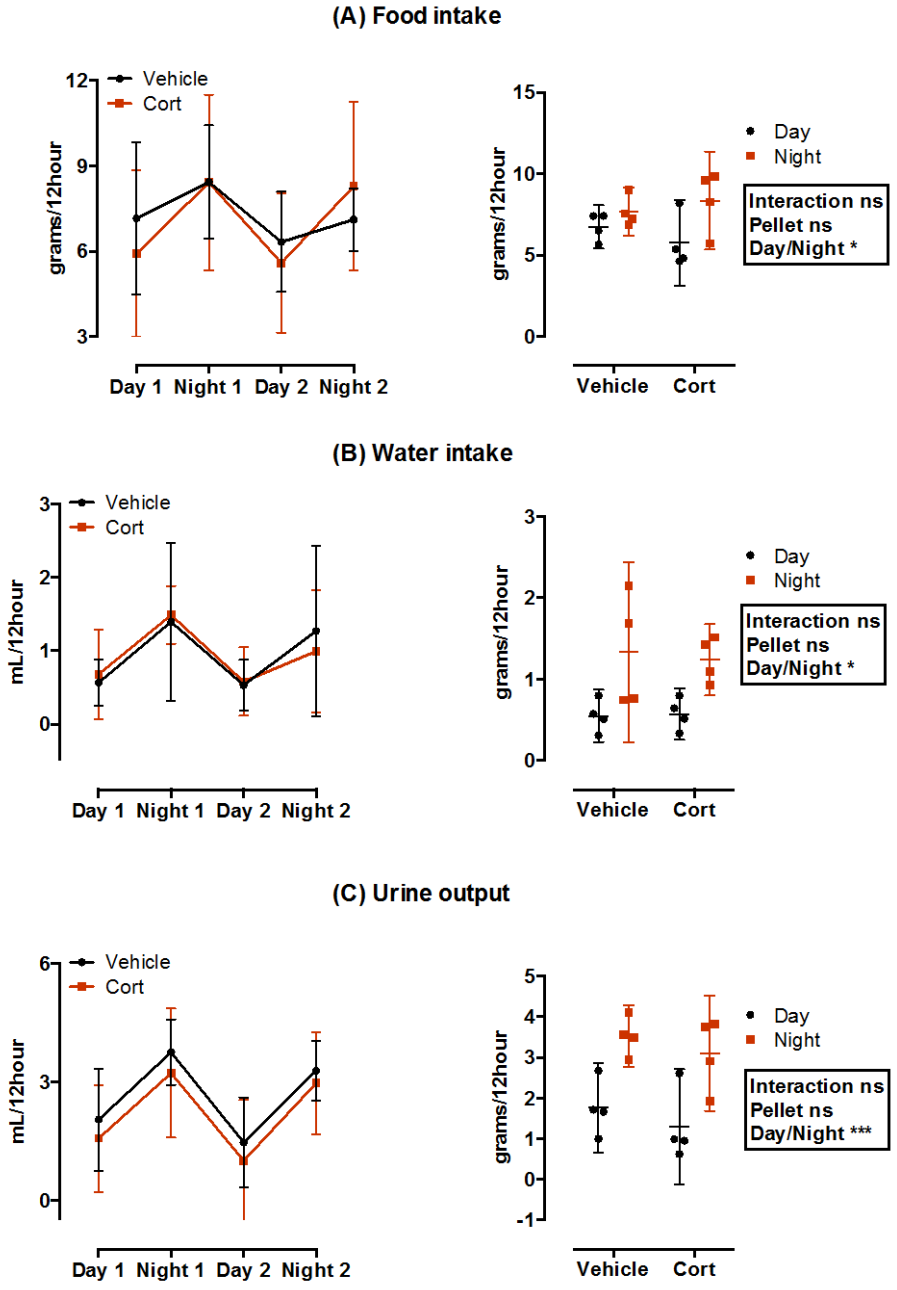

Figure 4.10: Food (A) and water intake (B) and urine output (C) over 2 consecutive days and nights in C57BL6 mice treated with corticosterone or vehicle.
All measured between ZT0 and ZT12 (day) and ZT12 and ZT 0 (night). The mean of the two days and nights is displayed in the right hand panel. Data are presented as mean±95% CI. Data were analysed by matched two way ANOVA where ***p<0.001, *p<0.05, ns p>0.05.

4.3.8. Effect of chronic corticosterone administration on the diurnal rhythm of electrolyte excretion

Urinary sodium excretion exhibited a strong diurnal rhythm in both corticosterone and vehicle treated groups (Figure 4.11 A). However, the corticosterone group had small but significant and reproducible reduction in sodium excretion during the night but interestingly not during the day when we see the NCC phosphorylation difference (Figure 4.11 A). There was no difference in overall mean 24-hour sodium balance over the 2 days, although faecal sodium was not measured (vehicle group values were 268.3±46.5 µmol/24 hour versus corticosterone group values of 280.3±62.6 µmol/24 hour with p= 0.64, by Student's t test, n=4). Potassium excretion was similar in both treatment groups with a strong diurnal rhythm of excretion (Figure 4.9 B).

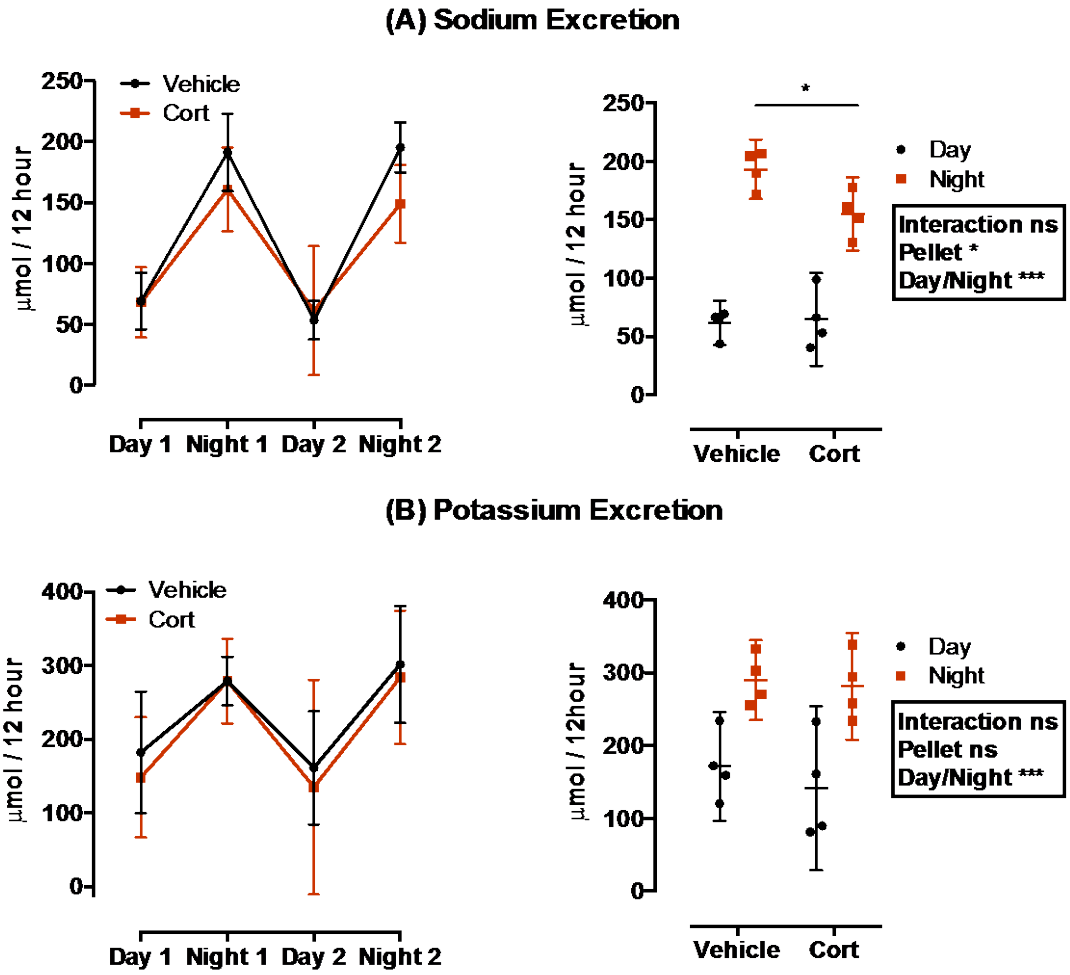

Figure 4.11: Sodium (A) and potassium output over 2 consecutive days and nights in C57BL6 mice treated with corticosterone or vehicle. All measured between ZT0 and ZT12 (day) and ZT12 and ZT 0 (night). The mean of the two days and nights is displayed in the right hand panel. Data presented as mean±95% CI. Data was analysed by two way ANOVA where ***p<0.001, *p<0.05, ns p>0.05.

4.4. Discussion

In this chapter the diurnal rhythm of NCC phosphorylation was found to be dependent upon a diurnal rhythm of plasma corticosterone. ADX, which reduced circulating GCs, reduced the NCC phosphorylation level and rhythm, whereas clamping corticosterone within a physiological intermediate range "held" NCC phosphorylation at a higher level.

4.4.1. Effect of ADX on levels of plasma corticosterone

Plasma corticosterone levels were significantly reduced compared to the control animals at the peak (ZT 12) and differences between plasma corticosterone levels at the time of cull (ZT 6 and ZT 18) were also not present in the ADX animals. Levels within this range 54.6 ±6.6 nmol/l (mean ±SEM) are consistent with literature reported values of <55nmol/l [181] and 61.2 ±13.0 nmol/l (mean ±SEM) [174]. While ADX removes a major source of corticosterone production, there are extrarenal sources, which still produce corticosteroids (reviewed in [182]). It is not clear whether this extra-adrenal corticosteroid excretion exhibits a circadian pattern of release but in these cohorts any diurnal rhythmicity of plasma corticosterone was blunted. Other plasma hormones levels that may be affected by ADX include aldosterone and epinephrine. These were not measured here due to welfare concerns but the literature suggests that ADX reduces aldosterone and epinephrine levels by at least 5 fold [181] and 20 fold respectively [183].

4.4.2. Effect of ADX on NCC phosphorylation, total protein and mRNA

The level and rhythm of NCC phosphorylation was significantly blunted in ADX animals compared to intact animals, with NCC phosphorylation being comparable during the day but failing to increase at night. Total NCC protein was significantly reduced at both time points but surprisingly mRNA was no different between ADX and intact animals. There was a reduction in total protein levels following ADX and this is consistent with the idea that adrenal hormones are required for the basal tone of thiazide-sensitive sodium transporter activity. It is curious that no changes were detected in mRNA, a phenomenon that has been reported previously by others [121, 184, 185]. One predicts that a similar quantity of NCC mRNA is produced and therefore there are two potential explanations for the changes seen in total protein: either a smaller proportion is translated or a significant amount of the protein product is turned over in the absence of adrenal hormones. The latter seems more feasible as NCC is constitutively internalised and phosphorylation both reduces this process of internalisation [101] and seems to protect NCC from ubiquitinylation through CUL3, KLHL3 and WNK-mediated pathways [95, 102, 186].

4.4.3. Effect of ADX on diurnal changes of renal transcript abundance

The adrenal gland has been described as the main temporal mediator of peripheral tissue oscillators [187] but intriguingly, ADX appeared to have very little effect on any of the renal transcripts examined here: differentially expressed genes that were present in the adrenal intact animals exhibited similar expression patterns in the ADX animals. It is possible that extra-adrenal corticosteroid sources release hormone rhythmically, but its amplitude was too low for detection in our setup but was enough to entrain the renal clock. However, whether extra-renal corticosteroid production exhibits rhythmicity is presently unknown. The second possibility is that the kidney has an intrinsic and autonomous clock that maintains a 24-hour rhythm that can oscillate independently of external cues if these cues are below a certain threshold. There are several lines of evidence that support the latter argument. ADX or specific targeted ablation of the adrenal clock does not abolish the rhythm of most renal clock genes, including clock, per2, bmal1 [75, 187] but does affect the rhythm of PER1 [75, 187] [72]. In the current chapter, detectable changes in PER1 expression in intact animals were not found at our time points. The circadian rhythm of PER1 has been defined with the circadian gene expression atlas (CIRCA: http://bioinf.itmat.upenn.edu/circa/). The CIRCA data by Hogenesch and colleagues indicate that our time points, ZT6 and ZT 18 are likely during the trough of PER1 expression in the kidney [43]. Therefore it is perhaps unsurprising that no major differences were detected in *per1* expression in this setting.

4.4.4. Effect of ADX on sodium balance

Welfare concerns prevented a metabolic cage experiment for an analysis of urinary output and sodium balance in these ADX versus intact animals. The literature does offer some insight. Previous findings in cats [188], dogs [189] and humans [190] have shown that ADX causes hyponatremia and volume constriction attributed to natriuresis and diuresis [191]. All ADX animals exhibit some degree of salt wasting, although morbidity and mortalities appear to be prevented by the replacement of drinking water with 0.9% saline. Consistent with the literature [192], the ADX animals in these experiments had a salt appetite. In rats, the circadian rhythm of sodium excretion was only mildly perturbed by ADX with acrophase appearing ~3 hours earlier with period comparable with intact rats [193]. Total sodium or the amplitude of sodium excretion in this case was not reported. Other transporters are also affected by ADX: the epithelial sodium transporter gamma subunit is markedly reduced in ADX animals [181] as is the net sodium transport within the loop of Henle [194].

In conclusion, the activity of sodium transporters is clearly reduced in ADX animals. The work in this chapter has further demonstrated this in the reduction of NCC phosphorylation following ADX. However, the rhythmicity of sodium excretion is likely to persist, conceivably through the action of a retained autonomous renal clock affecting renal function but also perhaps as a result of the retention of normal circadian patterns of feeding and drinking behaviour.

4.4.5. Effect of chronic corticosterone treatment on plasma and urinary corticosterone and urinary aldosterone

Corticosterone levels were effectively clamped at an intermediate level using silastic slow release pellets, with daytime plasma levels markedly raised and nighttime levels slightly dampened. The day/night difference in urine corticosterone excretion levels was also markedly reduced in the corticosterone pellet group compared to the vehicle treated animals. The other major corticosteroid, aldosterone is unlikely to have been greatly affected by corticosterone in this context. Corticosterone feedback mechanisms may reduce ACTH levels, which could in turn affect the rhythm of aldosterone synthesis. However, several experiments in humans suggest that the circadian rhythms of ACTH and aldosterone are uncoupled, with aldosterone being more reliant on levels of angiotensin II and renin secretion in non-diseased states [195, 196]. Our data is in agreement with this, as corticosterone pellets, which may conceivably reduce ACTH levels, had no effect on the urinary excretion levels of aldosterone.

4.4.6. Effect of chronic corticosterone treatment on NCC phosphorylation and total NCC

The rhythm of NCC phosphorylation at T53 was perturbed in the corticosterone-clamped mice. The vehicle treated mice exhibited a robust difference in phosphorylation at pT53 at night compared to the day. Interestingly, a small difference in phosphorylation was also found at S71 in the vehicle treated group. It is unclear why this may be the case in these control animals but not in the previous cohort but one possible explanation is that the slightly larger sample size permitted the detection of this change. Again, this difference in pS71 was not seen in the corticosterone-treated animals. No change in total protein was seen in either treatment group. This either indicates that glucocorticoids cannot alter NCC protein levels but activate an existing pool controlled by other systems, or that the intermediate levels of GC over 5 days was not of long enough duration or magnitude to evoke a change in protein levels. There is currently no data in the literature describing the long-term effects of GC on

total NCC protein levels. But salt restriction, accompanied by an increase in both aldosterone and angiotensin II, evoked an increase in total NCC within 3 days in rats [197]. Our analysis was performed after 5 days; therefore it's likely the small physiological change in GC levels was not a large enough stimulus to evoke total protein changes. Other investigators attribute the diurnal rhythm of NCC phosphorylation to aldosterone [160] showing that chronic MR blockade (with eplerenone) abolishes the phosphorylation rhythm. This does not necessarily prove aldosterone is causal as GCs can bind both MR and GR, but it does suggests that MR regulates the diurnal rhythm of NCC.

4.4.7. Effect of chronic corticosterone treatment on the diurnal variation of renal transcripts

Both GILZ and sgk1 expression was increased only during the daytime in corticosterone-treated mice. This is consistent with the idea that the corticosterone treatment clamped various genes "ON". *Sgk1* and *GILZ* are expressed throughout the kidney. *Sgk1* has a key role in both NCC and ENaC regulation, promoting the increase of both transporters' activity. GILZ acts to recruit and stabilise SGK1 in the ENaC regulatory pathways [198]. The effect of GILZ in the NCC regulatory cascade is not well defined but appears to oppose the activity of sgk1 [199]. It is unclear therefore why GILZ was upregulated at night in our vehicle treated animals and during both night and day in our corticosterone treated animals, when NCC phosphorylation is increased. *GILZ* could be acting as part of a negative feedback system, acting in opposition to *sgk1* to begin the process of turning NCC phosphorylation off. Another explanation is that since the qPCR data presented here are from whole kidney; these changes could reflect an increase in *GILZ* expression in other parts of the nephron. Indeed the pattern of the *GILZ* circadian rhythm is considerably shallower and very slightly phase shifted in CCD compared to DCT/CNT segments [42].

While ADX did not affect circadian clock genes, clamped plasma corticosterone levels increased the daytime levels of *cry1* and *bmal1* and induced *per1* at nighttime and daytime while *per2* expression rhythms were unchanged. Many studies have shown similar changes in clock genes following GC treatment [75, 187] [72]. *Per1* is particularly affected by GCs and this may be directly relevant to NCC activation. A proposed working model for how clamped corticosterone may affect per1 and the downstream consequences is illustrated in Figure 4.12. Recently Richard's et al demonstrated that per1 could bind to WNK1, WNK4 and slc12a3 promoters [56]. No differences were found in NCC or WNK4 transcript in this chapter, but changes in WNK1-KS were not explored. WNK1-KS does not require

posttranslational modifications to be activated and therefore a change in its transcription could directly affect NCC phosphorylation, but this remains to be explored. The authors did not investigate any per1-induced posttranslational modifications of proteins within the NCC regulation cascade, so it remains to be seen whether these changes are possible or relevant.

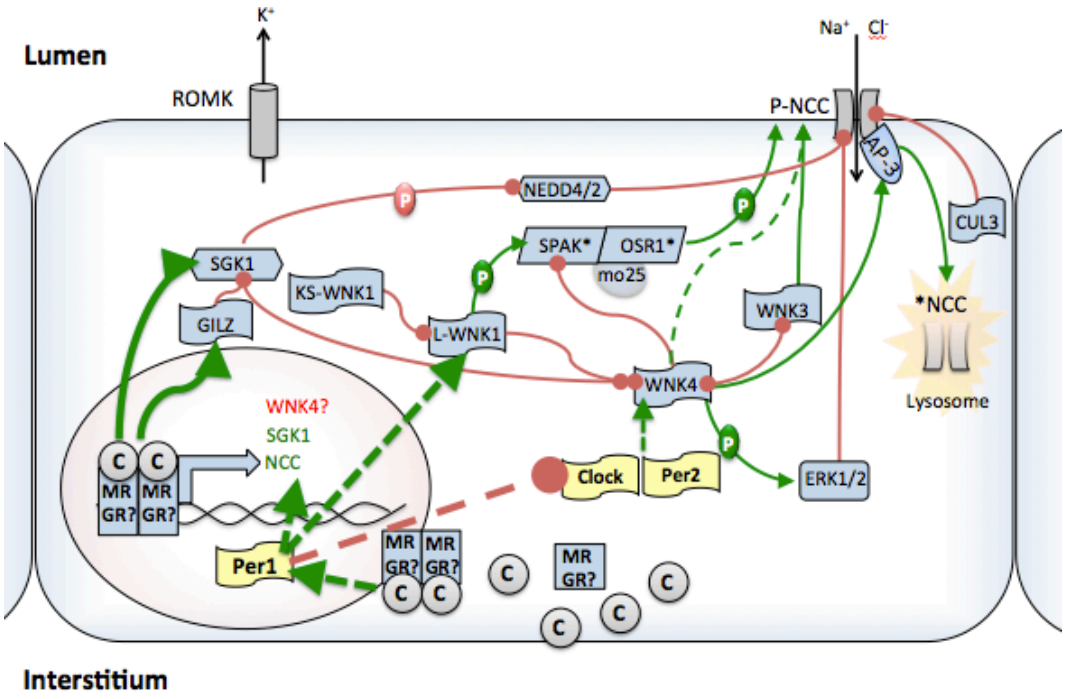

Figure 4.12: Diagram illustrating the current paradigm for the regulation of the sodium chloride co-transporter (NCC) including implicated clock genes. Enlarged arrows highlight the pathways affected by clamped corticosterone levels.
Corticosteroid (C) induced MR or GR activation, dimerization and translocation to the nucleus, promotes the transcription of NCC and inhibits WNK4 expression following prolonged corticosteroid exposure. WNK4 is generally accepted to be an inhibitory regulatory kinase of NCC and how WNK4 is activated is still unknown. SGK1 and L-WNK1 inhibit WNK4 and thus promote NCC activity through relief of WNK4-mediated inhibition of the STE20/SPS-1-related-proline/alanine-rich kinase and oxidative stress response kinase 1 (SPAK/OSR1) complex. Mouse protein 25 (mo25) is a positive regulator of SPAK/OSR1. SGK1 is also postulated to inhibit Nedd4/2, which can also ubiquitinylate NCC. GILZ on the other hand acts in opposition to SGK1. Kidney specific WNK1 (KS-WNK1) is a negative regulator of L-WNK1 and thus promotes WNK4 driven inhibition of NCC. Further WNK4-mediated inhibitory pathways include inhibition of the NCC-stimulatory kinase WNK3 and stimulation of inhibitory protein ERK1/2 and the adaptor protein 3 (AP3). AP-3 facilitates lysosomal transport and thus WNK4 redirects NCC to the lysosome. Cullin 3 (CUL3) acts to promote NCC ubiquitinylation. Per1 can promote NCC and WNK1 transcription and prevent the binding of clock and per2 to the WNK4 promoter. (Red connectors represent inhibition through phosphorylation (P) or otherwise, while green arrows indicate stimulation by phosphorylation (P) or otherwise. Interrupted green arrows represent speculative or controversial events).

4.4.8. Effect of chronic corticosterone administration on sodium handling

Clamped plasma corticosterone reduced the amount of sodium excreted at nighttime. This was not an effect of altered sodium intake, as food intake was similar between groups. The literature has conflicting reports on the effect of GCs on sodium excretion. Chronic GC treatment evokes natriuresis, but can also activate anti-natriuretic sodium transporters in both the DCT [103] and the ASDN [200]. Systemic GR expression means that GCs have pleotropic actions that are often countervailing [92]. In this case a physiologically subtle change in GC levels did not drastically alter natriuresis but reduced natriuresis only at night. Conceivably this could be as a result of increased NCC activation although it is unclear why this is not temporally aligned with NCC activation (aberrant NCC activation as measured by phosphorylation levels occurs in corticosterone clamped animals at midday but dampened-natriuresis appears during the 12 hour night urine collection with no differences in the 12 hour day collection). It is possible that our urine collections lacked the temporal resolution required to reveal any differences present during the day. During the daytime it is possible that the mice are retaining sodium but a reduction in micturition and bladder retention of urine that occurs during the day means that differences that may have occurred as a result of daytime sodium excretion can only be seen at night when this urine is voided. It is interesting that Bankir et al suggest that BP is raised during rest as a result of an inability to excrete sufficient sodium during wakefulness [26]. It certainly appears that there is reduced sodium excretion during wakefulness in corticosterone-clamped mice but whether this leads to changes in BP is yet to be determined.

4.4.9. Summary of Chapter findings

1) ADX blunted NCC phosphorylation rhythm and reduced the total NCC protein.
2) Rhythms of clock proteins bmal1, cry1, per2 are retained in ADX animals
3) The implantation of slow release corticosterone pellets suppressed the rhythmicity of plasma corticosterone without changing urinary aldosterone excretion.
4) Clamped plasma corticosterone levels abrogated the diurnal rhythm of NCC phosphorylation at T53 without any changes in total NCC.
5) Day time levels of Bmal1, cry1, GILZ and SGK1 were raised in mice with clamped corticosterone levels
6) Both day and nighttime levels of per1 were increased while per2 was unaffected in mice with clamped corticosterone levels.
7) Clamped plasma corticosterone caused perturbations in the rhythm of sodium excretion that could not be attributed to changes in sodium intake.

5. Role of NCC and GCs in the circadian regulation of BP and sodium balance

5.1. Introduction

In the previous chapter it was shown that GCs affect the diurnal rhythm of NCC phosphorylation: NCC phosphorylation is inappropriately elevated during the day in mice with chronically clamped plasma corticosterone levels. NCC reabsorbs 5-10 % of the total filtered load and plays important roles in BP homeostasis. Therefore this chapter aims to investigate the functional consequences of this perturbed NCC phosphorylation rhythm. The two major aims of the experiments in this chapter were to assess whether day and night differences in NCC phosphorylation translated into day and night differences in thiazide-sensitive sodium transport and to investigate the effect of corticosterone clamping of NCC activity on the circadian rhythm of BP.

To carry out these experiments we collaborated with iPRECIO (Japan, http://www.iprecio.com), a company that have designed state-of-the art programmable micro-osmotic minipumps (model SMP300, iPRECIO) suitable for implantation in mice. This product was in the late beta testing phase and we were one of the first centres to use these pumps in experimental animals. This chapter addresses the series of experiments leading up to the design of a small pilot experiment using these programmable pumps.

5.1.1. Aims

1. To investigate whether there is a difference in thiazide sensitive sodium transport during the day compared to the night.
2. To assess the effects of chronically clamped corticosterone and HCTZ treatment on BP, HR and activity.

5.1.2. Strategy for addressing the chapter aims:

1. A series of pilot experiments was designed in order to select an appropriate NCC inhibitor and dose for use in the beta phase testing experiments using iPRECIO micro-osmotic programmable mini-pumps. The second half of this chapter outlines the series of experiments and the final pilot experiments performed in an attempt to resolve diurnal differences in NCC-mediated sodium reabsorption.
2. In order to assess rhythmic blood pressure changes, recordings need to be made in conscious unrestrained animals using radio-telemetry. Following 10 days of baseline

measurements, mice were randomised to receive either vehicle or corticosterone slow release pellets. Initial experiments were designed with the intention to resolve differences in nighttime and daytime dosing of HCTZ by injection. However, pilot experiments showed that any blood pressure lowering effects of HCTZ were masked by large increases in blood pressure caused by handling and injection of the drug; therefore a simple chronic approach was taken. All the telemetered mice were treated with a dose of ~80 mg/kg/day HCTZ in their drinking water. This minimised experimenter interference, allowing changes in rhythmicity to be more clearly defined.

5.2. Methods

Detailed methods of each of the major procedures in this chapter are described in the main methods chapter. For clarity, an outline of the experiments is presented here. The full experimental protocols for the programmable minipump experiments are also described here.

5.2.1. Experimental work up for micro-osmotic minipump experiment

Several key experiments lead to the decision to use HCTZ at 20 mg/kg in the final "Programmable micro-osmotic mini-pump" pilot experiment. These are explored in this chapter. The limitations of the iPRECIO pumps meant that the selection criteria for a suitable drug were strict. The drug should display:

Criteria:

1) Specific and efficacious inhibition of NCC
2) Good bioavailability via subcutaneous administration
3) Solubility to achieve desired concentration in 200 µl reservoir and achieve desired dosing with a maximum delivery rate of 10 µl/hour

5.2.1.1. Thiazide diuretic choice

Both bendroflumethiazide (BFMZ) and hydrochlorothiazide (HCTZ) have been used in experimental animals [147, 201]. BFMZ has greater selectivity for NCC [202] whereas HCTZ can also inhibit carbonic anhydrase [202]. At higher doses thiazide diuretics can reduce GFR through tubulo-glomerular feedback effects [203]. The first experiments, performed in terminally anaesthetised C57BL6 mice, compared the effects of BFMZ and HCTZ on renal blood flow, GFR and sodium handling. Mice (n=8-12) underwent renal clearance surgery (described in detail in Methods 2.8) and following 40-minute baseline urinary collections, either 6 mg/kg BFMZ, 20 mg/kg HCTZ or 2% DMSO was administered

(i.v.). Following 20 minutes equilibration, urine was collected for 40 minutes. Urine was analysed as outlined in the main methods section (2.8.3).

5.2.1.2. Bioactivity of BFMZ

These experiments were designed to test whether BFMZ was effective when administered subcutaneously and therefore suitable for use in the programmable mini-pumps. A secondary aim was to assess the time course for natriuresis so that we could design experiments to capture the "peak" natriuresis. C57BL6 mice (n=10) were housed in metabolic cages and fed a gelled diet (outlined in main methods section). Following acclimatisation (5 days) mice were injected (i.p. or s.c.) with BFMZ or 50 % DMSO at ZT 12 (7 pm local time) and urine was collected for 12 hours. A further 12-hour collection was made without any prior injection. 24 hours was allowed between injections to allow for the clearance of the drug. An initial dose of 6 mg/kg BFMZ was used but evoked no natriuresis. The maximum that was soluble in 50 % DMSO (24 mg/kg) was then tested. An injection volume of 40 μl was used to mimic the maximum volume that would be delivered by micro-osmotic mini-pumps at any single time-point.

In order to test whether natriuresis was followed by a period of anti-natriuresis, which could mask the natriuretic effect of BFMZ, hourly urine collections were performed during the day after BFMZ or vehicle injection at ZT 0. Urinary sodium and potassium concentration were measured by ion sensitive electrode (9180 Roche Electrolyte Analyser, Roche Diagnostics, UK). BFMZ did not cause natriuresis at any point during these experiments and was therefore rejected as a suitable drug for use in micro-osmotic mini-pump experiments.

5.2.1.3. Bioactivity of HCTZ

Two experiments were performed to assess the extent and time course of natriuresis in response to HCTZ (20 mg/kg). First, C57BL6 mice (n=10) were acclimatised in standard cages to a reverse day/night cycle (for 14 days) and then acclimatised to metabolic cages with standard powdered chow for 5 days. HCTZ (20 mg/kg in volume of 150 μl/30 gbw in 2 % DMSO i.p.) or vehicle (2 % DMSO) was administered at 8am (ZT 1) and urine collected for 6 hours. The second experiment tested whether subcutaneous administration of HCTZ produced natriuresis. A small group (n=4) of mice underwent renal clearance surgery under terminal inactin anaesthetic (as described in Main Methods). A 30-minute baseline collection was made followed by injection (s.c.) of 30 μl 20 mg/kg HCTZ and urine was collected

every 30 minutes for 2 hours thereafter. These 2 studies were used to decide upon the thiazide diuretic for the micro-osmotic mini-pump experiment.

5.2.2. Programmable micro-osmotic pump experiments

5.2.2.1. In vitro testing of programmable micro- osmotic mini-pumps

The drug administration protocol was first assessed *in vitro*. One pump was programmed to release pink tissue culture fluid at a rate of 10 μl/hour for 4 hours (Figure 5.1, B). The pump was positioned on a fine balance (ISO9001, Sartorius) and the pump catheter placed into a 2 ml eppendoff tube, which was positioned off the balance. The volume released by the pump was calculated by loss of weight of the pump. The eppendoff was weighed at the end and fluid loss from the pump matched the fluid gained by the tube.

5.2.2.2. Surgical implantation of micro-osmotic mini-pumps

As the mice would be housed in metabolic cages throughout the duration of the experiment, the placement of the micro-osmotic mini-pumps needed to be carefully considered. Implantation down the flank through an incision made at the nape of the neck was chosen as the wound would be difficult for the mice to manipulate and the pump position would place limited pressure on the wound. The orientation of the incision site (Figure 5.1 D) meant that movement of the head did not open the wound but instead put pressure on wound closure.

Mice were anaesthetised under isofluorane using a 5 ml syringe nose-cone adaptation, given vetergesic (0.05 mg/kg) and positioned in ventral recumbency. Hair was removed from the dorsal cervical area with clippers and scrubbed with iodine scrub and ethanol. A ~15 mm transverse dorsal cervical incision was made and a subcutaneous pocket to the right of the midline. The device was prepared by trimming the catheter and the antenna was wrapped around the width of the device. These manipulations made the device more compact for implantation. The wound was then held open with forceps and device gently inserted, catheter-end first, using clean, gloved hand. The device was positioned down the left side, well away from the wound so as to not put any pressure on the wound.

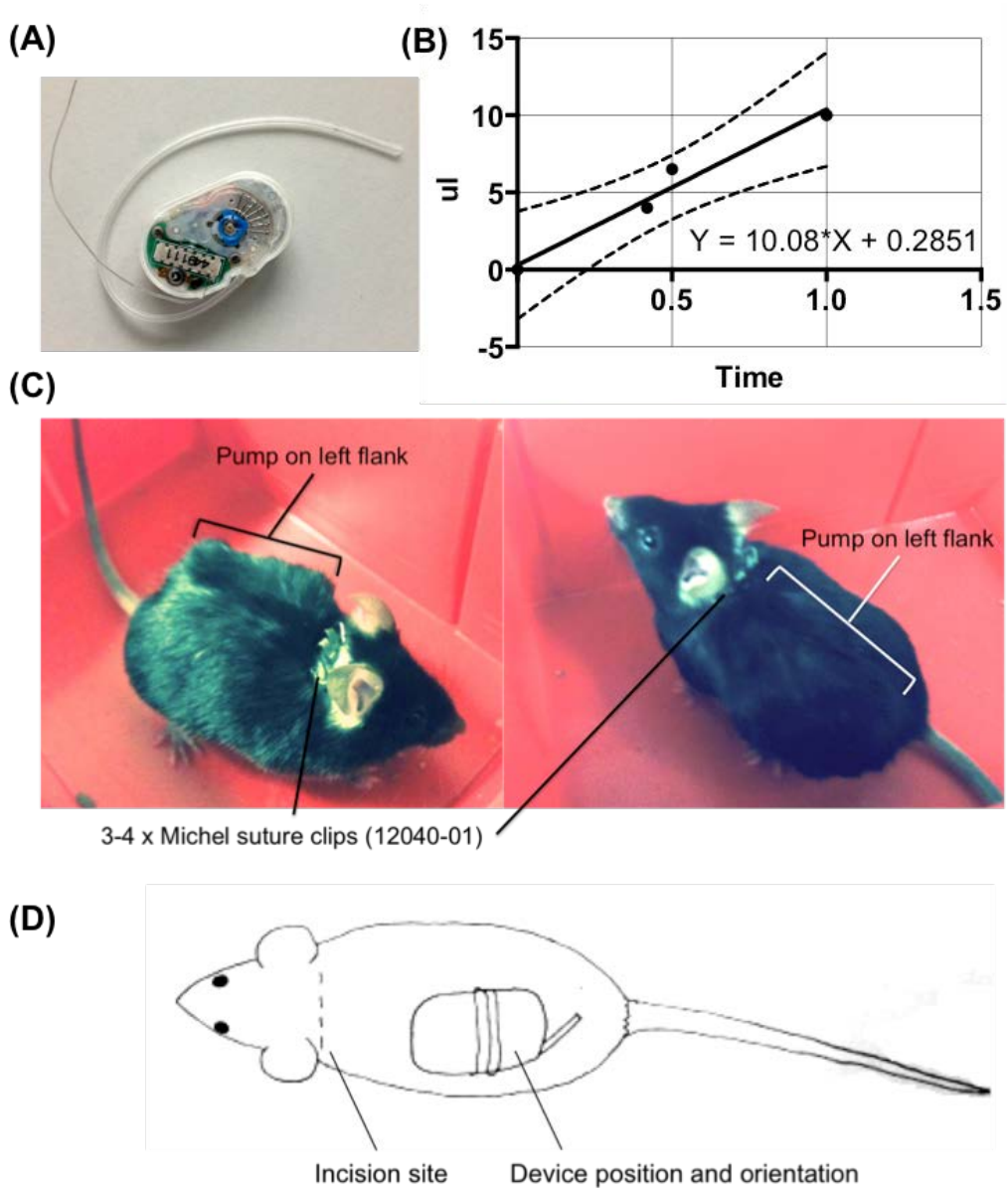

Figure 5.1: Micro-osmotic mini-pump (A), *in vitro* testing (B) & implantation site (C-D)
A programmable micro-osmotic mini-pump (A) SMP-300 (iPRECIO, Japan) was programmed to release at a rate of 10 µl/hour. The pump was placed on a fine balance with the long catheter emptying into an eppendoff tube. The release rate (B) was estimated by the reduction of weight over the programmed time period. Following programming pumps were implanted subcutaneously down the left flank in >25 g C57BL6 mice via a dorsal cervical incision (C, D).

The wound was closed with 3-4 Michel suture clips (7.5 x 1.75 mm). Mice regained consciousness in a hotbox (34^{o}C) within 5-15 minutes and were returned to their metabolic cages. Mice were given soft mash and vetergesic jelly for 24hours post op and were checked twice daily until the wound was healed.

5.2.2.3. Experimental setup for micro-osmotic pump experiments

A pilot experiment using programmable micro-osmotic mini-pumps (iPRECIO, Japan) was designed to administer HCTZ in conscious unrestrained mice without handling or injection. 8 male C57BL6 mice were acclimatised to metabolic cages for 6 days. The acclimatisation period included cage changeovers of all metabolic cage parts that come into contact with urine, i.e. funnel, filter, pots and metal grid at 12-hour intervals. Gelled diet dries out after 24 hours and requires daily replacement. The mice tend to eat large quantities of gelled diet when they are first introduced it to it, therefore if this was performed daily it would cause a surge of eating and urinarting at the point of food introduction. To evenly distribute this bias between day and night fresh gel diet was given at 12-hourly intervals. After acclimatisation micro-osmotic pumps and either vehicle or corticosterone slow release pellets were implanted under isofluorane anaesthetic. These pumps were pre-programmed via wireless technology using the accompanying software and programme set to start several hours after surgical implantation. The programmable pumps could only administer one drug and with a limited supply of pumps (we were donated a total of 10 pumps, two of which were used for *in vitro* experiments and surgical optimisation), a vehicle group could not be included. A "no drug" period of urine collections, which was performed at the same times but on the consecutive day/night after drug release when the pumps were set to release at a rate of 0 μl/hour was used as a control in the absence of a vehicle group.

The experimental protocol is illustrated in Figure 5.2. The pump rate was set at 0 μl for the first 3 days after implantation to allow recovery. This was the maximum length of time the pumps could be programmed to release at a rate of 0 μl/hour without compromising drug release. Furthermore the maximum battery life for the devices was ~10 days. HCTZ was administered at a rate of 10 μl/hour over 3 hours local time 11.30-14h30 (ZT 4.5-7.5) to achieve a dose of 20 mg/kg. Following a 33-hour break, where the pumps were programmed to administer at a rate of 0 μl/hour, HCTZ was released again between 23.30-2h30am (ZT 16.5-19.5). These HCTZ-administration times were chosen to span the period over which kidneys had previously been taken for NCC phospho-analysis (i.e. at 1am and 1pm local time). At these time points the difference in NCC phosphorylation was at least 2 fold and therefore we hypothesised that differences in thiazide-sensitive sodium transport should be high at these points. This cycle of dosing was repeated. Overall this experiment produced 2 day and 2 night collections under: (i) no drug and (ii) HCTZ infusion. During the first cycle of dosing, urine was collected hourly over 6 hours to span the period of drug release. However the experimenter (Ivy/Bailey) noted significant disturbance of the animals, most

evident during the “sleep” period, rendering unambiguous interpretation of the data difficult. During the second cycle, therefore, 5-hour urine collections were made to minimise disturbance of the animals. Only these data are presented here (Urine samples 5-8).

Figure 5.2 (overleaf): Timeline of experimental setup for micro-osmotic minipump experiment
8 male C57BL6 were individually housed in metabolic cages. After 6 days acclimatisation, mice were anaesthetised under isofluorane and implanted with programmable micro-osmotic minipumps and either vehicle or corticosterone slow-release pellets (n=4). Pumps were programmed to release no drug (i.e. at a rate of 0 μl/hour) for 3 days to allow recovery from anaesthetic. After this, pumps released HCTZ at a rate of 10 μl/hour for 3 hours at ZT 4.5 – 7.5 to give a dose of 20 mg/kg this was followed by a 33-hour gap in drug release during which control urine collections were performed. HCTZ was administered again for 3 hours at a rate of 10 μl/hour at ZT 16.5-19.5 followed by another 33-hour gap in drug release. This protocol was repeated and urinary collections from two rounds of day and night HCTZ release and two rounds of no HCTZ release were obtained.

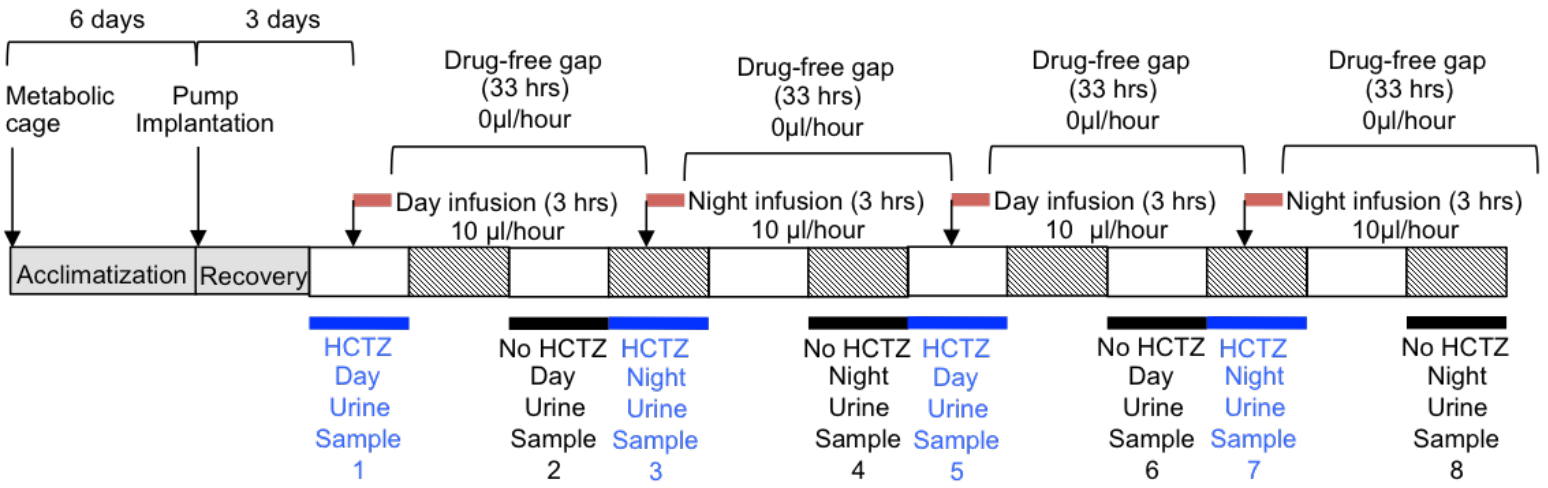
6 days
3 days
Metabolic cage
Pump Implantation
Drug-free gap (33 hrs) 0µl/hour
Drug-free gap (33 hrs) 0µl/hour
Drug-free gap (33 hrs) 0µl/hour
Drug-free gap (33 hrs) 0µl/hour
Day infusion (3 hrs) 10 µl/hour
Night infusion (3 hrs) 10 µl/hour
Day infusion (3 hrs) 10 µl/hour
Night infusion (3 hrs) 10µl/hour
Acclimatization
Recovery
HCTZ Day Urine Sample 1
No HCTZ Day Urine Sample 2
HCTZ Night Urine Sample 3
No HCTZ Night Urine Sample 4
HCTZ Day Urine Sample 5
No HCTZ Day Urine Sample 6
HCTZ Night Urine Sample 7
No HCTZ Night Urine Sample 8

5.2.3. Experimental setup for radio-telemetry experiments

Radio-telemeter devices were implanted and experiments were performed in a single cohort of 14 C57BL6 mice. Telemetry implantation surgery was performed as outlined in Methods Chapter and mice were single-housed in quiet 12-hour light dark conditions. BP waveforms were assessed once a week for quality control. In 3 of the 14 mice, blood pressure waveforms were inconsistent (Figure 5.3), with shallow waveforms (Figure 5.3 B, E) or huge fluctuating measurements after 2 weeks of recording (Figure 5.3 H). These devices were from both vehicle and corticosterone groups with one from the vehicle group (Figure 5.3. A, B, C) and two from the corticosterone treated group (D, E, F & G, H, I). All three of these mice were excluded from the analysis and all three device failures reported to the manufacturers (DSI) for further investigation.

The experimental timeline is outlined in Figure 5.4. Routine husbandry and HCTZ administration were performed under red light during the active phase (between ZT 12 and ZT 0) to minimise inactive phase disturbances. Water bottles were weighed in order to estimate the concentration of HCTZ required for a ~80 mg/kg/day dose and further weighed post dosing. The mice did not change their intake of water following HCTZ dosing. Adequate HCTZ dosing was assessed by mass spectrometry of terminal plasma samples taken between ZT 14-ZT 16 (Methods 2.9). In order to verify that the plasma corticosterone clamping was sustained throughout the experiment, blood was sampled at ZT 0 and ZT 12 in vehicle and corticosterone treated mice on the last day of the telemetry experiment i.e. four weeks after implantation.

Figure 5.3 (overleaf): Wave forms from before and after device failure
Three/fourteen devices produced inconsistent readings during this experiment and were therefore excluded from the analysis. Waveforms were steady during recovery post surgery (A, D, G), but each deteriorated at different points during experimental recording (B, E, H). The inconsistencies in the recordings can be seen in the moving average systolic blood pressure data for the entire experiment where each failed recording is compared to vehicle moving average (C, F, I).

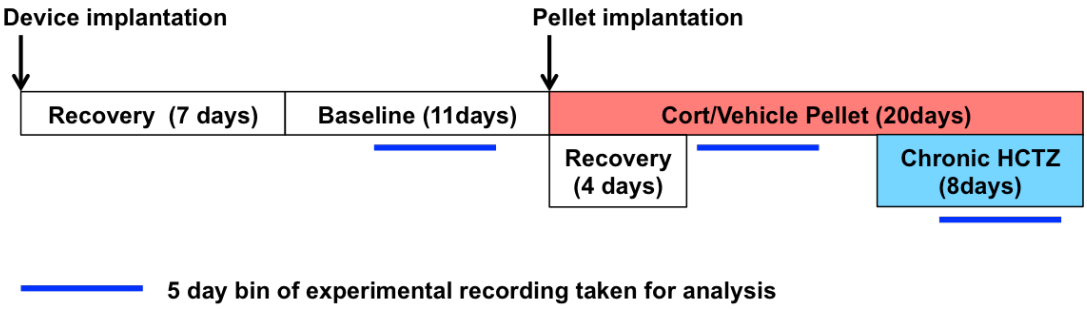

Figure 5.4: Time line of experimental setup for telemetry experiment.
Male C57BL6 were implanted with radio telemeter devices under isofluorane anaesthetic. After 7 days of recovery 11 days of baseline recordings were made. Corticosterone or vehicle pellets were then implanted under isofluorane anaesthetic. Following 4 days recovery further recordings were taken. For the final 8 days of the experiment drinking water was replaced with HCTZ to achieve a dose of 80 mg/kg.

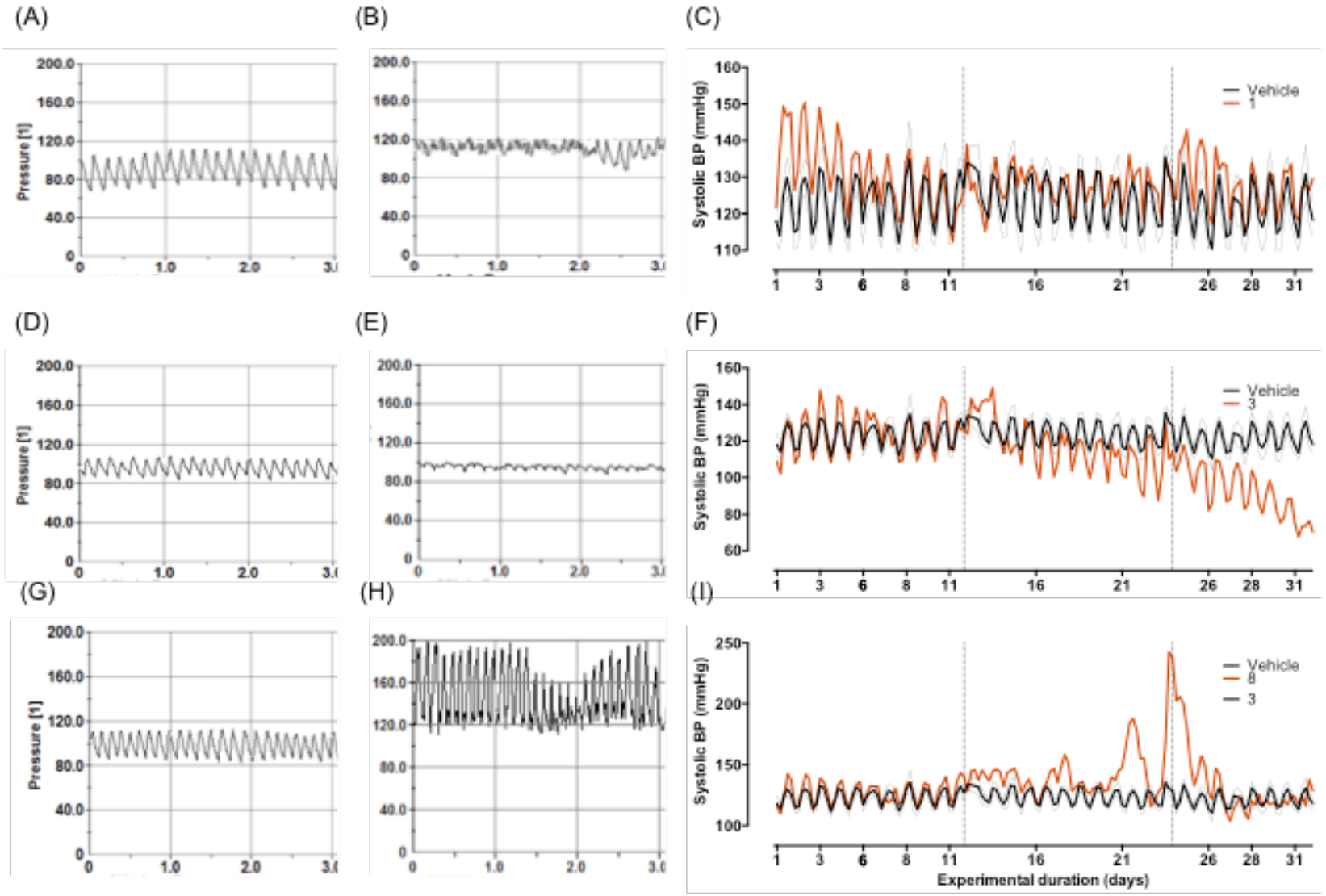
(A)
(B)
(C)
(D)
(E)
(F)
(G)
(H)
(I)
Pressure [1]
Systolic BP (mmHg)
Vehicle
1
3
8
Experimental duration (days)

5.2.4. Analysis of telemetry data

Recordings were taken for 1 minute every 30 minutes throughout the duration of the experimental timeline. Five-day bins of experimental recordings were taken forward for the analyses; these were chosen on the basis that systolic blood pressure was in steady state during these windows (by visual assessment of the entire data set). Data analysis was performed using several different methods. In the first instance, to allow better visualisation of the data, the data were smoothed using a simple moving average over 5 hours (performed using DSI Data Quest ART software). Day versus night differences were compared by using the mean day (ZT 3-8) or mean night (ZT 15-20) averaged over the selected 5 days. Finally as systolic blood pressure is most associated with pathology [204] we next undertook a more sophisticated cosinor analysis of these data. The method for this is detailed in the main methods chapter (Methods 2.6.3).

5.3. Results

A series of experiments was conducted with the primary objective of designing an experiment using programmable minipumps (iPRECIO, Japan) to administer NCC inhibitors differentially at night/day in conscious unrestrained animals.

5.3.1.1. Drug choice: BFMZ or HCTZ

Renal clearance experiments in anaesthetised C57BL6 mice were designed to test the effect of vehicle (2% DMSO), HCTZ (20 mg/kg) or BFMZ (6 mg/kg) on electrolyte excretion and renal function. Both diuretics caused a marked increase in sodium excretion ($p=0.0002$, HCTZ and $p<0.0001$ for BFMZ, Figure 5.5, A). Both diuretics increased potassium excretion ($p=0.0002$, HCTZ and $p<0.0001$ for BFMZ, Figure 5.5, B). GFR as measured by inulin clearance was unchanged by vehicle ($p=0.15$) or BFMZ ($p=0.98$) but decreased with HCTZ treatment ($p=0.013$, Figure 5.5 C). BFMZ and vehicle had little effect on renal blood flow ($p=0.18$, $p=0.83$ respectively) but HCTZ increased renal blood flow ($p=0.03$, Figure 5.5, D). The change in fractional sodium excretion with diuretic was greatest with BFMZ at ~8% of the total load, with HCTZ ~6% of the total sodium load (Figure 5.5 E). BFMZ offered considerably better stability of renal function and therefore was taken forward for further testing.

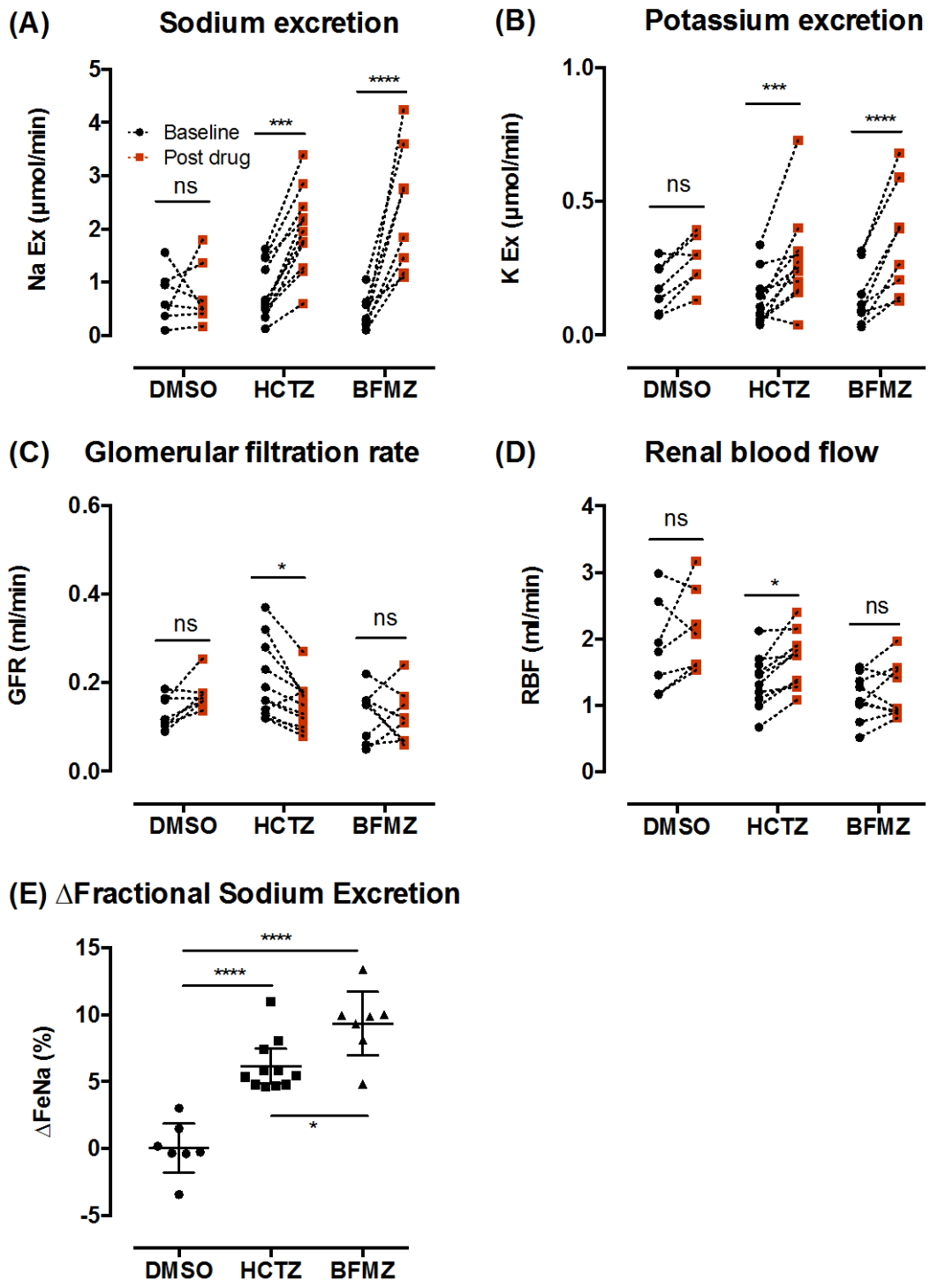

Figure 5.5: Renal clearance parameters and electrolyte excretion in anaesthetised C57BL6 mice at baseline and following a bolus injection of 2% DMSO, hydrochlorothiazide (HCTZ) or bendroflumethiazide (BFMZ)

Sodium excretion, (A) potassium excretion (B), glomerular filtration rate (GFR, C) and renal blood flow (RBF, D) in anaesthetised C57BL6 mice at baseline and following bolus injection of 2% DMSO, HCTZ (20mg/kg), or BFMS (6mg/kg). Change in fractional sodium excretion from baseline following DMSO, HCTZ, BFMZ (E). Data were analysed by matched two-way ANOVA with post hoc Sidak tests (n=7, DMSO, n=11, HCTZ, n=7 BFMS).

5.3.1.2. Does subcutaneous BFMZ injection induce natriuresis?

6 mg/kg BFMZ was administered (s.c.) and urine collected over the next 12 hours. This dose did not cause natriuresis therefore the dose was increased to the maximum soluble in 50% DMSO for a volume of 40 µl, which was 24 mg/kg. This was injected s.c. and i.p. and urine collected over 12 hours after injection. 24 hours was allowed between injections to allow the drug to clear (half life ~6-8 hours [205]). Sodium excretion following injection (s.c. or i.p.) was not different to sodium excretion following vehicle injection or following no injection (Figure 5.6, A). Potassium excretion was also unchanged by any injection (Figure 5.6 B). Diuretic braking can occur in response to loop diuretics and involves a period of compensatory sodium retention post diuretic administration [206]. To test whether this phenomenon was affecting these experiments, hourly urine collections were carried out following s.c. injection of BFMZ (during the day). Sodium excretion was comparable at every time point following sub-cutaneous injection of BFMZ or vehicle (50% DMSO) (Figure 5.6, C). We hypothesised that BFMZ may have poor bioactivity when administered subcutaneously. Further increases in BFMZ dose would not be possible in the mini-pump experiment so BFMZ was rejected as a suitable drug for these experiments.

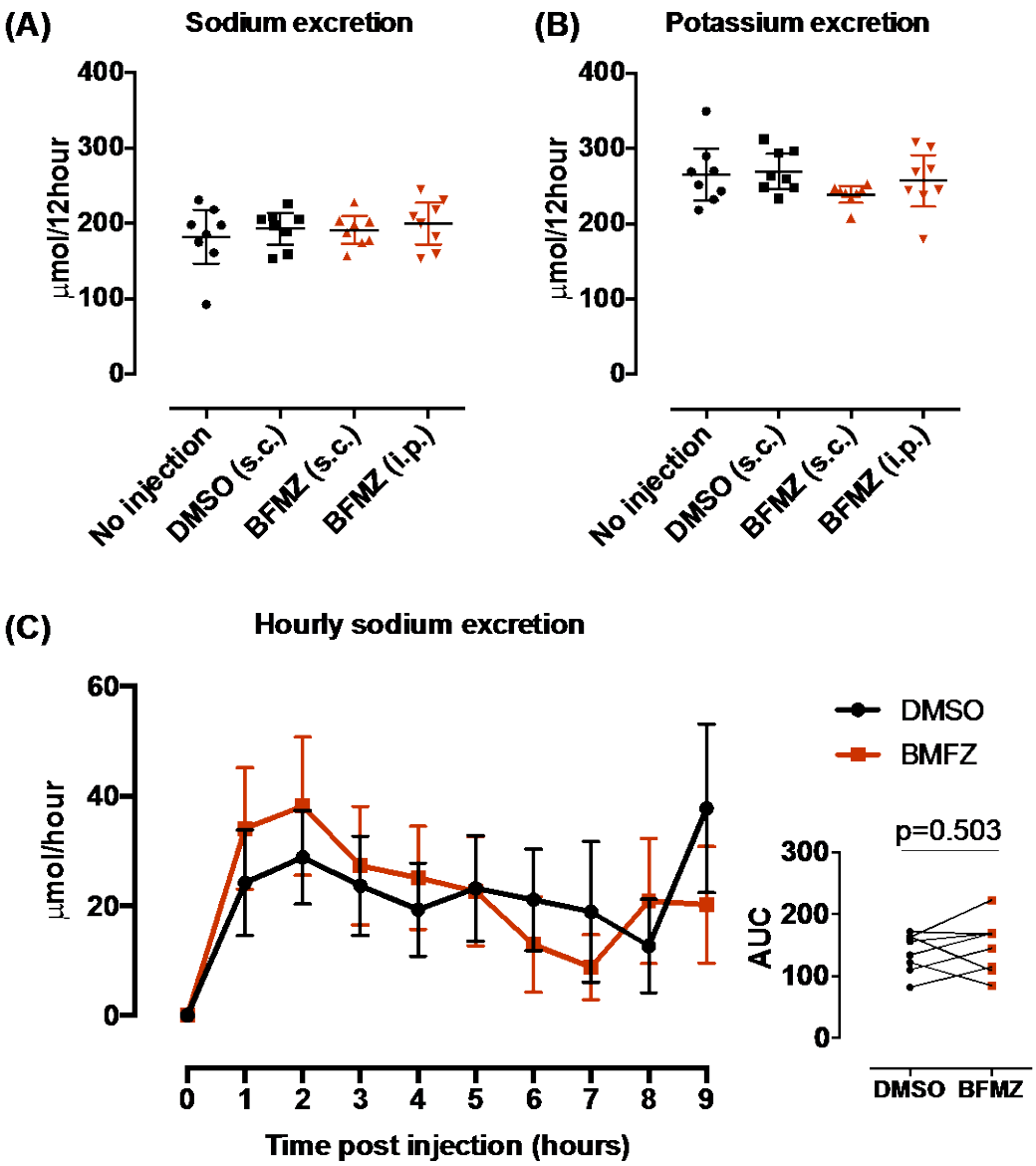

Figure 5.6: Sodium (A) and potassium (B) excretion 12 hours following 24 mg/kg BFMZ or vehicle (50% DMSO) subcutaneous (s.c.) and (C) intra-peritoneal (i.p) injection and hourly sodium excretion following 24 mg/kg BFMZ or vehicle injection (s.c)

Data in (A) and (B) was analysed by repeated measures one way ANOVA, no differences were found between BMFZ and controls. Area under the curve (AUC) data was analysed by a paired t test. Data are mean± 95% CI, n=8.

5.3.1.3. Bioactivity of HCTZ

HCTZ also inhibits NCC and is considerably more soluble than BFMZ. Urine was collected in C57BL6 mice for 6 hours following HCTZ (20 mg/kg) injection (i.p). HCTZ injection caused natiuresis (Figure 5.7 A, p=0.0058, n=10) in 8 out of 10 mice. However, this was via the i.p. route and micro-osmotic mini-pump experiments would require s.c. administration. Therefore, experiments were conducted in anaesthetised mice to assess whether HCTZ was efficacious via s.c. route. A dose of 20 mg/kg caused natriuresis in anaesthetised mice within 30 minutes of s.c. injection, which lasted for 2 hours (Figure 5.7 B). Therefore this drug was taken forward for use in micro-osmotic mini pump experiments.

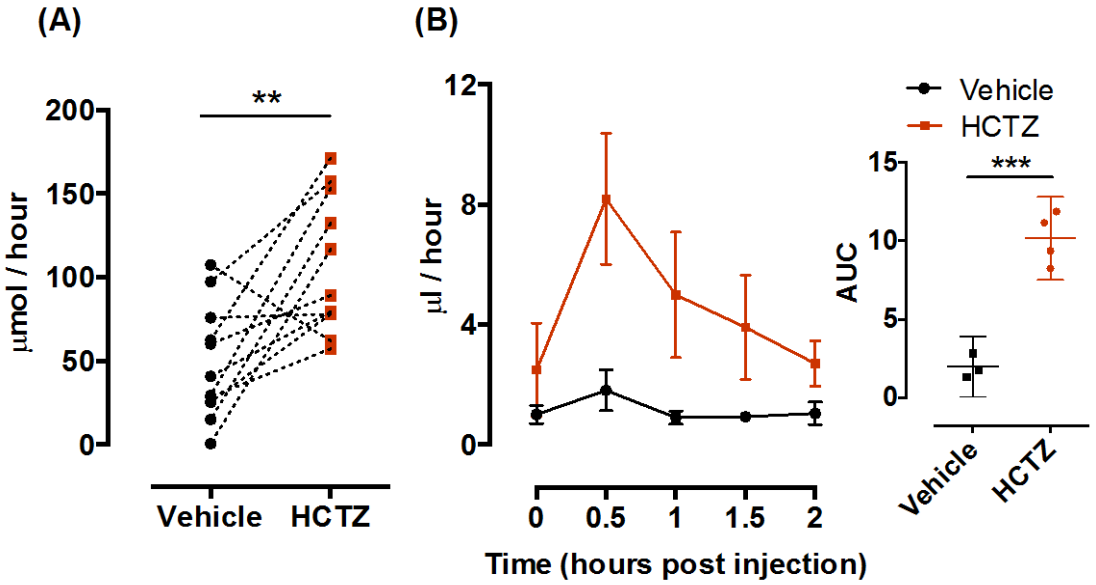

Figure 5.7: Sodium excretion following 20 mg/kg HCTZ injection (i.p) in conscious (A) and anaesthetised (B) C57BL6 mice.
Urinary sodium excretion in conscious animals (A) was analysed by paired t test, n=10. Urinary excretion in anaesthetised animals (B) was analysed t-test analysis of the area under the curve with n=3 (vehicle) and n=4 (HCTZ). Data are mean ± 95% CI.

5.3.2. Micro-osmotic mini-pump experiment

All the pump reservoirs were empty at the end of the experiments, indicating release of HCTZ. To confirm release, urinary HCTZ was measured by mass spectroscopy in the "intra-drug" 5-hour urinary collection period during HCTZ release and during "no drug" release. Samples used here were the nighttime samples as this is the period where the most urine was available. Urinary HCTZ excretion was low in the "no drug" time period (Figure 5.8) but was not 0 (mean = 0.81 μg/hour, p=0.0003, one-sample t-test against a theoretical mean of 0). HCTZ was detected in all urine collected during HCTZ administration. However, the rate of urinary HCTZ excretion varied from 17 μg/hour to 224 μg/hour.

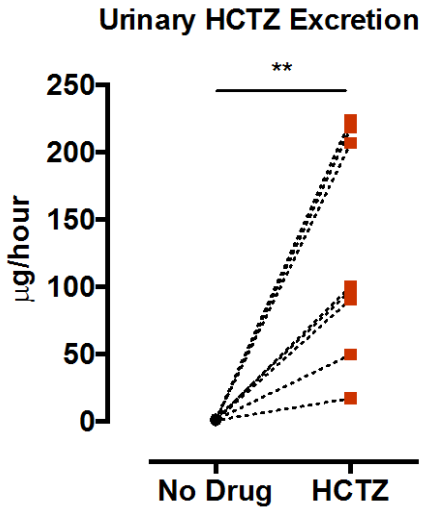

Figure 5.8: Urinary HCTZ excretion during no drug or HCTZ administration via programmable micro-osmotic mini-pump
Urinary HCTZ was measured by tandem liquid chromatography mass spectroscopy (LCMS) in mice administered HCTZ at a dose of 20 mg/kg via programmable micro-osmotic minipumps (iPRECIO, Japan) and during "no drug" administration. Urinary excretion data were analysed by paired t-tests.

Urinary sodium excretion was measured before and during HCTZ administration in mice treated with chronic vehicle or corticosterone. This was assessed for both night and day dosing. As expected, the overall rate of urinary sodium excretion was higher at night (306 ± 59 μmol/hour vehicle and 289 ± 70 μmol/hour, corticosterone) compared to the day (118± 41 μmol/hour, vehicle and 161 ± 38 μmol/hour, corticosterone) in both vehicle and cort groups. The day/night difference in sodium excretion was significantly blunted in the corticosterone treated animals compared to the vehicle group (p=0.018, Student's t-test, n=4), consistent with the findings of Chapter 4. HCTZ did not cause statistically significant natriuresis in any group (corticosterone or vehicle) at any time point (day or night, Figure 5.9

A, C). Urinary sodium excretion during the baseline or "pre" drug period was then subtracted from the "intra" drug period to get ΔHCTZ/no drug values. The change in urinary excretion with HCTZ or no drug was not different at any time or in any group (Figure 5.9, B, C).

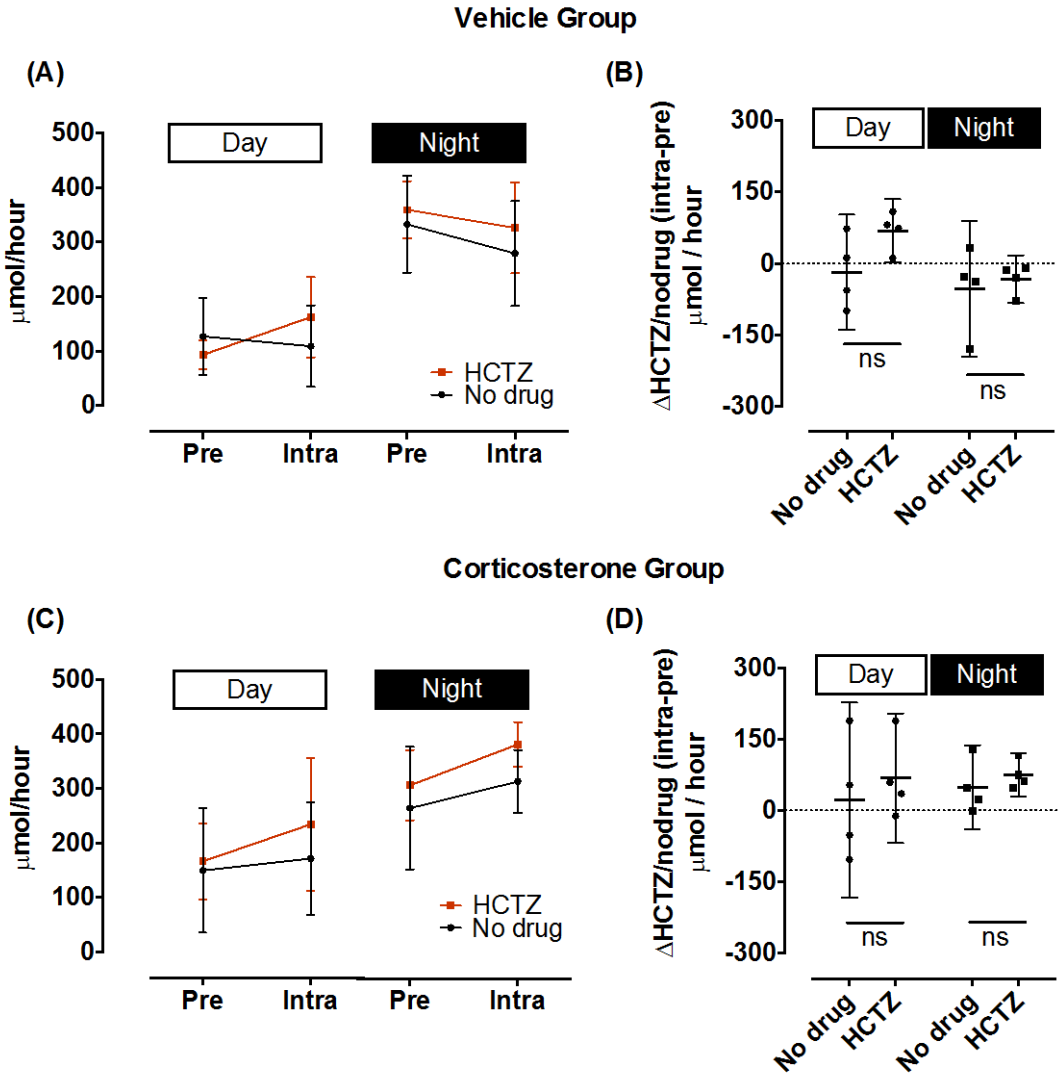

Figure 5.9: Urinary sodium excretion in C57BL6 mice implanted with programmable micro-osmotic mini-pumps and vehicle (A, B) or corticosterone (C, D) silastic slow release pellets

Pre-drug urinary sodium excretion was measured from ZT 0/12 (7 am/pm) to ZT 3.5/15.5 (10.30am/pm), intra-drug sodium excretion was measured from ZT 3.5/15.5 (10.30 am/pm) to ZT 8.5/20.5 (3.30 am/pm). HCTZ/no drug summary values are "pre" drug urinary sodium subtracted from the "intra" drug/no drug sodium excretion during the day and night. These summary data were analysed by matched two-way ANOVAs with post hoc Sidak tests.

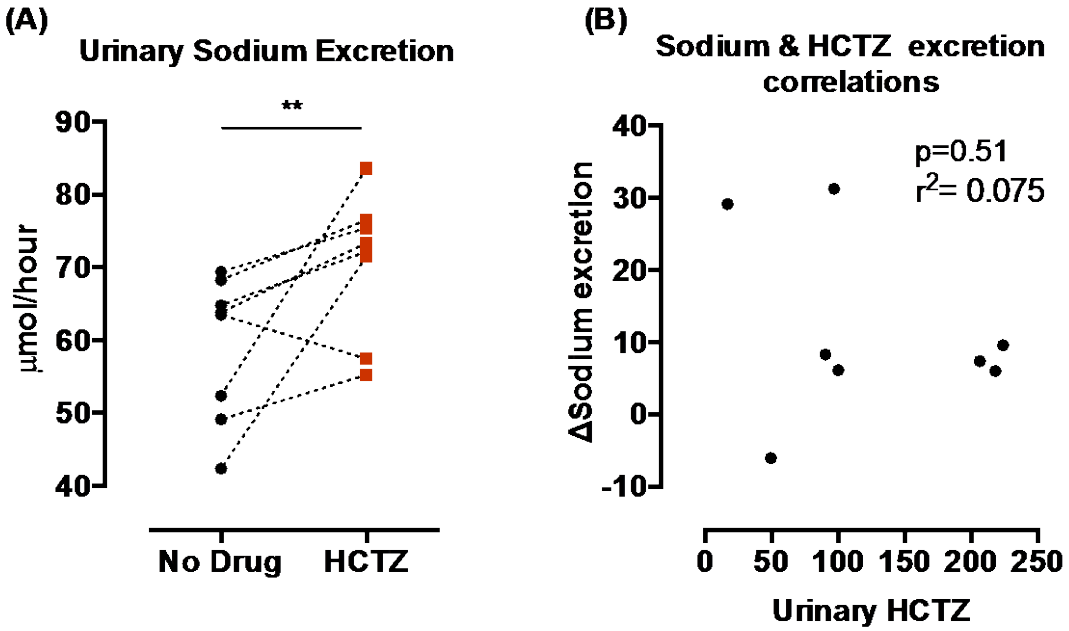

Figure 5.10: Urinary sodium excretion during nighttime HCTZ or "no drug" administration via programmable micro-osmotic mini-pump (A) and corresponding correlation between urinary HCTZ excretion and urinary sodium excretion (B)
Urinary excretion data were analysed by paired t-tests. Pearson correlation was performed on delta sodium excretion versus urinary HCTZ data.

HCTZ was released by the micro-osmotic mini-pumps as evidenced by the substantial increase in urinary HCTZ excretion during the release period (Figure 5.8). Interestingly, the variation in HCTZ excretion (Figure 5.8) was considerably larger than the variation seen in the sodium excretion for the same time periods (Figure 5.10 A) and there was no correlation between urinary HCTZ and a change in sodium excretion with HCTZ ($p=0.51$, $r^2=0.075$ by Pearson's correlation Figure 5.10 B).

5.3.3. Effect of corticosterone and HCTZ treatment on BP

We next addressed the role of NCC and corticosterone on the diurnal rhythm of BP. To verify that the clamping of plasma corticosterone persists throughout 4 weeks of pellet implantation, plasma was sampled at ~7am (ZT 0) and ~ 7pm (ZT 12). In vehicle treated mice, a significant difference was seen in plasma corticosterone in blood sampled by tail venesection at ZT 0 compared to that from ZT 12 (Figure 5.11 A) but this was not seen in the corticosterone treated animals, which exhibited slightly higher day time plasma corticosterone and slightly lower night time corticosterone (Figure 5.11 A). In order to verify that the dose of HCTZ taken by the mice was sufficient, plasma HCTZ was measured in terminal samples by mass spectroscopy. HCTZ levels were similar between vehicle and corticosterone treated animals (p=0.54, Figure 5.11 B) being on average ~15 μmol/l, ~ 40X higher than required in hypertensive humans for a 20 mmHg drop in mean blood pressure [207]. This value for human therapeutic level is indicated on the graph by a dotted line (Figure 5.11 B). Therefore in theory, the HCTZ dose was in an efficacious range in these studies.

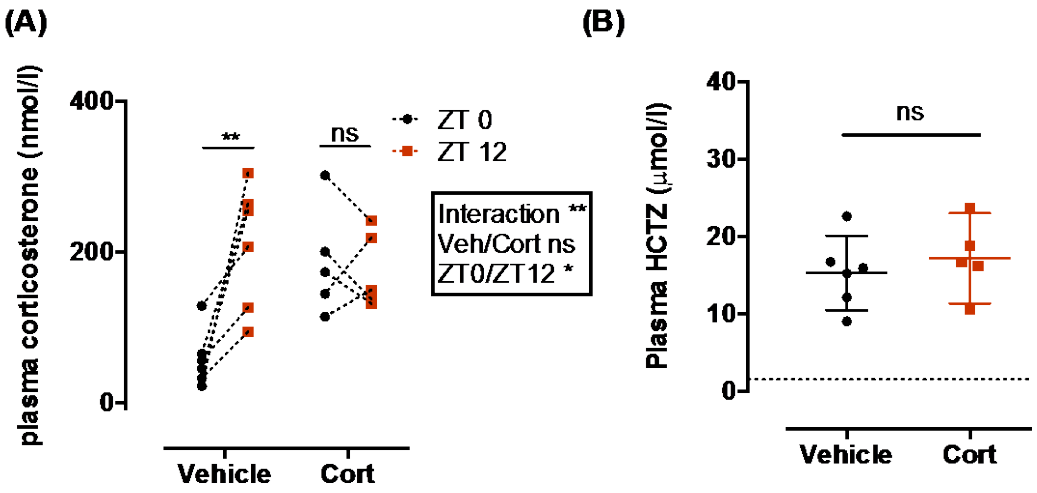

Figure 5.11: Plasma corticosterone at week 4 post vehicle/corticosterone silastic pellet implantation (A) and plasma HCTZ following 1 week of HCTZ treatment (B). Following 4 weeks with slow-release silastic pellet implantation blood was sampled at ZT0 and ZT 12 in conscious mice via tail venesection. After 1 week of chronic HCTZ treatment administered in drinking water mice were culled and a terminal plasma sample analysed for HCTZ by LCMS. The dotted line indicates the human plasma concentration at which a 20mmHg blood pressure drop occurs in hypertensive individuals. Data are mean± 95% CI. Plasma corticosterone data was analysed by matched two-way ANOVA with post hoc Sidak tests. Plasma HCTZ data was analysed by Student's t tests. **p<0.01, ns p>0.05, n=6 (vehicle) n=5 (corticosterone).

5.3.4. BP is increased with corticosterone treatment and rescued with HCTZ

Systolic blood pressure (SBP) was measured in conscious unrestrained C57BL6 mice. At baseline, both groups had identical daily rhythms of SBP (Figure 5.12 A, B, C, F). All mice were then anaesthetised with isofluorane and silastic slow release corticosterone pellets were implanted. Following recovery from anaesthetic, the vehicle group immediately regained its daily rhythm of SBP (Figure 5.12 A), which was no different from pre-implant values (Figure 5.12 E, F). The corticosterone-treated group took longer to regain their daily rhythm of SBP and when they did (~3 days post surgery, Figure 5.12 A) their daytime SBP was raised compared to baseline values (Figure 5.12 A, C, E). All the mice were then treated with HCTZ in their drinking water. This treatment did not affect daytime or nighttime SBP in the vehicle group (Figure 5.12 A, E, F) but improved daytime SBP in the corticosterone treated group (Figure 5.12 A, E, F) with no effect on nighttime SBP.

At baseline, both groups have identical rhythms of diastolic blood pressure (DBP, Figure 5.13 A). Corticosterone treatment increased both daytime and nighttime DBP (Figure 5.13 A, B, C). Daytime DBP was reduced by HCTZ treatment but nighttime DBP remained elevated. There were no changes in nighttime or daytime DBP following vehicle treatment or HCTZ treatment in the vehicle group. Pulse pressure steadily decreased throughout the experiment (Figure 5.13 D) and was significantly reduced in both vehicle and corticosterone groups following pellet implantation and decreased further following HCTZ treatment. There were no differences in pulse pressure between vehicle and corticosterone groups (Figure 5.13 E). It is unclear why pulse pressure should reduce over time but it is unlikely to be a physiological phenomenon and may relate to the deterioration of the catheter patency over the 6-week period.

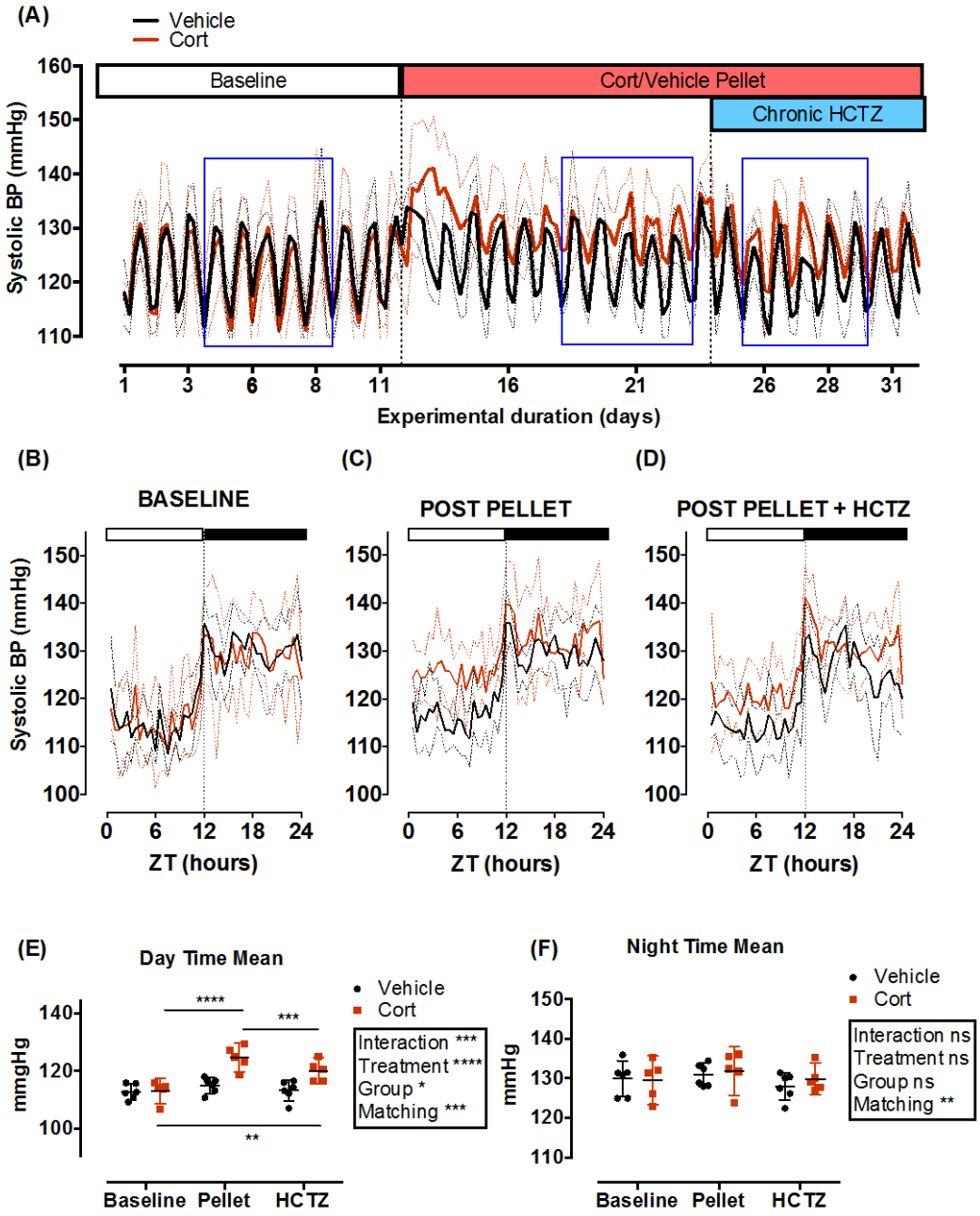

Figure 5.12: Systolic blood pressure (SBP) in C57BL6 mice following treatment with corticosterone or vehicle and chronic HCTZ.
SBP was measured by radio telemetry in C57BL6 mice. (A) Moving averages (over 5 hours) throughout the duration of the experiment. After baseline recordings (11 days), all mice were anaesthetised under isofluorane and received either vehicle or corticosterone slow-release silastic pellets (s.c.). After 8 days recording all mice were treated with chronic HCTZ (80 mg/kg) in their drinking water. The blue rectangles indicate 5-day bins that were taken forward for further analysis. In the first instance a mean over 5-day bin for each half hour for 24 hours was displayed at baseline (B), post corticosterone/vehicle pellet (C) and following HCTZ treatment (D). Mean daytime (E) and nighttime (F) blood pressure was obtained by taking the mean systolic blood pressure over the 5-day bins between ZT 3-8 (day) and ZT 15-20 (night), data are mean± 95% CI. Data were analysed by matched two-way ANOVA with post hoc Sidak tests. ****p<0.0001, ***p<0.001, **p<0.01 n=6 (vehicle) n=5 (corticosterone).

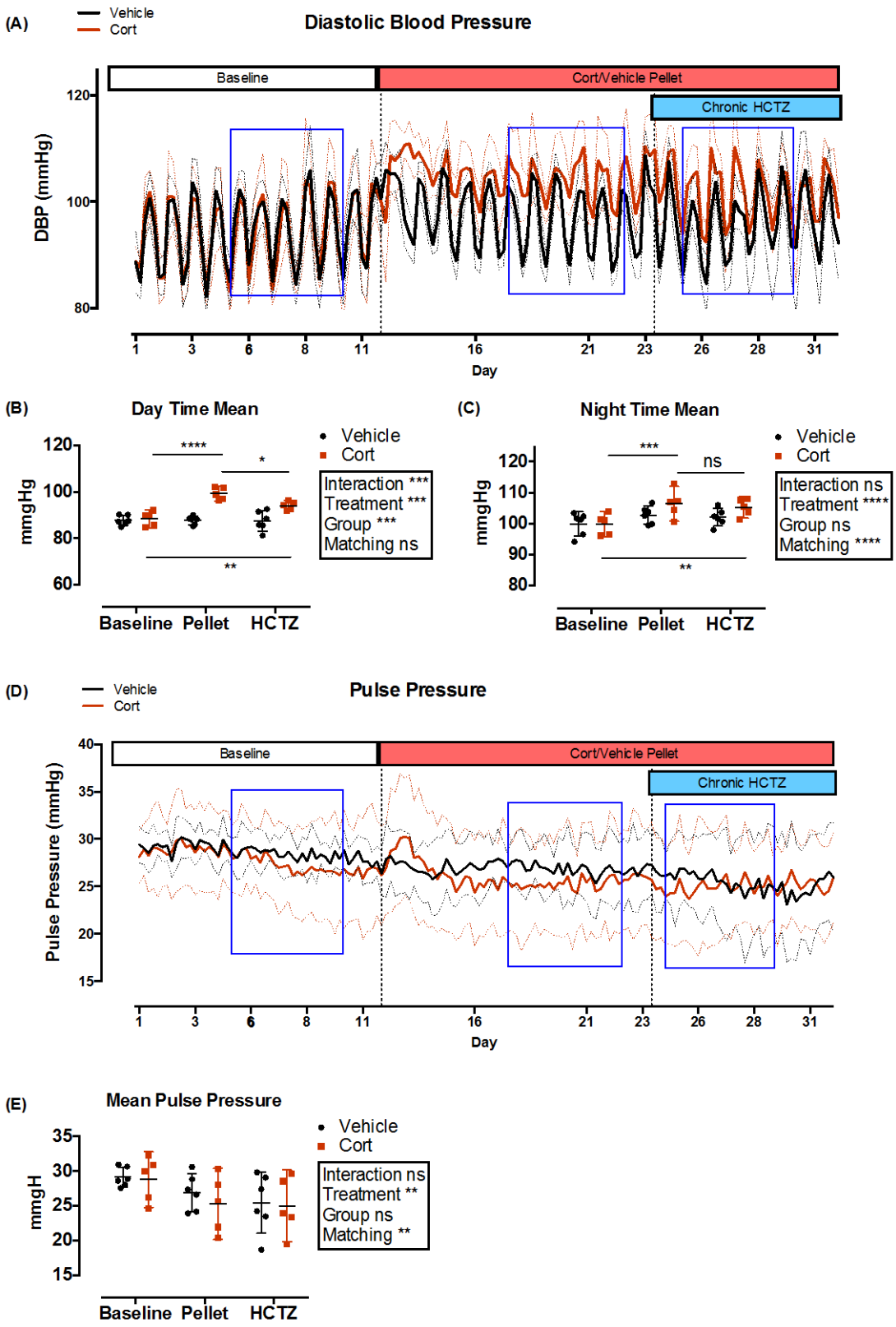

Figure 5.13: Diastolic blood pressure (DBP) and pulse pressure in C57BL6 mice following treatment with corticosterone or vehicle and chronic HCTZ. (details overleaf)

DBP was measured by radio telemetry in C57BL6 mice. (A) Moving averages (over 5 hours) of diastolic (A) and pulse pressure (D) throughout the duration of the experiment. After baseline recordings (11 days), all mice were anaesthetised under isofluorane and received either vehicle or corticosterone slow-release silastic pellets (s.c.). After 8 days recording all mice were treated with chronic HCTZ (80mg/kg) in their drinking water. The blue rectangles indicate 5-day bins that were taken forward for further analysis. Summary mean daytime (E) and nighttime (F) diastolic pressure was obtained by taking the mean diastolic pressure over the 5-day bins between ZT 3-8 (day) and ZT 15-20 (night). Mean pulse pressure is the 24 hour mean over each 5 day bin (E). Data are mean± 95% CI. Summary mean were analysed by matched two-way ANOVA with post hoc Sidak tests. ****p<0.0001, ***p<0.001, **p<0.01, *p<0.05 ns, not significant p>0.05, n=6 (vehicle) n=5 (corticosterone).

5.3.5. HR and activity are unchanged by corticosterone treatment

At baseline both groups had identical daily rhythms of HR (Figure 5.14 A, B, C). Following recovery from surgery, animals in the vehicle group regained their daily rhythms of HR, with mean HR returning to pre-implant values. The corticosterone group exhibited a transiently lower heart rate than the vehicle group for the first 4 days following corticosterone implantation, and in the 5 proceeding days nighttime heart rate was significantly lower than prior to corticosterone pellet implantation (Fig 5.14 C), with no change in daytime HR (Figure 5.14 B). HR appeared to decrease over time throughout the experiment in both groups: heart rate following HCTZ was lower than baseline HR. No differences were found in daytime or nighttime HR between corticosterone and vehicle groups with any treatment (Figure 5.14 B, C). Activity as measured by radiotelemetry device, exhibited strong day-night differences and was unchanged by either corticosterone or HCTZ treatment (Figure 5.14 D, E, F).

Figure 5.14 (overleaf): Heart rate (HR) and activity in C57BL6 mice following treatment with corticosterone or vehicle and chronic HCTZ

HR and activity was measured by radio telemetry in C57BL6 mice. Data displayed here are the moving average (over 5 hours) of heart rate (A) and activity (D) throughout the duration of the experiment. After baseline recordings (11 days), all mice were anaesthetised under isofluorane and received either vehicle or corticosterone slow-release silastic pellets (s.c.). After 8 days recording all mice were treated with chronic HCTZ (80 mg/kg) in their drinking water. The blue rectangles indicate 5-day bins that were taken forward for further analysis. Summary mean daytime and nighttime heart rate (B, C) and activity (E, F) were obtained by taking the mean over the 5-day bins between ZT 3-8 (day) and ZT 15-20 (night). Data are mean± 95% CI. Summary data were analysed by matched two-way ANOVA with post hoc Sidak tests. ****p<0.0001, ***p<0.001, **p<0.01, *p<0.05 ns, not significant p>0.05, n=6 (vehicle) n=5 (corticosterone).

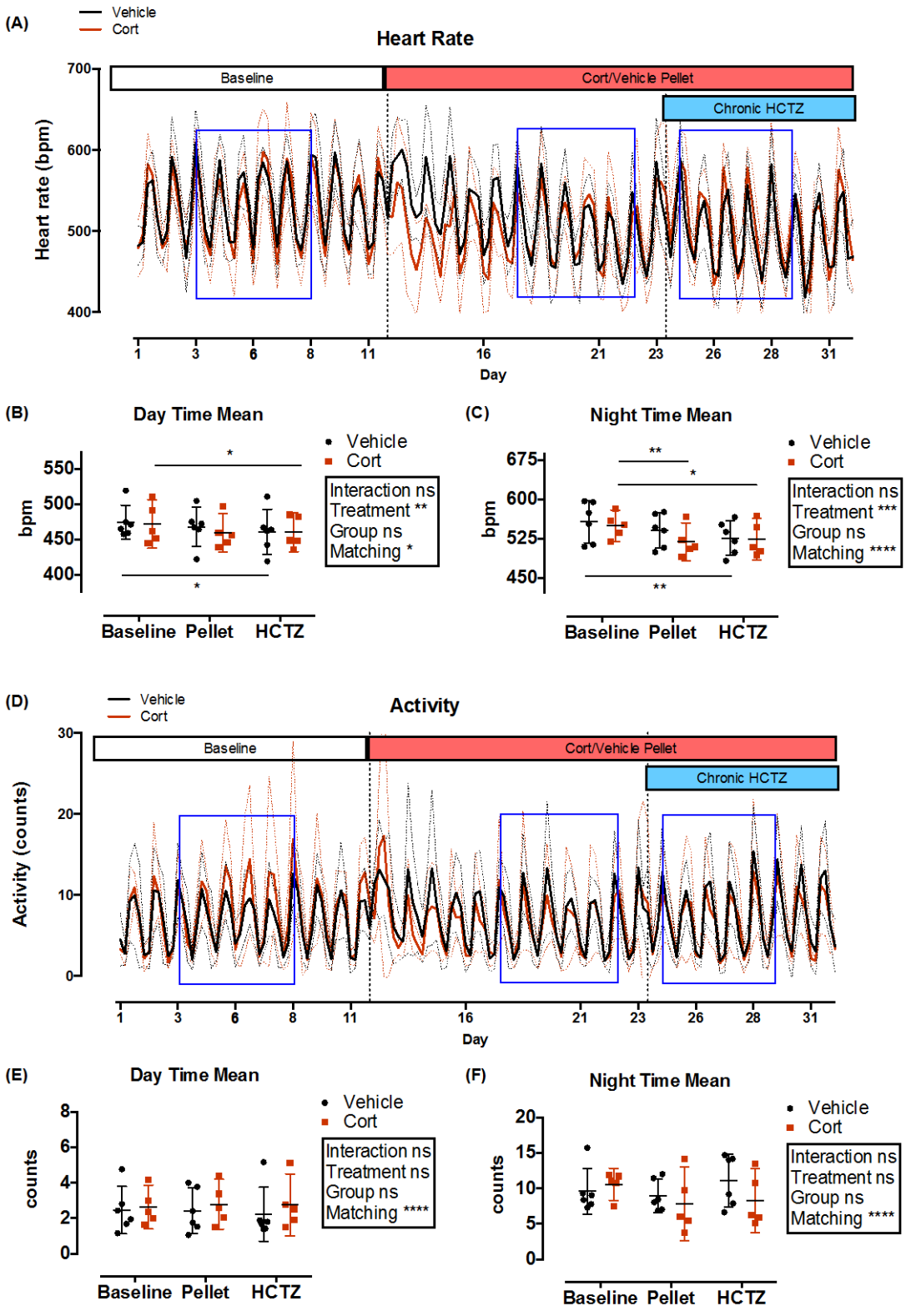
(A)
Vehicle
Cort
Heart Rate
Baseline
Cort/Vehicle Pellet
Chronic HCTZ
Heart rate (bpm)
Day
(B)
Day Time Mean
bpm
Vehicle
Cort
Interaction ns
Treatment **
Group ns
Matching *
Baseline Pellet HCTZ
(C)
Night Time Mean
bpm
Vehicle
Cort
Interaction ns
Treatment ***
Group ns
Matching ****
Baseline Pellet HCTZ
(D)
Vehicle
Cort
Activity
Baseline
Cort/Vehicle Pellet
Chronic HCTZ
Activity (counts)
Day
(E)
Day Time Mean
counts
Vehicle
Cort
Interaction ns
Treatment ns
Group ns
Matching ****
Baseline Pellet HCTZ
(F)
Night Time Mean
counts
Vehicle
Cort
Interaction ns
Treatment ns
Group ns
Matching ****
Baseline Pellet HCTZ

Table 5.1: Results of cosinor analysis of SBP in C57BL6 mice treated with chronic corticosterone or vehicle followed by chronic HCTZ treatment (80 mg/kg).

	Baseline		Pellet		HCTZ	
	Vehicle	**Cort**	**Vehicle**	**Cort**	**Vehicle**	**Cort**
Period (hours)	24h10 ± 0h16	24h12 ± 0h20	24h05 ± 0h13	23.12 ± 4h25	23h40±0h34	24h18±0h34
Acrophase (ZT)	16h59 ± 0h37	16h50 ± 0h53	16h56 ± 0h47	14h50 ±0 h53	17h16 ± 1h12	16h13 ± 1h29
Amplitude (mmHg)	9.9 ± 2.6	9.3 ± 2.9	8.4 ± 1.9	**4.4 ± 3.2******	8.6 ± 1.1	**6.7 ± 2.3****
MESOR (mmHg)	123.1 ± 3.2	122.5 ± 6.2	123.4 ± 1.8	**129.5 ± 5.0*****	121.3 ± 3.4	126.2 ± 3.0
Robustness (%)	72.5 ± 11.2	76.2 ± 7.4	73.1 ± 9.4	**39.6 ± 28.0*****	70.5 ± 12.6	62.7 ± 15.9

Data are mean ± 95% CI. Data analysed by matched two-way ANOVA with post hoc Sidak comparisons between baseline, pellet and HCTZ. Underlined values are significantly different from baseline values, where ****p<0.0001 ***p<0.001 **p<0.01.

5.3.6. Cosinor analysis of SBP

A cosinor analysis was performed on SBP data from the "bins" of experimental time periods highlighted in Figure 5.12 A. All the descriptive data produced from this analysis is presented in Table 5.1 with the same data plotted in Figures 5.15 and 5.16 for better visualisation. The MESOR was similar between vehicle and corticosterone groups at baseline (i.e. prior to pellet implantation). MESOR of the vehicle is unchanged by vehicle pellet implantation or HCTZ treatment. However, corticosterone treatment caused an increase in MESOR ($p<0.0001$, Figure 5.15 B), which was reduced by HCTZ treatment ($p=0.012$, Figure 5.15 B) to levels similar to baseline MESOR ($p=0.07$, Figure 5.15 B). The amplitude of SBP rhythm was again similar between groups at baseline. Corticosterone treatment induced a reduction in SBP amplitude ($p<0.0001$, Figure 5.15 A), which was increased by HCTZ treatment ($p=0.013$, Figure 5.15 A). Vehicle SBP amplitude was unchanged by pellet implantation ($p=0.12$, Figure 5.15 A) or HCTZ treatment ($p=0.99$, Figure 5.15 A). Robustness is a measure of how "rhythmic" the data is or rather how well a cosinor curve can be fitted to the data. Robustness levels of <20% are defined as not different from noise or "not rhythmic"[144, 208]. Robustness was high and similar between groups at baseline at ~ 75%. Robustness remained consistent in the vehicle-treated group throughout the entire experiment. Corticosterone treatment caused a sharp reduction in robustness to about 40% ($p=0.0002$, Table 5.1, Figure 5.15 C, post hoc Sidak test) and HCTZ treatment restored robustness to ~63% (Table 5.1 $p=0.0092$, Figure 5.15, post hoc Sidak test).

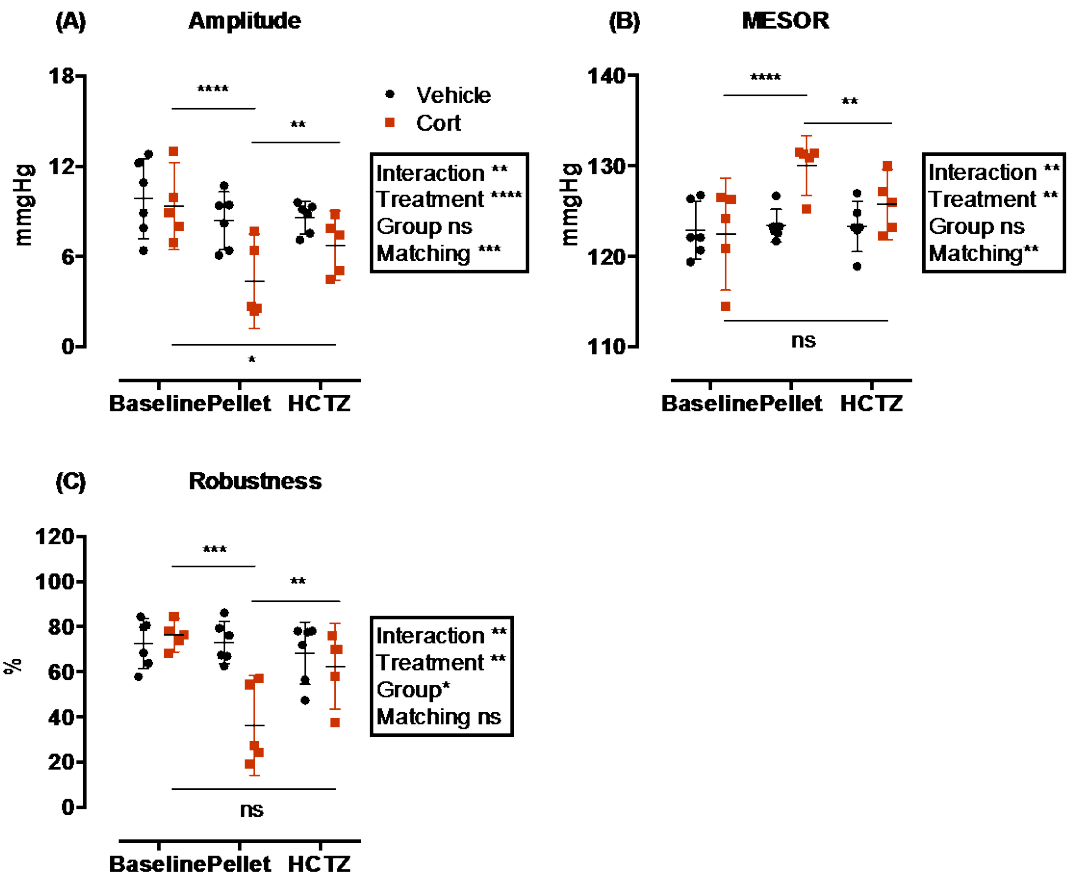

Figure 5.15: Analysis of rhythmic parameters of SBP in C57BL6 mice following treatment with corticosterone or vehicle followed by chronic HCTZ.
SBP was measured by radio telemetry in C57BL6 mice. Following baseline measurements mice received vehicle or corticosterone slow release silastic pellets, this was followed by chronic HCTZ treatment (80mg/kg). SBP data from 5-day bins during each treatment period: baseline, after pellet and after HCTZ treatment was subject to cosinor analysis. Data are mean ± 95% CI. Data were analysed by matched two-way ANOVA followed by post hoc Sidak tests, where ****p<0.0001, ***p<0.001, **p<0.01, *p<0.05, n.s p>0.05.

Acrophase is the time point at which oscillating variables, such as systolic blood pressure here, reach their peak. Figure 5.16 is a polar plot that displays acrophase against amplitude. There were no statistically significant differences between any of the groups' acrophases but there are some trends particularly with regard to the spread of the acrophase data with treatment. At baseline both groups' acrophases were between ~14-17 ZT (Figure 5.16 A). Following pellet implantation, the vehicle group's acrophases remained between ~14-17 ZT (Figure 5.16, B). The corticosterone group exhibited a greater distribution of acrophases after pellet implantation with values between ~10 - 18 ZT (Figure 5.16, B). HCTZ treatment shifted the corticosterone group's acrophases to between ~13-16 ZT but also appeared to cause a greater spread of the vehicle group's acrophases ~ 14 - 18 ZT (Figure 15.16, C).

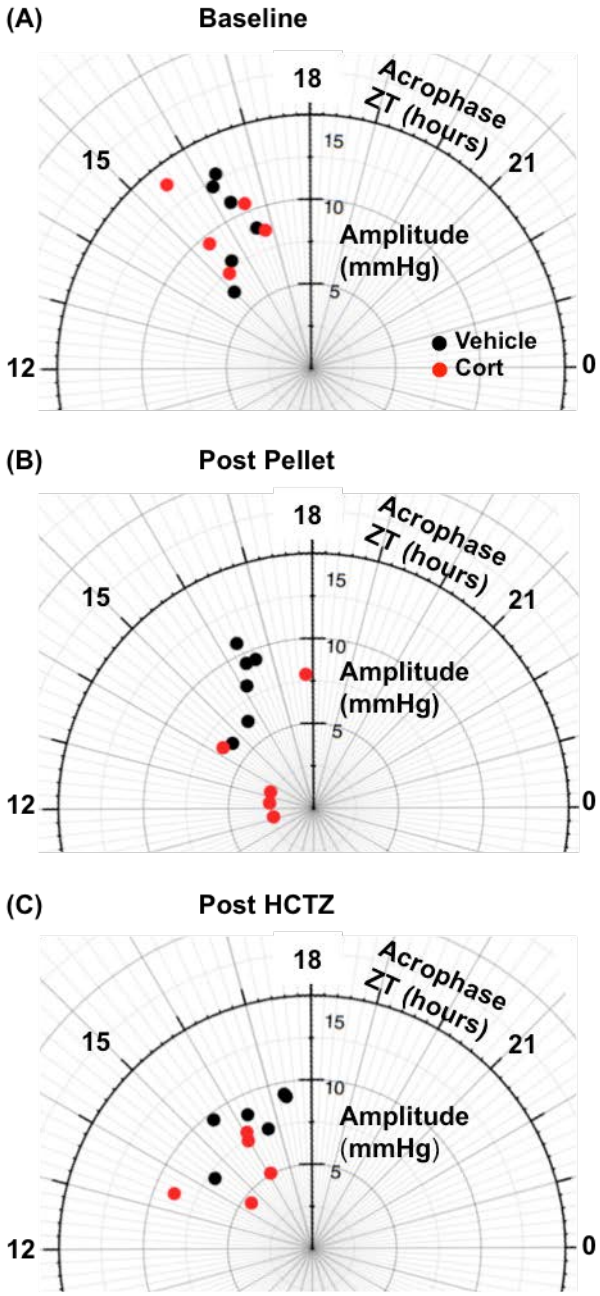

Figure 5.16: Polar diagram of acrophase and amplitude of SBP in C57BL6 mice at baseline (A) following corticosterone or vehicle treatment (B) and following chronic HCTZ treatment (C).

SBP was measured by radio telemetry in C57BL6 mice. Following baseline measurements mice received vehicle or corticosterone slow release silastic pellets, this was followed by chronic HCTZ treatment (80 mg/kg). SBP data from 5-day bins during each treatment period: baseline, after pellet and after HCTZ treatment was subject to cosinor analysis. Data are individual amplitude and corresponding acrophases for each mouse.

5.4. Discussion

5.4.1. What are the functional consequences of NCC phosphorylation?

The major aim of this chapter was to assess the functional consequence of a perturbed day/night rhythm of NCC phosphorylation. NCC phosphorylation is associated with increased activation in many *in vitro* [98, 100] [99] and *in vivo* studies [86]. However its use as a surrogate reporter of NCC activity should be taken with caution as reports from our lab [86] and others [105, 159] indicate that NCC phosphorylation and thiazide-sensitive sodium transport are not always associated. For example, in 11βHSD2 null mice, NCC phosphorylation at all residues as well as total NCC protein is increased but thiazide-sensitive sodium transport is not elevated above wild-type levels [86]. Therefore it was important to investigate what the diurnal rhythm of NCC phosphorylation means functionally. The major challenge of the work in this chapter was how to design an experiment to detect circadian changes in NCC function.

5.4.2. Thiazide diuretic choice: How to inhibit NCC?

One way of assessing NCC function in vivo is to measure the natriuretic effect of NCC inhibitors (thiazide diuretics). This thiazide-sensitive sodium excretion gives an estimate of how much of the sodium reabsorption is occurring through NCC. To this end, two thiazide diuretics were investigated for potential use in thiazide-sensitivity experiments: hydrochlorothiazide (HCTZ) and bendroflumethiazide (BFMZ). Both inhibit NCC but BFMZ is considerably more potent than HCTZ [209]. Thiazide diuretics reduce GFR through their effects on tubuloglomerular feedback [210-212]. HCTZ has greater carbonic anhydrase inhibiting capacity and can cause dilatation of blood vessels through alkalinisation of smooth muscle cells [202]. In our experiments in anaesthetised animals, HCTZ had a greater effect on renal haemodynamics: 20 mg/kg HCTZ significantly lowered GFR in anesthetised mice but there was no such difference with 6 mg/kg BFMZ. HCTZ also caused a mild elevation of RBF. Both drugs induced a large and rapid natriuresis. The change in fractional sodium excretion was 5-10 % consistent with the reported proportion of filtered sodium reabsorbed by NCC [150, 213]. Therefore in terms of specificity and potency BFMZ was superior but is also 7X less soluble than HCTZ (108 mg/l compared to 722 mg/l at 25^{o}C) and no natriuretic effects could be seen at the maximum dose soluble in our required volume of 50% DMSO (25 mg/kg). HCTZ was chosen for use in thiazide-sensitivity studies as it did induce natriuresis in conscious C57BL6 mice and was considerably more soluble.

5.4.3. How to design a functional circadian experiment to test NCC activity?

The next major challenge was how to administer HCTZ. We first considered administration by injection. This has the advantage that one would know the exact timing of drug administration. However this route was rejected as restraint and handling of mice causes large increases in corticosterone levels [174, 214]. Indeed, our pilot telemetry experiments showed injection of saline vehicle during the day caused a sustained surge in BP to levels normally seen during peak activity at night. We also considered a renal clearance approach, as it would allow measurement of renal function and HCTZ-sensitive fractional sodium excretion measurements. However, this approach requires anaesthetic, surgery and saline infusion. Studies in rats found that circadian variations in renal function seen in conscious animals did not persist when anaesthetised and the renal clearance preparation abolished the aldosterone rhythm [215]. Finally oral HCTZ was considered as the diuretic has good oral bioavailability and large intake would mean the low solubility would be less of an issue. However, this approach was rejected, as it would be difficult to control when HCTZ dosing occurs without resorting to gavage.

Finally, we were given the opportunity beta test a new miniaturised programmable micro-osmotic minipump system SMP-300 (iPRECIO, Japan). These pumps can accurately administer one substance at a maximum rate of 10 μl/hour. It is pre-programmable, so no animal handling is required for drug administration. Studies using the same technology in larger SMP-200 devices have established the accuracy and reliability of the osmotic pump technology [216].

5.4.4. Experiments using micro-osmotic minipumps to deliver HCTZ

In our experiments the SMP-300 mouse device exhibited great accuracy *in vitro* (within ~4%). The *in vivo* results were also promising with high levels of HCTZ appearing in urine collected during infusion periods; little HCTZ was detected when the pump was programmed to be off. There was however, huge variability in HCTZ excretion rates with a 13-fold difference between the highest and lowest HCTZ excretion rate. This could either be a result of pump variability or a biological phenomenon (filtration/secretion/micturition). There are several points at which biological variability could occur: these can be thought of in terms of either absorption or elimination. In terms of reabsorption, 70% of HCTZ is absorbed by the GI tract [217] and although HCTZ has been administered subcutaneously in many experimental settings [218-220] there is a paucity of data on the pharmacokinetics of

this route of administration. More variability could be present during HCTZ elimination. At least 95% of an intravenous dose of HCTZ is excreted, unchanged by the kidneys [217] and as 90% of plasma HCTZ is bound to protein tubular secretion is thought to be the major route of HCTZ elimination. OAT1 channels are major contributors to HCTZ secretion allowing uptake across the basolateral membrane [221] but it is unclear whether these transporters undergo dynamic regulation. However, that HCTZ elimination may not undergo considerable regulation is evidenced by experiments in anaesthetised animals and in the clinic. Using the same LCMS methods as used here the proportion of urinary HCTZ excretion only varied in proportion to the intravenous dose administered [147]. This has also been found in patients receiving different oral doses [207]. Therefore it is unlikely that HCTZ secretion was a major factor in the variability seen here. The other possibility for biological variation was the timing of bladder emptying. i.e. the mouse with the lowest reported HCTZ levels may have urinated right at the start of the 5 hours of urine collection, prior to HCTZ secretion and the animal with the highest may have urinated at the peak time for HCTZ secretion. 24-hour urinary HCTZ elimination experiments would have been helpful to rule out this possibility. It would also have been useful to include in the pump reservoir a freely filtered labelled tracer (such as FITC-inulin) or dye in order to determine the variability of the pumping rates *in vivo*.

5.4.5. What was the biological outcome of the experiment?

In previous chapters, it was shown that NCC phosphorylation was twice as high at night compared to the daytime. Corticosterone treatment eliminated this day/night difference. However, we were unable to detect any increases in thiazide-sensitive sodium transport at night compared to the daytime in this cohort of mice. Moreover, although there were changes in rhythmic sodium excretion, no such differences in thiazide-sensitive sodium transport were detected between vehicle and corticosterone treated groups. We have shown that HCTZ caused a reduction in GFR in renal clearance experiments, and this may result in an underestimation of sodium excretion. We do not know the renal haemodynamic profile of these mice. Normalising urinary excretion data to creatinine was considered as other groups [222] employ this approach. However, creatinine has a secretory rhythm that restricts its use as a reliable marker of GFR in circadian experiments [223] and so this strategy was not employed in these experiments. As we have explored, variability in HCTZ excretion was very large. Furthermore, there were no correlations between urinary concentration of HCTZ and sodium excretion ($p= 0.57$, $r^2=0.056$, Pearson's Correlation). A lack of correlation between peak plasma levels and urinary sodium excretion has also been seen in healthy

volunteers [207]. The thiazide-sensitive excretion studies in this chapter must be treated as preliminary as they are underpowered and there were clear limitations in these experiments. It is interesting to note that considerably higher doses of HCTZ are required to achieve detectable and reproducible natriuresis in conscious mice and rats [220, 222] compared to humans or indeed anaesthetised mice. This may be indicative of compensatory changes that occur in mice, which are blocked by anaesthetic.

5.4.6. Effect of HCTZ on rhythmicity on BP: an alternative approach

We also developed a complementary strategy to test whether HCTZ affected the diurnal rhythm of BP in mice implanted with vehicle or corticosterone pellets. The SMP300 iPRECIO system was no longer available to us and therefore a change in strategy was required. A chronic oral dose of HCTZ was chosen based on [222]. This large dose (~80 mg/kg/day) was chosen in order to achieve high plasma levels throughout the 24-hour cycle. We do not know the 24-hour plasma HCTZ levels. However, based on the estimated half-life ~6 hours [205] and the plasma HCTZ levels, which were sampled at ~ 13 ZT i.e. during the main feeding/drinking time in the active phase, it is likely that the plasma concentration of HCTZ does not decrease below therapeutic levels [207] (Figure 5.17). This approach may still introduce some variability in amount drank by each mouse and the timing of ingestion but the substantial dose should mean that the level of plasma HCTZ was consistently in an efficacious range.

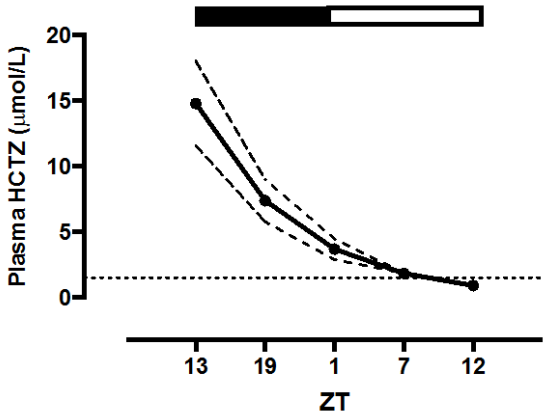

Figure 5.17: Hypothetical worst-case scenario for estimated HCTZ elimination in C57BL6 mice treated chronically with 80 mg/kg HCTZ (p.o.) HCTZ treatment (C).
Hypothetical worst-case scenario estimated HCTZ elimination in C57BL6 mice treated chronically with 80 mg/kg HCTZ (p.o.). HCTZ was measured in termainal plasma sampled at ~13 ZT. This estimate assumes the 13 ZT sample was at the plasma HCTZ peak, that no further ingestion would take place overnight. This very rough estimation also uses the shortest reported half-life for HCTZ (6 hours). Using this rough projection, HCTZ levels would only reach below the therpeautic plasma levels for hypertensive humans at ZT 12, whereby the animals enter the active phase again. Data are mean ± 95% CI of all vehicle and corticosterone treated animals.

5.4.7. BP rhythmicity following corticosterone treatment and NCC inhibition

SBP was increased in corticosterone-treated animals during the daytime but was unchanged at nighttime. HCTZ improved daytime BP in corticosterone-treated animals but did not affect vehicle SBP. One of the consequences of corticosterone-treatment (explored in-depth in Chapter 4) is an inappropriate elevation of daytime NCC phosphorylation. The observation that HCTZ can decrease daytime BP in corticosterone-treated mice gives weight to the role of NCC in diurnal BP rhythm. The cosinor analysis of SBP gave very similar conclusions to the day/night mean analysis. Importantly this type of analysis makes use of each point within the 24-hour cycle and therefore gives a more accurate and complete description of the data. The amplitude of SBP was greatly decreased by corticosterone treatment and the MESOR was increased. The day/night mean analysis shows that these changes are likely a result of elevated daytime BP without any major changes in nighttime BP. There were no changes in period length but corticosterone and indeed HCTZ treatment appeared to cause a slight change in the phase as denoted by acrophase, although this did not reach statistical significance. These changes appeared to introduce greater group variation of the acrophases rather than shifting of all of the data points. Robustness or prominence of the cosinor fit was drastically reduced by corticosterone treatment, indicating a loss of rhythmicity [144]. This can be as a result of increased noise; corticosterone could increase the mice's sensitivity to sleep disturbances [224]. Another reason for a change in rhythmicity is a non-repeating phase of the daily rhythm or in other words, a loss of stationarity. This means that the SBP curve may not be repeating reproducibly every day, leading to a perceived loss of rhythmicity. HCTZ partially restored this rhythmicity of SBP increasing robustness levels back to baseline levels.

5.4.8. HR following corticosterone & HCTZ treatment

The major changes in BP with corticosterone and HCTZ do not appear to be as a result of any changes in HR or activity. Aside from a small, transient reduction in heart rate in the first 4 days immediately following corticosterone pellet implantation, HR was not affected by corticosterone or HCTZ treatment. A reduction in HR following acute GC treatment has been reported in healthy volunteers [225] and the finding that diurnal HR rhythm remains intact despite alterations to SBP rhythm with GC treatment has been reported in the literature, where both Cushing's patients and those treated with high levels of GCs have no nocturnal dip despite having an intact HR dip [226] [227]. It is peculiar that heart rate decreased over time. This occurred to a similar extent in all mice in both vehicle and

corticosterone groups. The reasons for this gradual decline are unclear but it may be linked to slow adaptations to single housing. The literature reports alterations to HR in single housed/versus pair-housed male mice [228], with lower HR in pair-housed mice than single housed. Unfortunately, single housing in this experimental setup was unavoidable. Every effort was made to minimise the stress of single housing: mice were acclimatised for 14 days before recordings were taken, 1 cage change was made (following pellet implantation) and the room was heated to 25^{o}C to limit the impact of temperature on the mice.

5.4.9. Mechanisms of HCTZ-induced restoration of BP rhythmicity

HCTZ lowers daytime BP in corticosterone treated mice. Corticosterone treated mice have elevated NCC phosphorylation during the day and have perturbed sodium excretion rhythms. However, we were unable to show that these findings specifically relate to a functional change in sodium handling by NCC. That HCTZ improves daytime BP and rhythmicity does give some evidence that NCC may be involved in the maintenance of diurnal BP rhythms. Furthermore, experiments where genetic alterations in the pathway molecules that regulate NCC have also shown interesting variations in their BP rhythm. A WNK4 hypomorphic mouse, with greatly reduced NCC phosphorylation, had a reduction in SBP amplitude characterised by reduced nighttime BP [229]. A mouse model of Gordon's syndrome, in which NCC is hyperactive, exhibits enhanced BP amplitude compared to wild type mice, accompanied by both increased daytime and night time SBP [108]. In clinical studies, a dipping profile of SBP was restored following 4 weeks of chronic HCTZ [27] or sodium restriction [28], indicating an important role for renal sodium transport in non-dipping. BP control and other cardiovascular indices such as left ventricular mass are improved by nighttime administration of HCTZ [230, 231].

However, non-renal effects of HCTZ cannot be ruled out. The route for BP lowering in acute HCTZ treatment is a reduction in cardiac output as a result of increased sodium excretion reducing extra-cellular fluid (ECF) and plasma volume [212, 232]. However this mechanism seems to be transient as ECF volume returns to baseline with chronic HCTZ use [233]. Reduction in total peripheral resistance is proposed as the major mechanism of BP lowering during steady state HCTZ treatment ([106] and Reviewed in [232]). HCTZ can directly alter vascular tone through changes in ion transport [234, 235] and carbonic anhydrase inhibition [202]. However, as previously explored, thiazides have different capacities for carbonic anhydrase inhibition, therefore if this is the major mechanism for BP lowering it follows that drugs like BFMZ, with low potency for carbonic anhydrase inhibition [232] would be poorer

anti-hypertensive drugs, which is not the case [209]. Furthermore, sodium depletion appears to be necessary for BP lowering [236] and BP in patients undergoing haemodialysis is unresponsive to HCTZ [237]. Chronic GC exposure (be it though Cushing's disease or iatrogenic) can cause sodium retention (Reviewed: [92] and increased vascular tone (Reviewed: [238]) both of which might be ameliorated by HCTZ. Finally HCTZ can also inhibit the sodium dependent chloride and bicarbonate exchanger (NDCBE, SLC4A8) in the CCD, which may also contribute to renal sodium absorption and regulation of sodium balance *in vivo* [222].

5.4.10. Summary of Chapter Findings:

1. We were unable to show any difference in HCTZ-sensitive sodium transport between day and night in vehicle or corticosterone treated C57BL6 mice
2. Daytime SBP and DBP were markedly increased by chronic corticosterone treatment.
3. Chronic corticosterone treatment disrupted rhythmicity of SBP: increasing MESOR and decreasing amplitude.
4. Chronic HCTZ treatment partially rescued raised daytime SBP and improved rhythmicity, increased amplitude and decreased MESOR.
5. HR was similar between vehicle and corticosterone treated animals before and after HCTZ treatment.

6. Acute regulation of NCC by glucocorticoids

6.1. Introduction

In Chapter 4, it was shown that corticosterone affected the diurnal NCC phosphorylation rhythm. However, the experimental setup is not readily tractable for investigations into the pathways involved. The available cell lines do not adequately model NCC transport *in vivo* ([239] and personal communication from Prof. Robert Fenton, University of Aarhus). Therefore the overarching aim of the experiments presented in this chapter was to establish an *in vivo* system within which these networks leading to NCC phosphorylation could be probed. In particular the steroid receptor (GR or MR) through which GCs act to induce NCC phosphorylation was investigated.

6.1.1. Aims

1. To investigate whether acute corticosterone administration in ADX mice can induce phosphorylation of NCC.
2. To investigate whether changes in NCC phosphorylation can be resolved in adrenal intact (AI) mice
3. To explore whether GC-mediated NCC phosphorylation is MR dependent.

6.1.2. Strategy for addressing the chapter aims:

1. ADX was initially used as a manoeuvre to reduce circulating adrenal hormones and thus minimise the background effect that these hormones may have on NCC phosphorylation. This was considered important as handling mice for injection evokes stress responses leading to an upregulation of plasma corticosterone or adrenaline [240, 241] This might contribute to the phosphorylation of NCC. Initial experiments used an acute dose of 500 μg/kg corticosterone and compared NCC phosphorylation after 4 hours.
2. In the second experiment, a pharmacological dose (6 mg/kg) was chosen to more robustly and reproducibly induce NCC phosphorylation. Concomitantly, a pilot experiment (n=2) tested whether NCC phosphorylation differences could be resolved in AI mice.
3. 6 mg/kg corticosterone evoked a robust increase in NCC phosphorylation in both ADX and AI mice. MR-antagonist experiments were therefore carried out in AI mice, as this is a more humane approach. Blockade of MR was chosen as this receptor has been implicated in rhythmic NCC phosphorylation [160].

6.2. Methods

Detailed methods of each of the procedures in this chapter are outlined in the main methods section, however for clarity, an outline of the experiments carried out and cohorts of mice used are presented here.

6.2.1. Acute physiological corticosterone treatment in ADX mice

In the first experiment, C57BL6 male mice were adrenalectomised. An AI group (n=8) was anaesthetised but not surgically manipulated. Post operatively, mice were single housed and the drinking water replaced with 0.9% saline. At day 9, post-op, ADX animals were injected at ZT 0 with either vehicle (n=8, vehicle: 2% DMSO in 0.9% sterile injectable saline, s.c.) or 0.5 mg/kg corticosterone (n=8) (Based on those used in [82]). All the animals were culled in pairs 4 hours after injection at ZT 4 by cervical dislocation (Methods 2.3.1). Intact animals (n=8) were not injected but culled at the same time as ADX animals. Kidneys were taken for western analysis (Methods 2.3).

6.2.2. Acute pharmacological corticosterone treatment in ADX mice

In these experiments a pharmacological dose (6 mg/kg, [174]) of corticosterone was administered acutely to assess whether this induced robust and reproducible effects on NCC phosphorylation. 20 animals were ADX (maximum of 4 surgeries a day) and allowed to recover with access to 0.9% saline. At day 9-post surgery, mice were injected at ZT 0 with either vehicle (n=10, vehicle: 2% DMSO in 0.9% sterile injectable saline, sub cut) or 6 mg/kg corticosterone (n=10). All mice were culled in pairs 4 hours later at ZT 4 (4 culls per day). In a small pilot experiment conducted concomitantly, AI animals were also injected with either vehicle or corticosterone (n=2) and culled 4 hours later. The objective being to assess whether an effect on NCC following corticosterone treatment could be resolved in AI animals with normal levels of adrenal hormones. Kidneys were taken for western analysis and qPCR (Methods 2.3 and 2.4 respectively)

6.2.3. Acute pharmacological corticosterone treatment of adrenal intact mice

Following the success of the small pilot experiment in adrenal intact mice, naïve C57BL6 mice were pair housed in a quiet room for 1 week. Mice were injected at ZT 0 with either vehicle (n=6, vehicle: 2% DMSO in 0.9% sterile injectable saline, s.c.) or 6 mg/kg corticosterone (n=6, s.c.). Mice were culled in pairs 4 hours later with a maximum of 3 pairs culled per day to minimise disturbance. Miss Theresa Peltz performed western analysis in

these experiments under the author's supervision during her Physiological Society-sponsored summer studentship.

6.2.4. MR inhibition followed by corticosterone treatment of adrenal intact mice

C57BL6 mice were acclimatised to pair housing in quiet room for 1 week. Mice were then anaesthetised under isofluorane and 2 x 30 mg silastic slow-release spironolactone pellets were implanted s.c (surgery described Methods 2.7.2). The mice were then injected with vehicle (n=6, vehicle: 2% DMSO in 0.9% sterile injectable saline, s.c.) or 6mg/kg corticosterone (n=7, s.c.). They were culled in pairs 4 hours later with a maximum of 3 pairs culled per day to minimise disturbance. Western analysis for pT53 NCC and total NCC was performed as in Methods 2.3.

6.3. Results

6.3.1. Acute physiological corticosterone treatment does not increase NCC phosphorylation

NCC phosphorylation at T53 was unchanged by acute physiological (0.5 mg/kg, s.c) corticosterone treatment (Figure 6.1 A, C) of ADX mice. AI mice (Figure 6.1) were investigated alongside ADX animals as a control to assess the success of the ADX surgery. As anticipated, total NCC levels were reduced by ADX (Figure 6.1, B, E).

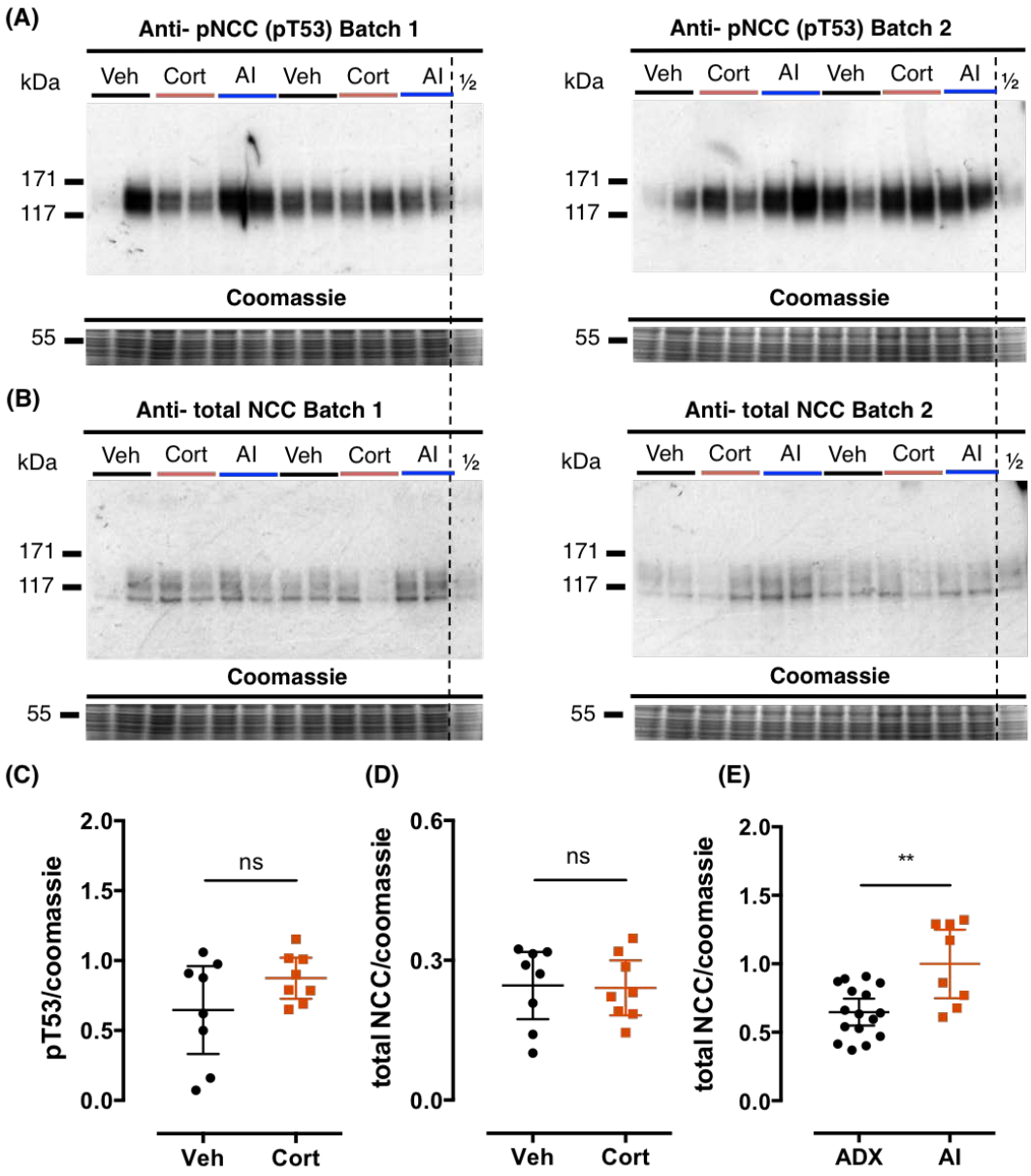

Figure 6.1: Western blots and corresponding densitometry analysis for pT53 NCC (A, C) and (B,D) total NCC in ADX C57BL6 mice 4 hours post 0.5 mg/kg corticosterone (cort) or vehicle (veh) injection

A group of untreated, adrenal intact (AI) animals were also culled contemporaneously as a control to assess the success of the ADX surgery. All ADX animals (cort and vehicle) versus AI animals total NCC levels are analysed in E. Data are mean ± 95% CI. Data was analysed by one way ANOVA with post hoc Holm-Sidak tests ** p<0.001 *p<0.05 (n=8)

6.3.2. *Acute pharmacological corticosterone treatment induces NCC phosphorylation in ADX mice*

pT53 NCC was increased by acute pharmacological corticosterone treatment (6 mg/kg, s.c.) compared to vehicle (2% DMSO in 0.9% saline) (p= 0.0002, Figure 6.2 A, Figure 6.3 A) in ADX C57BL6 mice. No such difference was evident for either pS71 (p=0.6299, Figure 6.2, 6.3 B) or total NCC (p=0.9030, Figure: 6.2, 6.3 C). AI animals are adrenal intact animals from a pilot experiment to test whether pT53 differences could be detected in adrenal-intact animals. pT53 in AI animals is slightly elevated in the corticosterone treated group by visual inspection (Fig 6.2 A batch 2 IN).

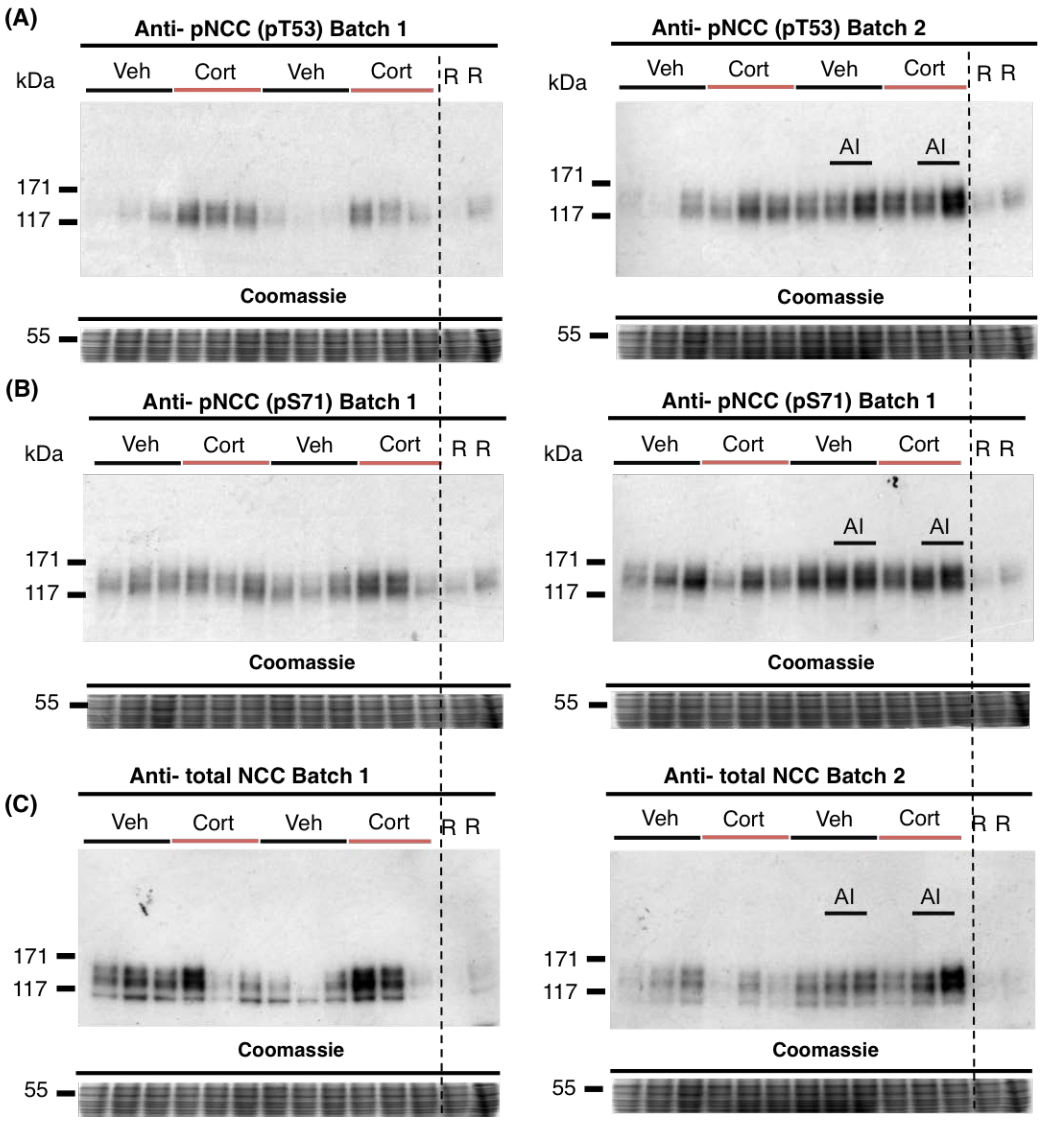

Figure 6.2: Western blots for (A) pT53 NCC, (B) pS71 and (C) total NCC in ADX or intact (AI) C57BL6 mice 4 hours post 6mg/lg corticosterone (cort) or vehicle (Veh) injection. "R" is 2 reference loads that were used to normalise across the western blots.

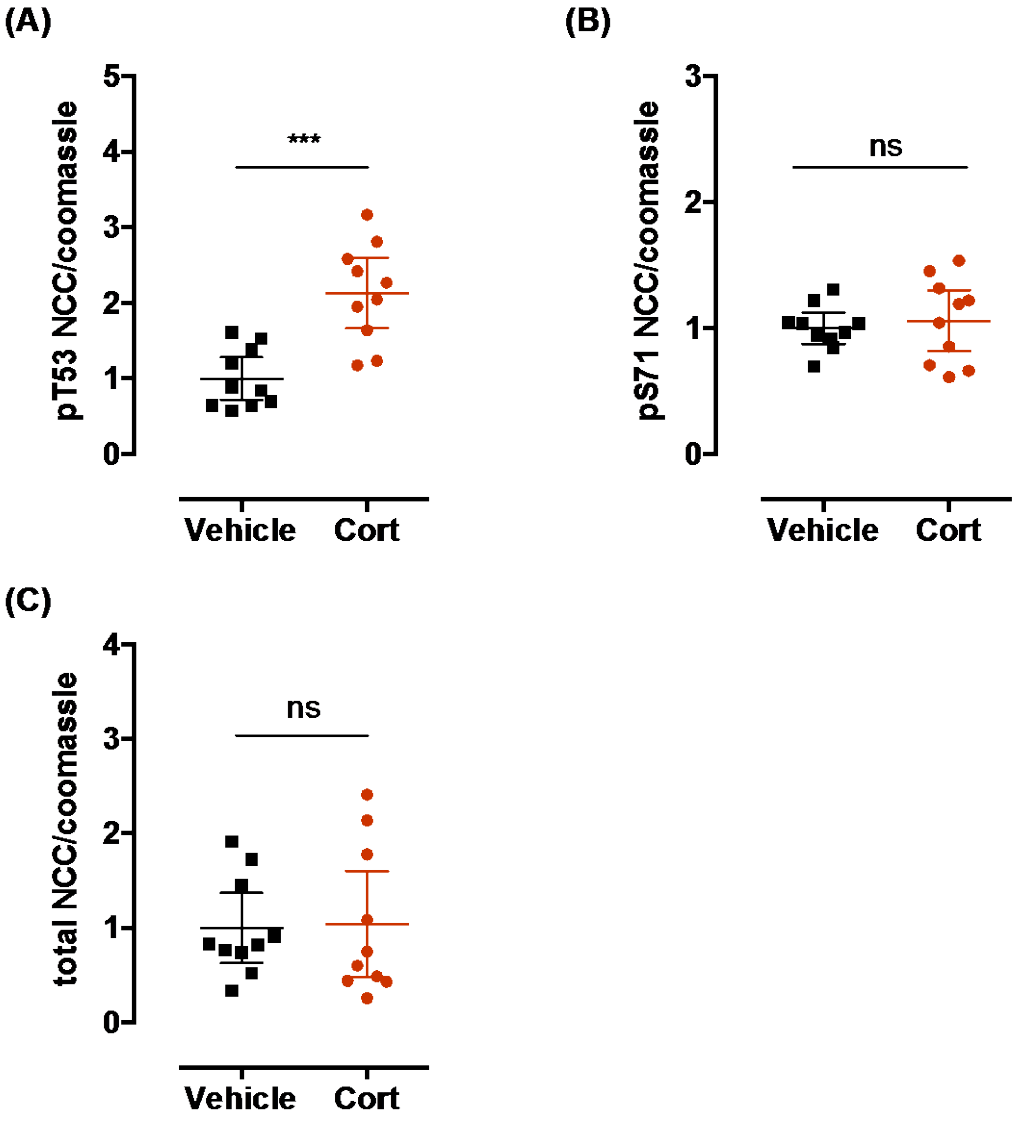

Figure 6.3: Densitometry analysis of Western blots for (A) pT53 NCC, (B) pS71 NCC, (C) total NCC in ADX C57BL6 mice after 6 mg/kg corticosterone (cort) or vehicle (veh) injection.

Data are mean ±95% CI. Unpaired Student's t tests were carried out on the densitometry analyses ***p<0.0001 **p<0.001 *p<0.05 ns p>0.05 (n=10). pT53:NCC was analysed using an unpaired Student's t test with Welch's correction for unequal variance.

6.3.3. Acute pharmacological corticosterone treatment induces NCC phosphorylation in adrenal intact mice

As shown in Figure 6.4, pT53 NCC and total NCC was measured in whole kidneys taken 4 hours post corticosterone (6 mg/kg, s.c.) or vehicle (2% DMSO in 0.9% saline, s.c.) in adrenal intact C57BL6 mice. NCC phosphorylation at T53 was markedly raised in the corticosterone treated compared to the vehicle treated animals (p= 0.004, Figure 6.4 A). No difference was evident for total NCC (p=0.21, Figure: 6.4 B). These data indicate that the effect of acute high dose corticosterone treatment on NCC phosphorylation can still be resolved in adrenal intact animals. This is a much-preferred experimental route as it avoids an invasive surgery and is better for animal welfare. Therefore this experimental setup was taken forward into inhibitor studies.

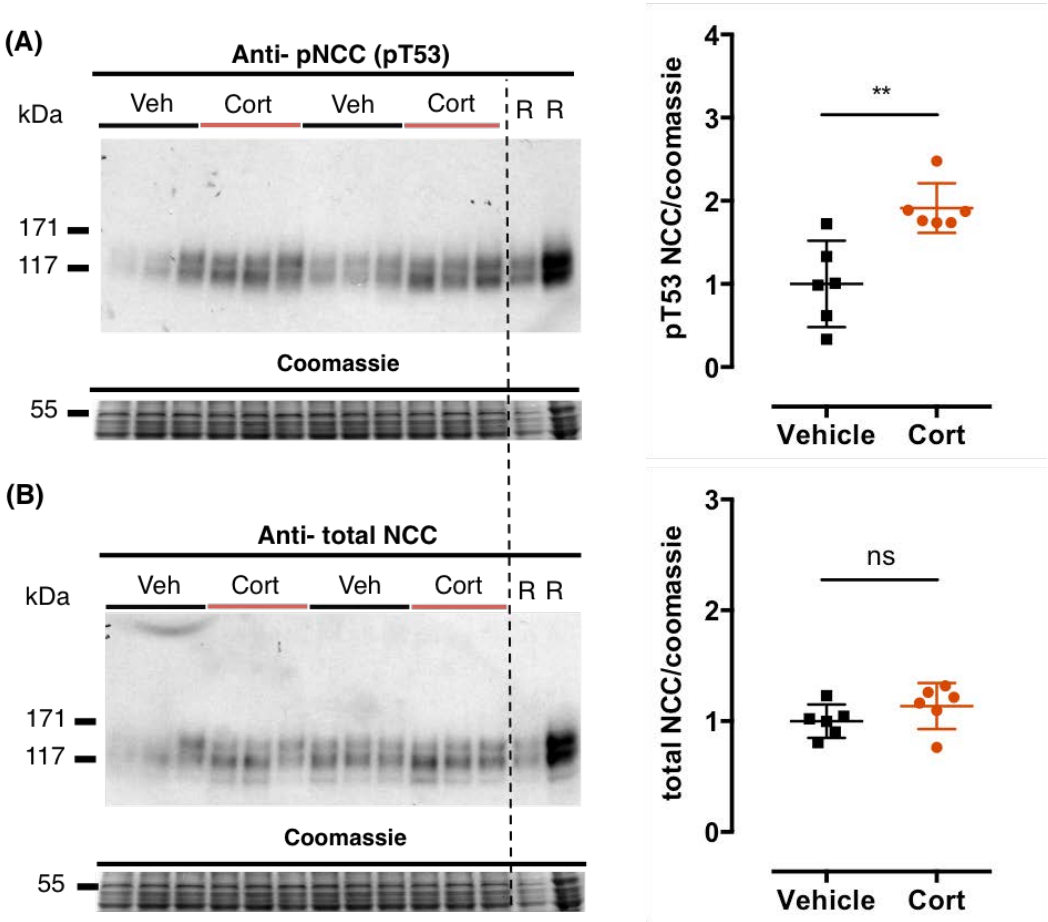

Figure 6.4: Western blots and corresponding densitometry analysis for (A) pT53 NCC and (B) total NCC in C57BL6 mice following a 6mg/kg corticosterone (cort) or vehicle (2%DMSO in 0.9% saline) injection.
Data are mean ±95% CI. Unpaired Student's t tests were carried out on the densitometry analyses ** p<0.001 ns p>0.05 (n=6).

6.3.4. Receptor pathways involved in NCC phosphorylation stimulation by corticosterone

In mice treated chronically with the MR inhibitor, spironolactone, NCC phosphorylation at T53 was markedly raised following corticosterone treatment compared to the vehicle treated animals (p= 0.017, Figure 6.5 A). There was no difference in total NCC between vehicle and corticosterone treated animals (p=0.40, Figure: 6.5 B). Therefore corticosterone-mediated NCC phosphorylation persists during MR inhibition.

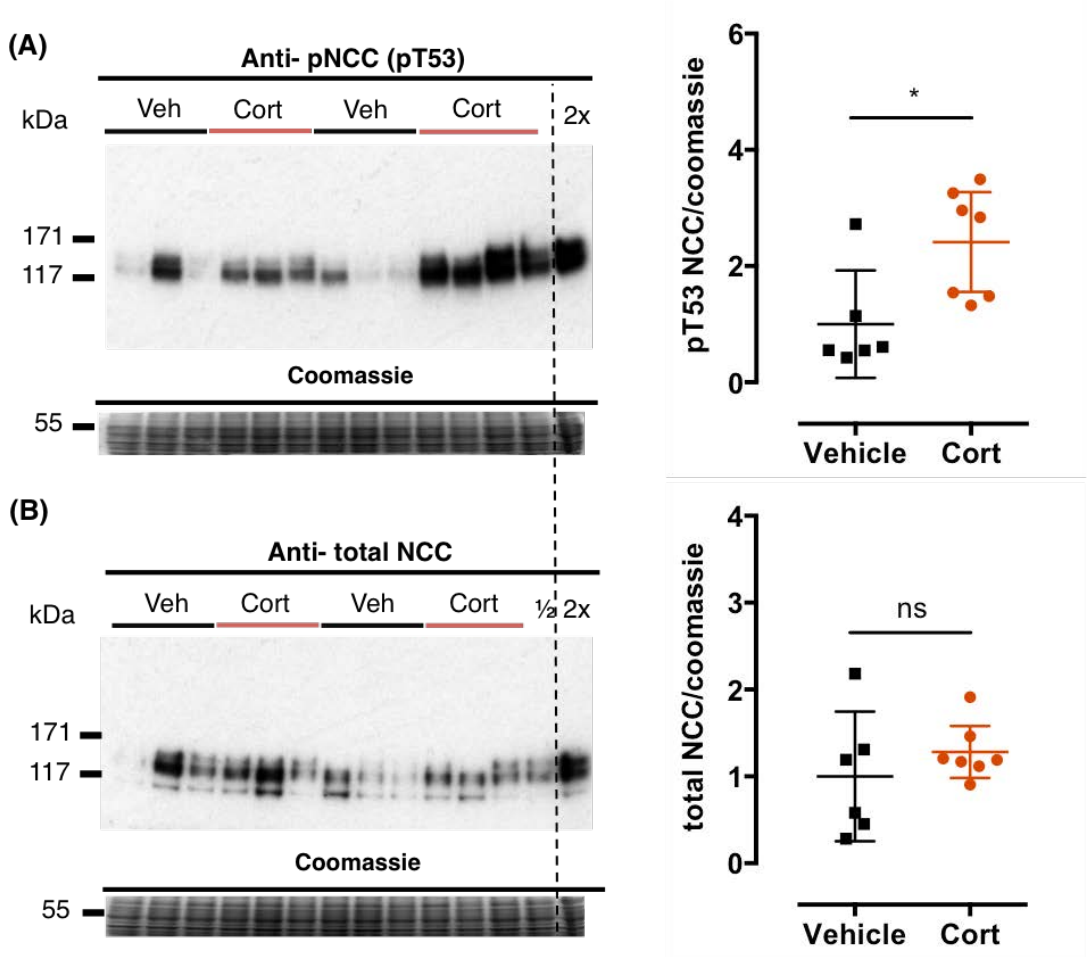

Figure 6.5: Western blots and corresponding densitometry analysis for (A) pT53 NCC and (B) total NCC in chronically spironolactone treated C57BL6 mice post 6 mg/kg corticosterone (cort) or vehicle (2 % DMSO in 0.9% saline) injections.
Data are mean ± 95% CI. Unpaired Student's t tests were carried out on the densitometry analyses * p<0.05 ns p>0.05 (n=6, vehicle group & n=7, cort group).

6.4. Discussion

The primary goal of this series of experiments was to design an *in vivo* system in which the pathways through which GCs can stimulate NCC phosphorylation could be investigated. Cell models were considered for this work but the current cell-lines available do not model NCC activity particularly well ([239] and personal communication from Prof. Robert Fenton, University of Aarhus). Therefore an *in vivo* system was chosen.

6.4.1. Physiological corticosterone and NCC phosphorylation

In the first instance, animals were adrenalectomised to minimise background corticosteroid levels and a high physiological dose was tested. The rationale for this dose was that it would mimic the daily peak plasma corticosterone levels. A very small rise in NCC phosphorylation was seen with corticosterone treatment but this did not reach statistical significance. The vehicle-treated group exhibited large variation in pT53 levels. It is possible that without corticosterone treatment, the vehicle group may have been more sensitive to other influences on rapid NCC phosphorylation such as feeding and saline drinking. It is also peculiar that the first sample from each gel has considerably low signal. This may be indicative of loading issues with these wells, but it is unclear how this arose. This approach was not carried forward, as any further pharmacological manipulations to the system would be difficult to interpret.

6.4.2. Pharmacological corticosterone and NCC phosphorylation

A 6 mg/kg dose of corticosterone robustly stimulated NCC phosphorylation within 4 hours in both adrenal intact and ADX animals. Experiments in C57BL6 mice show that this dose achieves a plasma concentration of ~ 3700 nmol/l within 15 minutes [174] that is sustained for at least 120 mins. This is ~2X the plasma corticosterone levels following acute restraint stress in C57BL6 mice (~1700 nmol/l, [174]). Interestingly a similar size of increase (~2X) in NCC phosphorylation compared to vehicle was evoked by corticosterone in both ADX and intact animals. ADX increases GR and MR levels [242], reduces circulating corticosteroids and may reduce 11βHSD2 levels, which need corticosterone to maintain activity [243]. In the ADX mice, it is likely that the difference in plasma corticosterone between corticosterone and vehicle treated groups would have been very large, with baseline corticosterone levels in ADX animals ~50 nmol/l (chapter 4) and stimulated levels ~3700 nmol/l. However ADX reduces total NCC and therefore the amount of total protein available to phosphorylate may have been the limiting factor. In intact animals the difference in plasma corticosterone levels between vehicle and corticosterone treated animals may not

have been as large (~1700 nmol/l estimate for handling for injection, [240] versus ≥3700 mmol/l) but total protein levels are higher allowing a higher maximum NCC phosphorylation.

NCC can undergo rapid phosphorylation and dephosphorylation: NCC dephosphorylates within 15 minutes following a K+ gavage and phosphorylates during a 15-minute vasopressin infusion [97]. However, there is very little data in the literature regarding the acute corticosteroid effects on NCC phosphorylation or activity. Most investigators have assessed the effect of several days of chronic infusion of aldosterone or corticosterone on NCC activity or phosphorylation [90, 91, 244]. In a DCT cell line, aldosterone stimulation induced NCC-dependent Na+ uptake within 12 hours; a shorter time frame was not investigated [157]. In an alternative approach, nuclear shutting of GR and MR occurred after 4 hours of aldosterone infusion [82]. Following the time course of NCC phosphorylation in response to a change in corticosterone would provide important information including the speed of response (any lag phases) and its maintenance and whether non-genomic effects are also observed. This may be particularly important in the context of circadian rhythms where temporal changes in plasma corticosteroids may precede effects on sodium reabsorption by several hours.

6.4.3. Role of MR in corticosterone-mediated NCC phosphorylation

An adrenal intact approach was taken forward for inhibitor experiments as this minimized animal suffering while still allowing detection of robust differences in NCC phosphorylation with corticosterone stimulation. Investigations on the role of MR in NCC phosphorylation were carried over GR as others demonstrated a role for MR in the diurnal rhythm of NCC phosphorylation [160]. These investigators found chronic eplerenone blockade inhibited the diurnal rhythm of NCC phosphorylation [160]. In our experiments however, upregulation of NCC phosphorylation occurred despite chronic MR blockade. There are several explanations for this finding: 1) incomplete inhibition of MR, 2) direct activation of GR in DCT or 3) indirect effects of GR activation elsewhere.

That MR may not have been adequately inhibited is unlikely. The same drug-formulation and dose was used to successfully block MR in 2 previous studies [200, 245]. Although not measured in the present study, this dosing regimen was previously shown to achieve terminal plasma levels of ~ 75 nmol/l canrenone, which was sufficient to induce BP lowering [200].

The other obvious explanation is that corticosterone induces NCC phosphorylation through direct interactions with GR in the distal nephron. GR has a 10X higher K_d for both corticosteroids than MR [246], i.e. MR will be fully occupied at 10X lower concentrations of hormone. It has been suggested that even if 11βHSD2 inactivated 99% of corticosterone in the ASDN, all of MR would be still bound to corticosterone [247]. In the DCT, total MR occupation by corticosterone is even more likely as 11βHSD2 expression is low [86](see Chapter 3). Therefore in AI animals it may be in the case that no further regulation can occur through MR and all dynamic regulation has to occur through GR. There is evidence to support this proposal in the literature. In ADX rats 1 μg/100gbw/d aldosterone induced the maximum thiazide-binding sites achievable for aldosterone. i.e. any further increases in aldosterone did not increase thiazide binding. However, RU-28362, a potent and highly selective GR agonist, on top of 1 μg/100gbw/d aldosterone induced a twofold increase in the thiazide binding sites. This indicates two mutually exclusive MR and GR pathways. A similar finding was reported by Velazques and co workers [91]. In conflict with this work, in an immortalised DCT cell line NCC activity was dependent on MR signalling and was not affected by GR inhibition with RU486. However, how this cell line work translates *in vivo* was not shown and it is not clear whether GR and MR expression levels are similar to *in vivo* levels [157].

There is strong evidence for the involvement of GR in pathological perturbations in sodium handling. Salt sensitive BP in 11βHSD2 heterozygous mice is unchanged by spironolactone but ameliorated by RU486 [245]. Aberrant ENaC regulation in these animals is also GR rather than MR dependent [248]. Recently, renal clearance experiments in these animals have revealed inappropriately raised thiazide-sensitive sodium transport following a high sodium diet compared to wild type controls (own observation, Appendix 9.1) suggesting a potential additional role for NCC in the aetiology of salt-sensitive blood pressure in these mice. Furthermore salt-sensitive BP induced by β-adrenergic stimulation was GR-dependent and accompanied by inappropriate NCC activation [103].

In immunofluorescent experiments *in vivo* low dose corticosterone infusion caused shuttling of GR to the nucleus of DCT cells [82] but not in principal cells of rat kidneys, where presumably GR is protected by 11βHSD2. However, MR shuttling to the nucleus of DCT cells also occurred with corticosterone infusion. MR certainly has a role in the regulation of NCC. Spironolactone treatment decreases the total amount of NCC protein [185]. Although not directly tested in this work, total NCC protein was likely reduced in our experiment: the

exposure time required to detect NCC protein in blots in these experiments was ~ 10X greater than that usually required for total NCC in untreated mice using the same protocols and antibodies. It might be that MR activation contributes to the setting of the level of NCC protein and then phosphorylation-dependent activation is then induced by GR.

GCs may indirectly affect NCC through extra-renal GR-activation. Dexamethasone induces an increase in blood pressure in mice that is GR, not MR dependent [249]. Interestingly, this DEX-induced high blood pressure is still evident in mice with conditional deletion of GR in the distal nephron (floxed using Ksp cadherin- CRE animals [250]). However, while the authors demonstrated a reduction of GR in AQP2-positive collecting ducts, no data was available for the presence of GR in NCC positive DCTs. Ksp cadherin is expressed in the DCT so one would expect at least a reduction in GR expression in DCT. It has therefore not been possible to definitely rule out GR-mediated NCC upregulation by DEX treatment. If tubular GR is not required for GC-induced high BP, this implicates extra-tubular GR in the genesis of GC-induced high blood pressure. This prompts the question: could the upregulation of NCC phosphorylation be an indirect result of GR activation? Both GFR and RBF increase with GC treatment within 2-3 hours [123, 251, 252]. An increase of GFR likely increases the delivery of sodium to the distal nephron [253], which will cause sodium-delivery dependent NCC activation [147, 254, 255]. Renal clearance experiments to measure thiazide sensitive sodium transport would allow the assessment of whether corticosterone-induced NCC phosphorylation has relevance for thiazide-sensitive sodium transport. Furthermore it would allow the assessment of any changes in renal haemodynamics with corticosterone treatment.

6.4.4. Limitations of experimental work

Financial and time constraints restricted the breadth of experimentation that could be conducted during this last phase of my PhD research. The limitations of these experiments are discussed here. Firstly, our data suggest that GCs do not activate NCC via MR but an alternative explanation is that we did adequately inhibit MR. Spironolactone is not the preferred MR antagonist as it has complex pharmacokinetics and off target effects. The majority of spironolactone's pharmacological effects are as a result of it's active metabolite canrenone. Spironolactone is rapidly metabolised to canrenone and both residual spironolactone and canrenone have off target effects [256]. A superior drug would have been eplerenone, which is highly specific but was prohibitively expensive for this work.

We have not measured canrenone in the samples taken from the current analysis due to the costs of the LCMS analysis. However, this is a key future experiment, as it will permit us to rule out inadequate MR inhibition as a reason for persistence of corticosterone-induced NCC phosphorylation in chronic MR blockade. Indeed, plasma analysis of canrenone may be particularly important to validate successful delivery in the vehicle treated group: this group has one outlier exhibiting both higher total NCC and higher pT53 than the other members of this group. This may be biological variation but could also indicate a failed spironolactone pellet.

These experiments are also restricted by the single dose used, followed by assessment at a single time point. A dose response curve experiment would yield valuable information about the relevance of GC signalling for "normal" physiology. The time point (4 hours post injection) chosen was an educated guess, based on a rough estimate for lag-time of genomic actions of corticosteroids ($\geq$ 1 hours, [165]) and on a previous experiment in which aldosterone infusion evoked changes in GR/MR nuclear translocation in renal tubules within 4 hours [82]. It is possible that changes in NCC phosphorylation may have occurred earlier and were not sustained at our 4-hour time point with the lower corticosterone dose but the larger dose caused sustained NCC phosphorylation that was detectable at 4 hours. Time course experiments would be useful in this regard. Experiments using RU486 to inhibit GR are necessary to confirm the importance of this receptor in NCC regulation.

6.4.5. Summary of Chapter Findings:

1. Acute corticosterone treatment induces NCC phosphorylation at T53
2. Chronic inhibition of MR with spironolactone does not prevent upregulation of pT53 NCC following acute corticosterone stimulation.

7. Discussion

The major findings of this thesis were that NCC has a diurnal rhythm of phosphorylation, which requires an intact GC rhythm. I further demonstrated that NCC phosphorylation is stimulated by corticosterone and that overstimulation reduces BP dipping, which is partially restored by thiazide diuretics.

7.1. Proposed model for role of NCC in diurnal rhythm of blood pressure

The kidney is important for the long-term control of BP homeostasis with the pressure natriuresis response serving to efficiently maintain extracellular fluid balance. Unsurprisingly evidence is accumulating for a role for renal sodium handling in the genesis of a circadian rhythm of BP ([26, 28] reviewed in: [257]). Our data indicates that NCC may contribute to BP rhythm; an effect on sodium balance would be the most plausible explanation for this but I was not able to demonstrate such an effect using the experimental approaches employed. My data (and that of others) suggest NCC's diurnal rhythm is not transcriptionally regulated at least at the level of the NCC transcript itself, but rather by phosphorylation of the protein [160].

The potential role of NCC and GCs is presented as a hypothesis in Figure 7.1. Here I propose that GCs regulate the circadian rhythm of NCC phosphorylation, which evokes rhythmic changes to sodium reabsorption; this in turn contributes to BP rhythmicity. Chronic GC treatment clamps NCC phosphorylation "on" during the day causing inappropriate sodium retention and elevated daytime BP. I showed that flattening the GC rhythms changed renal clock gene rhythms, altered daytime NCC phosphorylation, caused a small shift in day:night sodium balance and reduced BP dipping. There are several components of this hypothesis that we were unable to demonstrate experimentally. This includes specific NCC-induced changes in sodium reabsorption between day and night (i.e. HCTZ sensitive transport experiments in Chapter 4) and it is unclear whether the clock genes have a direct role to play in the regulation of NCC phosphorylation. Further experiments testing the assumptions of this model are needed. These should define GC-induced changes in NCC activity and identify whether natriuresis is the mechanism for BP lowering following HCTZ treatment in corticosterone-treated mice. Experiments in renal-specific clock mutants would allow the assessment of the role of the renal clock in NCC phosphorylation rhythms. A major limitation of this work is the use of only two time points for the assessment of NCC phosphorylation and transcriptional changes over 24 hours. These time points were initially

chosen to coincide with the peak and trough of blood pressure however, dynamic changes in NCC activation may occur before and facillitate this peak/trough in BP. Greater resolution of NCC phosphorylation over 24 hours is needed to investigate this possibility.

In a fully integrated system BP rhythmicity is the product of many interacting factors. In this regard, the model has limitations: 24-hour sodium balance is the product of total renal sodium transporter activity (including that in the proximal tubules, loop of Henle and distal nephron). Furthermore, transporter activity is influenced by multiple hormonal systems e.g. the RAAS, insulin, vasopressin and rSNA and changes in ultrafiltration capacity over 24 hours will also influence BP. Finally, GCs, through their effect on peripheral organ circadian clocks, will evoke multi-system effects outwith the kidney. Although limited, this figure is used here as a framework for a discussion on the clinical implications of this work.

7.2. Stimulation of NCC by GCs

The major emphasis of this work has been the role of GCs in the regulation of NCC phosphorylation. Two groups discovered a role for GCs in the regulation of NCC activity in the 1990s. These included experiments that showed an increase in metolazone-binding sites with dexamethasone treatment in adrenalectomised rats [90] and thiazide-sensitive sodium transport was increased by dexamethasone in micropuncture experiments [91]. Furthermore, GR was required for salt sensitive hypertension induced by β adrenergic receptor stimulation via modification of the WNK4 promoter [103]. This hypertension was accompanied by inappropriately raised HCTZ-sensitive sodium transport [103].

We have shown via 2 routes that GCs can evoke changes in NCC phosphorylation: (i) chronic administration of GCs alters the diurnal rhythm of NCC phosphorylation and (ii) acutely GCs stimulate NCC phosphorylation within 4 hours. This is a clinically relevant finding. There are many pathophysiological situation in which high or chronic GC levels feature, particularly in salt sensitive hypertension. Polymorphic variants of both the gene encoding GR (NR3C1) and 11βHSD2 (hsd211b), both involved in GC-sensitivity are found in the human population. GR (NR3C1) polymorphisms are associated with obesity and high BP [258, 259] and 11βHSD2 polymorphisms with salt sensitive hypertension [260] [261]. Whilst specific changes in NCC activity in humans with GC excess have not been documented, subtler GC abnormalities often feature in salt sensitive hypertension. Salt sensitive individuals exhibit augmented stress-induced activation of the HPA axis [262] and attenuated clearance of GCs [263].

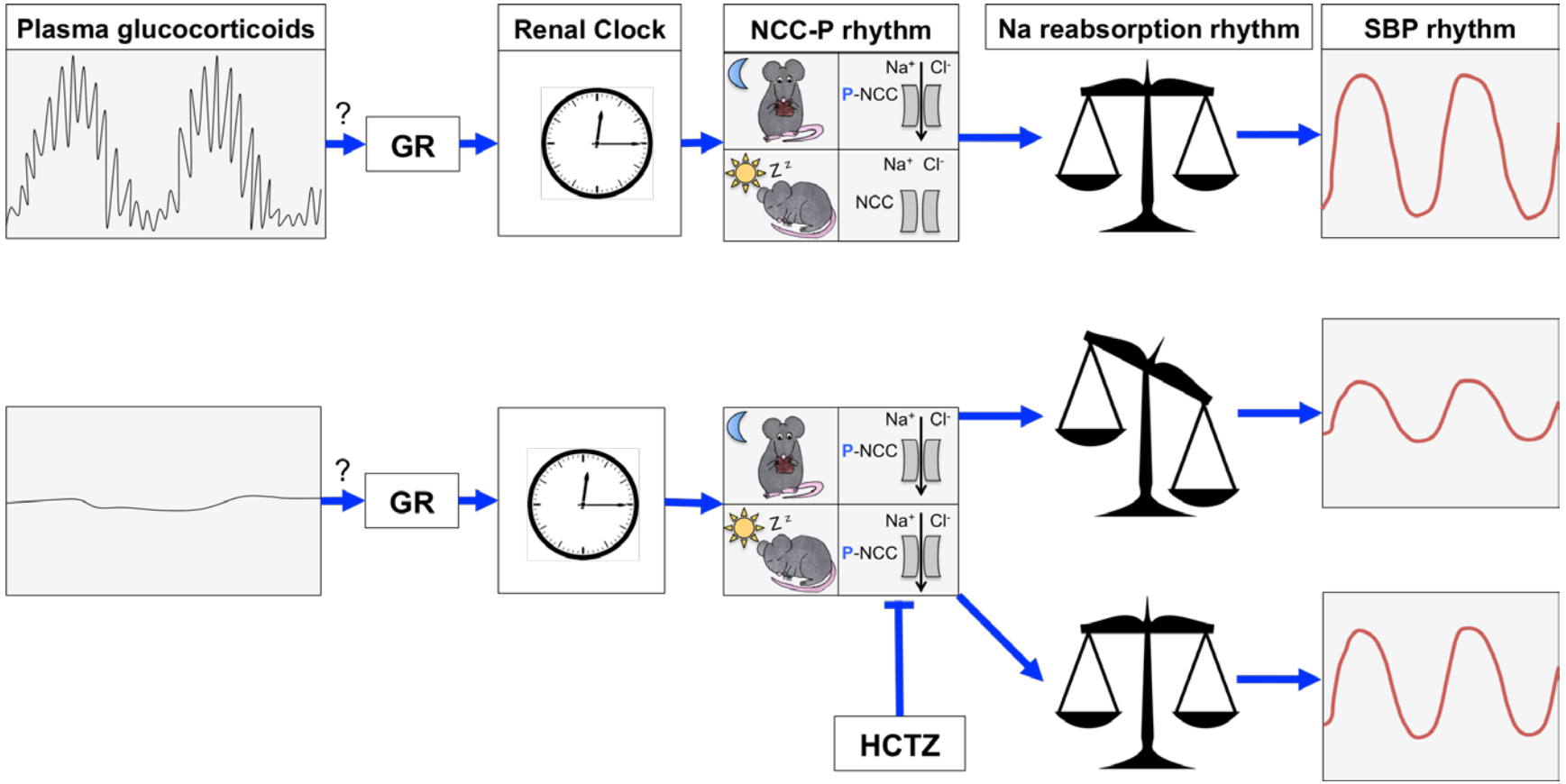

Figure 7.1: Hypothesis for the involvement of NCC and glucocorticoids (GCs) in the regulation of BP rhythm
Plasma GC rhythms may act through the GC receptor (GR) to entrain renal clocks, which may regulate the NCC phosphorylation rhythm. NCC activity through its contribution to the daily rhythm of sodium reabsorption affects the daily SBP (systolic blood pressure) rhythm. If the circadian rhythm of GCs is abolished through chronic treatment NCC phosphorylation is clamped on during the day leading to abrogation of sodium reabsorption rhythm and dampening of SBP rhythmicity. NCC inhibition with HCTZ through restoration of sodium reabsorption rhythms partially rescues SBP rhythmicity.

Furthermore, metabolic syndrome, which is highly prevalent in the western world, features the upregulation of GC tissue availability [264] and salt-sensitive hypertension [265] [266] [267].

Two mouse models within our lab featuring altered GC signalling indicate NCC perturbations contribute to their BP phenotypes. 11βHSD2 heterozygous mice, which exhibit salt sensitive hypertension [245], fail to downregulate BFMZ-sensitive sodium transport when on a high sodium diet (own observations, Appendix 9.1). Similarly GR haplo-insufficient mice [268] have salt sensitive BP and inappropriately elevated HCTZ-sensitive sodium transport upon high sodium feeding [269, 270]. Both have rhythms of corticosterone with a peak at ~ZT 12 and trough at ~ZT 0 but in the GR haploinsufficient mice both peak and trough levels are raised and in the 11βHSD2 heterozygous mice high sodium feeding causes an elevation in the peak levels but no change in the trough [248]. It would be intriguing to investigate both the GC rhythms and NCC phosphorylation rhythms are present in the full 11βHSD2 knock out mouse, which model the syndrome of apparent mineralocorticoid excess (SAME). In other labs, NCC activity is enhanced in salt-sensitive norepinephrine and isoproterenol-infused mice [103]. This is dependent on GR signalling and is abolished with RU486 treatment or adrenalectomy [103].

Our data would suggest that targeting NCC with thiazide diuretics might be a strategy for attenuating BP arhythmicity in metabolic syndrome or chronic stress. Indeed, in an experimental model of metabolic syndrome NCC phosphorylation was enhanced [271]. Conversely, chronic stress combined with salt loading caused high SBP in baboons that was not attenuated with HCTZ although BP rhythm was not studied [272]. Chlorthalidone, which is a thiazide-like diuretic with a longer half-life than HCTZ, has cardiovascular benefit in metabolic syndrome [273]. However, thiazide diuretics also exacerbate metabolic derangements and cause endothelial dysfunction [274]. It has been argued that the cardiovascular benefits outweigh the adverse metabolic side effects [275] and it has also been suggested that correcting hyperuriceamia and hypokalaemia may prevent the adverse metabolic side-effects associated with thiazide treatment while maintaining the BP lowering benefits [274].

7.3. How do GCs and the clock integrate with the NCC regulatory system?

The mechanism through which GCs and the clock integrate with intracellular pathways regulating NCC is unknown. Our work (in Chapter 6) suggests that this might be through the

GR but MR involvement cannot be ruled out and further investigations to this end are in progress using pharmacological approaches. However ideally further experiments to interrogate the receptor pathways underlying GC regulation of rhythmic NCC phosphorylathion would be undertaken using inducible kidney-specific GR/MR knock out mice.

The regulatory networks that link receptor activation to NCC phosphorylation/activation have also not been elucidated. GCs can alter the level of per1, per2 and rev-erbα directly through GREs and thus can directly influence the renal clock [76-79]. We confirmed this effect in a cohort of ADX mice, which showed induction of cry1, bmal1, per1 and per2 within 4 hours of corticosterone treatment (Figure 7.3). But this acute GC treatment also induced SGK1 and GILZ expression (Figure 7.3) and both are involved in the NCC regulatory cascade (discussed in Chapter 4). We have no temporal profile for these GC-induced genes. Furthermore these experiments were carried out in whole kidney. Therefore these findings prompt many more questions. Firstly what does the GC-induced gene expression profile look like in DCT? What is the order of gene induction? Does GILZ/SGK1 upregulation precede or result from clock gene induction or are these pathways independent? Finally are all or only a selection of these genes required for a change in NCC phosphorylation? What other genes are involved?

One way of approaching some of these questions would be to investigate whether NCC upregulation via GCs can occur in the absence of clock genes. Here, GC stimulation of NCC-p in a renal specific (or better yet DCT-specific) knock out of multiple clock genes would be informative. Furthermore defining any abnormalities in the intra-cellular regulatory kinases (WNKs/SPAK/OSR1) in these mouse models would be valuable in determining which parts of the regulatory pathways (if any) are affected.

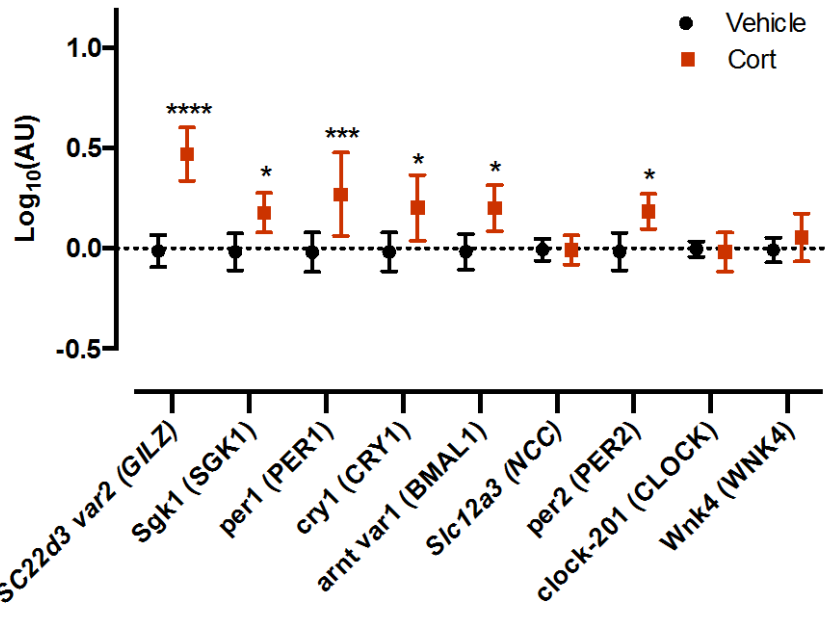

Figure 7.2: Gene expression in kidneys of ADX C57BL6 mice 4 hours following corticosterone (6mg/kg) or vehicle (2% DMSO in 0.9% saline) injection.
Protein the gene transcribes is in brackets. Expression of each gene was normalised to the average expression of 18S, TBP and HPRT. Data are mean±95% CI. Data were analysed by two way ANOVA with post hoc Sidak tests ****p<0.0001, ***p<0.001, *p<0.05 (n=10).

7.4. The importance of GCs in rhythmic BP

In our experiments we found a loss of rhythmicity, decrease in amplitude and increase in MESOR of BP in C57BL6 mice treated chronically with corticosterone. The finding that perturbations in GC signalling can evoke changes in BP rhythms is not new. In the clinic, both an excess of GCs, as seen in Cushing's disease [226] or with exogenous GC intake [227], and deficiency, as seen in Addison's disease [276] are associated with a lack of BP rhythmicity. The mice described in Chapter 5 exhibit marked changes to their BP rhythms despite having physiological levels of corticosterone. This gives further credence to the concept that it not only the level of GCs but also their temporal release that plays a role in disease [44, 277].

Alterations to the circadian rhythm of plasma GCs may be fairly common in the population featuring in jetlag, shift-work, chronic stress, metabolic syndrome and depression. Jetlag is the result of a rapid switch of external light/dark cues causing a misalignment of the internal circadian clocks and external time This is also accompanied by desynchrony of the tissue clocks as a result of differing kinetics of the peripheral oscillators and central clock. Although it is transient and perhaps of little long-term consequence for most holiday goers, those who travel frequently for business or indeed flight workers risk the long-term

consequences of chronic jet lag. These include adverse metabolic changes [278], increases in MAP [278], [279] and accelerated mortality with age [280].

Misalignment of circadian clocks also occurs with shift work, which is defined as employment in any work schedule that is not during regular daytime hours (9am to 5pm). A meta-analysis of ~ 2 million people from 34 studies links shift work to an increased risk of myocardial infarction, and ischaemic stroke [281]. Rotation shift work seems to pose a particular problem with a higher risk of death by cardiovascular disease than fixed-schedule work found in both Japanese [282] and African American but not in Caucasian workers [283]. Disruption of GC signalling is implicated in peripheral clock desynchrony in both shift work and jetlag [73, 284]. Interventions using timed GC treatment to resynchronise the peripheral clocks [74] may be a valuable approach for protection against the long term effects of jetlag and shift work. However, the practicalities of GC treatment are complicated by the need for both circadian and ultradian GC signalling for normal physiology as discussed later.

Jetlag and shift working are examples where external lighting cues or behaviours affect circadian rhythms of several systems as a result of mistimed sleep/feeding/awake cycles. However, there are also common examples of "internal" disruption of circadian GC rhythms for example in metabolic syndrome [285], chronic stress [286] and depression [287, 288]. This may have implications for circadian BP control with higher incidence of non-dipping BP reported in metabolic syndrome [289], depression [290], and chronic stress [291]. Renal sodium handling is implicated in the metabolic syndrome (reviewed: [292]) and in a rat model of metabolic syndrome NCC activity is inappropriately upregulated [271]. The role of sodium transporters in BP accompanying affective disorders has not been explored but may be an overlooked consequence of these disorders.

7.5. Chronotherapy: timely treating

In humans, non-dipping SBP is more closely associated with cardiovascular-associated morbidity and mortality than office BP or MAP [293] [13] [294]. In this work we have shown that NCC phosphorylation has a diurnal rhythm that is important for diurnal BP control in mice. Therefore some patients with non-dipping BP might too have miss-timed regulation of renal transporters. Evidence for this includes transformation of non-dipper to a dipper profile following sodium restriction or diuretic treatment in patients with essential hypertension [27, 28]. However, these individuals may benefit from targeting transporters at

the time at which they are most aberrant. This strategy, aptly named chronotherapy, is the timed administration of therapies to complement intrinsic circadian rhythms.

The MAPEC trial investigated the effect of taking at least one anti-hypertensive medication at bedtime rather than the conventional morning dosing schedule [295]. MAPEC was an open label, blinded end-point trial involving 2156 patients with essential hypertension taking at least 1 antihypertensive agent. Bedtime dosing improved mean arterial pressure control, decreased prevalence of non-dipping and importantly decreased cardiovascular morbidity and mortality [294, 295]. Furthermore nighttime dosing improved outcomes in resistant hypertension, hypertension during chronic kidney disease and hypertension with diabetes (reviewed in: [296]). There are several small trials that look at HCTZ chronotherapy in particular. In a randomised, open-label, blinded end-point study, HCTZ was added to the treatment regimen for 204 essential hypertension patients as BP was poorly controlled in patients with valsartan alone [231]. They found here that nighttime dosing increased the proportion of non-dipping patients [231]. HCTZ monotherapy was trialled in 165 African patients with essential hypertension with either bedtime or waking dosing regimen [230]. The major limitation of this work was that ambulatory BP was not measured. However, there was evidence of reduced target organ damage with bedtime dosing: left ventricular mass was reduced and diastolic function improved. MAP failed to reach significance ($p=0.07$, [230]).

According to our model for NCC's involvement in the circadian rhythm of BP, it might be assumed that HCTZs would be an effective treatment for BP alterations in states of high GCs such as Cushing's syndrome. As discussed earlier HCTZ treatment can exacerbate hypokalaemia in these individuals. An alternative strategy to target the BP effects of misaligned GC rhythms might be to try and mimic the circadian rhythm of GCs but this is no trivial task. In normal physiology temporal release of GCs can be spilt into both circadian and ultradian release. GCs are released in 1-2 ultradian pulses every hour, which increase in both amplitude and frequency towards the daily circadian peak and decrease towards the trough [297]. The ultradian GC release causes GR-mediated gene pulses. These pulses seem to modulate stress responses in rodents [298] but it is not clear what effect these might have on sodium balance and cardiovascular disease.

Currently available technology is unable to deliver pulsatile GCs and thereby replicate the true ultradian pattern of HPAA activity *in vivo* [277]. Nevertheless, attempts have been made to mimic the circadian rhythm of GCs in order to circumvent the disturbances to circadian

BP. In double blind cross over study in ADX patients investigators examined the difference between two treatment regimens: administration of 10 mg hydrocortisone first thing in the morning followed by 20 mg at night or 20 mg first thing in the morning followed by 10mg at night. The concept being that the higher dose first thing in the morning may more closely mirror the "morning surge" of cortisol experienced in adrenal intact individuals. They found little improvement in office MAP with either regimen and day/night differences in MAP remained minimal in both groups [299]. However, neither regimen replicated the physiological GC rhythm: causing two surges of cortisol at the beginning and end of the day. Modified release hydrocortisone has been more successful in mimicking the diurnal pattern of cortisol in patients [300]. This has very recently been shown to improve SBP compared to conventional cortisol replacement in Addison's patients [301].

There are two major reasons why chronotherapy is so important for treatment efficacy. Firstly consideration of any inherent circadian rhythms of the drug targets themselves is crucial. For example, HCTZs may have better efficacy at night because that's when NCC is inappropriately active and this corrects the aberrant sodium transport and restores the dipping SBP profile. Secondly, systems pertinent to the pharmacokinetics of drugs also have circadian rhythms. Gastric pH, emptying and motility have circadian rhythms that are important for absorption of oral drugs [302]. The liver, the organ with the highest number of circadian genes [43], is key in drug metabolism. GFR has a circadian rhythm with reduced GFR at night reducing excretion of drugs at night [303]. A recent study has shown that over 50% of the drugs on the market today target the product of a genes with a circadian rhythm and importantly almost half of these drugs have half lives <6 hours [43] and therefore timing of the dosing of these drugs in particular will be important for their efficacy.

In this work we have made a case for chronotherapeutic administration of thiazide diuretics and GCs but this is just the tip of the iceberg. A greater understanding of how we can harness the circadian rhythms of the intrinsic clocks controlling both drug targets and pharmacokinetics will mean better control of pathologies. Advances in our understanding of the mechanisms involved in the GC-induced entrainment of peripheral clocks may aid with the development of strategies to evade the health consequences of a 24-hour society.

8. References

1. Lim, S.S., T. Vos, A.D. Flaxman, G. Danaei, K. Shibuya, H. Adair-Rohani, M. Amann, H.R. Anderson, K.G. Andrews, M. Aryee, C. Atkinson, L.J. Bacchus, A.N. Bahalim, K. Balakrishnan, J. Balmes, et al., *A comparative risk assessment of burden of disease and injury attributable to 67 risk factors and risk factor clusters in 21 regions, 1990-2010: A systematic analysis for the global burden of disease study 2010.* Lancet, 2012. **380**(9859): p. 2224-60.
2. Kearney, P.M., M. Whelton, K. Reynolds, P. Muntner, P.K. Whelton, J. He, *Global burden of hypertension: Analysis of worldwide data.* The Lancet, 2005. **365**(9455): p. 217-223.
3. Clement, D.L., M.L. De Buyzere, D.A. De Bacquer, P.W. de Leeuw, D.A. Duprez, R.H. Fagard, P.J. Gheeraert, L.H. Missault, J.J. Braun, R.O. Six, P. Van Der Niepen, E. O'Brien, *Prognostic value of ambulatory blood-pressure recordings in patients with treated hypertension.* New England Journal of Medicine, 2003. **348**(24): p. 2407-2415.
4. Hansen, T.W., J. Jeppesen, S. Rasmussen, H. Ibsen, C. Torp-Pedersen, *Ambulatory blood pressure monitoring and risk of cardiovascular disease: A population based study.* Am J Hypertens, 2006. **19**(3): p. 243-50.
5. de la Sierra, A., J. Segura, J.R. Banegas, M. Gorostidi, J.J. de la Cruz, P. Armario, A. Oliveras, L.M. Ruilope, *Clinical features of 8295 patients with resistant hypertension classified on the basis of ambulatory blood pressure monitoring.* Hypertension, 2011. **57**(5): p. 898-902.
6. White, W.B., *Importance of blood pressure control over a 24-hour period.* J Manag Care Pharm, 2007. **13**(8 Suppl B): p. 34-9.
7. Pickering, T.G., K. Kario, *Nocturnal non-dipping: What does it augur?* Curr Opin Nephrol Hypertens, 2001. **10**(5): p. 611-6.
8. Verdecchia, P., G. Schillaci, M. Guerrieri, C. Gatteschi, G. Benemio, F. Boldrini, C. Porcellati, *Circadian blood pressure changes and left ventricular hypertrophy in essential hypertension.* Circulation, 1990. **81**(2): p. 528-36.
9. Vasunta, R.L., Y.A. Kesaniemi, A. Ylitalo, O. Ukkola, *Nondipping pattern and carotid atherosclerosis in a middle-aged population: Opera study.* Am J Hypertens, 2012. **25**(1): p. 60-6.
10. Bianchi, S., R. Bigazzi, G. Baldari, G. Sgherri, V.M. Campese, *Diurnal variations of blood pressure and microalbuminuria in essential hypertension.* Am J Hypertens, 1994. **7**(1): p. 23-9.
11. Yamamoto, Y., I. Akiguchi, K. Oiwa, M. Hayashi, T. Ohara, K. Ozasa, *The relationship between 24-hour blood pressure readings, subcortical ischemic lesions and vascular dementia.* Cerebrovasc Dis, 2005. **19**(5): p. 302-8.

12. Routledge, F.S., J.A. McFetridge-Durdle, C.R. Dean, *Night-time blood pressure patterns and target organ damage: A review.* The Canadian Journal of Cardiology, 2007. **23**(2): p. 132-138.
13. Ohkubo, T., A. Hozawa, J. Yamaguchi, M. Kikuya, K. Ohmori, M. Michimata, M. Matsubara, J. Hashimoto, H. Hoshi, T. Araki, I. Tsuji, H. Satoh, S. Hisamichi, Y. Imai, *Prognostic significance of the nocturnal decline in blood pressure in individuals with and without high 24-h blood pressure: The ohasama study.* J Hypertens, 2002. **20**(11): p. 2183-9.
14. Lurbe, E., J. Redon, A. Kesani, J.M. Pascual, J. Tacons, V. Alvarez, D. Batlle, *Increase in nocturnal blood pressure and progression to microalbuminuria in type 1 diabetes.* New England Journal of Medicine, 2002. **347**(11): p. 797-805.
15. Hermida, R.C., L. Chayan, D.E. Ayala, A. Mojon, M.J. Dominguez, M.J. Fontao, R. Soler, I. Alonso, J.R. Fernandez, *Association of metabolic syndrome and blood pressure nondipping profile in untreated hypertension.* Am J Hypertens, 2009. **22**(3): p. 307-13.
16. Farmer, C.K., D.J. Goldsmith, J. Cox, P. Dallyn, J.C. Kingswood, P. Sharpstone, *An investigation of the effect of advancing uraemia, renal replacement therapy and renal transplantation on blood pressure diurnal variability.* Nephrol Dial Transplant, 1997. **12**(11): p. 2301-7.
17. Timio, M., S. Venanzi, S. Lolli, G. Lippi, C. Verdura, C. Monarca, E. Guerrini, *"Non-dipper" hypertensive patients and progressive renal insufficiency: A 3-year longitudinal study.* Clin Nephrol, 1995. **43**(6): p. 382-7.
18. Mansoor, G.A., *Sleep actigraphy in hypertensive patients with the 'non-dipper' blood pressure profile.* J Hum Hypertens, 2002. **16**(4): p. 237-42.
19. Dhaun, N., R. Moorhouse, I.M. MacIntyre, V. Melville, W. Oosthuyzen, R.A. Kimmitt, K.E. Brown, E.D. Kennedy, J. Goddard, D.J. Webb, *Diurnal variation in blood pressure and arterial stiffness in chronic kidney disease: The role of endothelin-1.* Hypertension, 2014. **64**(2): p. 296-304.
20. Sherwood, A., F.S. Routledge, W.K. Wohlgemuth, A.L. Hinderliter, C.M. Kuhn, J.A. Blumenthal, *Blood pressure dipping: Ethnicity, sleep quality, and sympathetic nervous system activity.* Am J Hypertens, 2011. **24**(9): p. 982-8.
21. Ivy, J.R., M.A. Bailey, *Pressure natriuresis and the renal control of arterial blood pressure.* J Physiol, 2014. **592**(Pt 18): p. 3955-67.
22. Pons, M., J. Cambar, J.M. Waterhouse, *Renal hemodynamic mechanisms of blood pressure rhythms.* Ann N Y Acad Sci, 1996. **783**: p. 95-112.
23. Firsov, D., O. Bonny, *Circadian regulation of renal function.* Kidney Int, 2010. **78**(7): p. 640-5.
24. Centonza, L., G. Castoldi, R. Chianca, G. Busca, R. Golin, A. Zanchetti, A. Stella, *Short-term analysis of the relationship between blood pressure and urinary sodium excretion in normotensive subjects.* Clin Sci (Lond), 2000. **98**(4): p. 495-500.

25. Bultasova, H., A. Veselkova, V. Brodan, P. Pinsker, *Circadian rhythms of urinary sodium, potassium and some agents influencing their excretion in young borderline hypertensives.* Endocrinol Exp, 1986. **20**(4): p. 359-69.
26. Bankir, L., M. Bochud, M. Maillard, P. Bovet, A. Gabriel, M. Burnier, *Nighttime blood pressure and nocturnal dipping are associated with daytime urinary sodium excretion in african subjects.* Hypertension, 2008. **51**(4): p. 891-8.
27. Uzu, T., G. Kimura, *Diuretics shift circadian rhythm of blood pressure from nondipper to dipper in essential hypertension.* Circulation, 1999. **100**(15): p. 1635-1638.
28. Uzu, T., K. Ishikawa, T. Fujii, S. Nakamura, T. Inenaga, G. Kimura, *Sodium restriction shifts circadian rhythm of blood pressure from nondipper to dipper in essential hypertension.* Circulation, 1997. **96**(6): p. 1859-1862.
29. Gatzka, C.D., H.P. Schobel, A.U. Klingbeil, H.H. Neumayer, R.E. Schmieder, *Normalization of circadian blood pressure profiles after renal transplantation.* Transplantation, 1995. **59**(9): p. 1270-4.
30. Wadei, H.M., H. Amer, S.J. Taler, F.G. Cosio, M.D. Griffin, J.P. Grande, T.S. Larson, T.R. Schwab, M.D. Stegall, S.C. Textor, *Diurnal blood pressure changes one year after kidney transplantation: Relationship to allograft function, histology, and resistive index.* Journal of the American Society of Nephrology, 2007. **18**(5): p. 1607-1615.
31. Guyton, A.C., A.W. Cowley, T.G. Coleman, J.W. Declue, R.A. Norman, R.D. Manning, *Hypertension - disease of abnormal circulatory control.* Chest, 1974. **65**: p. 328-338.
32. Guyton, A.C., T.G. Coleman, D.B. Young, T.E. Lohmeier, J.W. Declue, *Salt balance and long-term blood-pressure control.* Annual Review of Medicine, 1980. **31**: p. 15-27.
33. Guyton, A.C., *The surprising kidney-fluid mechanism for pressure control - its infinite gain.* Hypertension, 1990. **16**: p. 725-730.
34. Guyton, A.C., *Renal-function curve - a key to understanding the pathogenesis of hypertension.* Hypertension, 1987. **10**: p. 1-6.
35. Fukuda, M., N. Goto, G. Kimura, *Hypothesis on renal mechanism of non-dipper pattern of circadian blood pressure rhythm.* Med Hypotheses, 2006. **67**(4): p. 802-6.
36. Mullins, L.J., M.A. Bailey, J.J. Mullins, *Hypertension, kidney, and transgenics: A fresh perspective.* Physiological Reviews, 2006. **86**: p. 709-746.
37. Moore-Ede, M.C., J.A. Herd, *Renal electrolyte circadian rhythms: Independence from feeding and activity patterns.* Am J Physiol, 1977. **232**(2): p. F128-35.
38. Minors, D.S., J.M. Waterhouse, *Circadian rhythms of urinary excretion: The relationship between the amount excreted and the circadian changes.* The Journal of Physiology, 1982. **327**: p. 39-51.
39. Dunlap, J.C., *Molecular bases for circadian clocks.* Cell, 1999. **96**(2): p. 271-290.
40. Etchegaray, J.-P., K.K. Machida, E. Noton, C.M. Constance, R. Dallmann, M.N. Di Napoli, J.P. DeBruyne, C.M. Lambert, E.A. Yu, S.M. Reppert, D.R. Weaver, *Casein kinase 1 delta*

regulates the pace of the mammalian circadian clock. Molecular and Cellular Biology, 2009. **29**(14): p. 3853-3866.

41. Zhang, E.E., S.A. Kay, *Clocks not winding down: Unravelling circadian networks.* Nat Rev Mol Cell Biol, 2010. **11**(11): p. 764-76.
42. Zuber, A.M., G. Centeno, S. Pradervand, S. Nikolaeva, L. Maquelin, L. Cardinaux, O. Bonny, D. Firsov, *Molecular clock is involved in predictive circadian adjustment of renal function.* Proceedings of the National Academy of Sciences, 2009. **106**(38): p. 16523-16528.
43. Zhang, R., N.F. Lahens, H.I. Ballance, M.E. Hughes, J.B. Hogenesch, *A circadian gene expression atlas in mammals: Implications for biology and medicine.* Proceedings of the National Academy of Sciences, 2014. **111**(45): p. 16219-16224.
44. Dickmeis, T., *Glucocorticoids and the circadian clock.* Journal of Endocrinology, 2009. **200**(1): p. 3-22.
45. Dibner, C., U. Schibler, U. Albrecht, *The mammalian circadian timing system: Organization and coordination of central and peripheral clocks.* Annual Review of Physiology, 2010. **72**(1): p. 517-549.
46. Saifur Rohman, M., N. Emoto, H. Nonaka, R. Okura, M. Nishimura, K. Yagita, G.T. van der Horst, M. Matsuo, H. Okamura, M. Yokoyama, *Circadian clock genes directly regulate expression of the na(+)/h(+) exchanger nhe3 in the kidney.* Kidney Int, 2005. **67**(4): p. 1410-9.
47. Gumz, M.L., L.R. Stow, I.J. Lynch, M.M. Greenlee, A. Rudin, B.D. Cain, D.R. Weaver, C.S. Wingo, *The circadian clock protein period 1 regulates expression of the renal epithelial sodium channel in mice.* J Clin Invest, 2009. **119**(8): p. 2423-34.
48. Meszaros, K., L. Pruess, A.J. Szabo, M. Gondan, E. Ritz, F. Schaefer, *Development of the circadian clockwork in the kidney.* Kidney Int, 2014. **86**(5): p. 915-22.
49. Curtis, A.M., Y. Cheng, S. Kapoor, D. Reilly, T.S. Price, G.A. FitzGerald, *Circadian variation of blood pressure and the vascular response to asynchronous stress.* Proceedings of the National Academy of Sciences, 2007. **104**(9): p. 3450-3455.
50. Rudic, R.D., P. McNamara, A.M. Curtis, R.C. Boston, S. Panda, J.B. Hogenesch, G.A. Fitzgerald, *Bmal1 and clock, two essential components of the circadian clock, are involved in glucose homeostasis.* PLoS Biol, 2004. **2**(11): p. e377.
51. Tokonami, N., D. Mordasini, S. Pradervand, G. Centeno, C. Jouffe, M. Maillard, O. Bonny, F. Gachon, R.A. Gomez, M.L.S. Sequeira-Lopez, D. Firsov, *Local renal circadian clocks control fluid–electrolyte homeostasis and bp.* Journal of the American Society of Nephrology, 2014.
52. Nikolaeva, S., S. Pradervand, G. Centeno, V. Zavadova, N. Tokonami, M. Maillard, O. Bonny, D. Firsov, *The circadian clock modulates renal sodium handling.* J Am Soc Nephrol, 2012. **23**(6): p. 1019-26.
53. Doi, M., Y. Takahashi, R. Komatsu, F. Yamazaki, H. Yamada, S. Haraguchi, N. Emoto, Y. Okuno, G. Tsujimoto, A. Kanematsu, O. Ogawa, T. Todo, K. Tsutsui, G.T. van der Horst, H.

Okamura, *Salt-sensitive hypertension in circadian clock-deficient cry-null mice involves dysregulated adrenal hsd3b6.* Nat Med, 2010. **16**(1): p. 67-74.

54. Lamia, K.A., S.J. Papp, R.T. Yu, G.D. Barish, N.H. Uhlenhaut, J.W. Jonker, M. Downes, R.M. Evans, *Cryptochromes mediate rhythmic repression of the glucocorticoid receptor.* Nature, 2011. **480**(7378): p. 552-556.
55. Stow, L.R., J. Richards, K.Y. Cheng, I.J. Lynch, L.A. Jeffers, M.M. Greenlee, B.D. Cain, C.S. Wingo, M.L. Gumz, *The circadian protein period 1 contributes to blood pressure control and coordinately regulates renal sodium transport genes.* Hypertension, 2012. **59**(6): p. 1151-6.
56. Richards, J., B. Ko, S. All, K.-Y. Cheng, R.S. Hoover, M.L. Gumz, *A role for the circadian clock protein per1 in the regulation of the nacl co-transporter (ncc) and the with-no-lysine kinase (wnk) cascade in mouse distal convoluted tubule cells.* Journal of Biological Chemistry, 2014. **289**(17): p. 11791-11806.
57. Richards, J., L.A. Jeffers, S.C. All, K.-Y. Cheng, M.L. Gumz, *Role of per1 and the mineralocorticoid receptor in the coordinate regulation of αenac in renal cortical collecting duct cells.* Front Physiol, 2013. **4**: p. 253.
58. Dallmann, R., C. Touma, R. Palme, U. Albrecht, S. Steinlechner, *Impaired daily glucocorticoid rhythm in per1 (brd) mice.* J Comp Physiol A Neuroethol Sens Neural Behav Physiol, 2006. **192**(7): p. 769-75.
59. Schmidt, T.M., S.-K. Chen, S. Hattar, *Intrinsically photosensitive retinal ganglion cells: Many subtypes, diverse functions.* Trends in neurosciences, 2011. **34**(11): p. 572-580.
60. Schibler, U., P. Sassone-Corsi, *A web of circadian pacemakers.* Cell, 2002. **111**(7): p. 919-922.
61. Guo, H., J.M. Brewer, M.N. Lehman, E.L. Bittman, *Suprachiasmatic regulation of circadian rhythms of gene expression in hamster peripheral organs: Effects of transplanting the pacemaker.* The Journal of Neuroscience, 2006. **26**(24): p. 6406-6412.
62. Clayton, J.D., C.P. Kyriacou, S.M. Reppert, *Keeping time with the human genome.* Nature, 2001. **409**(6822): p. 829-31.
63. Schwartz, M.D., H.F. Urbanski, A.A. Nunez, L. Smale, *Projections of the suprachiasmatic nucleus and ventral subparaventricular zone in the nile grass rat (arvicanthis niloticus).* Brain Res, 2011. **1367**: p. 146-61.
64. Todd, W.D., A.J. Gall, J.A. Weiner, M.S. Blumberg, *Distinct retinohypothalamic innervation patterns predict the developmental emergence of species-typical circadian phase preference in nocturnal norway rats and diurnal nile grass rats.* J Comp Neurol, 2012. **520**(14): p. 3277-92.
65. Nader, N., G.P. Chrousos, T. Kino, *Interactions of the circadian clock system and the hpa axis.* Trends Endocrinol Metab, 2010. **21**(5): p. 277-86.
66. Rosenfeld, P., J.A.M. van Eekelen, S. Levine, E.R. de Kloet, *Ontogeny of corticosteroid receptors in the brain.* Cellular and Molecular Neurobiology, 1993. **13**(4): p. 295-319.

67. Cascio, C.S., J. Shinsako, M.F. Dallman, *The suprachiasmatic nuclei stimulate evening acth secretion in the rat.* Brain Res, 1987. **423**(1-2): p. 173-8.
68. Chung, S., G.H. Son, K. Kim, *Circadian rhythm of adrenal glucocorticoid: Its regulation and clinical implications.* Biochimica et Biophysica Acta (BBA) - Molecular Basis of Disease, 2011. **1812**(5): p. 581-591.
69. Meier, A.H., *Daily variation in concentration of plasma corticosteroid in hypophysectomized rats.* Endocrinology, 1976. **98**(6): p. 1475-9.
70. Ottenweller, J.E., A.H. Meier, *Adrenal innervation may be an extrapituitary mechanism able to regulate adrenocortical rhythmicity in rats.* Endocrinology, 1982. **111**(4): p. 1334-8.
71. Reddy, A.B., E.S. Maywood, N.A. Karp, V.M. King, Y. Inoue, F.J. Gonzalez, K.S. Lilley, C.P. Kyriacou, M.H. Hastings, *Glucocorticoid signaling synchronizes the liver circadian transcriptome.* Hepatology, 2007. **45**(6): p. 1478-1488.
72. Pezük, P., J.A. Mohawk, L.A. Wang, M. Menaker, *Glucocorticoids as entraining signals for peripheral circadian oscillators.* Endocrinology, 2012. **153**(10): p. 4775-4783.
73. Cuesta, M., N. Cermakian, D.B. Boivin, *Glucocorticoids entrain molecular clock components in human peripheral cells.* Faseb j, 2015. **29**(4): p. 1360-70.
74. Balsalobre, A., S.A. Brown, L. Marcacci, F. Tronche, C. Kellendonk, H.M. Reichardt, G. Schütz, U. Schibler, *Resetting of circadian time in peripheral tissues by glucocorticoid signaling.* Science, 2000. **289**(5488): p. 2344-2347.
75. Sujino, M., K. Furukawa, S. Koinuma, A. Fujioka, M. Nagano, M. Iigo, Y. Shigeyoshi, *Differential entrainment of peripheral clocks in the rat by glucocorticoid and feeding.* Endocrinology, 2012. **153**(5): p. 2277-86.
76. So, A.Y.-L., T.U. Bernal, M.L. Pillsbury, K.R. Yamamoto, B.J. Feldman, *Glucocorticoid regulation of the circadian clock modulates glucose homeostasis.* Proceedings of the National Academy of Sciences, 2009. **106**(41): p. 17582-17587.
77. Yamamoto, T., Y. Nakahata, M. Tanaka, M. Yoshida, H. Soma, K. Shinohara, A. Yasuda, T. Mamine, T. Takumi, *Acute physical stress elevates mouse period1 mrna expression in mouse peripheral tissues via a glucocorticoid-responsive element.* Journal of Biological Chemistry, 2005. **280**(51): p. 42036-42043.
78. Cheon, S., N. Park, S. Cho, K. Kim, *Glucocorticoid-mediated period2 induction delays the phase of circadian rhythm.* Nucleic Acids Research, 2013. **41**(12): p. 6161-6174.
79. Torra, I.P., V. Tsibulsky, F. Delaunay, R. Saladin, V. Laudet, J.C. Fruchart, V. Kosykh, B. Staels, *Circadian and glucocorticoid regulation of rev-erbalpha expression in liver.* Endocrinology, 2000. **141**(10): p. 3799-806.
80. Nader, N., G.P. Chrousos, T. Kino, *Circadian rhythm transcription factor clock regulates the transcriptional activity of the glucocorticoid receptor by acetylating its hinge region lysine cluster: Potential physiological implications.* The FASEB Journal, 2009. **23**(5): p. 1572-1583.

81. Le Minh, N., F. Damiola, F. Tronche, G. Schütz, U. Schibler, *Glucocorticoid hormones inhibit food-induced phase-shifting of peripheral circadian oscillators.* The EMBO Journal, 2001. **20**(24): p. 7128-7136.
82. Ackermann, D., N. Gresko, M. Carrel, D. Loffing-Cueni, D. Habermehl, C. Gomez-Sanchez, B.C. Rossier, J. Loffing, *In vivo nuclear translocation of mineralocorticoid and glucocorticoid receptors in rat kidney: Differential effect of corticosteroids along the distal tubule.* American Journal of Physiology-Renal Physiology, 2010. **299**: p. F1473-F1485.
83. Todd-Turla, K.M., J. Schnermann, G. Fejes-Toth, A. Naray-Fejes-Toth, A. Smart, P.D. Killen, J.P. Briggs, *Distribution of mineralocorticoid and glucocorticoid receptor mrna along the nephron.* American Journal of Physiology - Renal Physiology, 1993. **264**(5): p. F781-F791.
84. Gaeggeler, H.P., E. Gonzalez-Rodriguez, N.F. Jaeger, D. Loffing-Cueni, R. Norregaard, J. Loffing, J.D. Horisberger, B.C. Rossier, *Mineralocorticoid versus glucocorticoid receptor occupancy mediating aldosterone-stimulated sodium transport in a novel renal cell line.* Journal of the American Society of Nephrology, 2005. **16**: p. 878-891.
85. Chapman, K., M. Holmes, J. Seckl, *11beta-hydroxysteroid dehydrogenases: Intracellular gate-keepers of tissue glucocorticoid action.* Physiol Rev, 2013. **93**(3): p. 1139-206.
86. Hunter, R.W., J.R. Ivy, P.W. Flatman, C.J. Kenyon, E. Craigie, L.J. Mullins, M.A. Bailey, J.J. Mullins, *Hypertrophy in the distal convoluted tubule of an 11beta-hydroxysteroid dehydrogenase type 2 knockout model.* J Am Soc Nephrol, 2015. **26**(7): p. 1537-48.
87. Naray-Fejes-Toth, A., G. Fejes-Toth, *Novel mouse strain with cre recombinase in 11beta-hydroxysteroid dehydrogenase-2-expressing cells.* Am J Physiol Renal Physiol, 2007. **292**(1): p. F486-94.
88. Campean, V., J. Kricke, D. Ellison, F.C. Luft, S. Bachmann, *Localization of thiazide-sensitive na(+)-cl(-) cotransport and associated gene products in mouse dct.* Am J Physiol Renal Physiol, 2001. **281**(6): p. F1028-35.
89. Bostanjoglo, M., W.B. Reeves, R.F. Reilly, H. Velazquez, N. Robertson, G. Litwack, P. Morsing, J. Dorup, S. Bachmann, D.H. Ellison, *11beta-hydroxysteroid dehydrogenase, mineralocorticoid receptor, and thiazide-sensitive na-cl cotransporter expression by distal tubules.* J Am Soc Nephrol, 1998. **9**(8): p. 1347-58.
90. Chen, Z.F., D.A. Vaughn, P. Blakely, D.D. Fanestil, *Adrenocortical steroids increase renal thiazide diuretic receptor density and response.* Journal of the American Society of Nephrology, 1994. **5**: p. 1361-1368.
91. Velazquez, H., A. Bartiss, P. Bernstein, D.H. Ellison, *Adrenal steroids stimulate thiazide-sensitive nacl transport by rat renal distal tubules*. Vol. 270. 1996. F211-F219.
92. Hunter, R.W., J.R. Ivy, M.A. Bailey, *Glucocorticoids and renal na+ transport: Implications for hypertension and salt sensitivity.* The Journal of Physiology, 2014. **592**(8): p. 1731-1744.
93. Simon, D.B., C. NelsonWilliams, M.J. Bia, D. Ellison, F.E. Karet, A.M. Molina, I. Vaara, F. Iwata, H.M. Cushner, M. Koolen, F.J. Gainza, H.J. Gitelman, R.P. Lifton, *Gitelman's variant*

of bartter's syndrome, inherited hypokalaemic alkalosis, is caused by mutations in the thiazide-sensitive na-cl cotransporter. Nature Genetics, 1996. **12**.

94. Mastroianni, N., A. Bettinelli, M. Bianchetti, G. Colussi, M. DeFusco, F. Sereni, A. Ballabio, C. Casari, *Novel molecular variants of the na-cl cotransporter gene are responsible for gitelman syndrome.* American Journal of Human Genetics, 1996. **59**.
95. Ohta, A., F.R. Schumacher, Y. Mehellou, C. Johnson, A. Knebel, T.J. Macartney, N.T. Wood, D.R. Alessi, T. Kurz, *The cul3-klhl3 e3 ligase complex mutated in gordon's hypertension syndrome interacts with and ubiquitylates wnk isoforms: Disease-causing mutations in klhl3 and wnk4 disrupt interaction.* Biochem J, 2013. **451**(1): p. 111-22.
96. Hadchouel, J., C. Delaloy, S. Fauré, J.-M. Achard, X. Jeunemaitre, *Familial hyperkalemic hypertension.* Journal of the American Society of Nephrology, 2006. **17**(1): p. 208-217.
97. Pedersen, N.B., M.V. Hofmeister, L.L. Rosenbaek, J. Nielsen, R.A. Fenton, *Vasopressin induces phosphorylation of the thiazide-sensitive sodium chloride cotransporter in the distal convoluted tubule.* Kidney International, 2010. **78**(2): p. 160-169.
98. Pacheco-Alvarez, D., P.S. Cristobal, P. Meade, E. Moreno, N. Vazquez, E. Munoz, A. Diaz, M.E. Juarez, I. Gimenez, G. Gamba, *The na+: Cl- cotransporter is activated and phosphorylated at the amino-terminal domain upon intracellular chloride depletion.* Journal of Biological Chemistry, 2006. **281**.
99. Richardson, C., F.H. Rafiqi, H.K.R. Karlsson, N. Moleleki, A. Vandewalle, D.G. Campbell, N.A. Morrice, D.R. Alessi, *Activation of the thiazide-sensitive na+-cl- cotransporter by the wnk-regulated kinases spak and osr1*. Journal of Cell Science, 2008. **121**.
100. Ko, B., A.C. Mistry, L. Hanson, R. Mallick, L.L. Cooke, B.K. Hack, P. Cunningham, R.S. Hoover, *A new model of the distal convoluted tubule.* American Journal of Physiology-Renal Physiology, 2012. **303**.
101. Rosenbaek, L.L., M.L. Kortenoeven, T.S. Aroankins, R.A. Fenton, *Phosphorylation decreases ubiquitylation of the thiazide-sensitive cotransporter ncc and subsequent clathrin-mediated endocytosis.* J Biol Chem, 2014. **289**(19): p. 13347-61.
102. Yang, S.-S., Y.-W. Fang, M.-H. Tseng, P.-Y. Chu, I.-S. Yu, H.-C. Wu, S.-W. Lin, T. Chau, S. Uchida, S. Sasaki, Y.-F. Lin, H.-K. Sytwu, S.-H. Lin, *Phosphorylation regulates ncc stability and transporter activity in vivo.* Journal of the American Society of Nephrology, 2013. **24**(10): p. 1587-1597.
103. Mu, S., T. Shimosawa, S. Ogura, H. Wang, Y. Uetake, F. Kawakami-Mori, T. Marumo, Y. Yatomi, D.S. Geller, H. Tanaka, *Epigenetic modulation of the renal [beta]-adrenergic-wnk4 pathway in salt-sensitive hypertension.* Nature medicine, 2011. **17**(5): p. 573-580.
104. Terker, A.S., C.L. Yang, J.A. McCormick, N.P. Meermeier, S.L. Rogers, S. Grossmann, K. Trompf, E. Delpire, J. Loffing, D.H. Ellison, *Sympathetic stimulation of thiazide-sensitive sodium chloride cotransport in the generation of salt-sensitive hypertension.* Hypertension, 2014. **64**(1): p. 178-84.

105. Lee, D.H., A.B. Maunsbach, A.D. Riquier-Brison, M.T.X. Nguyen, R.A. Fenton, S. Bachmann, A.S. Yu, A.A. McDonough, *Effects of ace inhibition and ang ii stimulation on renal na-cl cotransporter distribution, phosphorylation, and membrane complex properties.* American Journal of Physiology-Cell Physiology, 2013. **304**: p. C147-C163.

106. Wilson, I.M., E.D. Freis, *Relationship between plasma and extracellular fluid volume depletion and the antihypertensive effect of chlorothiazide.* Circulation, 1959. **20**: p. 1028-36.

107. Wilson, F.H., S. Disse-Nicodeme, K.A. Choate, K. Ishikawa, C. Nelson-Willams, I. Desitter, M. Gunel, D.V. Milford, G.W. Lipkin, J.M. Achard, M.P. Feely, B. Dussol, Y. Berland, R.J. Unwin, H. Mayan, et al., *Human hypertension caused by mutations in wnk kinases.* Science, 2001. **293**(5532).

108. Lalioti, M.D., J. Zhang, H.M. Volkman, K.T. Kahle, K.E. Hoffmann, H.R. Toka, C. Nelson-Williams, D.H. Ellison, R. Flavell, C.J. Booth, Y. Lu, D.S. Geller, R.P. Lifton, *Wnk4 controls blood pressure and potassium homeostasis via regulation of mass and activity of the distal convoluted tubule.* Nature Genetics, 2006. **38**.

109. McCormick, J.A., C.-L. Yang, D.H. Ellison, *Wnk kinases and renal sodium transport in health and disease - an integrated view.* Hypertension, 2008. **51**.

110. Cai, H., V. Cebotaru, J.H. Wang, X.M. Zhang, L. Cebotaru, S.E. Guggino, W.B. Guggino, *Wnk4 kinase regulates surface expression of the human sodium chloride cotransporter in mammalian cells.* Kidney International, 2006. **69**.

111. Subramanya, A.R., J. Liu, D.H. Ellison, J.B. Wade, P.A. Welling, *Wnk4 diverts the thiazide-sensitive nacl cotransporter to the lysosome and stimulates ap-3 interaction.* Journal of Biological Chemistry, 2009. **284**.

112. Lai, L.Y., X.Y. Feng, D.F. Liu, J. Chen, Y.Q. Zhang, B.W. Niu, Y. Gu, H. Cai, *Dietary salt modulates the sodium chloride cotransporter expression likely through an aldosterone-mediated wnk4-erk1/2 signaling pathway.* Pflugers Archiv-European Journal of Physiology, 2012. **463**: p. 477-485.

113. Castaneda-Bueno, M., L. Graciela Cervantes-Perez, N. Vazquez, N. Uribe, S. Kantesaria, L. Morla, N.A. Bobadilla, A. Doucet, D.R. Alessi, G. Gamba, *Activation of the renal na+:Cl- cotransporter by angiotensin ii is a wnk4-dependent process.* PROCEEDINGS OF THE NATIONAL ACADEMY OF SCIENCES OF THE UNITED STATES OF AMERICA, 2012. **109**.

114. Dimke, H., *Exploring the intricate regulatory network controlling the thiazide-sensitive nacl cotransporter (ncc).* Pflugers Arch, 2011. **462**(6): p. 767-77.

115. Wang, Z.H., C.L. Yang, D.H. Ellison, *Comparison of wnk4 and wnk1 kinase and inhibiting activities.* Biochemical and Biophysical Research Communications, 2004. **317**.

116. Pablo Arroyo, J., C. Ronzaud, D. Lagnaz, O. Staub, G. Gamba, *Aldosterone paradox: Differential regulation of ion transport in distal nephron.* Physiology, 2011. **26**.

117. Subramanya, A.R., C.L. Yang, X.M. Zhu, D.H. Ellison, *Dominant-negative regulation of wnk1 by its kidney-specific kinase-defective isoform.* American Journal of Physiology-Renal Physiology, 2006. **290**.

118. O'Reilly, M., E. Marshall, T. MacGillivray, M. Mittal, W. Xue, C.J. Kenyon, R.W. Brown, *Dietary electrolyte–driven responses in the renal wnk kinase pathway in vivo.* Journal of the American Society of Nephrology, 2006. **17**(9): p. 2402-2413.

119. Sandberg, M.B., A.B. Maunsbach, A.A. McDonough, *Redistribution of distal tubule na(+)-cl(-) cotransporter (ncc) in response to a high-salt diet.* American Journal of Physiology-Renal Physiology, 2006. **291**.

120. Gonzalez-Nunez, D., M. Morales-Ruiz, A. Leivas, S.C. Hebert, E. Poch, *In vitro characterization of aldosterone and camp effects in mouse distal convoluted tubule cells.* American Journal of Physiology-Renal Physiology, 2004. **286**.

121. Abdallah, J.G., R.W. Schrier, C. Edelstein, S.D. Jennings, B. Wyse, D.H. Ellison, *Loop diuretic infusion increases thiazide-sensitive na+/cl--cotransporter abundance: Role of aldosterone.* Journal of the American Society of Nephrology, 2001. **12**: p. 1335-1341.

122. Rozansky, D.J., T. Cornwall, A.R. Subramanya, S. Rogers, Y.-F. Yang, L.L. David, X. Zhu, C.-L. Yang, D.H. Ellison, *Aldosterone mediates activation of the thiazide-sensitive na-cl cotransporter through an sgk1 and wnk4 signaling pathway.* Journal of Clinical Investigation, 2009. **119**.

123. Mangos, G.J., J.A. Whitworth, P.M. Williamson, J.J. Kelly, *Glucocorticoids and the kidney.* Nephrology, 2003. **8**.

124. Wakabayashi, M., T. Mori, K. Isobe, E. Sohara, K. Susa, Y. Araki, M. Chiga, E. Kikuchi, N. Nomura, Y. Mori, H. Matsuo, T. Murata, S. Nomura, T. Asano, H. Kawaguchi, et al., *Impaired klhl3-mediated ubiquitination of wnk4 causes human hypertension.* Cell Rep, 2013. **3**(3): p. 858-68.

125. Shibata, S., J. Zhang, J. Puthumana, K.L. Stone, R.P. Lifton, *Kelch-like 3 and cullin 3 regulate electrolyte homeostasis via ubiquitination and degradation of wnk4.* Proc Natl Acad Sci U S A, 2013. **110**(19): p. 7838-43.

126. Roy, A., L. Al-Qusairi, B.F. Donnelly, C. Ronzaud, A.L. Marciszyn, F. Gong, Y.P.C. Chang, M.B. Butterworth, N.M. Pastor-Soler, K.R. Hallows, O. Staub, A.R. Subramanya, *Alternatively spliced proline-rich cassettes link wnk1 to aldosterone action.* J Clin Invest, 2015. **125**(9): p. 3433-3448.

127. Flatman, P.W., *Regulation of na–k–2cl cotransport by phosphorylation and protein–protein interactions.* Biochimica et Biophysica Acta (BBA) - Biomembranes, 2002. **1566**(1–2): p. 140-151.

128. Traslavina, R.P., E.J. King, A.S. Loar, E.R. Riedel, M.S. Garvey, R. Ricart-Arbona, F.R. Wolf, S.S. Couto, *Euthanasia by co2 inhalation affects potassium levels in mice.* Journal of the American Association for Laboratory Animal Science, 2010. **49**: p. 316-322.

129. Sorensen, M.V., S. Grossmann, M. Roesinger, N. Gresko, A.P. Todkar, G. Barmettler, U. Ziegler, A. Odermatt, D. Loffing-Cueni, J. Loffing, *Rapid dephosphorylation of the renal sodium chloride cotransporter in response to oral potassium intake in mice.* Kidney International, 2013. **83**: p. 811-824.

130. Hunter, R.W., *The renal distal convoluted tubule in apparent mineralocorticoid excess*, in *Centre for Cardiovascular Science*. 2013, University of Edinburgh: Edinburgh. p. 313.

131. Gamba, G., A. Miyanoshita, M. Lombardi, J. Lytton, W.S. Lee, M.A. Hediger, S.C. Hebert, *Molecular cloning, primary structure, and characterization of two members of the mammalian electroneutral sodium-(potassium)-chloride cotransporter family expressed in kidney.* Journal of Biological Chemistry, 1994. **269**(26): p. 17713-22.

132. Hoover, R.S., E. Poch, A. Monroy, N. Vazquez, T. Nishio, G. Gamba, S.C. Hebert, *N-glycosylation at two sites critically alters thiazide binding and activity of the rat thiazide-sensitive na(+):Cl(-) cotransporter.* J Am Soc Nephrol, 2003. **14**(2): p. 271-82.

133. McCormick, J.A., J.H. Nelson, C.-L. Yang, J.N. Curry, D.H. Ellison, *Overexpression of the sodium chloride cotransporter is not sufficient to cause familial hyperkalemic hypertension.* Hypertension, 2011. **58**(5): p. 888-894.

134. Liu, Z., J. Xie, T. Wu, T. Truong, R.J. Auchus, C.-L. Huang, *Downregulation of ncc and nkcc2 cotransporters by kidney-specific wnk1 revealed by gene disruption and transgenic mouse models.* Human Molecular Genetics, 2010.

135. Pech, V., M. Thumova, Y.H. Kim, D. Agazatian, E. Hummler, B.C. Rossier, A.M. Weinstein, M. Nanami, S.M. Wall, *Enac inhibition stimulates cl− secretion in the mouse cortical collecting duct through an nkcc1-dependent mechanism.* Vol. 303. 2012. F45-F55.

136. Richardson, C., K. Sakamoto, P. de los Heros, M. Deak, D.G. Campbell, A.R. Prescott, D.R. Alessi, *Regulation of the nkcc2 ion cotransporter by spak-osr1-dependent and -independent pathways.* Journal of Cell Science, 2011. **124**(5): p. 789-800.

137. Cicinnati, V.R., G.C. Shen Q Fau - Sotiropoulos, A. Sotiropoulos Gc Fau - Radtke, G. Radtke A Fau - Gerken, S. Gerken G Fau - Beckebaum, S. Beckebaum, *Validation of putative reference genes for gene expression studies in human hepatocellular carcinoma using real-time quantitative rt-pcr.* (1471-2407 (Electronic)).

138. Majewski, J., J. Ott, *Distribution and characterization of regulatory elements in the human genome.* Genome Research, 2002. **12**(12): p. 1827-1836.

139. Schmid, H., C.D. Cohen, A. Henger, S. Irrgang, D. Schlondorff, M. Kretzler, *Validation of endogenous controls for gene expression analysis in microdissected human renal biopsies.* Kidney Int, 2003. **64**(1): p. 356-360.

140. Hoenderop, J.G.J., A.W.C.M. van der Kemp, C.M. Urben, S.A. Strugnell, R.J.M. Bindels, *Effects of vitamin d compounds on renal and intestinal ca2+ transport proteins in 25-hydroxyvitamin d3-1[alpha]-hydroxylase knockout mice1.* Kidney Int, 2004. **66**(3): p. 1082-1089.

141. Al-Dujaili, E.A.S., L.J. Mullins, M.A. Bailey, R. Andrew, C.J. Kenyon, *Physiological and pathophysiological applications of sensitive elisa methods for urinary deoxycorticosterone and corticosterone in rodents.* Steroids, 2009. **74**: p. 938-944.

142. Al-Dujaili, E.A.S., L.J. Mullins, M.A. Bailey, C.J. Kenyon, *Development of a highly sensitive elisa for aldosterone in mouse urine: Validation in physiological and pathophysiological states of aldosterone excess and depletion.* Steroids, 2009. **74**: p. 456-462.

143. Hoogstraten-Miller, S.L., P.A. Brown, *Techniques in aseptic rodent surgery.* Current protocols in immunology / edited by John E. Coligan ... [et al.], 2008. **CHAPTER**: p. Unit-1.12-14.

144. Refinetti, R., G.C. Lissen, F. Halberg, *Procedures for numerical analysis of circadian rhythms.* Biological rhythm research, 2007. **38**(4): p. 275-325.

145. Levinsky, N., W. Lieberthal, *Clearance techniques*, in *Comprehensive physiology*. 1992. p. 227-247.

146. Craigie, E., *Investigating mechanisms of salt-sensitive hypertension in 11β-hsd2 heterozygote mice*, in *Department of Molecular Physiology*. 2011, The University of Edinburgh: Edinburgh. p. 284.

147. Hunter, R.W., E. Craigie, N.Z.M. Homer, J.J. Mullins, M.A. Bailey, *Acute inhibition of ncc does not activate distal electrogenic na(+) reabsorption or kaliuresis.* American Journal of Physiology - Renal Physiology, 2014. **306**(4): p. F457-F467.

148. Possidente, B., S. Birnbaum, *Circadian rhythms for food and water consumption in the mouse, mus musculus.* Physiol Behav, 1979. **22**(4): p. 657-60.

149. Ameringer, S., R.C. Serlin, S. Ward, *Simpson's paradox and experimental research.* Nursing research, 2009. **58**(2): p. 123-127.

150. Subramanya, A.R., D.H. Ellison, *Distal convoluted tubule.* Clinical Journal of the American Society of Nephrology, 2014. **9**(12): p. 2147-2163.

151. Ho, A., A. Chin, *Circadian feeding and drinking patterns of genetically obese mice fed solid chow diet.* Physiol Behav, 1988. **43**(5): p. 651-656.

152. Edgar, D.M., T.S. Kilduff, C.E. Martin, W.C. Dement, *Influence of running wheel activity on free-running sleep/wake and drinking circadian rhythms in mice.* Physiol Behav, 1991. **50**(2): p. 373-378.

153. Boemke, W., U. Palm, M. Corea, E. Seeliger, H.W. Reinhardt, *Endogenous variations and sodium intake-dependent components of diurnal sodium excretion patterns in dogs.* The Journal of Physiology, 1994. **476**(3): p. 547-552.

154. Manchester, R.C., *The diurnal rhythm in water and mineral exchange.* J Clin Invest, 1933. **12**(6): p. 995-1008.

155. Shin, J., E. Xu, Y. Lim, B. Choi, B. Kim, Y. Lee, M. Kim, M. Mori, Y. Yamori, *Erratum to: Relationship between nocturnal blood pressure and 24-h urinary sodium excretion in a rural population in korea.* Clinical Hypertension, 2015. **21**(1): p. 1-1.

156. Dyer, A.R., R. Stamler, R. Grimm, J. Stamler, R. Berman, F.C. Gosch, L.A. Emidy, P. Elmer, J. Fishman, N. Van Heel, et al., *Do hypertensive patients have a different diurnal pattern of electrolyte excretion?* Hypertension, 1987. **10**(4): p. 417-24.
157. Ko, B., A.C. Mistry, L. Hanson, R. Mallick, B.M. Wynne, T.L. Thai, J.L. Bailey, J.D. Klein, R.S. Hoover, *Aldosterone acutely stimulates ncc activity via a spak-mediated pathway.* Am J Physiol Renal Physiol, 2013. **305**(5): p. F645-52.
158. Ashek, A., R.I. Menzies, L.J. Mullins, C.O.C. Bellamy, A.J. Harmar, C.J. Kenyon, P.W. Flatman, J.J. Mullins, M.A. Bailey, *Activation of thiazide-sensitive co-transport by angiotensin ii in the cyp1a1-ren2 hypertensive rat.* Plos One, 2012. **7**.
159. Yang, S.-S., Y.-F. Lo, C.-C. Wu, S.-W. Lin, C.-J. Yeh, P. Chu, H.-K. Sytwu, S. Uchida, S. Sasaki, S.-H. Lin, *Spak-knockout mice manifest gitelman syndrome and impaired vasoconstriction.* Journal of the American Society of Nephrology, 2010. **21**(11): p. 1868-1877.
160. Susa, K., E. Sohara, K. Isobe, M. Chiga, T. Rai, S. Sasaki, S. Uchida, *Wnk-osr1/spak-ncc signal cascade has circadian rhythm dependent on aldosterone.* Biochemical and Biophysical Research Communications, 2012. **427**: p. 743-747.
161. Castagna, A., F. Pizzolo, L. Chiecchi, F. Morandini, S.K. Channavajjhala, P. Guarini, G. Salvagno, O. Olivieri, *Circadian exosomal expression of renal thiazide-sensitive nacl cotransporter (ncc) and prostasin in healthy individuals.* Proteomics Clin Appl, 2015. **9**(5-6): p. 623-9.
162. Dear, J.W., J.M. Street, M.A. Bailey, *Urinary exosomes: A reservoir for biomarker discovery and potential mediators of intrarenal signalling.* PROTEOMICS, 2013. **13**(10-11): p. 1572-1580.
163. Hughes, M.E., J.B. Hogenesch, K. Kornacker, *Jtk_cycle: An efficient nonparametric algorithm for detecting rhythmic components in genome-scale data sets.* Journal of Biological Rhythms, 2010. **25**(5): p. 372-380.
164. Cuesta, M., N. Cermakian, D.B. Boivin, *Glucocorticoids entrain molecular clock components in human peripheral cells.* The FASEB Journal, 2014.
165. Connell, J.M.C., E. Davies, *The new biology of aldosterone.* Journal of Endocrinology, 2005. **186**.
166. Reddy, T.E., F. Pauli, R.O. Sprouse, N.F. Neff, K.M. Newberry, M.J. Garabedian, R.M. Myers, *Genomic determination of the glucocorticoid response reveals unexpected mechanisms of gene regulation.* Genome Research, 2009. **19**(12): p. 2163-2171.
167. Gibson, P.G., N. Saltos, K. Fakes, *Acute anti-inflammatory effects of inhaled budesonide in asthma: A randomized controlled trial.* Am J Respir Crit Care Med, 2001. **163**(1): p. 32-6.
168. Lipworth, B.J., *Therapeutic implications of non-genomic glucocorticoid activity.* The Lancet. **356**(9224): p. 87-89.

169. van der Lubbe, N., C.H. Lim, R.A. Fenton, M.E. Meima, A.H. Jan Danser, R. Zietse, E.J. Hoorn, *Angiotensin ii induces phosphorylation of the thiazide-sensitive sodium chloride cotransporter independent of aldosterone.* Kidney Int, 2011. **79**(1): p. 66-76.

170. Rittig, S., T.B. Matthiesen, E.B. Pedersen, J.C. Djurhuus, *Circadian variation of angiotensin ii and aldosterone in nocturnal enuresis: Relationship to arterial blood pressure and urine output.* J Urol, 2006. **176**(2): p. 774-80.

171. Rittig, S., U.B. Knudsen, J.P. Norgaard, E.B. Pedersen, J.C. Djurhuus, *Abnormal diurnal rhythm of plasma vasopressin and urinary output in patients with enuresis*. Vol. 256. 1989. F664-F671.

172. Schwartz, W.J., R.J. Coleman, S.M. Reppert, *A daily vasopressin rhythm in rat cerebrospinal fluid.* Brain Research, 1983. **263**(1): p. 105-112.

173. Somers, V.K., M.E. Dyken, A.L. Mark, F.M. Abboud, *Sympathetic-nerve activity during sleep in normal subjects.* New England Journal of Medicine, 1993. **328**(5): p. 303-307.

174. Flint, M.S., S.S. Tinkle, *C57bl/6 mice are resistant to acute restraint modulation of cutaneous hypersensitivity*. Toxicological Sciences, 2001. **62**(2): p. 250-256.

175. Geerling, J.C., A.D. Loewy, *Central regulation of sodium appetite.* Experimental Physiology, 2008. **93**(2): p. 177-209.

176. Rowland, N.E., M.J. Fregly, *Characteristics of thirst and sodium appetite in mice (mus-musculus).* Behavioral Neuroscience, 1988. **102**(6): p. 969-974.

177. Nakamura, K., T. Shimizu, T. Yanagita, T. Nemoto, K. Taniuchi, S. Shimizu, F. Dimitriadis, T. Yawata, Y. Higashi, T. Ueba, M. Saito, *Angiotensin ii acting on brain at1 receptors induces adrenaline secretion and pressor responses in the rat.* Sci. Rep., 2014. **4**.

178. Benedict, C.R., M. Fillenz, C. Stanford, *Changes in plasma noradrenaline concentration as a measure of release rate*. British Journal of Pharmacology, 1978. **64**(2): p. 305-309.

179. Yagil, Y., L.R. Krakoff, *The differential effect of aldosterone and dexamethasone on pressor responses in adrenalectomized rats.* Hypertension, 1988. **11**(2): p. 174-8.

180. Mironova, E., V. Bugaj, K.P. Roos, D.E. Kohan, J.D. Stockand, *Aldosterone-independent regulation of the epithelial na+ channel (enac) by vasopressin in adrenalectomized mice.* Proceedings of the National Academy of Sciences, 2012. **109**(25): p. 10095-10100.

181. MacDonald, P., S. MacKenzie, L.E. Ramage, J.R. Seckl, R.W. Brown, *Corticosteroid regulation of amiloride-sensitive sodium-channel subunit mrna expression in mouse kidney*. J Endocrinol, 2000. **165**(1): p. 25-37.

182. Taves, M.D., C.E. Gomez-Sanchez, K.K. Soma, *Extra-adrenal glucocorticoids and mineralocorticoids: Evidence for local synthesis, regulation, and function.* American Journal of Physiology - Endocrinology and Metabolism, 2011. **301**(1): p. E11-E24.

183. Ricordi, C., S.D. Shah, P.E. Lacy, W.E. Clutter, P.E. Cryer, *Delayed extra-adrenal epinephrine secretion after bilateral adrenalectomy in rats.* American Journal of Physiology - Endocrinology and Metabolism, 1988. **254**(1): p. E52-E53.

184. Abdallah, J.G., B. Wyse, S.D. Jennings, D.H. Ellison, *Mechanisms of aldosterone regulation of the thiazide-sensitive na-cl cotransporter.* Journal of the American Society of Nephrology, 2000. **11**(Program and Abstract Issue): p. 24A.

185. Nielsen, J., T.-H. Kwon, S. Masilamani, K. Beutler, H. Hager, S. Nielsen, M.A. Knepper, *Sodium transporter abundance profiling in kidney: Effect of spironolactone*. Vol. 283. 2002. F923-F933.

186. Hossain Khan, M.Z., E. Sohara, A. Ohta, M. Chiga, Y. Inoue, K. Isobe, M. Wakabayashi, K. Oi, T. Rai, S. Sasaki, S. Uchida, *Phosphorylation of na-cl cotransporter by osr1 and spak kinases regulates its ubiquitination.* Biochem Biophys Res Commun, 2012. **425**(2): p. 456-61.

187. Son, G.H., S. Chung, H.K. Choe, H.-D. Kim, S.-M. Baik, H. Lee, H.-W. Lee, S. Choi, W. Sun, H. Kim, S. Cho, K.H. Lee, K. Kim, *Adrenal peripheral clock controls the autonomous circadian rhythm of glucocorticoid by causing rhythmic steroid production.* Proceedings of the National Academy of Sciences, 2008.

188. Marine, D., E.J. Baumann, *Duration of life after suprarenalectomy in cats and attempts to prolong it by injections of solutions containing sodium salts, glucose and glycerol.* American Journal of Physiology -- Legacy Content, 1927. **81**(1): p. 86-100.

189. Harrop, G.A., L.J. Soffer, R. Ellsworth, J.H. Trescher, *Studies on the suprarenal cortex : Iii. Plasma electrolytes and electrolyte excretion during suprarenal insufficiency in the dog.* The Journal of Experimental Medicine, 1933. **58**(1): p. 17-38.

190. Lipsett, M.B., O.H. Pearson, *Sodium depletion in adrenalectomized humans.* J Clin Invest, 1958. **37**(10): p. 1394-402.

191. Loeb, R.F., D.W. Atchley, E.M. Benedict, J. Leland, *Electrolyte balance studies in adrenalectomized dogs with particular reference to the excretion of sodium.* The Journal of Experimental Medicine, 1933. **57**(5): p. 775-792.

192. Stricker, E.M., K.S. Gannon, J.C. Smith, *Salt appetite induced by doca treatment or adrenalectomy in rats: Analysis of ingestive behavior.* Physiol Behav, 1992. **52**(4): p. 793-802.

193. Poulis, J.A., F. Roelfsema, D. van der Heide, *Circadian urinary excretion rhythms in adrenalectomized rats.* American Journal of Physiology - Regulatory, Integrative and Comparative Physiology, 1986. **251**(3): p. R441-R449.

194. Stanton, B.A., *Regulation by adrenal corticosteroids of sodium and potassium transport in loop of henle and distal tubule of rat kidney.* J Clin Invest, 1986. **78**(6): p. 1612-1620.

195. Kem, D.C., M.H. Weinberger, C. Gomez-Sanchez, N.J. Kramer, R. Lerman, S. Furuyama, C.A. Nugent, *Circadian rhythm of plasma aldosterone concentration in patients with primary aldosteronism.* Journal of Clinical Investigation, 1973. **52**(9): p. 2272-2277.

196. Sonoyama, T., M. Sone, N. Tamura, K. Honda, D. Taura, K. Kojima, Y. Fukuda, N. Kanamoto, M. Miura, A. Yasoda, H. Arai, H. Itoh, K. Nakao, *Role of endogenous acth on*

circadian aldosterone rhythm in patients with primary aldosteronism. Endocrine Connections, 2014. **3**(4): p. 173-179.

197. Masilamani, S., X. Wang, G.H. Kim, H. Brooks, J. Nielsen, S. Nielsen, K. Nakamura, J.B. Stokes, M.A. Knepper, *Time course of renal na-k-atpase, nhe3, nkcc2, ncc, and enac abundance changes with dietary nacl restriction.* Am J Physiol Renal Physiol, 2002. **283**(4): p. F648-57.
198. Soundararajan, R., J. Wang, D. Melters, D. Pearce, *Glucocorticoid-induced leucine zipper 1 stimulates the epithelial sodium channel by regulating serum- and glucocorticoid-induced kinase 1 stability and subcellular localization.* Journal of Biological Chemistry, 2010. **285**.
199. Rashmi, P., R. Soundararajan, J. Wang, M. Ng, G.L. Colussi, *Gilz regulates sodium and potassium balance in the distal nephron*, in *Renin-angiotensin-aldosterone system/endocrine hypertension*. p. OR40-5-OR40-5.
200. Bailey, M.A., J.J. Mullins, C.J. Kenyon, *Mineralocorticoid and glucocorticoid receptors stimulate epithelial sodium channel activity in a mouse model of cushing syndrome.* Hypertension, 2009. **54**: p. 890-896.
201. Zhao, D., D.M. Seth, L.G. Navar, *Enhanced distal nephron sodium reabsorption in chronic angiotensin ii–infused mice.* Hypertension, 2009. **54**(1): p. 120-126.
202. Pickkers, P., R.S. Garcha, M. Schachter, P. Smits, A.D. Hughes, *Inhibition of carbonic anhydrase accounts for the direct vascular effects of hydrochlorothiazide.* Hypertension, 1999. **33**: p. 1043-1048.
203. Skøtt, P., E. Hommel, S. Arnold-Larsen, H.H. Parving, *Effect of carbonic anhydrase inhibitors on glomerular filtration rate in diabetic nephropathy.* British Medical Journal (Clinical research ed.), 1987. **294**(6571): p. 549-549.
204. He, J., P.K. Whelton, *Elevated systolic blood pressure and risk of cardiovascular and renal disease: Overview of evidence from observational epidemiologic studies and randomized controlled trials.* Am Heart J, 1999. **138**(3 Pt 2): p. 211-9.
205. Carter, B.L., M.E. Ernst, J.D. Cohen, *Hydrochlorothiazide versus chlorthalidone: Evidence supporting their interchangeability.* Hypertension, 2004. **43**(1): p. 4-9.
206. Loon, N.R., C.S. Wilcox, R.J. Unwin, *Mechanism of impaired natriuretic response to furosemide during prolonged therapy.* Kidney Int, 1989. **36**(4): p. 682-689.
207. Beermann, B., M. Groschinsky-Grind, *Antihypertensive effect of various doses of hydrochlorothiazide and its relation to the plasma level of the drug.* European Journal of Clinical Pharmacology, 1978. **13**(3): p. 195-201.
208. Piccione, G., G. Caola, R. Refinetti, *Daily rhythms of blood pressure, heart rate, and body temperature in fed and fasted male dogs.* J Vet Med A Physiol Pathol Clin Med, 2005. **52**(8): p. 377-81.
209. Peterzan, M.A., R. Hardy, N. Chaturvedi, A.D. Hughes, *Meta-analysis of dose-response relationships for hydrochlorothiazide, chlorthalidone, and bendroflumethiazide on blood pressure, serum potassium, and urate.* Hypertension, 2012. **59**(6): p. 1104-9.

210. Okusa, M.D., A.E. Persson, F.S. Wright, *Chlorothiazide effect on feedback-mediated control of glomerular filtration rate.* Am J Physiol, 1989. **257**(1 Pt 2): p. F137-44.
211. VILLARREAL, H., J.E. EXAIRE, A. REVOLLO, J. SONÍ, *Effects of chlorothiazide on systemic hemodynamics in essential hypertension.* Circulation, 1962. **26**(3): p. 405-408.
212. Ellison, D.H., J. Loffing, *Thiazide effects and side effects: Insights from molecular genetics.* Hypertension, 2009. **54**(2): p. 196-202.
213. Hierholzer, K., M. Wiederholt, *Some aspects of distal tubular solute and water transport.* Kidney Int, 1976. **9**(2): p. 198-213.
214. Ridder, S., S. Chourbaji, R. Hellweg, A. Urani, C. Zacher, W. Schmid, M. Zink, H. Hörtnagl, H. Flor, F.A. Henn, G. Schütz, P. Gass, *Mice with genetically altered glucocorticoid receptor expression show altered sensitivity for stress-induced depressive reactions.* The Journal of Neuroscience, 2005. **25**(26): p. 6243-6250.
215. Walter, S.J., T. Zewde, D.G. Shirley, *The effect of anesthesia and standard clearance procedures on renal-function in the rat.* Quarterly Journal of Experimental Physiology and Cognate Medical Sciences, 1989. **74**: p. 805-812.
216. Tan, T., S.W. Watts, R.P. Davis, *Drug delivery: Enabling technology for drug discovery and development. Iprecio(®) micro infusion pump: Programmable, refillable, and implantable.* Frontiers in Pharmacology, 2011. **2**: p. 44.
217. Beermann, B., M. Groschinsky-Grind, *Pharmacokinetics of hydrochlorothiazide in man.* European Journal of Clinical Pharmacology, 1977. **12**(4): p. 297-303.
218. Rabkin, S.W., O. Roob, *Effect of chronic diuretics on epinephrine-induced ventricular arrhythmias: A comparison of hydrochlorothiazide and amiloride in the rat.* J Cardiovasc Pharmacol, 1987. **10**(2): p. 238-45.
219. Loffing, J., D. Loffing-Cueni, I. Hegyi, M.R. Kaplan, S.C. Hebert, M. Le Hir, B. Kaissling, *Thiazide treatment of rats provokes apoptosis in distal tubule cells.* Kidney Int, 1996. **50**(4): p. 1180-90.
220. Nijenhuis, T., J.G. Hoenderop, J. Loffing, A.W. van der Kemp, C.H. van Os, R.J. Bindels, *Thiazide-induced hypocalciuria is accompanied by a decreased expression of ca2+ transport proteins in kidney.* Kidney Int, 2003. **64**(2): p. 555-64.
221. Hasannejad, H., M. Takeda, K. Taki, H.J. Shin, E. Babu, P. Jutabha, S. Khamdang, M. Aleboyeh, M.L. Onozato, A. Tojo, A. Enomoto, N. Anzai, S. Narikawa, X.L. Huang, T. Niwa, et al., *Interactions of human organic anion transporters with diuretics.* Journal of Pharmacology and Experimental Therapeutics, 2004. **308**: p. 1021-1029.
222. Leviel, F., xE, oise, xFc, C.A. bner, P. Houillier, L. Morla, S. El Moghrabi, G. Brideau, xEb, lle, H. Hatim, M.D. Parker, I. Kurth, A. Kougioumtzes, et al., *The na+-dependent chloride-bicarbonate exchanger slc4a8 mediates an electroneutral na+ reabsorption process in the renal cortical collecting ducts of mice.* J Clin Invest, 2010. **120**(5): p. 1627-1635.

223. van Acker, B.A., G.C. Koomen, M.G. Koopman, R.T. Krediet, L. Arisz, *Discrepancy between circadian rhythms of inulin and creatinine clearance.* J Lab Clin Med, 1992. **120**(3): p. 400-10.

224. Fehm, H.L., R. Benkowitsch, W. Kern, G. Fehm-Wolfsdorf, P. Pauschinger, J. Born, *Influences of corticosteroids, dexamethasone and hydrocortisone on sleep in humans.* Neuropsychobiology, 1986. **16**(4): p. 198-204.

225. Brotman, D.J., J.P. Girod, M.J. Garcia, J.V. Patel, M. Gupta, A. Posch, S. Saunders, G.Y.H. Lip, S. Worley, S. Reddy, *Effects of short-term glucocorticoids on cardiovascular biomarkers.* The Journal of Clinical Endocrinology & Metabolism, 2005. **90**(6): p. 3202-3208.

226. Imai, Y., K. Abe, S. Sasaki, N. Minami, M. Nihei, M. Munakata, O. Murakami, K. Matsue, H. Sekino, Y. Miura, et al., *Altered circadian blood pressure rhythm in patients with cushing's syndrome.* Hypertension, 1988. **12**(1): p. 11-9.

227. Imai, Y., K. Abe, S. Sasaki, N. Minami, M. Munakata, M. Nihei, H. Sekino, K. Yoshinaga, *Exogenous glucocorticoid eliminates or reverses circadian blood pressure variations.* J Hypertens, 1989. **7**(2): p. 113-20.

228. Spani, D., M. Arras, B. Konig, T. Rulicke, *Higher heart rate of laboratory mice housed individually vs in pairs.* Lab Anim, 2003. **37**(1): p. 54-62.

229. Ohta, A., T. Rai, N. Yui, M. Chiga, S.S. Yang, S.H. Lin, E. Sohara, S. Sasaki, S. Uchida, *Targeted disruption of the wnk4 gene decreases phosphorylation of na-cl cotransporter, increases na excretion and lowers blood pressure.* Hum Mol Genet, 2009. **18**(20): p. 3978-86.

230. Okeahialam, B.N., E.N. Ohihoin, J.N.A. Ajuluchukwu, *Diuretic drugs benefit patients with hypertension more with night-time dosing.* Therapeutic Advances in Drug Safety, 2012. **3**(6): p. 273-278.

231. Hermida, R.C., D.E. Ayala, A. Mojón, M.J. Fontao, J.R. Fernández, *Chronotherapy with valsartan//hydrochlorothiazide combination in essential hypertension: Improved sleep-time blood pressure control with bedtime dosing.* Chronobiology International: The Journal of Biological & Medical Rhythm Research, 2011. **28**(7): p. 601-610.

232. Duarte, J.D., R.M. Cooper-DeHoff, *Mechanisms for blood pressure lowering and metabolic effects of thiazide and thiazide-like diuretics.* Expert review of cardiovascular therapy, 2010. **8**(6): p. 793-802.

233. Tarazi, R.C., H.P. Dustan, E.D. Frohlich, *Long-term thiazide therapy in essential hypertension. Evidence for persistent alteration in plasma volume and renin activity.* Circulation, 1970. **41**(4): p. 709-17.

234. Calder, J.A., M. Schachter, P.S. Sever, *Potassium channel opening properties of thiazide diuretics in isolated guinea pig resistance arteries.* J Cardiovasc Pharmacol, 1994. **24**(1): p. 158-64.

235. Pickkers, P., A.D. Hughes, F.G. Russel, T. Thien, P. Smits, *Thiazide-induced vasodilation in humans is mediated by potassium channel activation.* Hypertension, 1998. **32**(6): p. 1071-6.
236. Winer, B.M., *The antihypertensive actions of benzothiadiazines.* Circulation, 1961. **23**: p. 211-8.
237. Bennett, W.M., W.J. McDonald, E. Kuehnel, M.N. Hartnett, G.A. Porter, *Do diuretics have antihypertensive properties independent of natriuresis?* Clin Pharmacol Ther, 1977. **22**(5 Pt 1): p. 499-504.
238. Ullian, M.E., *The role of corticosteroids in the regulation of vascular tone*. Vol. 41. 1999. 55-64.
239. Markadieu, N., P. San-Cristobal, A.V. Nair, S. Verkaart, E. Lenssen, K. Tudpor, F. van Zeeland, J. Loffing, R.J. Bindels, J.G. Hoenderop, *A primary culture of distal convoluted tubules expressing functional thiazide-sensitive nacl transport.* Am J Physiol Renal Physiol, 2012. **303**(6): p. F886-92.
240. Benedetti, M., R. Merino, R. Kusuda, M.I. Ravanelli, F. Cadetti, P. dos Santos, S. Zanon, G. Lucas, *Plasma corticosterone levels in mouse models of pain.* Eur J Pain, 2012. **16**(6): p. 803-15.
241. Kanemi, O., X. Zhang, Y. Sakamoto, M. Ebina, R. Nagatomi, *Acute stress reduces intraparenchymal lung natural killer cells via beta-adrenergic stimulation.* Clinical and Experimental Immunology, 2005. **139**(1): p. 25-34.
242. Kalman, B.A., R.L. Spencer, *Rapid corticosteroid-dependent regulation of mineralocorticoid receptor protein expression in rat brain.* Endocrinology, 2002. **143**(11): p. 4184-95.
243. Gaeggeler, H.P., H. Duperrex, S. Hautier, B.C. Rossier, *Corticosterone induces 11 beta-hsd and mineralocorticoid specificity in an amphibian urinary bladder cell line*. Vol. 264. 1993. C317-C322.
244. van der Lubbe, N., C.H. Lim, M.E. Meima, R. van Veghel, L.L. Rosenbaek, K. Mutig, A.H.J. Danser, R.A. Fenton, R. Zietse, E.J. Hoorn, *Aldosterone does not require angiotensin ii to activate ncc through a wnk4–spak–dependent pathway.* Pflügers Archiv, 2012. **463**(6): p. 853-863.
245. Bailey, M.A., E. Craigie, D.E.W. Livingstone, Y.V. Kotelevtsev, E.A.S. Al-Dujaili, C.J. Kenyon, J.J. Mullins, *Hsd11b2 haploinsufficiency in mice causes salt sensitivity of blood pressure*. Hypertension, 2011. **57**: p. 515-U322.
246. Arriza, J., C. Weinberger, G. Cerelli, T. Glaser, B. Handelin, D. Housman, R. Evans, *Cloning of human mineralocorticoid receptor complementary DNA: Structural and functional kinship with the glucocorticoid receptor.* Science, 1987. **237**(4812): p. 268-275.
247. Funder, J., K. Myles, *Exclusion of corticosterone from epithelial mineralocorticoid receptors is insufficient for selectivity of aldosterone action: In vivo binding studies.* Endocrinology, 1996. **137**(12): p. 5264-8.
248. Craigie, E., J. Mullins, M. Bailey, *Failure to down-regulate the epithelial sodium channel causes salt-sensitivity in 11bhsd2 heterozygote mice.* Hypertension, 2012.

249. Goodwin, J.E., D.S. Geller, *Glucocorticoid-induced hypertension.* Pediatric Nephrology, 2012. **27**: p. 1059-1066.

250. Goodwin, J.E., J.H. Zhang, H. Velazquez, D.S. Geller, *The glucocorticoid receptor in the distal nephron is not necessary for the development or maintenance of dexamethasone-induced hypertension.* Biochemical and Biophysical Research Communications, 2010. **394**: p. 266-271.

251. Baylis, C., R.K. Handa, M. Sorkin, *Glucocorticoids and control of glomerular filtration rate.* Semin Nephrol, 1990. **10**(4): p. 320-9.

252. Baylis, C., B.M. Brenner, *Mechanism of glucocorticoid-induced increase in glomerular-filtration rate.* American Journal of Physiology, 1978. **234**.

253. Palmer, L.G., J. Schnermann, *Integrated control of na transport along the nephron.* Clin J Am Soc Nephrol, 2015. **10**(4): p. 676-87.

254. Ellison, D.H., H. Velazquez, F.S. Wright, *Thiazide-sensitive sodium chloride cotransport in early distal tubule*. Vol. 253. 1987. F546-F554.

255. Monroy, A., C. Plata, S.C. Hebert, G. Gamba, *Characterization of the thiazide-sensitive na+-cl− cotransporter: A new model for ions and diuretics interaction*. Vol. 279. 2000. F161-F169.

256. Delyani, J.A., *Mineralocorticoid receptor antagonists: The evolution of utility and pharmacology.* Kidney Int, 2000. **57**(4): p. 1408-11.

257. Sachdeva, A., A.B. Weder, *Nocturnal sodium excretion, blood pressure dipping, and sodium sensitivity.* Hypertension, 2006. **48**(4): p. 527-33.

258. Di Blasio, A.M., E.F. van Rossum, S. Maestrini, M.E. Berselli, M. Tagliaferri, F. Podesta, J.W. Koper, A. Liuzzi, S.W. Lamberts, *The relation between two polymorphisms in the glucocorticoid receptor gene and body mass index, blood pressure and cholesterol in obese patients.* Clin Endocrinol (Oxf), 2003. **59**(1): p. 68-74.

259. Manenschijn, L., E.L. Van Den Akker, S.W. Lamberts, E.F. Van Rossum, *Clinical features associated with glucocorticoid receptor polymorphisms.* Annals of the New York Academy of Sciences, 2009. **1179**(1): p. 179-198.

260. Alikhani-Koupaei, R., F. Fouladkou, P. Fustier, B. Cenni, A.M. Sharma, H.C. Deter, B.M. Frey, F.J. Frey, *Identification of polymorphisms in the human 11beta-hydroxysteroid dehydrogenase type 2 gene promoter: Functional characterization and relevance for salt sensitivity.* Faseb j, 2007. **21**(13): p. 3618-28.

261. Mariniello, B., V. Ronconi, C. Sardu, A. Pagliericcio, F. Galletti, P. Strazzullo, M. Palermo, M. Boscaro, P.M. Stewart, F. Mantero, G. Giacchetti, *Analysis of the 11beta-hydroxysteroid dehydrogenase type 2 gene (hsd11b2) in human essential hypertension.* Am J Hypertens, 2005. **18**(8): p. 1091-8.

262. Weber, C.S., J.F. Thayer, M. Rudat, A.M. Sharma, F.H. Perschel, K. Buchholz, H.C. Deter, *Salt-sensitive men show reduced heart rate variability, lower norepinephrine and enhanced cortisol during mental stress.* J Hum Hypertens, 2008. **22**(6): p. 423-31.

263. Kerstens, M.N., F.G. van der Kleij, A.H. Boonstra, W.J. Sluiter, J. Koerts, G. Navis, R.P. Dullaart, *Salt loading affects cortisol metabolism in normotensive subjects: Relationships with salt sensitivity.* J Clin Endocrinol Metab, 2003. **88**(9): p. 4180-5.

264. Pereira, C.D., I. Azevedo, R. Monteiro, M.J. Martins, *11beta-hydroxysteroid dehydrogenase type 1: Relevance of its modulation in the pathophysiology of obesity, the metabolic syndrome and type 2 diabetes mellitus.* Diabetes Obes Metab, 2012. **14**(10): p. 869-81.

265. Fuenmayor, N., E. Moreira, L.X. Cubeddu, *Salt sensitivity is associated with insulin resistance in essential hypertension.* Am J Hypertens, 1998. **11**(4 Pt 1): p. 397-402.

266. Hoffmann, I.S., L.X. Cubeddu, *Increased blood pressure reactivity to dietary salt in patients with the metabolic syndrome.* J Hum Hypertens, 2007. **21**(6): p. 438-44.

267. Chen, J., D. Gu, J. Huang, D.C. Rao, C.E. Jaquish, J.E. Hixson, C.S. Chen, J. Chen, F. Lu, D. Hu, T. Rice, T.N. Kelly, L.L. Hamm, P.K. Whelton, J. He, *Metabolic syndrome and salt sensitivity of blood pressure in non-diabetic people in china: A dietary intervention study.* Lancet, 2009. **373**(9666): p. 829-35.

268. Michailidou, Z., R.N. Carter, E. Marshall, H.G. Sutherland, D.G. Brownstein, E. Owen, K. Cockett, V. Kelly, L. Ramage, E.A.S. Al-Dujaili, M. Ross, I. Maraki, K. Newton, M.C. Holmes, J.R. Seckl, et al., *Glucocorticoid receptor haploinsufficiency causes hypertension and attenuates hypothalamic-pituitary-adrenal axis and blood pressure adaptions to high-fat diet.* Faseb Journal, 2008. **22**: p. 3896-3907.

269. Ivy, J.R.E., Louise C.; Richardson, Rachel V., Flatman, Peter W.; Chapman, Karen E.; Kenyon, Christopher J.; Bailey, Matthew A. . *Abnormal regulation of ncc in glucocorticoid receptor haploinsufficient mice*. in *Experimental Biology 2013*. 2013. Boston, USA: The FASEB Journal.

270. Ivy, J.R.E., Louise C.; Richardson, Rachel V., Flatman, Peter W.; Chapman, Karen E.; Kenyon, Christopher J.; Bailey, Matthew A. . *Glucocorticoid receptor haploinsufficiency causes salt-sensitivity and dysregulation of the thiazide-sensitive na-cl cotransporter*. in *37th Congress of IUPS*. 2013. Birmingham, UK: Proceeding's of The Physiological Society.

271. Komers, R., S. Rogers, T.T. Oyama, B. Xu, C.-L. Yang, J. McCormick, D.H. Ellison, *Enhanced phosphorylation of na-cl cotransporter in experimental metabolic syndrome – role of insulin.* Clinical science (London, England : 1979), 2012. **123**(11): p. 635-647.

272. Turkkan, J.S., D.S. Goldstein, *Stress and sodium hypertension in baboons: Neuroendocrine and pharmacotherapeutic assessments.* J Hypertens, 1991. **9**(10): p. 969-75.

273. Ferdinand, K.C., *Obesity and hypertension: It's about more than the numbers.* Obesity, 2013. **21**(4): p. 657-658.

274. Reungjui, S., T. Pratipanawatr, R.J. Johnson, T. Nakagawa, *Do thiazides worsen metabolic syndrome and renal disease? The pivotal roles for hyperuricemia and hypokalemia.* Current Opinion in Nephrology and Hypertension, 2008. **17**(5): p. 470-476.

275. Mendoza, M.D., J.J. Stevermer, *Hypertension with metabolic syndrome: Think thiazides are old hat? Allhat says think again.* The Journal of Family Practice, 2008. **57**(5): p. 306-310.

276. Fallo, F., G. Fanelli, A. Cipolla, C. Betterle, M. Boscaro, N. Sonino, *24-hour blood pressure profile in addison's disease.* Am J Hypertens, 1994. **7**(12): p. 1105-9.

277. Henley, D.E., S.L. Lightman, *Cardio-metabolic consequences of glucocorticoid replacement: Relevance of ultradian signalling.* Clin Endocrinol (Oxf), 2014. **80**(5): p. 621-8.

278. Scheer, F.A.J.L., M.F. Hilton, C.S. Mantzoros, S.A. Shea, *Adverse metabolic and cardiovascular consequences of circadian misalignment.* Proceedings of the National Academy of Sciences, 2009. **106**(11): p. 4453-4458.

279. Cho, K., A. Ennaceur, J.C. Cole, C.K. Suh, *Chronic jet lag produces cognitive deficits.* J Neurosci, 2000. **20**(6): p. Rc66.

280. Davidson, A.J., M.T. Sellix, J. Daniel, S. Yamazaki, M. Menaker, G.D. Block, *Chronic jet-lag increases mortality in aged mice.* Current biology : CB, 2006. **16**(21): p. R914-R916.

281. Vyas, M.V., A.X. Garg, A.V. Iansavichus, J. Costella, A. Donner, L.E. Laugsand, I. Janszky, M. Mrkobrada, G. Parraga, D.G. Hackam, *Shift work and vascular events: Systematic review and meta-analysis*. Vol. 345. 2012.

282. Fujino, Y., H. Iso, A. Tamakoshi, Y. Inaba, A. Koizumi, T. Kubo, T. Yoshimura, *A prospective cohort study of shift work and risk of ischemic heart disease in japanese male workers.* Am J Epidemiol, 2006. **164**(2): p. 128-35.

283. Lieu, S.J., G.C. Curhan, E.S. Schernhammer, J.P. Forman, *Rotating night shift work and disparate hypertension risk in african-americans.* J Hypertens, 2012. **30**(1): p. 61-6.

284. Kiessling, S., G. Eichele, H. Oster, *Adrenal glucocorticoids have a key role in circadian resynchronization in a mouse model of jet lag.* J Clin Invest, 2010. **120**(7): p. 2600-2609.

285. Pasquali, R., V. Vicennati, M. Cacciari, U. Pagotto, *The hypothalamic-pituitary-adrenal axis activity in obesity and the metabolic syndrome.* Ann N Y Acad Sci, 2006. **1083**: p. 111-28.

286. Razzoli, M., C. Karsten, J.M. Yoder, A. Bartolomucci, W.C. Engeland, *Chronic subordination stress phase advances adrenal and anterior pituitary clock gene rhythms.* Am J Physiol Regul Integr Comp Physiol, 2014. **307**(2): p. R198-205.

287. Yehuda, R., M.H. Teicher, R.L. Trestman, R.A. Levengood, L.J. Siever, *Cortisol regulation in posttraumatic stress disorder and major depression: A chronobiological analysis.* Biological Psychiatry, 1996. **40**(2): p. 79-88.

288. Jarcho, M.R., G.M. Slavich, H. Tylova-Stein, O.M. Wolkowitz, H.M. Burke, *Dysregulated diurnal cortisol pattern is associated with glucocorticoid resistance in women with major depressive disorder.* Biol Psychol, 2013. **93**(1): p. 150-8.

289. Uzu, T., G. Kimura, A. Yamauchi, M. Kanasaki, K. Isshiki, S. Araki, T. Sugiomoto, Y. Nishio, H. Maegawa, D. Koya, M. Haneda, A. Kashiwagi, *Enhanced sodium sensitivity and disturbed circadian rhythm of blood pressure in essential hypertension.* J Hypertens, 2006. **24**(8): p. 1627-32.

290. Clays, E., K. Van Herck, M. De Buyzere, M. Kornitzer, F. Kittel, G. De Backer, D. De Bacquer, *Behavioural and psychosocial correlates of nondipping blood pressure pattern among middle-aged men and women at work.* J Hum Hypertens, 2012. **26**(6): p. 381-7.

291. Vrijkotte, T.G.M., L.J.P. van Doornen, E.J.C. de Geus, *Effects of work stress on ambulatory blood pressure, heart rate, and heart rate variability.* Hypertension, 2000. **35**(4): p. 880-886.

292. Strazzullo, P., A. Barbato, F. Galletti, G. Barba, A. Siani, R. Iacone, L. D'Elia, O. Russo, M. Versiero, E. Farinaro, F.P. Cappuccio, *Abnormalities of renal sodium handling in the metabolic syndrome. Results of the olivetti heart study.* J Hypertens, 2006. **24**(8): p. 1633-9.

293. Staessen, J.A., L. Thijs, R. Fagard, E.T. O'Brien, D. Clement, P.W. de Leeuw, G. Mancia, C. Nachev, P. Palatini, G. Parati, J. Tuomilehto, J. Webster, *Predicting cardiovascular risk using conventional vs ambulatory blood pressure in older patients with systolic hypertension. Systolic hypertension in europe trial investigators.* Jama, 1999. **282**(6): p. 539-46.

294. Hermida, R.C., D.E. Ayala, A. Mojón, J.R. Fernández, *Decreasing sleep-time blood pressure determined by ambulatory monitoring reduces cardiovascular risk.* Journal of the American College of Cardiology, 2011. **58**(11): p. 1165-1173.

295. Hermida, R.C., D.E. Ayala, A. Mojon, J.R. Fernandez, *Influence of circadian time of hypertension treatment on cardiovascular risk: Results of the mapec study.* Chronobiol Int, 2010. **27**(8): p. 1629-51.

296. Hermida, R.C., D.E. Ayala, M.H. Smolensky, J.R. Fernandez, A. Mojon, J.J. Crespo, M.T. Rios, A. Moya, F. Portaluppi, *Chronotherapeutics of conventional blood pressure-lowering medications: Simple, low-cost means of improving management and treatment outcomes of hypertensive-related disorders.* Curr Hypertens Rep, 2014. **16**(2): p. 412.

297. Chrousos, G.P., *Ultradian, circadian, and stress-related hypothalamic-pituitary-adrenal axis activity--a dynamic digital-to-analog modulation.* Endocrinology, 1998. **139**(2): p. 437-40.

298. Sarabdjitsingh, R.A., B.L. Conway-Campbell, J.D. Leggett, E.J. Waite, O.C. Meijer, E.R. de Kloet, S.L. Lightman, *Stress responsiveness varies over the ultradian glucocorticoid cycle in a brain-region-specific manner.* Endocrinology, 2010. **151**(11): p. 5369-79.

299. Jyothinagaram, S.G., P. Neary, D.M. Watson, I.M. McGinley, P.L. Padfield, *Role of corticosteroids in the diurnal rhythm of blood pressure.* J Hypertens Suppl, 1989. **7**(6): p. S68-9.

300. Debono, M., C. Ghobadi, A. Rostami-Hodjegan, H. Huatan, M.J. Campbell, J. Newell-Price, K. Darzy, D.P. Merke, W. Arlt, R.J. Ross, *Modified-release hydrocortisone to provide circadian cortisol profiles.* The Journal of Clinical Endocrinology & Metabolism, 2009. **94**(5): p. 1548-1554.

301. Morelli, V., ; Messina, E.; Mendola, M.; Cairoli, E.; Ambrosi, B.;, Cannavò, S.; Chiodini, I.; Spada, A. *Beneficial effects of replacement therapy with modified-release hydrocortisone in patients with adrenal insufficiency*. in *17th European Congress of Endocrinology*. 2015. Dublin, Ireland: Bioscientifica.

302. Levi, F., U. Schibler, *Circadian rhythms: Mechanisms and therapeutic implications.* Annu Rev Pharmacol Toxicol, 2007. **47**: p. 593-628.

303. Koopman, M.G., G.C. Koomen, R.T. Krediet, E.A. de Moor, F.J. Hoek, L. Arisz, *Circadian rhythm of glomerular filtration rate in normal individuals.* Clin Sci (Lond), 1989. **77**(1): p. 105-11.

9. Appendix

9.1. Thiazide-sensitive sodium transport in 11βHSD2 heterozygous mice

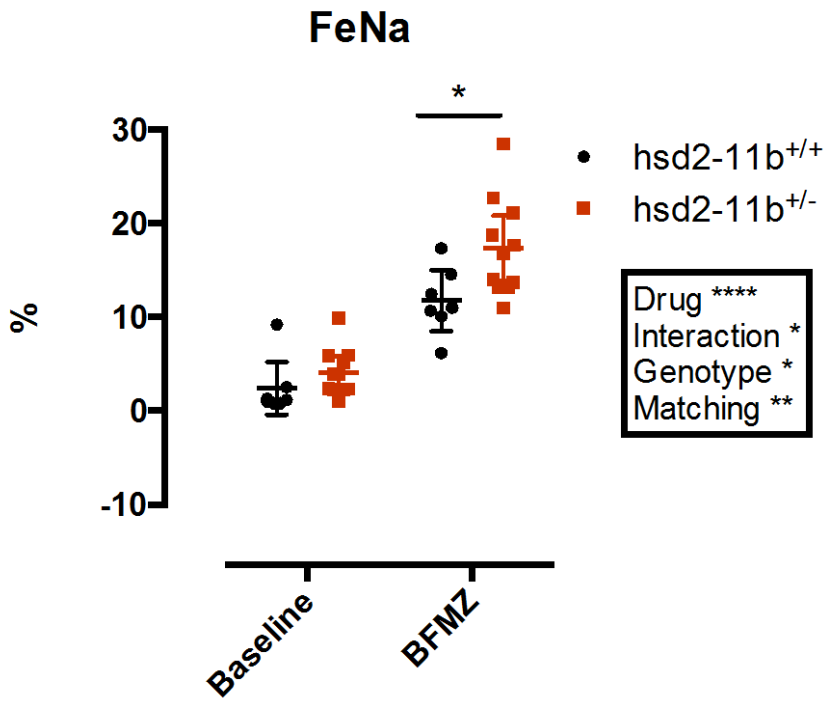

Figure 9.1: Fractional sodium excretion (FeNa) in HSD2-11b wild type (+/+) and heterozygous (+/-) mice
Hsd2-11b wild type and heterozygous littermate mice underwent renal clearance surgery. The experimenter was blinded to the genotype. Following a 40-minute baseline urine collection, mice were given bendroflumethiazide (BFMZ, 6 mg/kg i.v.) and a further 40-minute collection was made. Data are mean±95% CI. Data were analysed by matched two-way ANOVA with post hoc Sidak tests, ****p<0.0001, **p<0.01, *p<0.05, n=13.

9.2. Grants:

2013 BHF travel grant to attend Experimental Biology, Boston

2013 The Physiological Society travel grant for International Union of Physiology Society meeting, Birmingham

2014 The Physiological Society travel grant for the Society Main Meeting in London

2015 The Physiological Society travel grant for the Society Main Meeting in Cardiff

9.3. Published Abstracts:

Ivy JR, Evans LC, Richardson RV, Flatman PW, Chapman KE, Kenyon CJ, Bailey MA. "Abnormal regulation of NCC in glucocorticoid receptor haploinsufficient mice" *Meeting Abstract Supplement FASEB, Experimental Biology Boston, 2013.* (poster presentation)

Ivy JR, Evans LC, Richardson RV, Flatman PW, Chapman KE, Kenyon CJ, Bailey MA. "Glucocorticoid receptor haploinsufficiency causes salt-sensitivity and disregulation of the thiazide-sensitive NC-Cl cotransporter" *37th Congress of IUPS, Birmingham, UK 2013* (poster presentation)

Ivy JR, Flatman PW, Bailey MA "Diurnal rhythm of the thiazide-sensitive sodium chloride cotransporter" *The Physiology Society Main Meeting, London, 2014* (poster presentation)

Ivy JR, Aldujaili E, Flatman PW, Bailey MA. "Glucocorticoids and the Diurnal Rhythm of Thiazide-sensitive NaCl Co-transporter" *Meeting Abstract Supplement FASEB, Experimental Biology, Boston, 2015.* (oral presentation)

Ivy JR, Aldujaili E, Flatman PW, Bailey MA "Glucocorticoids affect the diurnal rhythm of the thiazide-sensitive NaCl co-transporter" *The Physiology Society Main Meeting, Cardiff, 2015*. (oral presentation)

9.4. Awards & achievements

2014 Figure from my Review article [21] was chosen for the cover of the Journal of Physiology

2015 Early Career researcher Oral Presentation Award from the Centre for Cardiovascular Society Annual Symposium

2015 Physiological Society Oral Communication Prize

The Journal of Physiology
15 September 2014 Volume 592 Number 18 3933–4096 WILEY Blackwell

The Journal of Physiology

Volume 592 / Number 18 / 15 September 2014

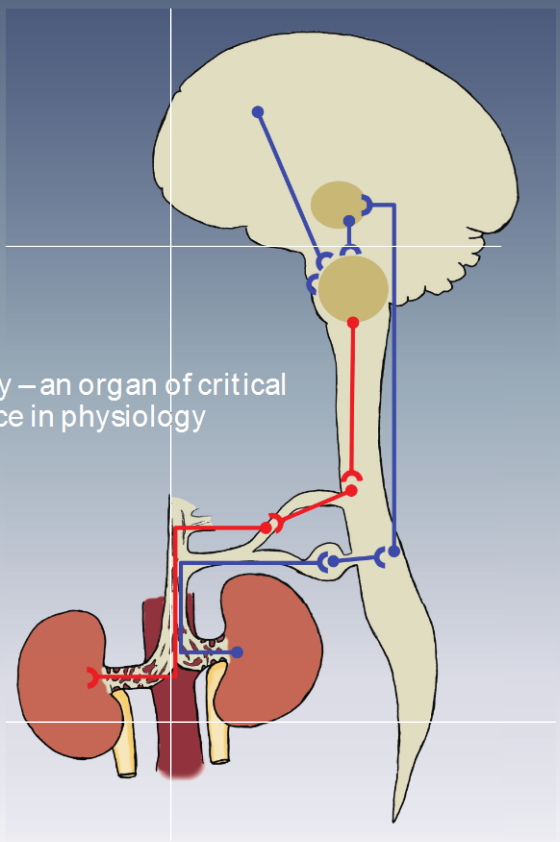

The kidney – an organ of critical importance in physiology

A publication of The Physiological Society